The Mechanics of Mitotic Cell Rounding

DISSERTATION

Zur Erlangung des akadmischen Grades

Doctor rerum naturalium (Dr. rer. nat.)

vorgelegt der Fakultät Mathematik und Naturwissenschaften der
Technischen Universität Dresden

von

Martin Philip Stewart

Geboren am 27.12.1983 in Sydney (Australien)

Erster Gutachter: Prof. Dr. Tony A. Hyman (MPI-CBG)

Zweiter Gutachter: Prof. Dr. Daniel J. Müller (TU Dresden/ETH Zürich)

Eingereicht am: 14.05.2012

Table of Contents

Table of Contents **2**

Thesis Summary **4**

Motivation **6**

Introduction **8**
- **Cell Shape, Cell Mechanics and the Cytoskeleton** **8**
- **The Cell Cycle is Linked to Cell Shape** **13**
- **Mitotic Cell Rounding** **16**

AFM Constant Force Experiments **18**
- The Trans-Mitotic Constant Force Assay 18

Observations on Shape and Adhesion of Round Cells **25**

AFM Constant Height Experiments **30**
- The Trans-Mitotic Constant Height Assay 30
- Selection of the 8 μm Constant Height Assay 33
- Comparison of Induced Interphase and Mitotic Cell Rounding 42
- Induced Cell Rounding via Phosphatase Inhibition 49
- **Pharmacological Dissection of Mitotic Cell Rounding** **50**
  - Actomyosin 51
  - Microtubules 52
  - Plasma Membrane Traffic and Surface Area 53
  - Ion Transporters 53
  - Summary of Inhibitor Results 64
  - Observations on Cell Rounding Rates with Inhibitors 66
  - Observations on Cell Blebbing with Inhibitors 68
- **Dynamic perturbations** **69**
  - Tonic shocks 70
  - Actomyosin 70
  - Na^+/H^+ Exchange 71
  - Plasma Membrane Permeability 72
  - Summary of Dynamic Perturbation Results 81

Discussion **85**
- **Physical Basis of MCR - Summary** **85**
- **Physical Basis of MCR - Details** **87**
  - Intracellular Pressure in Cell Mechanics 87
  - Intracellular Pressure in MCR 88
  - Intracellular Pressure in Cell Shape and Movement 92
  - Volume Regulation 94
  - Na^+/H^+ Exchange and the Physical Properties of Cells 98
  - Cell Volume and α-toxin Plasma Membrane Permeabilization 100
  - Deformation and Cell Volume 101
  - Cell Volume Trans-Mitosis 102
  - Plasma Membrane-Actomyosin Cortex Coupling 102
  - Changes in Cell Surface Area During Cell Rounding 104
  - Changes in Adhesion During Cell Rounding 105
- **Signaling Pathways and Proteins in MCR** **109**
  - Cdk1 and Mitosis 109

Cdk1 Modulation of Actomyosin ... 113
Cdk1 Modulation of Cell Adhesion ... 115
Cdk1 Modulation of Intermediate Filaments and Spectrin ... 116
General Cell Rounding ... 117
The Adhesion versus Surface Tension Paradigm ... 117
Rounding Mode 1 – Actomyosin Surface Tension ... 124
Cell Rounding by the RhoA Pathway ... 124
Signals Inducing Cell Rounding by the RhoA Pathway ... 125
Cell Rounding by Eicosanoids ... 126
Cell Rounding by Ephrins ... 127
Cell Rounding by Protease-Activated Receptors: Thrombin & Trypsin ... 127
Cell Rounding by the PAK Pathway ... 130
Cell Rounding by Phosphatase Inhibition ... 131
Rounding Mode 2 – Weakening of Internal Structures ... 131
Cell Rounding by Perturbation of Actin and Focal Adhesions ... 132
Cell Rounding by Upstream Regulators of Actin and Focal Adhesions ... 132
Cell Rounding by Pathogenic Disruption of Actin and Focal Adhesions ... 133
Rounding Mode 3 – Interference with External Adhesion Receptors ... 135
Cell Rounding by Interference with Integrins ... 135
Cell Rounding via the Action of Cell-Matrix Modulators ... 136
Rounding Mode 4 – Surface Coating ... 137
Cell Rounding by Lectins ... 137
The Adhesion versus Surface Tension Paradigm in Tissue Barriers ... 140
Discussion Summary ... 143

Outlook ... 144
MCR as a Model Problem in Cell Mechanics ... 144
The Mechanics of Cell Rounding Beyond Mitosis ... 144
Improved Cell Mechanics Methodology ... 145
Understanding Cell Compression ... 146
Ongoing AFM-based Screening for MCR Pathways ... 147

Conclusions ... 150

Methods ... 151
Equipment ... 151
Reagent Setup ... 152
Protocols ... 154
Setting up AFM, Optical Microscope and Cantilever Calibration ... 154
Performing an AFM Constant Force/Height Assay ... 156
Mid-Experiment Dynamic Perturbations ... 159
Methods Discussion ... 160
Methods in Cell Mechanics ... 160
AFM in Cell Mechanics ... 161
The AFM Constant Height Assay to Analyze Cell Mechanics and Volume ... 162
Other AFM Methods to Analyze Cell Mechanics and Volume ... 163
Outlook for Methods in Cytomechanics and "Systems Physiology" ... 166

Terms and Abbreviations ... 168

List of Publications ... 170

Acknowledgements ... 171

References ... 172

Declaration of Originality ... 193

Thesis Summary

During mitosis, adherent animal cells undergo a drastic shape change, from essentially flat to round, in a process known as mitotic cell rounding (MCR). The aim of this thesis was to critically examine the physical and biological basis of MCR.

The experimental part of this thesis employed a combined optical microscope-atomic force microscope (AFM) setup in conjunction with flat tipless cantilevers to analyze cell mechanics, shape and volume. To this end, two AFM assays were developed: the constant force assay (CFA), which applies constant force to cells and measures the resultant height, and the constant height assay (CHA), which confines cell height and measures the resultant force. These assays were deployed to analyze the shape and mechanical properties of single cells trans-mitosis. The CFA results showed that cells progressing through mitosis could increase their height against forces as high as 50 nN, and that higher forces can delay mitosis in HeLa cells. The CHA results showed that mitotic cells confined to ~50% of their normal height can generate forces around 50-100 nN without disturbing mitotic progression. Such forces represent intracellular pressures of at least 200 Pascals and cell surface tensions of around 10 nN/μm. Using the CHA to compare mitotic cell rounding with induced cell rounding, it was observed that the intracellular pressure of mitotic cells is at least 3-fold higher than rounded interphase cells. To investigate the molecular basis of the mechanical changes inherent in mitotic cell rounding, inhibitors and toxins were used to pharmacologically dissect the role of candidate cellular processes. These results implicated the actomyosin cortex and osmolyte transporters, the most prominent of which is the Na^+/H^+ exchanger, in the maintenance of mechanical properties and intracellular hydrostatic pressure. Observations on blebbing cells under the cantilever supported the idea that the actomyosin cortex is required to sustain hydrostatic pressure and direct this pressure into cell shape changes. To gain further insight into the

relationship between actomyosin activity and intracellular pressure, dynamic perturbation experiments were conducted. To this end, the CHA was used to evaluate the pressure and volume of mitotic cells before, during and after dynamic perturbations that included tonic shocks, influx of specific inhibitors, and exposure to pore-forming toxins. When osmotic pressure gradients were depleted, pressure and volume decreased. When the actomyosin cytoskeleton was abolished, cell volume increased while rounding pressure decreased. Conversely, stimulation of actomyosin cortex contraction triggered an increase in rounding pressure and a decrease in volume. Taken together, the dynamic perturbation results demonstrated that the actomyosin cortex contracts against an opposing intracellular pressure and that this relationship sets the surface tension, pressure and volume of the cell.

The discussion section of this thesis provides a comprehensive overview of the physical basis of MCR by amalgamating the experimental results of this thesis with the literature. Additionally, the biochemal signaling pathways and proteins that drive MCR are collated and discussed. An exhaustive and unprecedented synthesis of the literature on cell rounding (approx. 750 papers as pubmed search hits on “cell rounding”, April 2012) reveals that the spread-to-round transition can be thought of in terms of a surface tension versus adhesion paradigm, and that cell rounding can be physically classified into four main modes, of which one is an MCR-like category characterized by increased actomyosin cortex tension and diminution of focal adhesions. The biochemical pathways and signaling patterns that correspond with these four rounding modes are catalogued and expounded upon in the context of the relevant physiology. This analysis reveals cell rounding as a pertinent topic that can be leveraged to yield insight into core principles of cell biophysics and tissue organization. It furthermore highlights MCR as a model problem to understand the adhesion versus cell surface tension paradigm in cells and its fundamentality to cell shape, mechanics and physiology.

Motivation

How this thesis work began

Daniel Müller suggested I test the mechanical response of cells subjected to constant forces. Therefore, I began a series of experiments using atomic force microscope (AFM) cantilevers to press MdCK cells with constant forces. In most experiments the cells yielded passively to the force, but in one prominent example the cell pushed back against the cantilever (Fig 1A). Curious to know why this cell was different, I tracked it with phase contrast microscopy for the next hour and observed that it rounded up, proceeded through mitosis, and divided. In order to repeat this experiment in a systematic way a method to predict which cells would enter mitosis was required. Therefore, Tony Hyman and Yusuke Toyoda suggested we identify cells early in mitosis cells by employing a HeLa cell line with fluorescently labeled histones. This enabled visualization of the cell cycle phase by chromatin morphology and with these cells it was possible to reproduce the initial observation on MdCK cells. In the first such successful attempt, I was able to track HeLa cell height against a constant force from early mitosis through to division (Fig 1B). At the beginning of mitosis, the cell had a protracted morphology. Then, against a 1 nN constant force, it elevated almost 10 μm and divided after 50 minutes. Fascinated by this phenomenon, I became motivated to investigate the mechanics and forces involved in mitotic cell rounding with AFM.

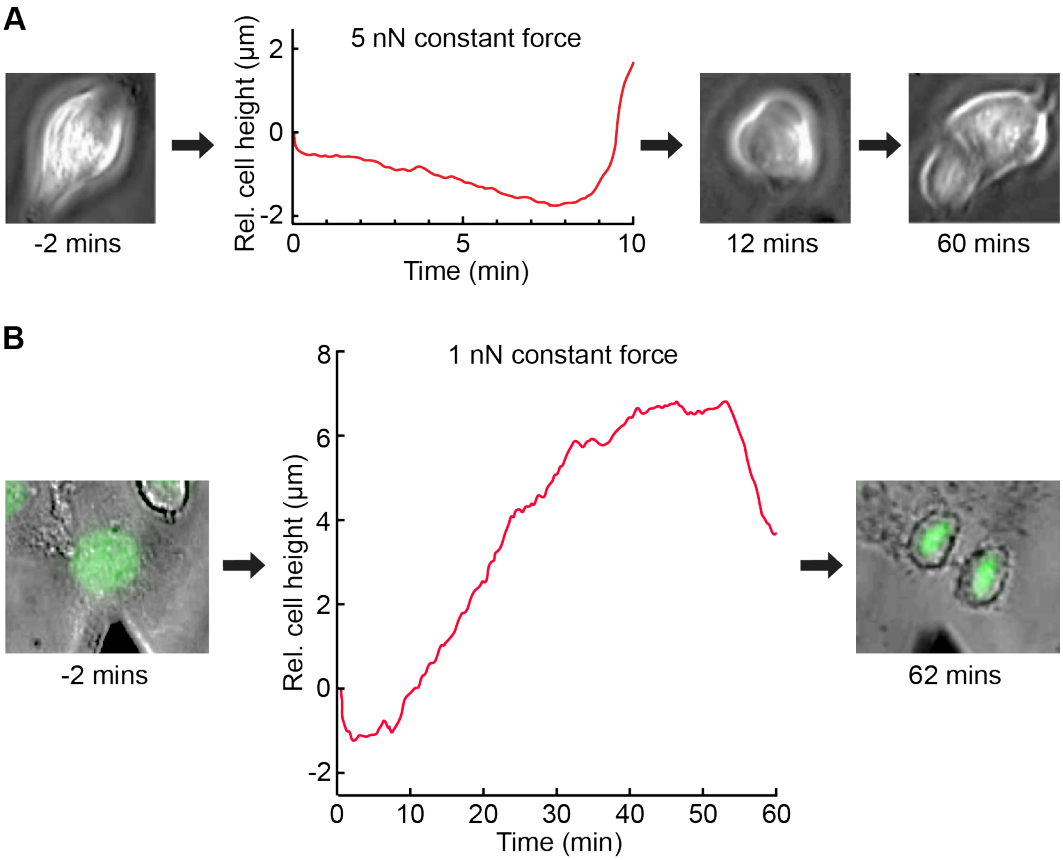

Figure 1: Initial observations of mitotic cell rounding against a constant force. **A** An MdCK cell was pressed from above with a flat atomic force microscope (AFM) cantilever at 5 nN constant force for a duration of 10 minutes. Rel. cell height is the relative cell height change where 0 is the height of the cell when the force is first applied. Note the abrupt increase in cell height in the final 2 minutes of the experiment. Phase contrast images comparing before (-2 mins) and after (60 mins) show that the cell divided. **B** A transgenic HeLa cell expressing a chromatin marker (Histone H2B-GFP) was identified at the beginning of mitosis by the appearance of condensed chromosomes (see methods, mitotic phase assignment) then pressed with a 1 nN constant force until the cell divided. Overlaid phase contrast and fluorescence GFP images show the cell before (-2 mins) and after (62 mins) division.

Introduction

Cell Shape, Cell Mechanics and the Cytoskeleton

Cell shape is of fundamental importance to the function of single cells and the tissues that they form. The shape of a given cell can be thought of as governed by three factors: the mechanical properties of its constituent components, the intrinsic forces generated by it, and extrinsic forces acting on it[1]. The first two of these factors are largely controlled by the cytoskeleton, which is thought to be primary determinant of cell shape, mechanics and intracellular spatial organization.

The Cytoskeleton

The cytoskeleton consists of a highly dynamic intracellular scaffolding of filamentous polymers, motor proteins, and accessory proteins[2]. Three main types of cytoskeletal polymer exist: actin filaments, microtubules and a category known collectively as intermediate filaments (IFs). Actin filaments (F-actin) form from the polymerization of actin monomers (G-actin) in an ATP dependent manner. Microtubules form hollow tubes based on a spiral-like assembly of tubulin heterodimers in a GTP dependent manner. Both have the ability to engage motor proteins, which are force-generating molecules that either move cargo along filaments or move filaments in relation to each other. Cytoskeletal motor proteins have been categorized into several groups including myosins, which form dynamic assemblies with F-actin, and kinesins and dyneins, which associate with microtubules. Unlike actin filaments and microtubules, IFs do not interact with specialized groups of motor proteins. Cytoskeletal networks are integral to many aspects of cellular homeostasis, and their function is dependent on regulatory signal networks and accessory proteins that link them to other cellular components[2].

Discovery and Identification of Cytoskeletal Components

In the early days of cell research cytoskeletal elements were observed by light microscopy as dynamic arrays of fibers in the cytoplasm of living cells[3, 4]. The advent of electron microscopy allowed researchers to zoom in on

these structures and classify them based on morphological features like size and assembly patterns. From the 1960s onwards, the development of key biochemical assays enabled the molecular identification of cellular cytoskeletal components. Assemblies of actin filaments and myosin motors (actomyosin), originally thought to be muscle specific, were found to be ubiqituous in almost all eukaryotic cells[5, 6]. The subunits that comprise microtubules were identified and named tubulin[7]. IFs were observed in skeletal muscle cells exhibiting an intermediate diameter (10 nm) relative to microtubules (25 nm), muscle-specific myosin filaments (15 nm) and actin filaments (7 nm)[8]. IFs were then shown to be present in many cell types and further defined by their resistance to biochemical treatments that disrupted other cytoskeletal components[9].

The Actomyosin Cytoskeleton

Knowledge of the molecular identity of cytoskeletal components was important because it provided the possibility to test for cellular function with specific biochemical and genetic tools. One theme that emerged from such studies was the apparent primacy of the actomyosin cytoskeleton in whole-cell shape and mechanics. Early on, actomyosin was found to be central to cellular processes such as adhesion[10-13], motility[14], cell division[15-17], and the homeostatis of mechanical properties[18-21]. Other proteins originally thought to be muscle-specific such as α-actinin were found in non-muscle cells and observed to localize to actin filaments and the plaque-like structures found at their terminal ends[22]. These actin-associated plaque-like structures were later shown to be key points of cell-substrate adhesive contact and aptly named “focal adhesions”[13]. Subsequently, proteins like vinculin, talin and paxillin were discovered and shown to participate in focal adhesion formation and structure[23-25]. In 1986 the trans-membrane links between focal adhesions and extracellular adhesion ligands were discovered and termed integrins[26-28]. Yet another major piece of the molecular puzzle fell into place with the identification of the Rho-family GTPases as master regulators of the actomyosin cytoskeleton and focal adhesions[29]. There are approximately 20 known Rho-GTPases but the three members considered most prominent are RhoA, Rac1 and Cdc42[30]. RhoA signaling stimulates

tension and contraction through increased actomyosin contractility. In contrast, it is thought that Rac1 and Cdc42 promote the formation of membrane extensions by triggering actin polymerization normal to the cell boundary and cause cell relaxation by down-modulating myosin contractility[31]. The abovementioned examples represent a handful of important actomyosin proteins but the human “actinome” is now known to include more than 500 gene products, of which the functions of many are still being characterized[32].

On a microstructural level actomyosin networks in cells generate forces through two main modes: pushing forces by polymerization and branching of actin networks, or pulling forces via the collective action of myosin motors drawing actin filaments together[2]. A classic example that incorporates both of these modes is the polarised motility of cells on planar surfaces. The leading edge is driven forward by broad, flat extensions called lamellipodia while the cell rear is pulled away from the substrate through myosin motor contractility[33-35]. Extension of the lamellipodium involves a process called treadmilling where polymerization pushes the plasma membrane forward at the front of the actin network and disassembly occurs at the trailing end. In synchrony with this, distinct cellular signaling pathways coordinate the formation and release of adhesion complexes at the front and rear respectively[36].

To explain how actomyosin networks bring about mechanical changes, the abovementioned modes of force generation must be understood in terms of cellular spatiotemporal distribution, anchorage, and organization. To illustrate this point, three examples show how the forces of actomyosin contraction can be channeled into different processes. The first example is cell division, where actomyosin localizes to form an equatorial contractile ring and is anchored to the plasma membrane to drive cleavage at the cell centre[37]. In the second example actomyosin is also tightly coupled to the plasma membrane but distributed in a homogenous and global manner to form an “actomyosin cortex”. This configuration serves to modulate whole-cell surface tension, which is an important parameter in tissue

morphogenesis[38, 39]. The third example is actomyosin contraction in bundled stress fibers, where the contractile force is directed linearly along actin cables between focal adhesions. This type of arrangement does not generate shape change in itself, but rather acts as a mechanosensor to gauge the mechanical properties of the surrounding environment. The feedback from such mechanosensitive components is translated into biochemical signals that can regulate cellular processes such as stem cell differentiation[40].

The architecture and self-assembly of actomyosin networks is governed by several classes of accessory proteins: nucleation-promoting factors, which initiate filament formation; capping proteins, which terminate filament growth; polymerases, which promote faster or more sustained filament growth; depolymerizing factors and severing factors, which disassemble filaments; crosslinkers and stabilizing proteins, which organize and reinforce higher-order network structures; and motor proteins, which generate movement and forces between filaments or a filament and another object[2]. The collective function of these accessory proteins gives rise to network properties such as turnover and fluctuation rate, and are key in determining the properties of actomyosin assemblies.

The Microtubule Cytoskeleton

In most animal cells microtubules are found in a star-like array emanating from the microtubule-organizing center, an organelle positioned adjacent to the nucleus that serves as a hub and nucleation point for microtubules. In this configuration the microtubule network governs certain aspects of intracellular organization by determining cell polarity, positioning of organelles, and the trafficking of molecular cargo by movement of motor proteins[41, 42]. This star-like configuration changes quickly when cells enter mitosis and microtubules reorganize into a bipolar mitotic spindle, a piece of cellular machinery essential for chromosome separation[43].

Microtubule assemblies can also form stable sub-cellular structures such as the core of cilia and flagella, which are specialized whip-like protrusions on the cell surface[44]. The mechanical functions of microtubules are well

established in the movement and persistence of cilia and flagella. In many cases, flagella act as rotors to propel cells through liquids and are essential for the motility of sperm cells and a number of prokaryotes.

The Intermediate Filament Cytoskeleton

IF proteins are defined by a conserved coiled coil alpha-helical domain responsible for assembly into characteristic 10 nm filaments[45]. Approximately 70 genes encode building blocks for 6 different types of IFs, most of which are expressed in a tissue specific manner[46]. For example, keratins, a group of IFs that constitute the main structural components of hair, skin and nails, are highly expressed in keratinocytes and epithelial cells. Improperly functioning keratins are involved in a number of severe skin diseases, which are thought to result from mechanical fragility of the tissue[47]. Another group of IFs called lamins are present in the nucleus where they are the main components of the nucleoskeleton, a structure that reinforces the nuclear envelope. Mutations in lamin genes cause softening of the nucleus and manifest a host of diseases referred to as laminopathies[48].

Mechanical experiments on IFs have demonstrated they are highly flexible, durable and extensible compared with microtubules and actin filaments, which rupture with minimal amounts of strain[49]. Indeed many IFs have been observed to stretch beyond 100% of their initial length, becoming thinner and exhibiting strain stiffening as a function of the extension[50]. In the face of such mechanical challenges IFs retain their elasticity and are able to recover their initial geometry. These properties probably arise due to the nanostructural features of IFs, where tetramer sub-filaments are able to slide past each other without longitudinal rupture[51]. Apart from their obvious role in forming the basis of select tissues, most research on IFs in cell mechanics indicates they simply serve as tissue-specific passive response elements to confer protection against large and sudden tensile stresses.

Mechanical and Non-Mechanical Functions of the Cytoskeleton

While it is clear that cytoskeletal components in cells have mechanical functions they may also play non-mechanical roles, particularly as platforms

for biochemical reactions and cargo transport. It used to be thought that membrane-bound compartments were required to concentrate the proteins responsible for a particular set of reactions in defined space. But the idea that the cytoskeleton can be employed for the same purpose and thereby facilitate biochemical sub-compartmentalization within the cytoplasm has recently gained prominence[52]. Untangling the contributions of mechanical and non-mechanical functions of the cytoskeleton is now a major challenge in cell mechanics. For example, it was once thought that microtubules served as rigid rod-like structures to counteract actomyosin contraction[53-55] but it was later discovered that disassembly of microtubules enhanced actomyosin contraction through biochemical means[56, 57]. Assembly of microtubules can also have a biochemical effect on actomyosin function by locally stimulating Rac1-based actin polymerization and lamellipodia formation[58]. These examples illustrate why it has often been difficult to relate the mechanical properties of *in vitro* reconstituted cytoskeletal systems to the cellular context. For example, while isolated stabilized microtubules are known to be the stiffest cytoskeletal polymer[59], their role in whole-cell mechanics has remained somewhat of a puzzle. Similarly to the case of microtubules, IFs are now known to exert a variety of non-mechanical signaling functions[46, 60]. Therefore, models of cell shape and mechanics must strive to take into account both the mechanical and non-mechanical functions of the cytoskeleton.

The Cell Cycle is Linked to Cell Shape

Cell growth and division follow a series of events known as the cell cycle. In cells with a nucleus (eukaryotes) the cell cycle can be classified into four different phases: gap 1 (G1), synthesis (S), gap 2 (G2), and mitosis (M) (Fig 2A). The first 3 phases are collectively termed interphase. G1 phase involves cell growth, S phase comprises the duplication of chromosomes, G2 phase represents further growth and preparation for division, and M phase culminates with the generation of two genetically identical daughter cells by partitioning the two sets of chromosomes to opposite poles of the cell as it divides through the midsection. Progression through the cell cycle is

controlled biochemically by a core set of regulators and stringent checkpoints that ensure the cell meets the requirements for passage into the next phase[61].

The maintenance of cell shape is central to many aspects of biology such as organism growth and form, but is especially important in cell division and mitosis. The role of the cytoskeleton is crucial in mitosis, which can be thought of as a series of dynamic structural transitions including nuclear envelope breakdown (NEBD), cell rounding, spindle assembly, and cytokinesis (Fig 2). At the beginning of mitosis cells abandon the protracted morphology characteristic of interphase and adopt a round shape[3, 4]. This rounding process is facilitated by the formation of a perimetric actomyosin cortex[62, 63]. At the same time, the microtubule cytoskeleton assembles to form the mitotic spindle, which functions as the central piece of machinery to organize and segregate chromosomes[43]. Mitosis then concludes with cytokinesis, which partitions the chromosomes, cytoplasm, organelles and plasma membrane into two daughter cells. This is accomplished through the action of an actomyosin contractile ring that forms around the cell equator and generates the forces required to divide the cell[37]. At the time of writing this thesis, the number of pubmed search hits for the terms “cytokinesis” (6750) and “mitotic spindle” (7744) demonstrates how intensely these fields have been studied. Subsequently, our understanding of these processes is now well developed. In comparison, “mitotic cell rounding” (14) has received little attention. In an attempt to gain insight into this intriguing problem, this thesis will focus on the topic of mitotic cell rounding.

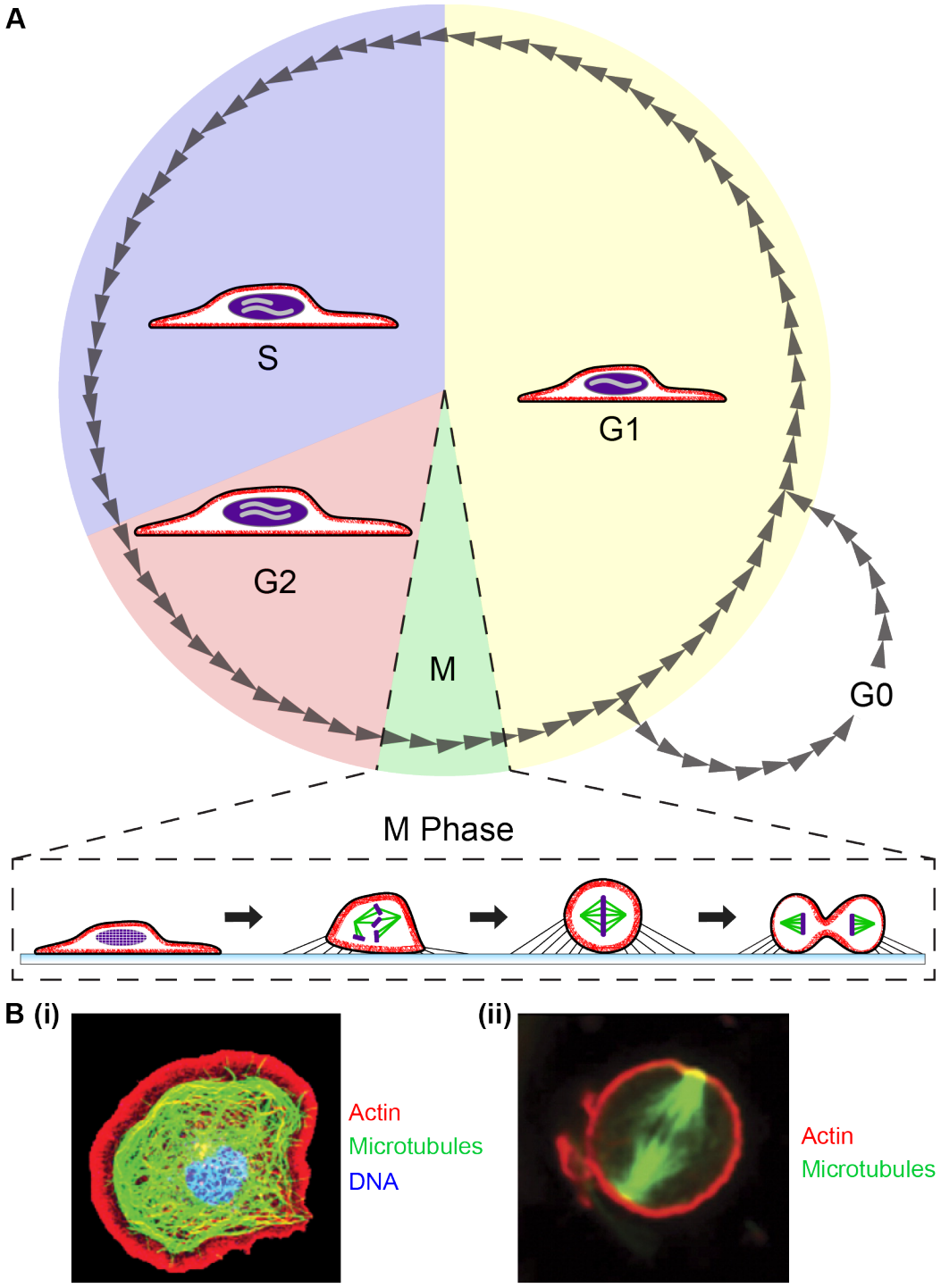

Figure 2: The cell cycle and associated changes in cell architecture. **A** Depicted are the phases of the cell cycle and typical cell shapes that accompany them. Cells remain adherent as they grow and replicate their DNA through interphase (G1, S, G2). In M phase (Mitosis) they undergo a marked transition from flat to round and then divide. Cell cycle segments are drawn in approximate proportion to duration. Cells outside the cell cycle are classified as being in G0, a quiescent resting phase. **B** Representative images of cell shape and arrangement of cytoskeletal components in **(i)** flat interphase and **(ii)** round mitotic cells. Images are of drosophila S2 cells from references[64, 65]. Note the diffuse organization of actin and microtubules in the adherent interphase cell and their subsequent rearrangement in the mitotic cell. The thick band of submembraneous actin in mitosis is characteristic of unspread cells and is known as the actomyosin cortex.

Mitotic Cell Rounding

Mitotic cell rounding (MCR) happens at the beginning of mitosis when cells abandon the protracted morphology characteristic of interphase and adopt a round shape. MCR has been observed to occur in the vast majority of animal cells both in culture[3, 66] and within living tissue[4, 67-70]. MCR has been proposed to facilitate organization within the mitotic cell and be necessary for the geometric requirements of division[67, 70-72]. Indeed, conditions that disturb MCR have been observed to be detrimental to spindle morphogenesis[64, 73] and orientation[70, 74], suggesting an interdependence between MCR and other aspects of mitosis. In a three-dimensional tissue environment a mitotic cell must exert forces on its surroundings in order to round up (Fig 3A). However, most studies of MCR to date primarily employed microscopy to monitor cultured cells on planar surfaces (Fig 3B). These studies observed a role for actin and associated proteins in cortical retraction and ridigity[62-64, 73, 75]. Importantly, Maddox and Burridge[63] and Kunda and colleagues[64] also made mechanical measurements of cell surface stiffness to further characterize the role of the actomyosin cytoskeleton in MCR. But to gain further insight there remains a need to measure the mechanics and driving forces of the rounding process with high temporal resolution throughout the process. To achieve such, this thesis presents the use of AFM and flat cantilevers to analyze rounding trans-mitosis: from mitotic entry until cytokinesis (Fig 3C). Importantly, the setup is versatile enough that the cantilever can be deployed in distinct modes to probe particular aspects of cell mechanics and shape. When deployed in constant height mode it acts as force sensor, facilitates measurement of cell size, and provides an impediment for the ex vivo simulation of rounding in tissue where mitotic cells push against their surroundings. When used in constant force mode, it can be used to probe cell shape as a function of applied force.

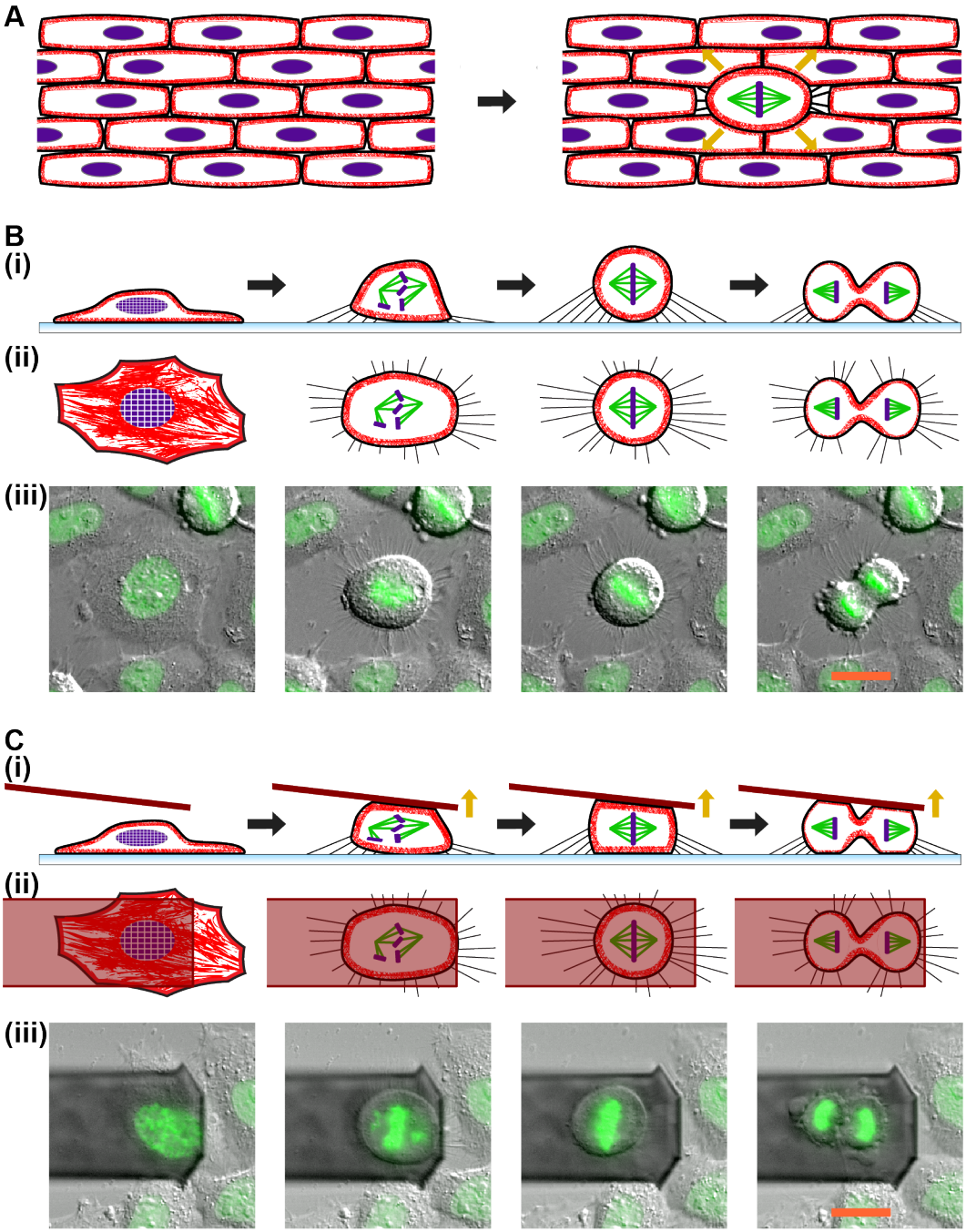

Figure 3: Mitotic cell rounding in various geometrical environments. **A** An illustration of mitotic cell rounding in animal tissue. Orange arrows represent outward directed force. In this and the following panels purple depicts DNA, green spindle microtubules, and red the actomyosin cortex. **B** Characteristic mitotic shape changes of animal cells cultured on flat substrates illustrated from (i) side and (ii) top view. (iii) Microscopy images of a transgenic HeLa cell expressing H2B-GFP throughout mitosis. Overlays consist of differential interference contrast (DIC) and fluorescence H2B-GFP images. Scale bar: 20μm. **C** Mitotic shape changes of animal cells cultured on flat substrates in the presence of a tipless AFM cantilever that can be deployed either as a force sensor or force actuator. The shape transitions are depicted schematically from (i) side and (ii) top view. Orange arrows represent upward directed force. (iii) Microscopy images of a transgenic HeLa cell expressing H2B-GFP undergoing mitosis in the presence of a two μm thick silicon tipless AFM cantilever. Overlays consist of DIC and fluorescence H2B-GFP images. Scale bar: 20μm.

AFM Constant Force Experiments

The Trans-Mitotic Constant Force Assay

To test the effect of constant forces on mitotic cell shape and progression, AFM was employed in conjunction with light microscopy. A flat tipless AFM cantilever was used to apply forces to single cells (Fig 3C). The first step in these experiments was to identify cells in early mitosis by the appearance of condensed chromosomes with fluorescence microscopy[76] in a transgenic H2B-GFP HeLa cell line[77]. The cantilever was then positioned above a candidate cell and the AFM used to engage a constant force feedback loop. Using this setup the height of a single cell could be tracked through mitosis as a function of force in what will henceforth be termed the trans-mitotic constant force assay (CFA). In the trans-mitotic CFA, mitotic cells were subjected to forces ranging from 1 nN to 100 nN (Fig 4). Flat prophase cells exhibited a stable, equilibrium height in response to applied forces. As cells underwent nuclear envelope breakdown (NEBD) and progressed into prometaphase, a notable increase in cell height was observed. Cells then attempted to round up against the cantilever and achieved a sustained height during metaphase. With progression into anaphase, a small transient increase in cell height was usually observed (Fig 4C, D, G) before the cells finally cleaved and resumed their spread morphology. These observations show that cell cycle events are tightly coupled to whole cell mechanics. This is particularly exemplified by the close correlation of MCR height increase with NEBD.

Next, the role of the actomyosin cortex in MCR against a constant force was examined. In early studies on MCR, Cramer and Mitchison used Cytochalasin D, an actin barbed end capper[78], to directly demonstrate a role for actin in the process[62]. Building on this result, Maddox and Burridge then showed that the mitotic actomyosin cortex is regulated by RhoA and its downstream effector Rho kinase (ROCK) by using Y-27632[63], an inhibitor of ROCK[79]. Here, the effect of these same inhibitors was characterized with the 50 nN trans-mitotic CFA (Fig 4 D-F). These treatments were found to

attenuate the normal increase of cell height at NEBD and retard rounding throughout mitosis.

A plot of cell height trajectories from prophase to mitotic maximum (Fig 5A) shows the effect of force on cell shape in mitosis in multiple experiments. As expected, the applied force was directly proportional to the height of the cell in both prophase and metaphase. However, for the drugs Y-27632 and Cytochalasin D at an applied force of 50 nN, the weakening effect was not observable in prophase. This was probably because inhibitor treated prophase cells appeared less spread to begin with. Additionally, the nucleus may have provided reinforcement. This suggests that actin cytoskeleton has a more prominent role in resistance to compression for metaphase cells compared with those in prophase.

Apart from the decrease in cell height, another effect was typically observed when using actomyosin perturbants. Cells treated with 50 nN constant force and cytochalasin D could not align their chromosomes and progress through mitosis (Fig 4F). This may have been because cytochalasin D treated cells could not increase their height upon mitotic entry, and therefore not generate sufficient space for the mitotic spindle to organize the chromosomes. Indeed, a plot of cell height:width ratio versus time taken from NEBD to anaphase (Fig 5B) shows a positive correlation between degree of compression and mitotic duration. Interestingly, uncompressed cells cultured with Cytochalasin D or Y-27632 alone were not slower through mitosis (data not shown). Therefore, these experiments suggest that biochemical disruption of the actomyosin cortex potentiates the effect of compressive forces to suppress mitotic cell shape and chromosome organization.

Inspired by the above result, it was postulated that there might be a threshold force capable of preventing mitosis. Therefore, cells were subjected to higher forces. But, cells compressed with 100 nN or greater in the trans-mitotic CFA were observed to slide along the 10° cantilever gradient, escape the compression, and then undergo mitosis. Interestingly, an analogous process called interkinetic nuclear migration (IKNM) has been

observed to occur in living tissue. IKNM is widely conserved among pseudostratified vertebrate neuroepithelia, where mitotic cells translocate to the apical side of the neural tube to undergo mitosis[80]. Tissue packing appears sparser in the apical side of the epithelial layer[69, 81], suggesting that MCR and de-adhesion facilitates movement of the cell into an area of reduced density, similar to what occurs ex vivo with slanted cantilevers. IKNM was also observed to be actomyosin dependent, because both Cytochalasin D and Y-27632 retarded mitotic translocation while the presence of constitutively active myosin II rescued it[69, 81]. In combination with the abovementioned knowledge on IKNM, the constant force results suggest that AFM-based force assays are capable of revealing insights into the role of MCR in tissue.

While attempting constant force experiments, a noteworthy observation was made. At forces of 150 nN, some cells slipped out in front of the cantilever. This caused the cantilever to scrape down one side of the cell and pin a portion of the plasma membrane against the substrate at a force of 150 nN (Fig 6A). The cytokinetic furrow was not able to gather and cleave this part of the membrane during division resulting in two daughter cells connected by a membrane bridge. These cells eventually merged to produce a multinuclear cell (Fig 6A, n=5). It is not clear to what extent the pinched membrane was accessible to actomyosin, or whether it existed as a flat sheet or a “donut” with a hole. High-resolution fluorescence microscopy may be able to answer these questions in future. In similar experiments from 1961, Rappaport used a glass rod to produce a donut shaped egg cell and thereby circumvent the first cell division by generating a membrane bridge[82] (Fig 6B). In conjunction with the early results of Rappaport, the AFM-based results suggest that one function of MCR and the actomyosin cortex in mitosis might be to gather in and control the plasma membrane in preparation for cytokinesis.

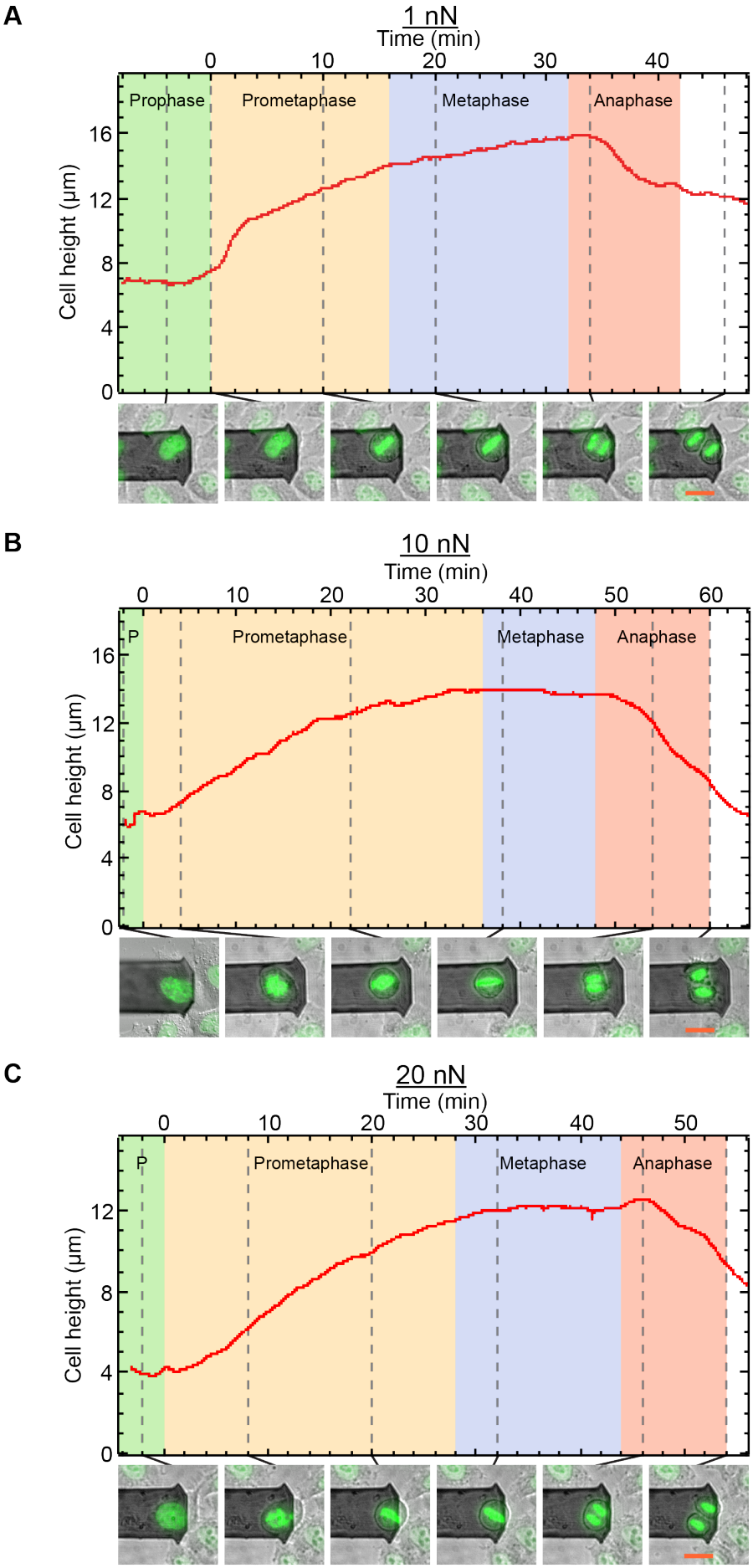
A
1 nN
Time (min)
0
10
20
30
40
Prophase
Prometaphase
Metaphase
Anaphase
Cell height (μm)
16
12
8
4
0
B
10 nN
Time (min)
0
10
20
30
40
50
60
P
Prometaphase
Metaphase
Anaphase
Cell height (μm)
16
12
8
4
0
C
20 nN
Time (min)
0
10
20
30
40
50
P
Prometaphase
Metaphase
Anaphase
Cell height (μm)
12
8
4
0

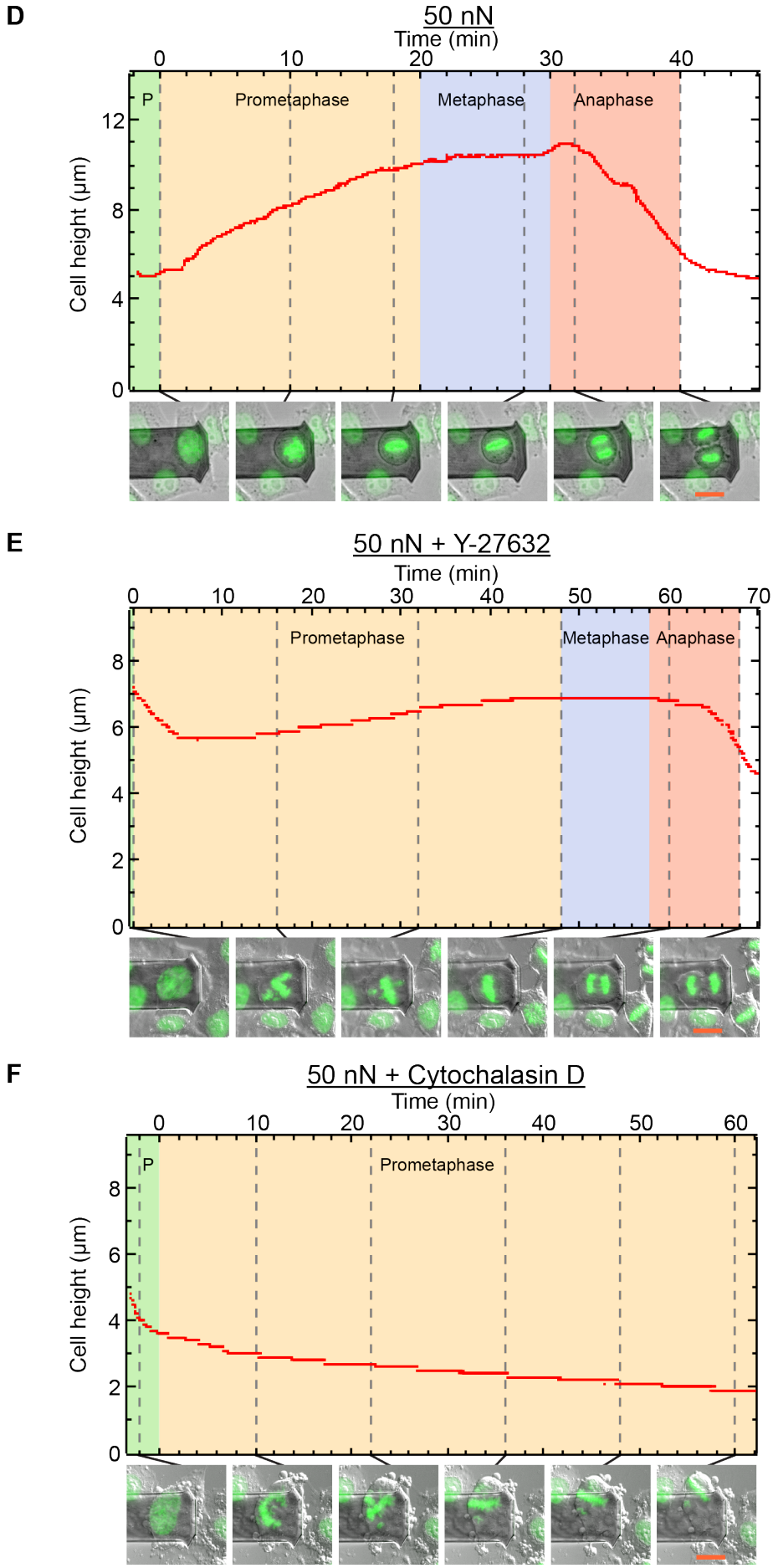
D
50 nN
Time (min)
0
10
20
30
40
P
Prometaphase
Metaphase
Anaphase
Cell height (μm)
0
4
8
12
E
50 nN + Y-27632
Time (min)
0
10
20
30
40
50
60
70
Prometaphase
Metaphase
Anaphase
Cell height (μm)
0
2
4
6
8
F
50 nN + Cytochalasin D
Time (min)
0
10
20
30
40
50
60
P
Prometaphase
Cell height (μm)
0
2
4
6
8

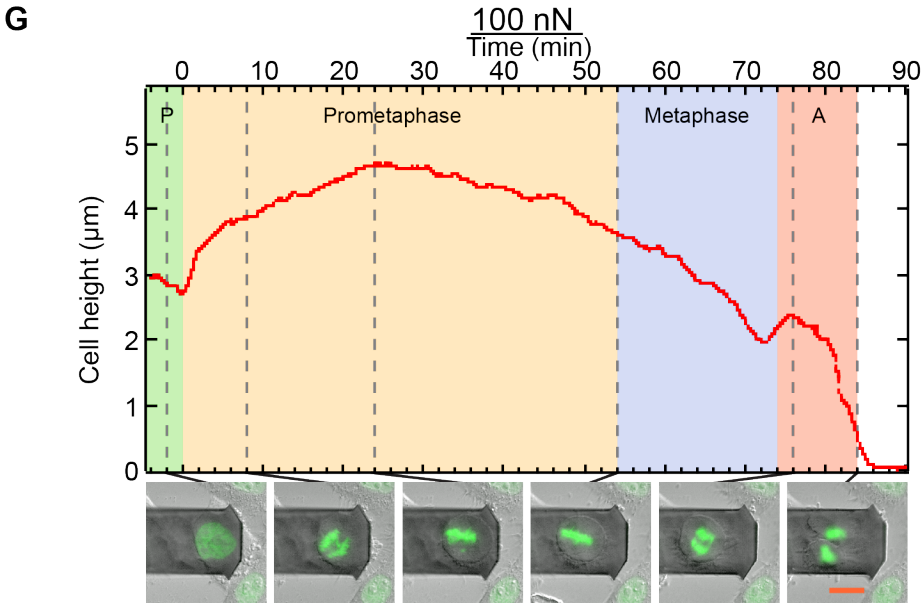

Figure 4: The trans-mitotic constant force assay (CFA) applied to single cells with following conditions: **A** 1 nN **B** 10 nN **C** 20 nN **D** 50 nN **E** 50 nN +10 µM Y-27632 **F** 50nN +500 nM Cytochalasin D **G** 100 nN. Forces were applied with flat tipless cantilevers fabricated from silicon (CSC/NSC series, Mikromasch). The height of the cantilever is continuously recorded by the AFM and used to determine cell height. Vertical gray dashed lines correspond with microscopy images shown at regulator intervals and consist of overlays of transmission microsopy (DIC or phase) and fluorescence H2B-GFP signals. Mitotic phases were assigned by the appearance of chromosomes (Fig 32). Images A-C use phase contrast while D-G employ DIC. Time zero is aligned to prometaphase onset as defined by nuclear envelope breakdown (NEBD). Scale bar: 20 µm.

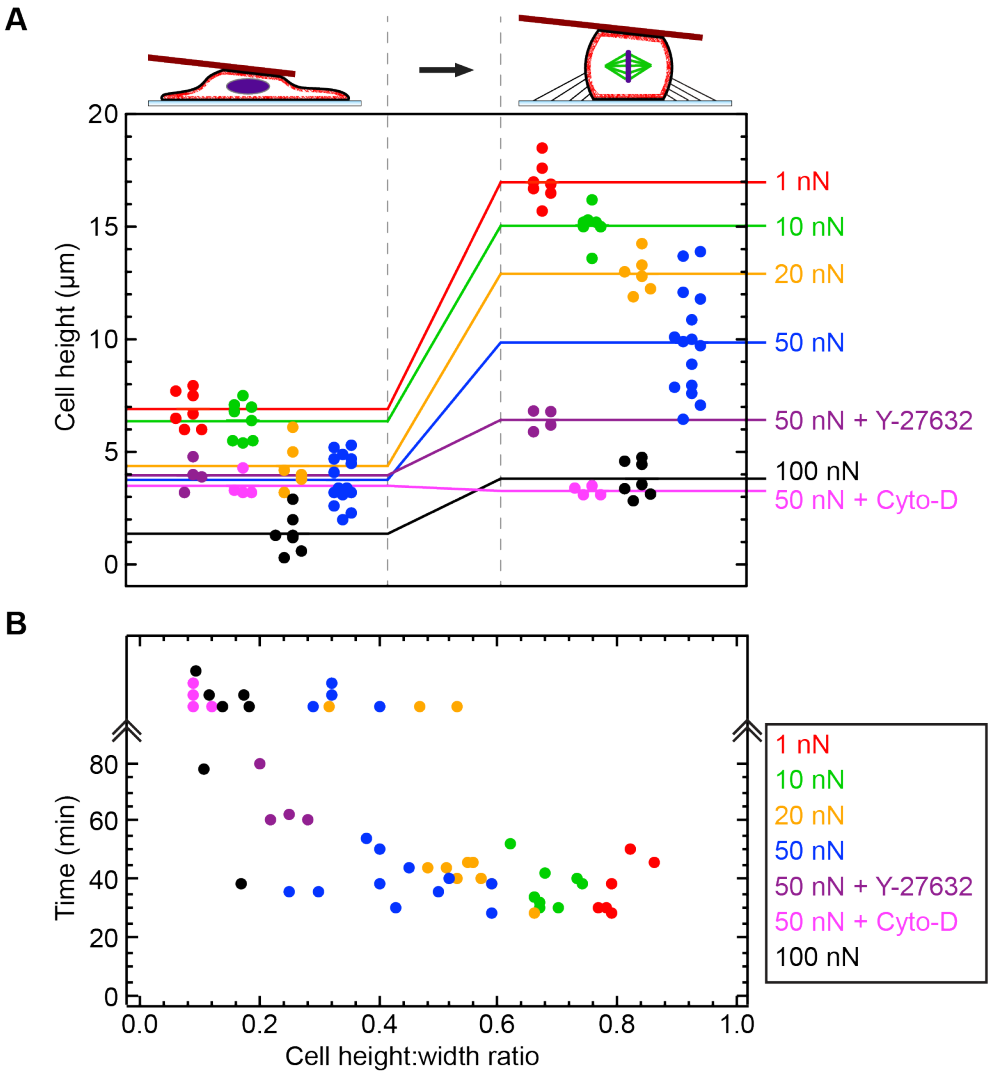

Figure 5: Constant forces affect cell shape and time taken through mitosis. **A** Cell height trajectories from prophase (left) to mitotic maximum (right) as a function of constant applied force and inhibitor treatment. The upper schematic represents cells in prophase (left) and metaphase (right). Concentrations of inhibitors were Y-27632 at 10 µM and Cytochalasin D 0.5 µM. Each dot represents an individual cell while horizontal lines depict averages. **B** Height:width ratios of cells at maximum mitotic height versus time taken from NEBD to anaphase. Height is measured with AFM and width with light microscopy. Cells that failed to enter anaphase within 80 mins are plotted above the double arrows.

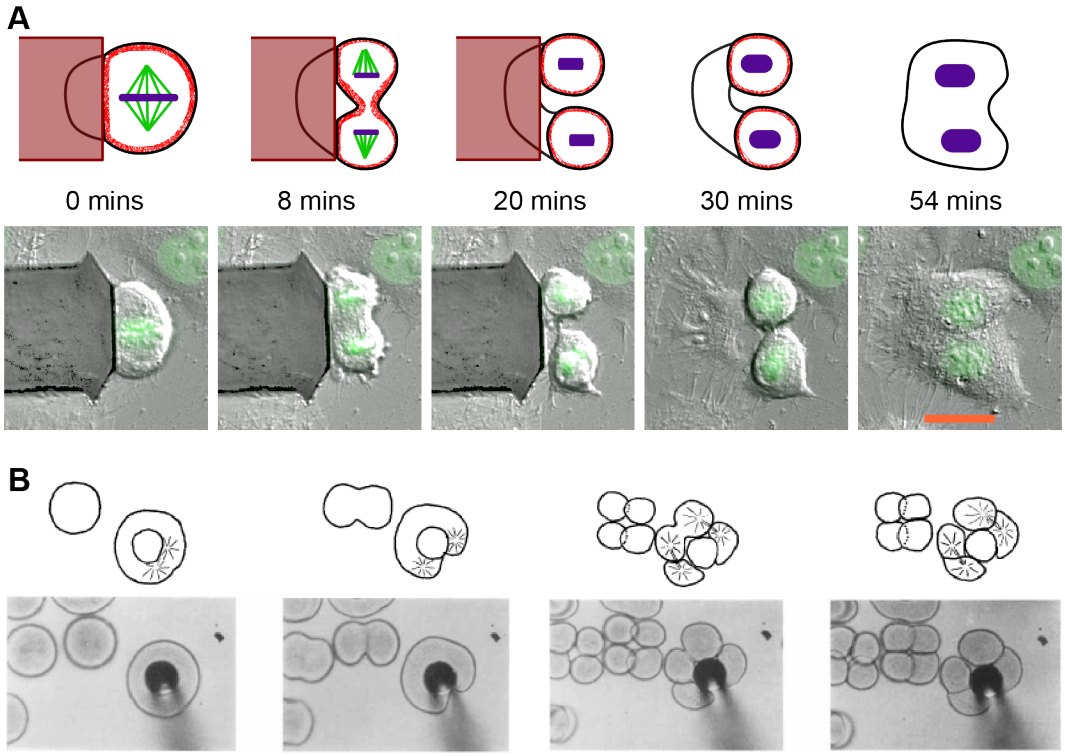

Figure 6: A The Rappaport experiment reproduced with cantilever micromanipulation on cultured cells shown schematically (top row) and with overlaid DIC/H2B-GFP images of HeLa cells (bottom row). A flat cantilever was used to pinch a portion of the cell membrane against the substrate during division resulting in a multinuclear cell. Colours correspond to cortical actomyosin (red), spindle microtubules (green), and DNA (purple). The experiment was repeated 5 times. Scale bar: 20 µm. **B** The original Rappaport experiment performed by pushing a glass rod through a sand dollar egg[82]. The sand dollar cells were subsequently competent to recover from the first failed division and generate mononuclear cells at the four-cell stage.

Observations on Shape and Adhesion of Round Cells

To examine the relationship between adhesion and shape on unperturbed round mitotic cells, AFM was used in a conventional manner to measure cell height, and transmitted light microscopy to measure cell width. Since the position of the cantilever can be measured with nanometer accuracy, this provides a precise measure of the cell dimensions. Metaphase HeLa cells had a height:width ratio of 0.86±0.04 (mean±SD, Fig 7B). Mitotic cells without retraction fibers were almost spherical, as were interphase cells detached with trypsin (Fig 7B,C). Therefore, it can be concluded that a detached, isolated cell will be nearly spherical independent of its cell cycle phase.

The trans-mitotic CFA data (Figs 4 and 5) and the results of others[62-64, 73, 75] implicate actin-based processes in MCR. Therefore, it was tested whether the actomyosin cytoskeleton has a role in maintaining a spherical shape by adding cytochalasin D to cells that were already round (Fig 7A,E). After treatment, both detached mitotic and interphase cells remained round. However, if retraction fibers were present, rounded cells sagged down to height:width ratios < 0.5 upon cytochalasin D treatment. This shows that the actomyosin cytoskeleton is necessary for upward forces to oppose the downward pull of adhesion in MCR.

To test for differences in cell-cell adhesion from interphase to mitosis, an AFM-based single cell force spectroscopy (SCFS) assay was implemented[83, 84]. Briefly, an interphase probe cell was bound to the AFM cantilever, brought into contact with the apical surface of an interphase or mitotic cell on the substrate, and then retracted to measure adhesion forces (Fig 8A). The deflection of the AFM cantilever was correlated with retraction distance to produce a force-distance curve from which detachment forces can be quantified (Fig 8B). The results showed that, at a contact time of 10 seconds, cell-cell detachment forces were not significantly different between interphase and mitosis (Fig 8A). This data corroborates well with observations that cell-cell adhesion is maintained in mitosis[85, 86].

Finally, these adhesion measurements (Fig 8) taken together with the cell shape observations (Fig 7) and CFA data (Figs 4 and 5) suggest that the presence of a functional actomyosin cytoskeleton is necessary to overcome the residual forces of adhesion in MCR.

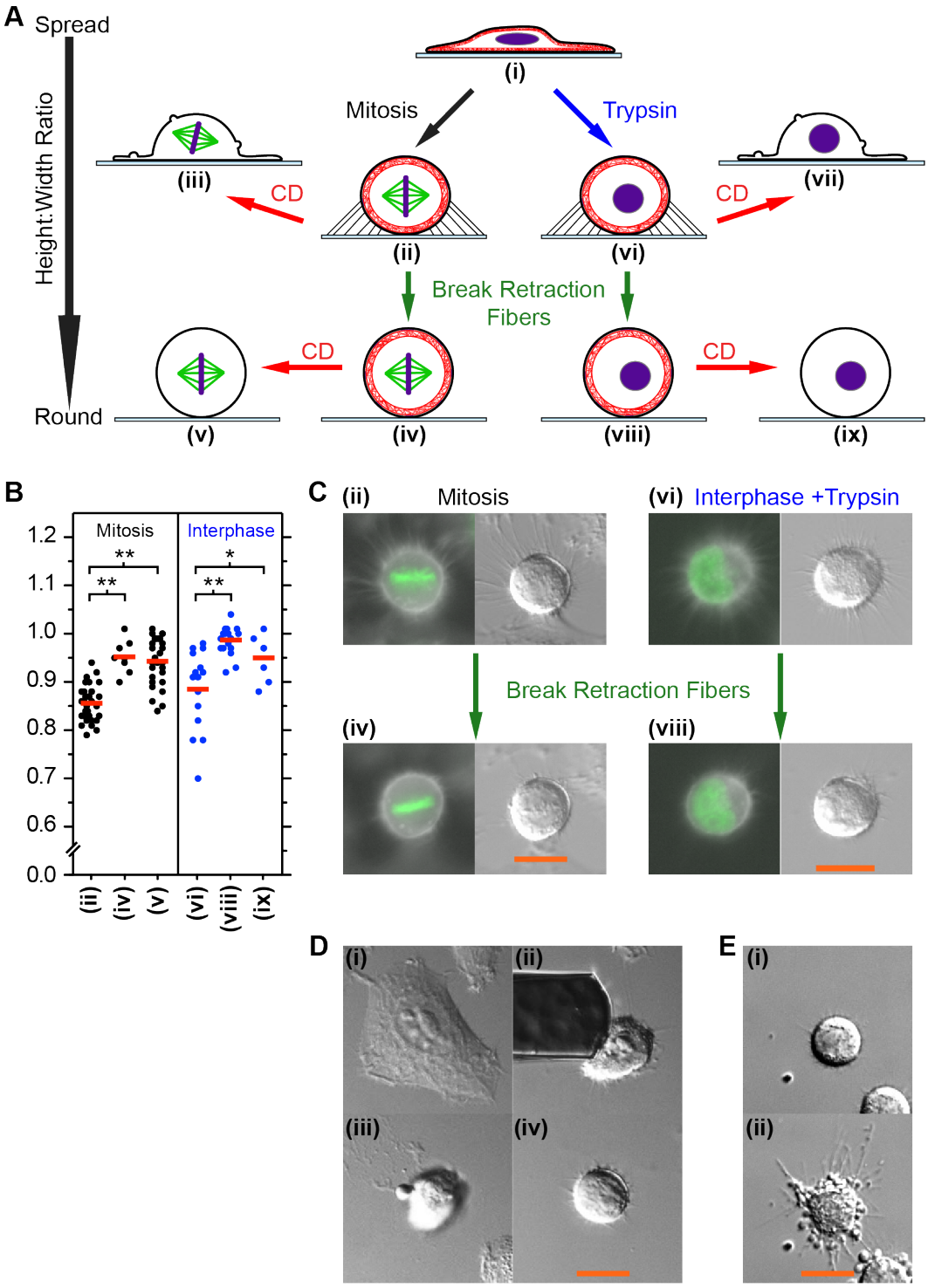

Figure 7: A Adhesion and retraction fibers restrain cells from achieving a spherical shape. Displayed is a schematic of the shape (the lower the more spherical) of mitotic and interphase cells subject to different combinations of perturbations to adhesion and actomyosin. Depicted are interphase cells **(i)**, mitotic cells **(ii)**, mitotic cells treated with 1 μM cytochalasin D (CD) **(iii)**, mitotic cells without retraction fibers **(iv)**, mitotic cells without retraction fibers treated with 1 μM cytochalasin D **(v)**, interphase cells rounded with trypsin **(vi)**, interphase cells rounded with trypsin treated with 1 μM cytochalasin D **(vii)**, interphase cells rounded with trypsin without retraction fibers **(vii)**, and interphase cells rounded with trypsin without retraction fibers treated with 1 μM cytochalasin D **(ix)**. The arrows represent entry into mitosis (black), trypsinization (blue), breaking of

retraction fibers with cantilever nudging method (green, see **D**), and treatment with cytochalasin D (red). Both mitotic and interphase cells are close to spherical in the absence of substrate connections even when treated with cytochalasin D. Chromatin is depicted in purple, actin in red, and spindle microtubules in green. **B** Plot of height:width ratios of cells from treatments designated in part A. Height and width of each cell were measured by AFM and light microscopy, respectively. The height:width ratios of partially adherent cells treated with cytochalasin D, **(iii)** and **(vii),** are not shown as they were approximated with light microscopy to be under 0.5 (see **E**). Dots represent measurements of individual cells and red bars the mean. p values (Mann-Whitney, two tailed) are designated * $p < 0.05$, ** $p < 0.001$. Absolute heights of spherical cells were typically around 20 μm. **C** Sets of twin fluorescent images (left) and DIC images (right) showing representative cells in schematic **A**. Fluorescent images constitute an overlay of membrane marker mCherry-CAAX (monochrome) and H2B-GFP (green) images. Green arrows denote the breaking of retraction fibers with the cantilever nudging method. **D** DIC images of the cantilever nudging method that was used to partially detach cells from supports. The cantilever is manually moved to “nudge” cells **(ii)** until only a small adhesive patch remains **(iii)**. After being allowed to recover for 1 minute, “nudged” cells were close to spherical **(iv)**. As well as rounding up interphase cells, the cantilever nudging method was used to break the retraction fibers of rounded cells. **E** DIC images of a typical round cell with retraction fibers **(i)** before and **(ii)** 70 minutes after cytochalasin D treatment, which causes the cell to sag down along its previous adhesion trajectories. Similar observations were made for both trypsinized interphase and mitotic rounded cells with retraction fibers. Scale bars, 20 μm.

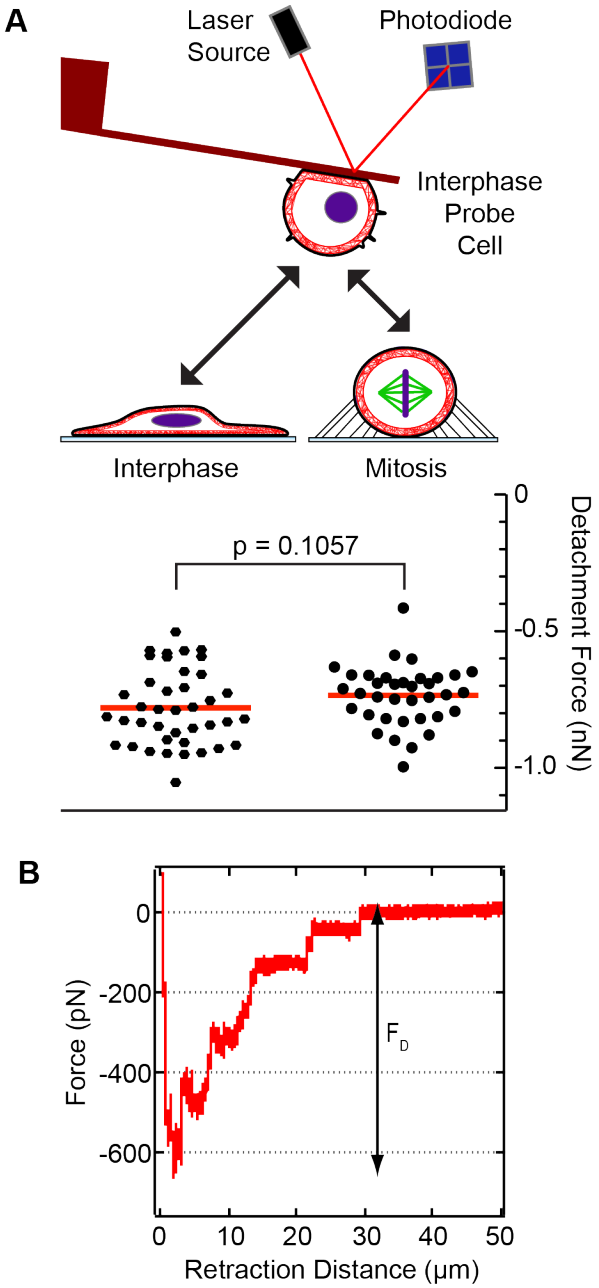

Figure 8: Short-term cell adhesion measurements of interphase-interphase and interphase-mitosis cell interactions performed with AFM single cell force spectroscopy (SCFS). **A** Schematic of the setup whereby an interphase probe cell bound to the cantilever via concanavalin A functionalization is brought into contact with the apical surface of interphase or mitotic cells on the substrate. After 10 seconds contact time the cells are pulled apart and detachment forces recorded. The interphase-interphase maximum detachment forces (left) are not significantly different to those of the interphase-mitosis combination (right). p value (Mann-Whitney, two-tailed) > 0.05 indicates insiginificance. **B** Typical force-distance profile upon retraction after 10 seconds contact. Maximum detachment force is labeled F_D. See Helenius et al. for further details regarding the SCFS technique[84].

AFM Constant Height Experiments

The Trans-Mitotic Constant Height Assay

To characterize the forces and mechanics of MCR, the constant height assay (CHA) was designed and implemented. In the CHA, a flat tipless cantilever was positioned over a prophase HeLa cell at a set height above the substrate and held there while the cell transitioned through mitosis (Fig 9A). In the case that the cantilever was held at 8 μm to confine a mitotic cell to ~50% of its spherical height (Fig 7B), a prometaphase cell commencing rounding came in contact with the cantilever and the upward force that it exerted could be measured with sub-nanonewton accuracy. Within ~10 minutes after NEBD cell shape reached an equilibrium at a barrel-like shape (Fig 9B, C) and remained in that shape until commencement of division. A three-dimensional rendering of cell shape by visualization of the plasma membrane with an mCherry-CAAX fluorescent marker showed that cell shape can be crudely approximated as a barrel with uniform radius (Fig 9C, D). Based on this geometry it is possible to calculate several useful parameters (Fig 9E), such as rounding pressure, $P_{rounding}$ (force divided by contact area), and cell volume, V.

In order to evaluate $P_{rounding}$ values from different experiments it is necessary to take into account relative deformation. However, inherent differences in cell size and position along the cantilver, x (Fig 9C), mean that degree of deformation in a CHA often varies over the time course of an experiment on a single cell or between experiments on different cells. To determine deformation, the height of the cell in an undeformed state, z_0, must be known. Although this cannot be directly measured during the CHA assay, it is possible to approximate it based on two assumptions: (1) that cell volume does not change markedly with deformation, and (2) that cell adhesion is minimal (Fig 9E). From this one can define the degree of deformation, or uniaxial strain, ε, as the ratio of uniaxial deformation ($z_0 - z_{cell}$) to undeformed cell height (z_0). Dividing equilibrium rounding pressure, $P_{rounding}$, by the uniaxial strain, ε, yields a whole cell "rounding modulus", $E_{rounding}$, of round cells analogous to the Young's modulus of solid materials, which is also determined by the ratio of

stress (force/area) to uniaxial strain[87]. The rounding modulus parameter is useful because it allows the prediction of the whole cell mechanical behavior under a given force or deformation. For example, a rounding modulus of 0.5 kPa says that a cell subject to 50% uniaxial deformation will exhibit a $P_{rounding}$ value of 0.25 kPa (Fig 9E). This is in contrast to indentation-based determination of mitotic cell surface stiffness, which gives only indirect indications of cellular forces[64, 88, 89]. While $P_{rounding}$ is the ideal parameter of interest, $E_{rounding}$ has the advantage of normalizing the discrepancy in deformation between experiments and will henceforth be used for the remainder of this thesis.

To analyze the mechanics of mitotic cells when constrained to different shapes, the trans-mitotic CHA (Fig 9) was implemented at heights ranging from 4 μm to 12 μm (Fig 10). At all heights, NEBD triggered a steep rise in force that stabilized into a plateau in prometaphase/metaphase. At anaphase, cells exhibited a transient force peak before they spread and lost contact with the cantilever upon completion of cytokinesis. Notably, the CFA data followed a similar pattern, albeit with height instead of force (Fig 4). Indeed, the CHA force data exhibited a consistent and reproducible force profile useful for analyzing the mechanical events of mitosis at high temporal resolution. Thus, AFM based assays can be used to capture and quantify the considerable forces that single cells generate against external impediments in mitosis.

In CHAs ranging from 4 to 6 μm the rounding forces were frequently recorded at greater than 100 nN, and, as a consequence, cells often slid along the 10° cantilever gradient (Fig 10B). This caused an unintended reduction in relative cell deformation throughout the experiment. In such cases, "rounding modulus" corrected for this aberration and showed that cellular mechanical properties (in contrast to raw measured forces) were stable from the end of prometaphase until anaphase onset (Fig 10B). This example demonstrates the usefulness of rounding modulus as a proxy to report on cellular mechanical properties in situations where deformation could not be held constant.

Above, trans-mitotic CHAs were implemented via progression of prophase cells into mitosis under a stationary cantilever (Fig 10). To test for

mechanosensitivity in mitotic cells, this method was compared to initiation of a CHA via the compression of an already round mitotic cell. In this variation, the cantilever was lowered onto a metaphase cell at a speed of 0.1 μm per second and held at a constant height (Fig 11A). In materials science, this type of experiment is known as a stress-relaxation assay and can provide information on the viscoelastic (time-dependent) mechanical properties of a sample[90]. Consistent with this notion, round quasi-metaphase cells showed an initially high resistance force that decayed to equilibrium (Fig 11A). The equilibrium forces, rounding pressures and rounding moduli for quasi-metaphase cells were then compared as a function of uniaxial strain between trans-mitotic and compression-initiated CHAs (Fig 11B). The data shows that both approaches yielded similar results, albeit with slightly more rigid cells for the compression-initiated experiments (for a given uniaxial strain (ε), rounding force was ∼10 nN greater). This slight difference could possibly be due to mechanosensitivity, which may cause down-modulation of rounding forces in response to the presence of long-term impediments such as a stiff cantilever. Alternatively, the difference may arise because compressed cells tended to exhibit fewer retraction fibers. This was probably due to the initial mechanical perturbation inherent in the compression-initiated CHA. This was because the 15 μm piezo range of the JPK Nanowizard I meant the cantilever was limited to being ≤ 14 μm from the substrate after an approach and quasi-metaphase HeLa cells are ∼18 μm high. Therefore the cell had to be nudged to get the cantilever over the cell and such nudging can break retraction fibers (Fig 7). Fink and colleagues recently showed that the combined forces of retraction fibers are ∼10 nN for HeLa cells in mitosis[91]. Therefore, the presence of fewer retraction fibers might explain why rounding force was ∼10 nN greater for a given uniaxial strain when measured with the compression method (Fig 11B). However, these differences are not extreme, and because similar mechanical trends were observed whether ‘constraining the cell’ or making a simple mechanical measurement on an already round one (Fig 11B), it can be concluded that both CHA approaches are applicable to studying the mechanics of round mitotic cells over a broad range of deformations and timescales.

Next, it was also examined whether the degree of cell compression affected cell volume (Fig 12A). For the trans-mitotic CHA (starting prophase) there appeared no correlation. However, for CHAs via compression, volume decreased slightly with increasing compression. This may have been because higher compressions tended to induce blebs, which could not be included in volume calculations because of difficulties assessing their complex morphology. On the short timescales of the compression (~1 minute) an increase in actomyosin cortex surface area during the shape transition from sphere to barrel might be sufficient to induce an increase in cortical tension, which could, in turn, trigger blebbing[92]. Hence, in the absence of dynamic deformations, cell volume did not appear to be strongly related to degree of cell deformation in mitosis. For this dataset, volume was additionally compared against equilibrium rounding pressure and rounding modulus (Fig 12B, C). The lack of a strong correlation between these parameters indicated that equilibrium cellular mechanical properties were independent of cell size or vice versa.

Selection of the 8 µm Constant Height Assay

In CHAs, the degree of deformation is an important parameter. Larger deformations can be advantageous because they reduce the uncertainty in the determining dimensions of the cell. For example, as the cell is increasingly compressed, $A_{contact}$ (which cannot feasibly be measured using DIC microscopy), approaches the easily determined A_{mid} and volume estimation becomes tractable (Fig 9). Larger deformations also increase the range of forces measured and improve the sensitivity of the assay in establishing differences between cellular states and perturbations. On the other hand, large compressive deformations tend to promote cell sliding along the cantilever gradient (Fig 10B); sometimes even causing escape from the assay, or potentially inhibit mitotic progression (Fig 5B). Mitotic cells in the 8 µm trans-mitotic CHA (Fig 10A) were generally constrained to ~50% of their undeformed height (Fig 11B). In this scenario sliding was not a major problem and cells transitioned from prophase to anaphase in an average 39.5 ±9.6 minutes (n=74), which was well within the normal 30-45 minute

window seen in unperturbed cells (Fig 5B). Because the 8 μm CHA offers a good compromise between the abovementioned considerations, it features in the remainder of this thesis.

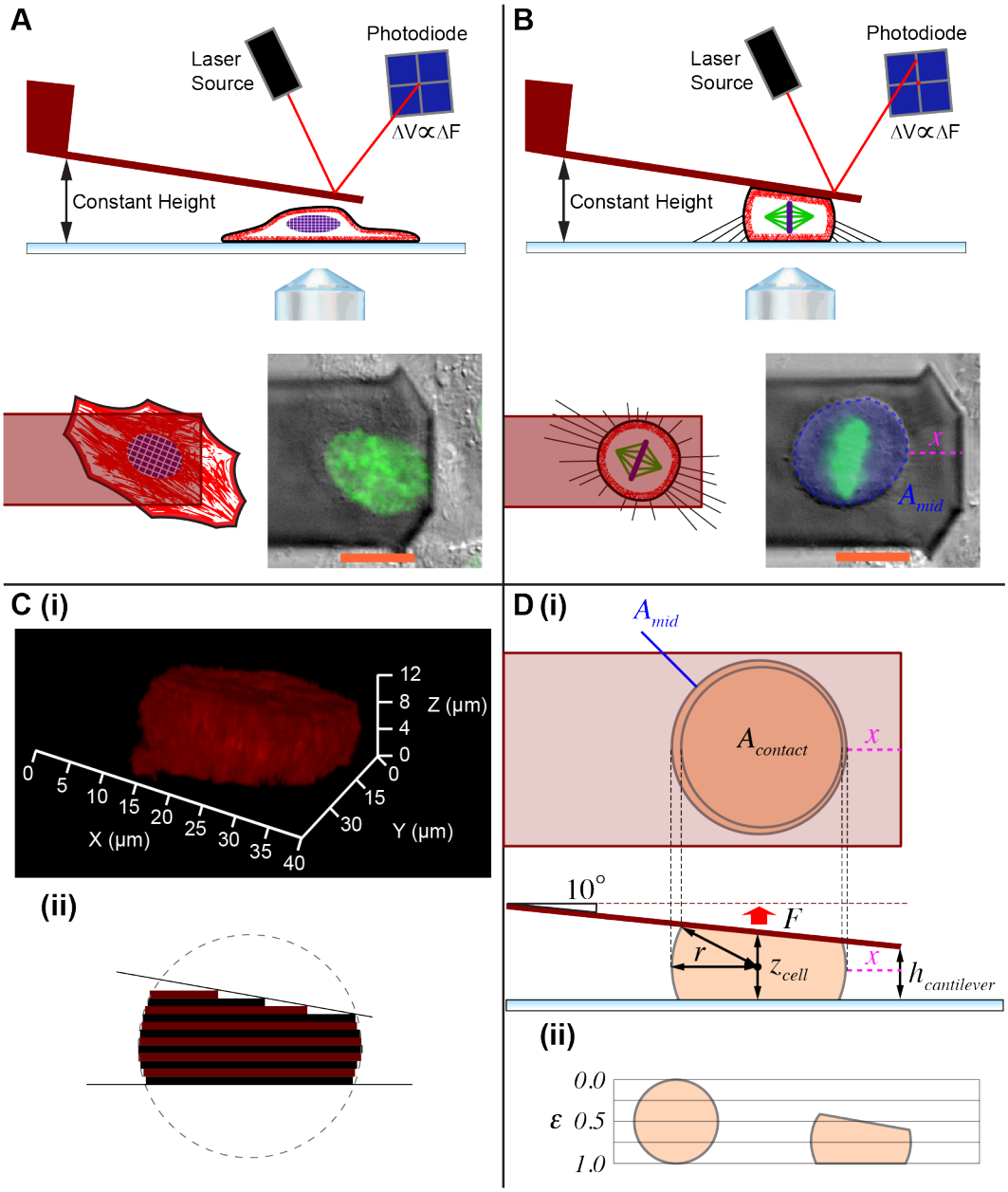

E

$$z_{cell} = \tan 10^{\circ}\left(x + \sqrt{\frac{A_{mid}}{\pi}}\right) + \frac{F}{k} + h_{cantilever}$$

$$z_0 = 2\sqrt[3]{\frac{3V}{4\pi}}$$

$$A_{contact} = A_{mid} - \frac{\pi z_{cell}^2}{4}$$

$$\varepsilon = 1 - \frac{z_{cell}}{z_0}$$

$$P_{Rounding} = \frac{F}{A_{contact}}$$

$$E_{Rounding} = \frac{P_{Rounding}}{\varepsilon}$$

$$V = \pi z_{cell}\left(\frac{A_{mid}}{\pi} - \frac{z_{cell}^2}{12}\right)$$

Figure 9: AFM constant height assay (CHA) with flat cantilevers. **A** Establishment of a CHA on a prophase HeLa cell. Note the appearance of condensed granular looking chromosomes characteristic of prophase in the DIC/H2B-GFP overlay image. V, Voltage signal at the AFM Photodiode, F, force. Scale bar: 20μm.

B Depiction and microscopy image of a barrel shaped metaphase cell in a CHA. Images were analyzed to extract the cross-sectional area, A_{mid} (blue) and the distance from the end of the cantilever, x (pink). Scale bar: 20 μm. **C** Cell shape under the cantilever in a CHA. **(i)** Three-dimensional rendering of a prometaphase/metaphase cell under the cantilever in an 8 μm CHA. Image is based on optical sections acquired with a zeiss apotome on a HeLa cell expressing a mCherry-CAAX membrane marker. **(ii)** The same image reconstituted to scale in a two-dimensional side projection. Each band represents a 1 μm slice. The fitted circle shows that the side profile of the compressed cell can be approximated as having a uniform radius from the cell centre. **D** Cellular geometry in the CHA. **(i)** $h_{cantilever}$, the height that the end of the cantilever is maintained above the substrate, F, force, A_{mid}, cross-sectional area of the cell, $A_{contact}$, contact area between the cantilever and the cell, r, cell radius, x, distance of the cell edge to the end of the cantilever, z_{cell}, height at the cell center. **(ii)** Schematic of the difference in cell shape between an undeformed round cell and one compressed 50% (ε = 0.5) by a 10 degree flat cantilever. **E** Equations to calculate volume and mechanical parameters of the cell. $P_{rounding}$, rounding pressure, V, volume, z_0, height of the undeformed cell, ε, z-axis uniaxial strain, $E_{rounding}$, rounding modulus. In CHA experiments, relatively stiff cantilevers (k≈0.3 N/m) were employed to ensure that the cell's upward force did not markedly alter the set height (for example, a k=0.3 N/m cantilever subject to 100 nN originally set at 8 μm would be displaced to 8.3 μm). Errors in $P_{Rounding}$, V, and $E_{Rounding}$ were estimated at ±2% by propagating uncertainty in the measurement of A_{mid} through the given equations.

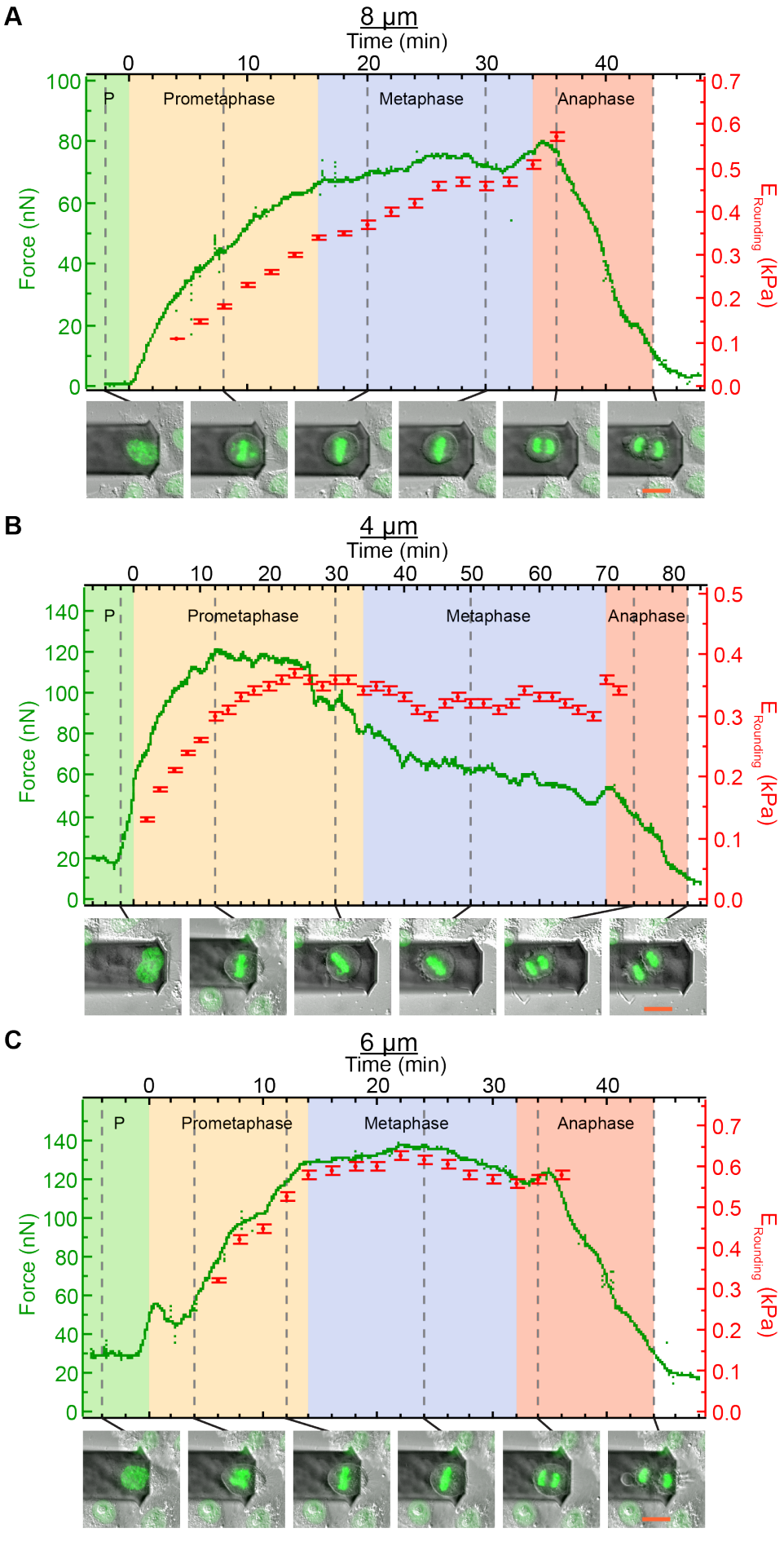
A
8 µm
Time (min)
0
10
20
30
40
P
Prometaphase
Metaphase
Anaphase
Force (nN)
E Rounding (kPa)
B
4 µm
Time (min)
0
10
20
30
40
50
60
70
80
P
Prometaphase
Metaphase
Anaphase
Force (nN)
E Rounding (kPa)
C
6 µm
Time (min)
0
10
20
30
40
P
Prometaphase
Metaphase
Anaphase
Force (nN)
E Rounding (kPa)

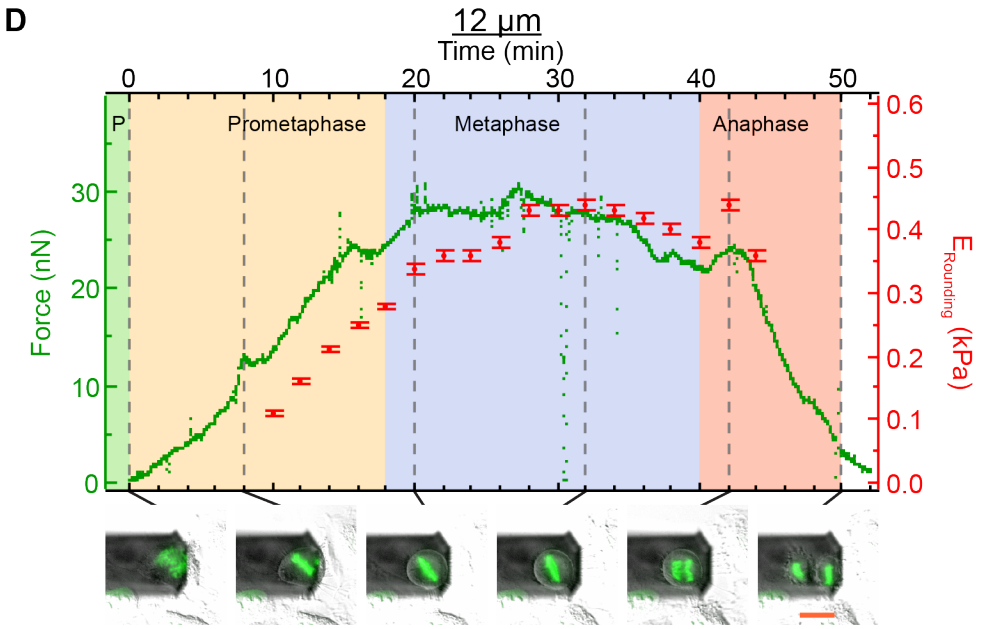

Figure 10: Probing the mechanics of mitotic cell rounding with the trans-mitotic constant height assay (CHA) at **A** 8 µm, **B** 4 µm, **C** 6 µm, and **D** 12 µm. $E_{rounding}$ error bars are ± 2% (see Fig 9). Forces were recorded at 1 Hz with flat tipless cantilevers fabricated from silicon (NSC series, Mikromasch). Microscopy images shown at regular intervals (grey dashed lines) consist of overlays of transmission microsopy (DIC or phase) and fluorescence H2B-GFP signals. Mitotic phases were assigned by the appearance of chromosomes (Fig 33). Time zero is aligned to prometaphase onset as defined by nuclear envelope breakdown (NEBD). Scale bar: 20 µm.

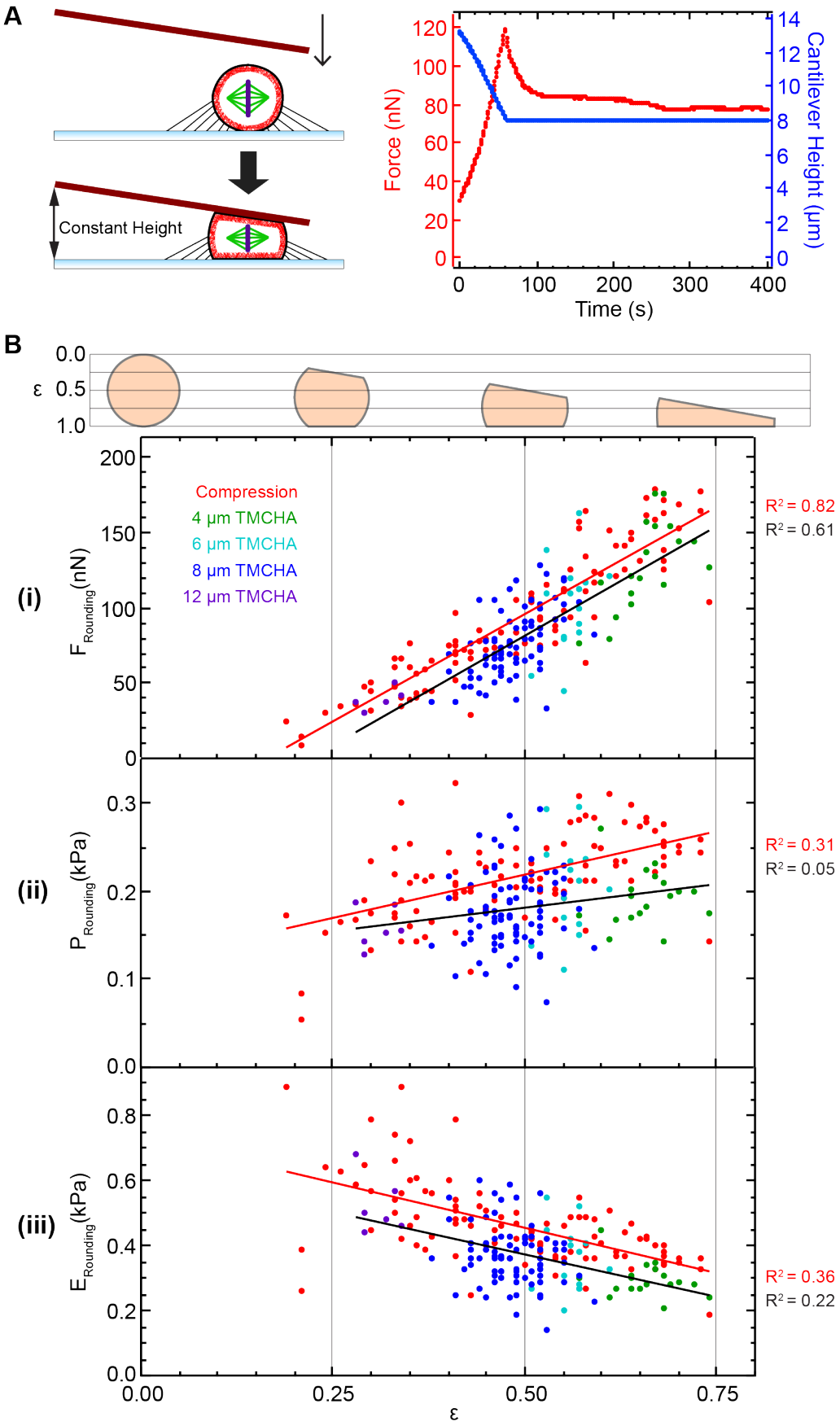

Figure 11: A Left: a schematic of CHA via compression performed on an already round metaphase HeLa cell. Right: a force-relaxation plot from the experiment shows behavior consistent with a viscoelastic sample: an initial decay of stress

followed by equilibrium. **B** Metaphase HeLa cell **(i)** equilibrium forces, **(ii)** rounding pressures and **(iii)** rounding moduli as a function of uniaxial strain (ε) for CHAs via compression and trans-mitotic CHAs (TMCHAs) performed at 4, 6, 8, and 12 μm. The strain axis is supplemented with a depiction of cell shape (top) aligned with vertical grey lines. As a visual aid only, linear fits are shown for compression (red) and TMCHAs (black) with R^2 values. n=100 (compression). n=123 (all TMCHAs combined). Note that due to differences in cell size and positioning along the cantilever, strain (ε) is not uniform for a TMCHA of a particular height.

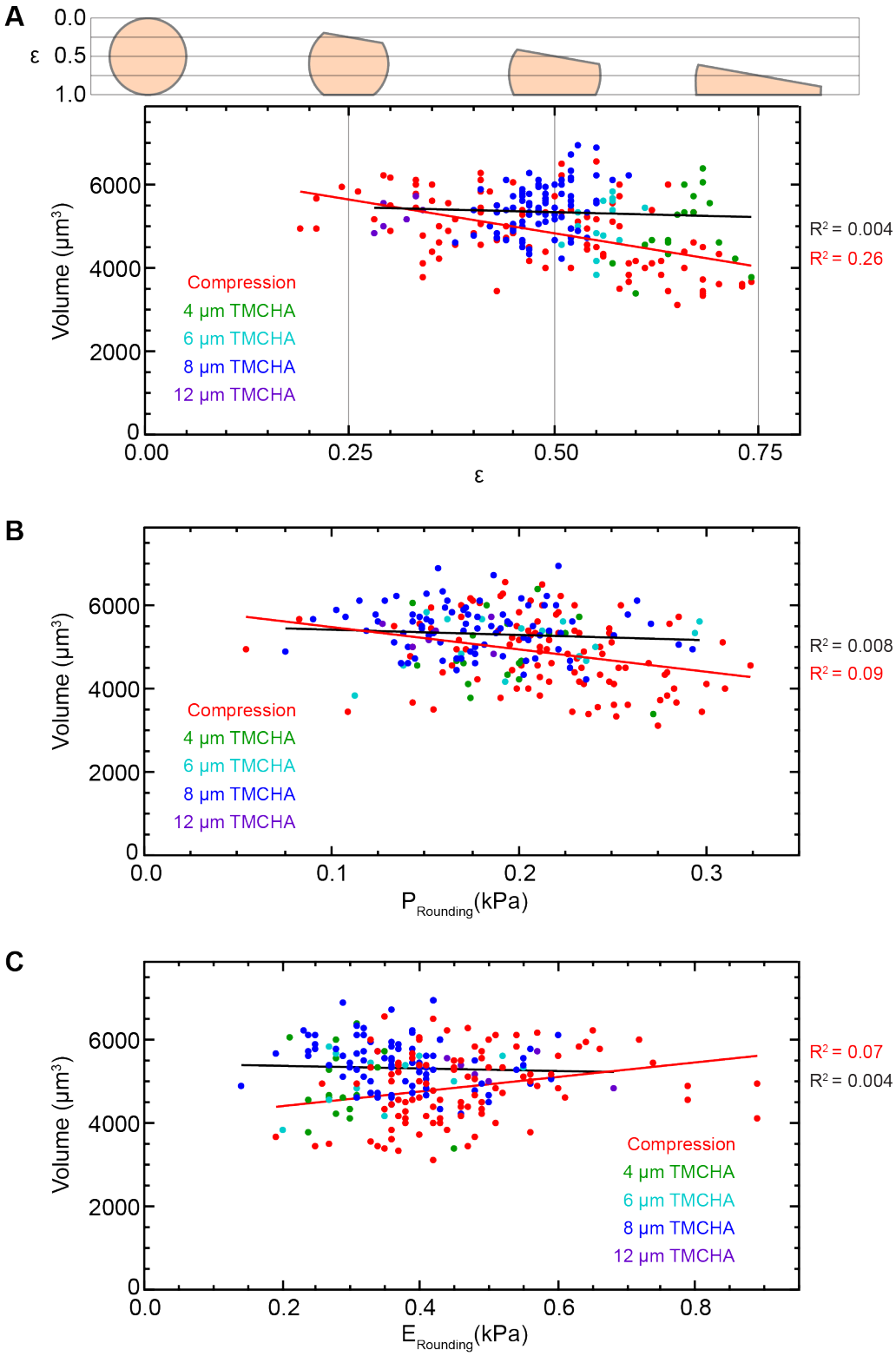

Figure 12: Metaphase HeLa cell volumes as a function of **A** uniaxial strain (ε), **B** rounding pressure ($P_{Rounding}$), and **C** rounding modulus ($E_{Rounding}$) for CHA via compression and trans-mitotic constant height assays (TMCHAs) performed at 4, 6, 8, and 12 μm. As a visual aid only, linear fits are shown for compression (red) and TMCHAs (black) with R^2 values. n=100 (compression). n=123 (all TMCHAs combined).

Comparison of Induced Interphase and Mitotic Cell Rounding

To compare MCR (Fig 10A) with the general effect of a flat cell de-adhering from a surface, the 8 μm CHA was used to analyze the dynamics of induced interphase rounding. In these experiments the cantilever was held above a flat interphase cell followed by injection of commonly used detachment agents, trypsin or EDTA, into the experimental media (Fig 13). Within ~2 minutes cells rounded up into the cantilever and adopted a barrel-like shape similar to that of mitotic cells. The forces and rounding moduli were greatest upon initial detachment and then decayed over the course of ~10 mins to settle at a steady value. The sustained rounding modulus for interphase cells was significantly lower than for mitotic cells. It can therefore be concluded that the elevated rounding pressures observed in mitosis are mitotic specific and not a general effect of de-adhesion.

Next, the behavior of prophase cells was tested with a similar experiment: at NEBD cell rounding was accelerated by addition of trypsin or EDTA (Fig 14). As in the case of interphase cells (Fig 13), a similar initial transient peak in cell rounding force was detected followed by a relaxation. But after several minutes the characteristic mitotic force regime assumed dominance as cells progressed through mitosis. Indeed, such curve profiles resemble the superimposition of MCR (Fig 10A) and induced interphase cell rounding (Fig 13). These results show that the mechanics of induced cell detachment and MCR are distinct. While MCR involves a sustained buildup of rounding pressure, trypsin- or EDTA-mediated rounding exhibits a transient peak before relaxation to a lower equilibrium. The transient characteristics of interphase rounding mechanics might be because of the timescales involved in dissipation of cytoskeletal prestress in cultured adherent cells[93, 94] upon detachment[95, 96] or due to changes in cellular signaling.

To investigate the changes in mechanical properties from interphase to mitosis in the absence of adhesion, pre-rounded cells were characterized through mitosis with the 8 μm CHA (Fig 15). Cells were first rounded up with EDTA or trypsin before being returned to normal media. Then, an already round prophase cell was engaged for investigation and tracked throughout

mitosis. Pre-rounded prophase cells exhibited a baseline similar to the equilibrium values of interphase cells. However, a pronounced increase in measured force and rounding modulus was observed concomitant with NEBD (Fig 15). The absence of adhesion therefore unmasks the stark nature of this mechanical transition at mitotic onset.

Taken together, the results from detachment-induced and mitotic cell rounding can be used to deduce a "trajectory" of mechanical properties as a function of cell cycle phase (Fig 16A). Induced rounding of interphase cells with trypsin yielded a transient rounding modulus of 0.38 ±0.11 kPa before relaxation to a stable plateau of 0.24 ±0.08 kPa (n=12) while the corresponding numbers for EDTA were 0.18 ±0.11 kPa to 0.05 ±0.03 kPa (n=9)(Fig 13). Prophase cells that were accelerated into a round state with trypsin showed a transient modulus of 0.37 ±0.14 kPa, before a short relaxation and then a metaphase peak at 0.48 ±0.08 kPa (n=8) while the corresponding results for EDTA were 0.10 ±0.04 kPa (n=5) and 0.35 ±0.10 kPa (n=10)(Fig 14). Furthermore, for trypsin and EDTA respectively, cells that were pre-rounded and then returned to normal media before commencement of a CHA showed prophase rounding moduli of 0.09 ±0.05 kPa (n=29) and 0.05 ±0.03 kPa (n=5) and metaphase rounding moduli of 0.38 ±0.08 kPa (n=29) and 0.33 ±0.06 kPa (n=5)(Fig 15). Untreated cells, which started from an adherent state, were also compared from the time they first reached a barrel-like shape in prometaphase 0.11 ±0.04 kPa (n=5) to their average metaphase maximums at 0.37 ±0.09 kPa (n=83)(Fig 10A).

Overall, two deductions can be made from these results. First, cell rounding modulus increases by approximately three fold from interphase to mitosis independent of changes in adhesion or cell shape. The differences could not be attributed to obvious variations in actin cortex morphology, as both trypsinized mitotic and interphase cells exhibited a well-formed homogenous actomyosin cortex (Fig 16B). Thus the mechanical changes and forces that drive MCR on a whole cell scale occur independently from changes in adhesion, and experiments such as presented in figure 15 are useful for characterizing these effects. Second, these results indicate that

trypsin treatment increases the rounding modulus of cells irrespective of cell cycle stage and adhesive state. This is exemplified in mitosis itself where metaphase cells maintained in trypsin exhibit a rounding modulus significantly greater ($p=0.006$) than those returned to normal media after trypsinization (Fig 16A(i)). In addition to this, trypsin-mediated detachment usually generated round cells with intact retraction fibers (Fig 7A,C). Because the distal ends of retraction fibers must be held in place by cell adhesion molecules[97, 98], trypsin-mediated rounding cannot be accounted for by proteolysis of extracellular cell adhesion receptor domains[13, 99-101]. This suggests that trypsin-mediated cell rounding may be partially due to an increase in rounding modulus and surface tension. Furthermore, this increase was unlikely to be due to apoptotic processes because cells were observed to transition through mitosis under these conditions.

For the analyzed cell cycle trajectories (Fig 16A(ii)) cell volume was also determined (Fig 16B(ii)). In the case of interphase-induced detachment, cell volume did not appreciably change over the course of the force-relaxation regime ($p=0.71$ for trypsin, and 0.22 for EDTA). For cells transitioning from prophase to metaphase, cells that were untreated or exposed to EDTA also showed an insignificant change in volume ($p=0.28$ Untreated, 0.51 in 5 mM continuous EDTA, and 0.55 for 5 mM EDTA pre-treatment). On the other hand, trypsinized cells, either incubated in trypsin or pre-rounded with it before return to normal media, showed a slight increase in volume from prophase to metaphase ($p=0.046$, 0.036 respectively). This could be because trypsin is known to activate a plethora of intracellular signaling pathways by way of interaction with protease-activated receptors[102], including activation of sodium channels known to promote cell volume increase[103].

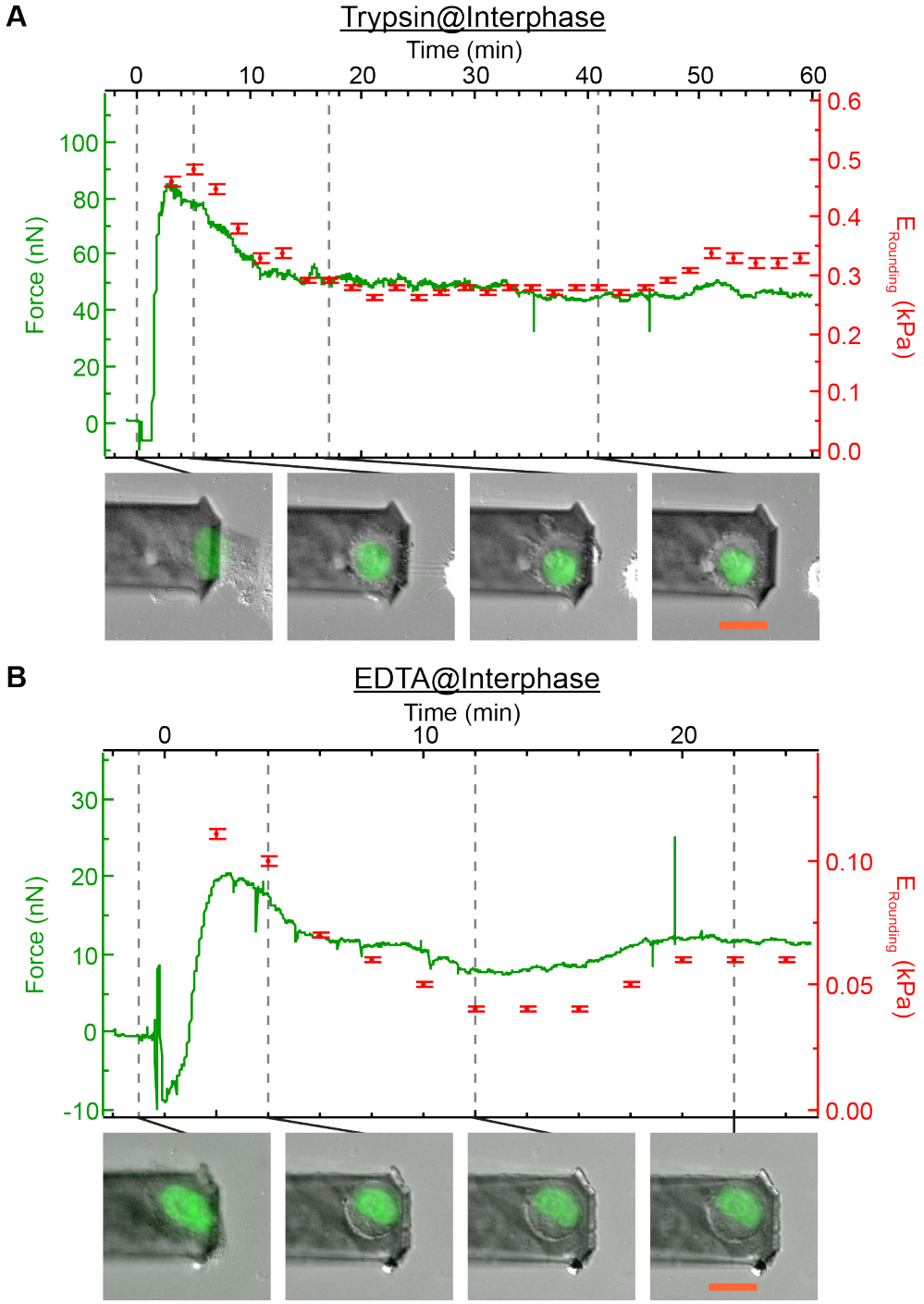

Figure 13: Probing the mechanics of interphase cell detachment with the 8 µm CHA. **A** 2.5 mg/L trypsin in DMEM lacking FCS (Fetal calf serum) or **B** 5 mM EDTA was introduced via injection at time zero. Scale bar: 20 µm. The cantilever was placed 8 µm above an isolated interphase cell before addition of respective detachment agents. See figures 9 and 10 for further experimental details on the 8 µm CHA.

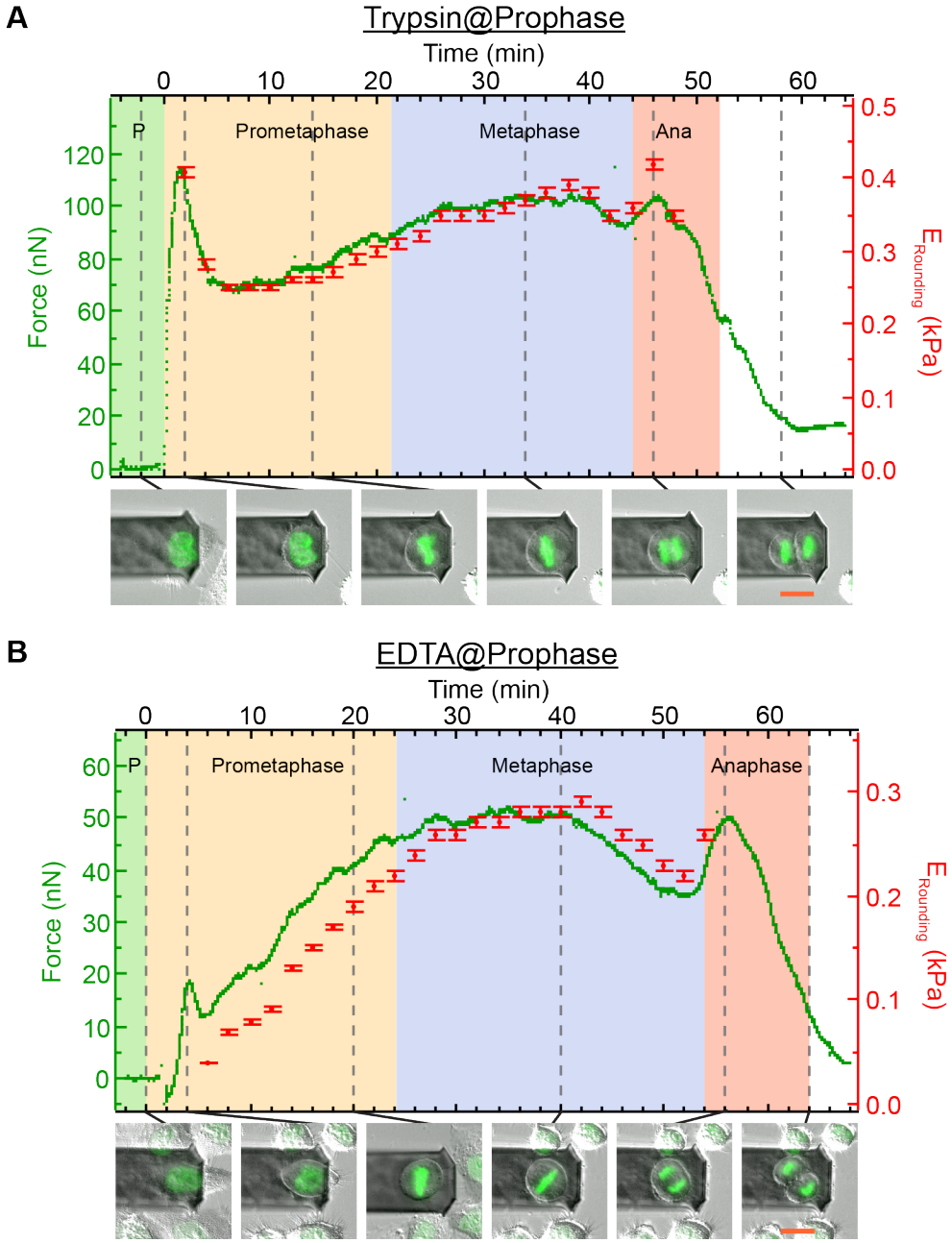

Figure 14: Probing the mechanics of induced cell detachment in late prophase/early prometaphase and subsequent mitosis. The 8 µm trans-mitotic CHA was setup on initially flat prophase cells subject to **A** 2.5 mg/L trypsin (added at 0 mins) in DMEM lacking FCS, or **B** 5 mM EDTA (added at 2 mins). Scale bar: 20 µm. See figures 9 and 10 for experimental details on the 8 µm trans-mitotic CHA.

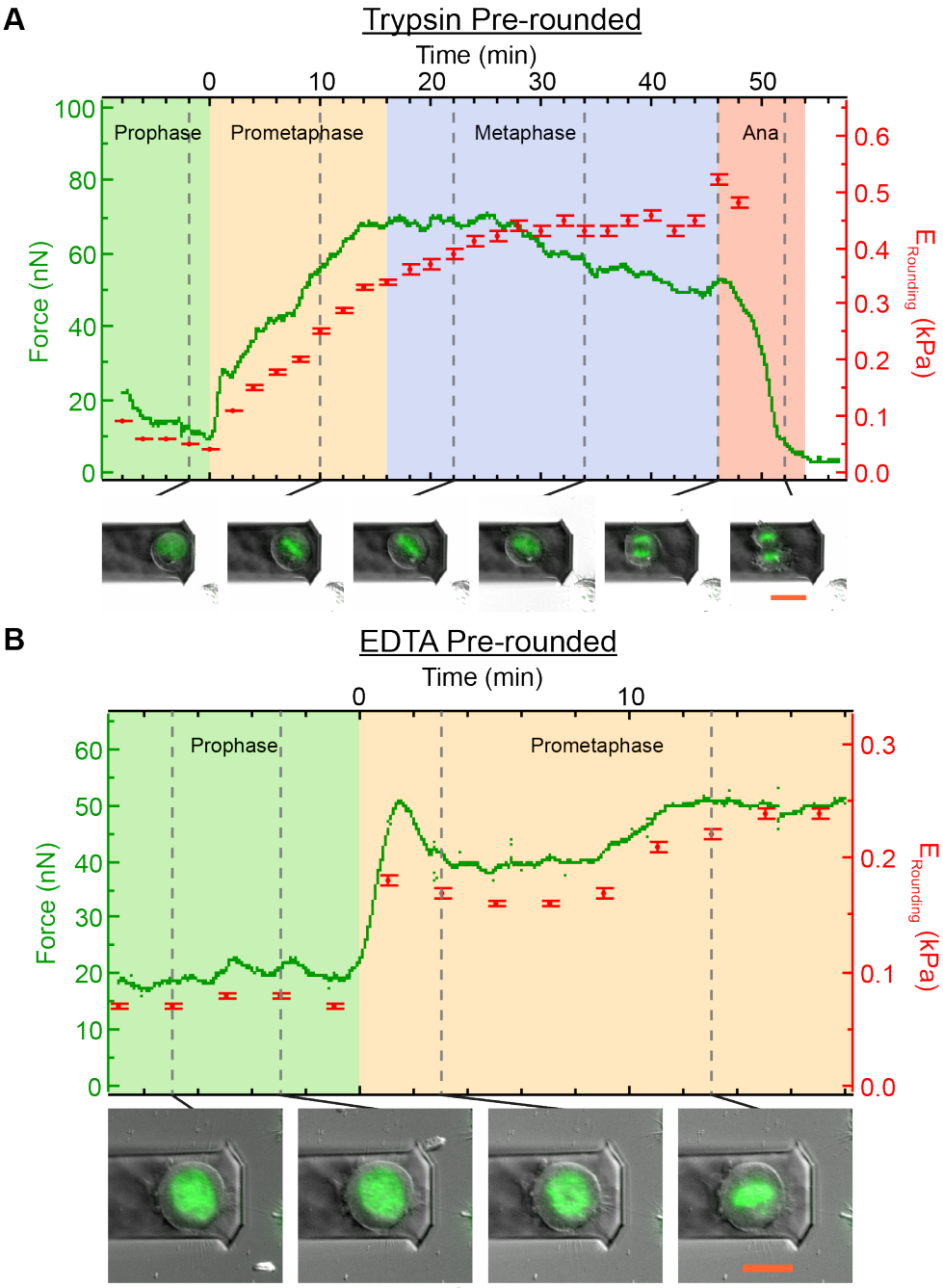

Figure 15: Probing the mechanics of pre-rounded mitotic cells with the 8 µm trans-mitotic CHA. Cells were pre-rounded with **A** trypsin, or **B** EDTA. For cells pre-rounded with trypsin, cells were allowed to round up in standard Dulbecco's Modified Eagle Media (DMEM) containing 2.5 mg/L trypsin without FCS. Medium was then exchanged back to standard DMEM with 10% FCS and cells incubated for at least 5 minutes before establishing an 8 µm CHA on a pre-rounded prophase cell. Scale bar: 20 µm. See figures 9 and 10 for experimental details on the 8 µm trans-mitotic CHA.

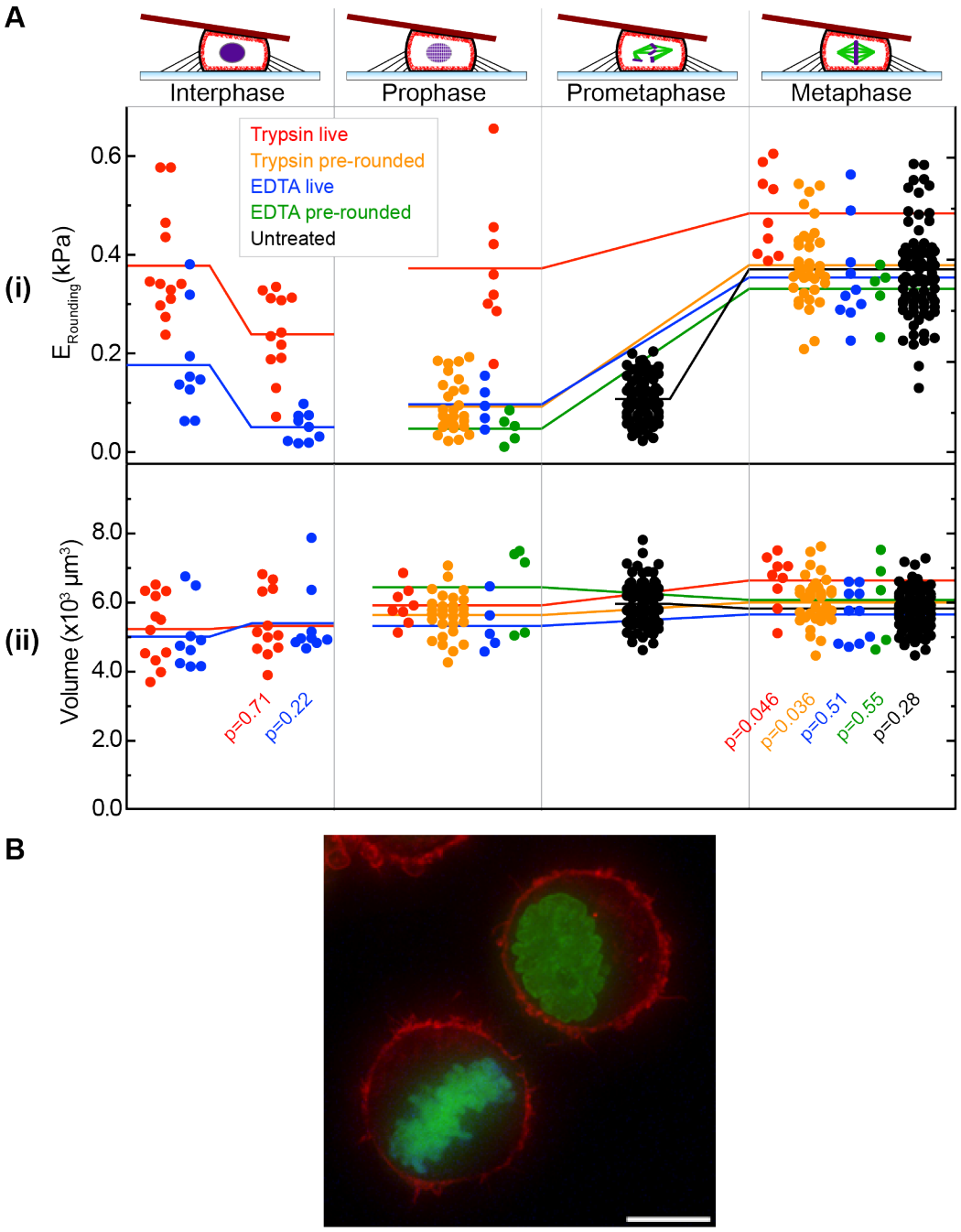

Figure 16: A Cell **(i)** rounding modulus ($E_{Rounding}$) and **(ii)** volume trajectories in the CHA as a function of detachment agents, time, and the cell cycle. Dots represent individual cells. Flat lines represent averages. Angular lines represent trajectories between indicated averages. "Trypsin" denotes 2.5 mg/L trypsin in DMEM without FCS. "EDTA" denotes 5 mM EDTA in normal media (DMEM with 10% FCS). "Live" denotes experiments where addition of agents occurred after commencement of the CHA and remained present throughout (Figs 13,14). "Pre-rounded" designates a switch back to normal media (DMEM with 10% FCS) and a ~5 min equilibration period before commencement of the CHA (Fig 15). Rounding moduli and volumes could only be calculated for untreated cells after first becoming round in prometaphase. Significance in volume changes over the indicated trajectory is indicated with a p value (Mann-Whitney, two-tailed). **B** Cortical F-actin morphology in trypsinized interphase and mitotic cells. To observe and compare the cortical actin morphology of round trypsinized cells in interphase and mitosis, H2B-GFP HeLa cells were trypsinized, quenched in

growth media, then spun onto poly-lysine-coated glass base dishes at 300 rpm (16 G) for 5 min. Then the cells were fixed in the PFA solution (3% paraformaldehyde, 5 mM EGTA, 1 mM $MgCl_2$ in PBS), and stained for actin and phosphorylated histone H3 at Ser 10 as a mitotic marker with rhodamine-phalloidin (Invitrogen) and an anti-phospho histone antibody (6G3, Cell Signaling Technology), respectively. The images were acquired at 0.3 μm intervals along the Z axis, deconvolved, and projected. Green, H2B-GFP; red, actin; blue; histone H3 phosphorylated at Ser 10. Scale bar, 10 μm. Image courtesy of Yusuke Toyoda.

Induced Cell Rounding via Phosphatase Inhibition

Besides cell rounding induced by the commonly used detachment agents presented above, calyculin A, an inhibitor of serine/threonine phosphatases 1 and 2A[104], has also been observed to trigger cell rounding[64, 105-107]. Although general phosphatase inhibition is highly non-specific, the mechanism of shape change is believed to be because it produces a population of constitutively phosphorylated cytoskeletal proteins[105, 108]. This in turn causes increased actomyosin contractility and promotes cytoskeletal reorganization. Some studies have gone so far as to employ calyculin A as a means to constitutively activate myosin contractility[109, 110].

The characteristics of calyculin A induced cell rounding in interphase cells were tested with CHAs (Fig 17, n=5). 10 to 90 mins after exposure to 5 nM of the inhibitor, cells abruptly detached from the substrate, generated forces similar to mitotic cells, and blebbed profusely. These cells also exhibited a severe loss of adhesion, which promoted acute sliding of cells along the cantilever gradient and eventual escape from the assay. Another feature of calyculin A treatment was the tendency to trigger chromosome condensation, as reported by others[111]. Events at mitotic entry are related to a global rise in protein phosphorylation and, more specifically, inhibition of phosphatases 1 and 2A[112]. Thus, phosphatase inhibition with calyculin A captures several biochemical and mechanical aspects of mitosis including loss of adhesion, chromosome condensation, and maintenance of sustained rounding forces.

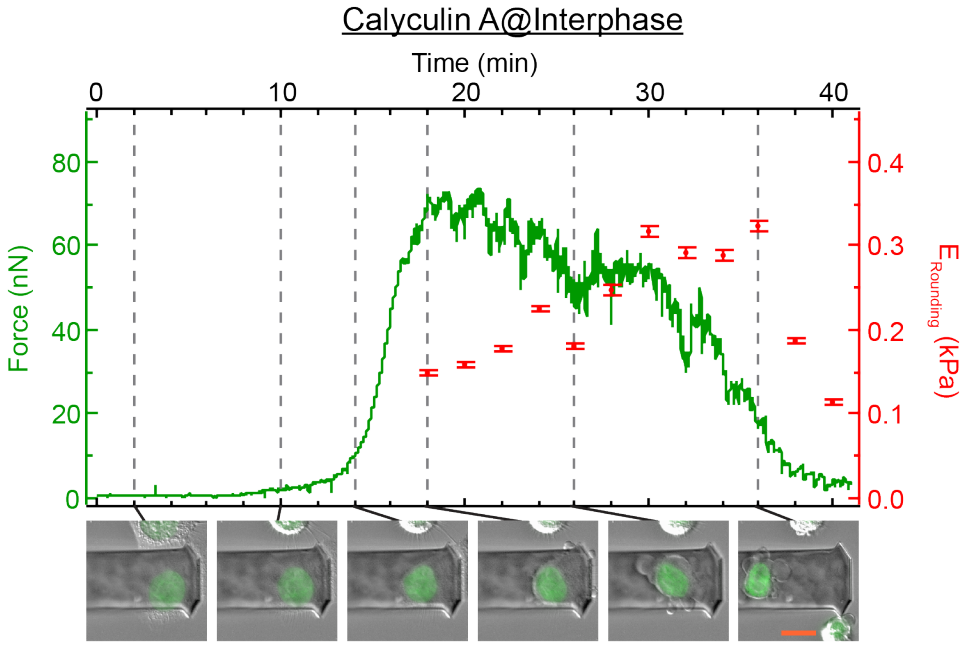

Figure 17: Probing the mechanics of interphase cell rounding induced with 5 nM Calyculin A using the 8 µm constant height assay (CHA). Calyculin A was added at t = -60 mins. Time zero is arbitrary. $E_{rounding}$ error bars are ± 2% (see Fig 9). Rounding commences at 14 minutes and blebbing follows quickly after. Chromosome condensation is visible from 26 minutes. Scale bar: 20 µm. See figures 9 and 10 for experimental details on the 8 µm CHA.

Pharmacological Dissection of Mitotic Cell Rounding

The mechanical properties of animal cells are governed by a wide array of cellular structures and processes across different cells types and organisms. Most research on animal cell mechanics has emphasized the role of cytoskeletal assemblies and associated force generating motor proteins[2]. However, the properties of the plasma membrane[113, 114], mechanics of the cytosol[115, 116], and the effects of intracellular hydrostatic pressure may also play a role[117-121]. Where available, the use of small molecule inhibitors is a useful strategy to elucidate the roles of such processes in a specific and temporally controlled manner[122]. To quantify the mechanical contribution of potential cellular processes and components in MCR, cells were preincubated with small molecule inhibitors and perturbants and tested in the 8 µm trans-mitotic CHA. Cells were then compared by using the rounding modulus parameter, which was 0.37±0.09 kPa (n=83) for untreated cells.

Actomyosin

Disruption of filamentous actin was brought about by application of latrunculin A, an actin monomer sequester[123, 124], cytochalasin D, an F-actin barbed end capper[78], or jasplakinolide, an F-actin stabilizer[125, 126]. With these treatments the rounding moduli decreased in a dose-response manner to 0.04±0.04 kPa (n=4) for 200 nM latrunculin A, 0.01±0.01 kPa (n=6) for 1 μM cytochalasin D, and 0.03±0.01 kPa (n=3) for 100 nM jasplakinolide respectively (Fig 18A-E). In addition to this, detectable force oscillations were often observed to occur concurrently with blebbing at particular concentrations of these inhibitors. Blebs form when a section of membrane detaches from the actomyosin cortex[127] and retract when the actomyosin cortex reassembles underneath the membrane and pulls the bleb back into the main cell body[128]. Blebbing was particularly pronounced in the case of 40 nM latrunculin A where, upon arrival at a threshold rounding pressure, large blebs cyclically formed and retracted over several minutes until division (Fig 18A(ii)). Bleb protrusion caused a ~50% reduction in rounding modulus and a ~15% decrease in volume of the main cell body followed by recovery upon retraction. Because rounding modulus is defined as the rounding pressure normalized to the degree of deformation (Fig 9E), the observed loss of pressure cannot be attributed to a size decrease of the main cell body. The concurrence of bleb formation and decrease of rounding pressure suggests that the cell was under hydrostatic pressure: the pressure inside the cell pushing the cantilever upward was partially released when a bleb formed[119]. This interpretation is supported by recent measurements quantitatively relating cortical actomyosin tension with bleb formation[92]. These results suggest that disrupting the structure of the actin cortex with biochemical inhibitors hinders a buildup of intracellular pressure during MCR.

Next, the role of actomyosin contractility in MCR was probed. To do this the following perturbants were employed: blebbistatin, an inhibitor of myosin II activity[129], ML-7, an inhibitor of myosin light chain kinase[130], and Y-27632, an inhibitor of ROCK, which regulates aspects of myosin contractility and actin dynamics[79]. Notably, ROCK has previously been

implicated in MCR through the RhoA pathway[63]. In the trans-mitotic CHA cells yielded rounding moduli of 0.04±0.01 kPa (n=6) for 100 μM blebbistatin, 0.24±0.11 kPa (n=4) for 30 μM ML-7, and 0.09±0.03 kPa (n=6) for 100 μM Y-27632 (Fig 18F-H). In addition to their deleterious effect on mechanics, it was observed that these inhibitors caused mitotic cells to exhibit slow shape change and a smooth periphery devoid of blebs. This indicated that perturbing the capacity of mitotic cells to generate tension through myosin contractility inhibited buildup of rounding pressure.

Taken together, the experiments with perturbants of actin archiecture and actomyosin contractility confirm that a well-formed and structurally intact homogenous contractile actomyosin cortex is required for rounding cells to generate a pressure against an external impediment.

Microtubules

Next, the role of the microtubule spindle in the mechanics of MCR was tested. To do this microtubule depolymerization agents, nocodazole[131] and vinblastine[132], the microtubule stabilization agent, taxol[133], and the kinesis eg-5 inhibitor, S-trityl-L-cysteine (STC)[134], were used. As expected, all of these inhibitors arrested mitotic cells in prometaphase due to spindle assembly defects. Compared to untreated cells, microtubule depolymerization agents accelerated the buildup of force against the cantilever before reaching a similar or slightly higher stable plateau (Fig 18 I,J). The maximum values for rounding moduli were 0.41±0.09 kPa (n=9) for nocadazole and 0.44±0.08 kPa (n=8) for vinblastine. Treatment with the microtubule stabilization agent taxol yielded an increase in rounding modulus of mitotic cells to 0.58±0.06 kPa (n=5) but without affecting the initial rounding rate (Fig 18K). Finally, the kinesin motor inhibitor STC appeared to have little effect on the mechanics of MCR as rounding modulus was determined to be 0.44±0.04 kPa (n=6) for a 2 μM dose. Together these results show that microtubules are not a necessary component of the force generating machinery in MCR.

Plasma Membrane Traffic and Surface Area

Previous reports have suggested that there is an interplay between plasma membrane surface area and cell surface tension level[135], and that this effect may be an important factor in MCR[114, 136]. Indeed, it has been proposed that an endocytosis-mediated reduction in plasma membrane surface area might provide a source of surface tension to drive MCR[114]. To test this idea dynamin, the primary motor that drives endocytosis, was inhibited with dynasore, a specific small molecule inhibitor[137]. Mitotic cells treated with 100 μM dynasore exhibited a slightly increased rounding modulus of 0.48±0.19 kPa (n=8) (Fig 18N) and featured aberrant spindles as previously reported[136]. Direct perturbation of membrane tension was also attempted with deoxycholate, a detergent that Raucher and Sheetz previously used to reduce the membrane tension of mitotic cells[114]. Deoxycholate was found to slightly reduce rounding modulus to 0.29±0.04 kPa (n=4) at 200 μM (Fig 18M). However, at these concentrations cell morphology was starkly affected, vacuoles formed, and non-specific toxic effects could not be ruled out. Therefore, while tight regulation of membrane traffic and tension is important for certain aspects of mitosis, such as cytokinesis[138], it appears not to underpin the mechanics of MCR. Such a conclusion is in accordance with the current theory in animal cell mechanics that the plasma membrane is not limiting, and that the apparent surface area of cells is rather governed by underlying cytoskeletal structures such as the spectrin network and actomyosin cortex[139].

Ion Transporters

The cell plasma membrane is highly permeable to water. As a result, water rapidly flows along its trans-membrane osmotic pressure gradient until equilibrium is achieved. In order to control volume, cells utilize a host of mechanisms to manipulate intracellular osmolarity and the flow of osmotically obliged water. In the short term (minutes) cells tend to employ ion transporters, while in the longer term (hours) cells control osmolyte concentrations through synthesis, release, or uptake of organic molecules[140]. For example, after cell swelling inorganic ions are rapidly

released in a process known as regulatory volume decrease (RVD). On the other hand, cell shrinkage triggers the uptake of ions through rapid activation of cellular transport mechanisms in a process known as regulatory volume increase (RVI)[140]. Cells deploy a host of transporters at the plasma membrane to control cytoplasmic osmolarity, pressure and volume with cellular response times ranging from milliseconds to minutes.

The role of several key ion transporters known to be involved in the homeostasis of cell volume[140] were tested for a contribution to MCR. The 8 μm trans-mitotic CHA was carried out on single cells with the following specific inhibitors: EIPA, an inhibitor selective for the NHE1 (SLC9A1) isoform of Na^+/H^+ exchangers[141], Ouabain, an inhibitor of the Na^+/K^+ ATPase[142], Bumetanide, an inhibitor of the Na^+-K^+-$2Cl^-$ symporter[143], and NPPB and DIDS, inhibitors of several chloride transport processes including Cl^-/HCO_3^- exchange[144](Fig 18 O-S). The results in terms of rounding moduli were as follows: 0.19±0.06 kPa (n=7) with 100 μM EIPA, 0.39±0.09 kPa (n=10) with 100 μM ouabain, 0.51±0.11 kPa (n=5) with 100 μM bumetanide, 0.41±0.12 kPa (n=7) with 100 μM NPPB, and 0.40±0.09 kPa (n=8) with 100 μM DIDS. Indeed, only the Na^+/H^+ exchange inhibitor, EIPA, affected a strong perturbation in the mechanics of MCR. The exchange of a proton with a Na^+ ion increases intracellular osmolarity because pH is strongly buffered in the cytoplasm. Thus, a Na^+ ion has a greater effect on osmolarity than a proton[140, 145-147]. Moreover, Na^+/H^+ exchange is known to be upregulated at the G2/M transition, play a role in permitting mitotic entry, and contribute to the elevated pH characteristic of mitosis[148, 149]. The EIPA results suggest that the activity of the Na^+/H^+ exchanger is required to maintain a substantial component of mitotic cell rounding pressure.

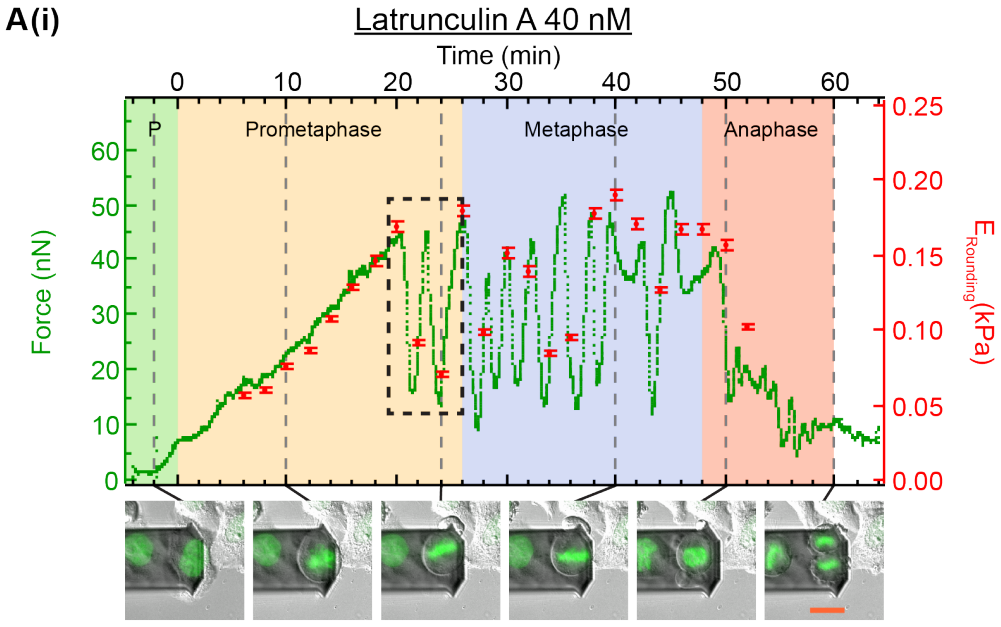
A(i)
Latrunculin A 40 nM
Time (min)
0
10
20
30
40
50
60
P
Prometaphase
Metaphase
Anaphase
Force (nN)
$E_{Rounding}$(kPa)
0.25
0.20
0.15
0.10
0.05
0.00

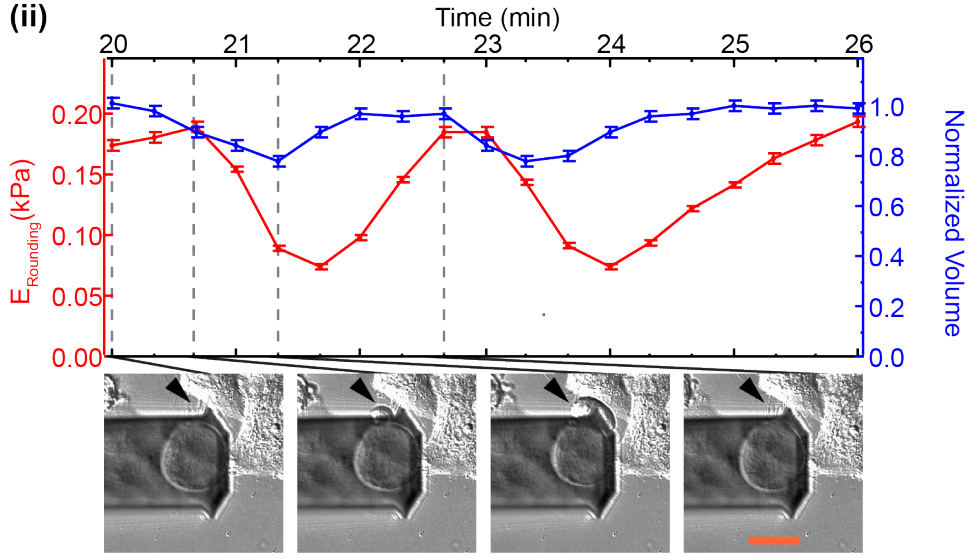
(ii)
Time (min)
20
21
22
23
24
25
26
$E_{Rounding}$(kPa)
Normalized Volume
1.0
0.8
0.6
0.4
0.2
0.0

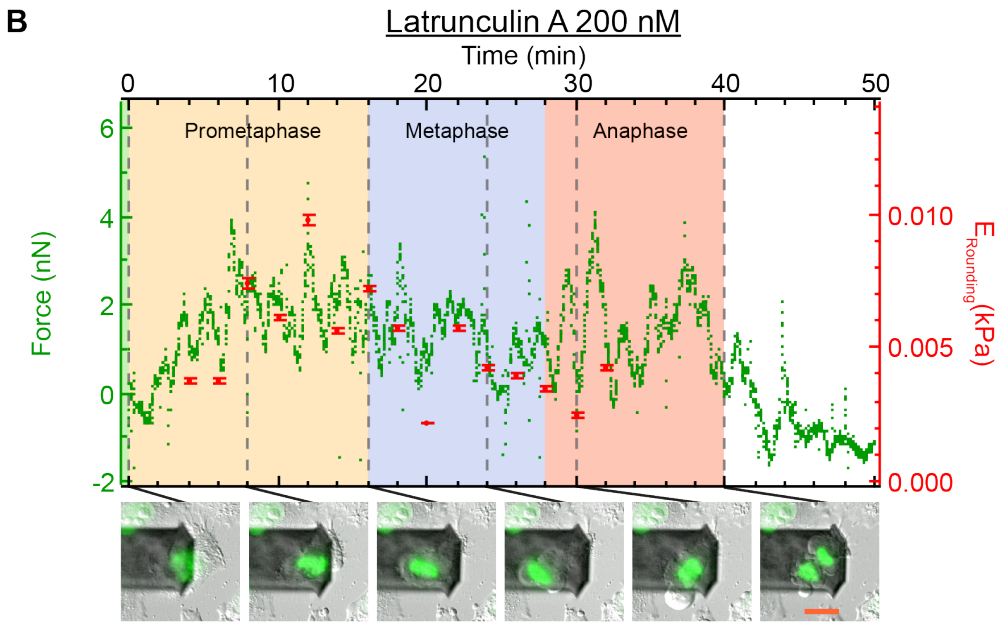
B
Latrunculin A 200 nM
Time (min)
0
10
20
30
40
50
Prometaphase
Metaphase
Anaphase
Force (nN)
$E_{Rounding}$(kPa)
0.010
0.005
0.000

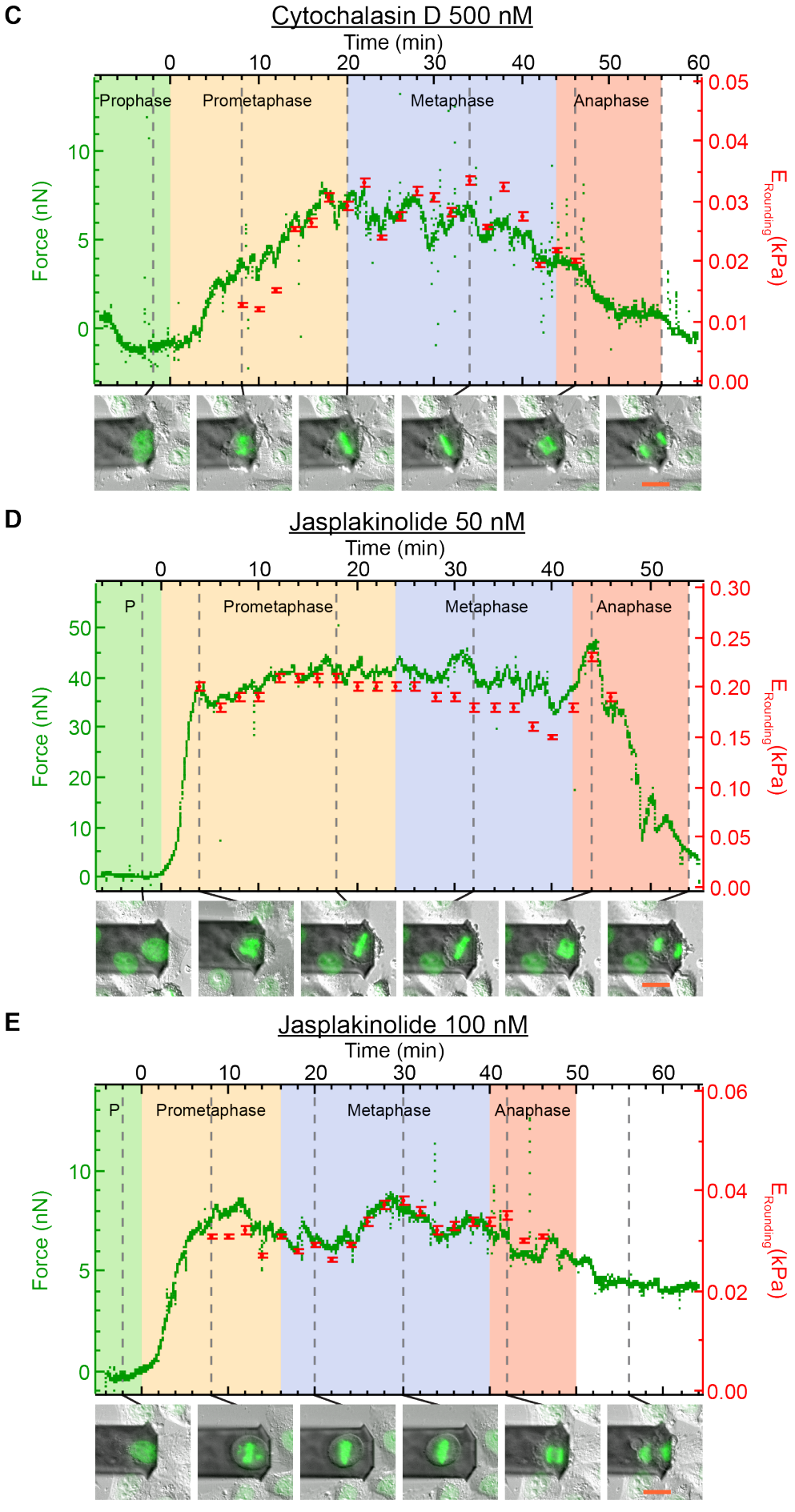
C
Cytochalasin D 500 nM
Time (min)
Prophase
Prometaphase
Metaphase
Anaphase
Force (nN)
E Rounding (kPa)
D
Jasplakinolide 50 nM
Time (min)
P
Prometaphase
Metaphase
Anaphase
Force (nN)
E Rounding (kPa)
E
Jasplakinolide 100 nM
Time (min)
P
Prometaphase
Metaphase
Anaphase
Force (nN)
E Rounding (kPa)

F

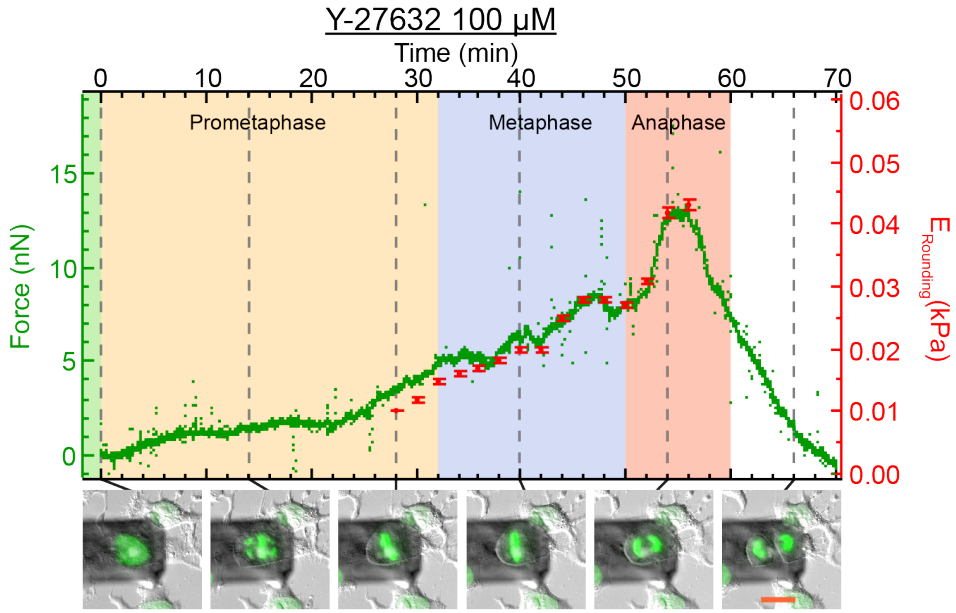
Y-27632 100 µM
Time (min)
0
10
20
30
40
50
60
70
Prometaphase
Metaphase
Anaphase
Force (nN)
0
5
10
15
E Rounding (kPa)
0.00
0.01
0.02
0.03
0.04
0.05
0.06

G

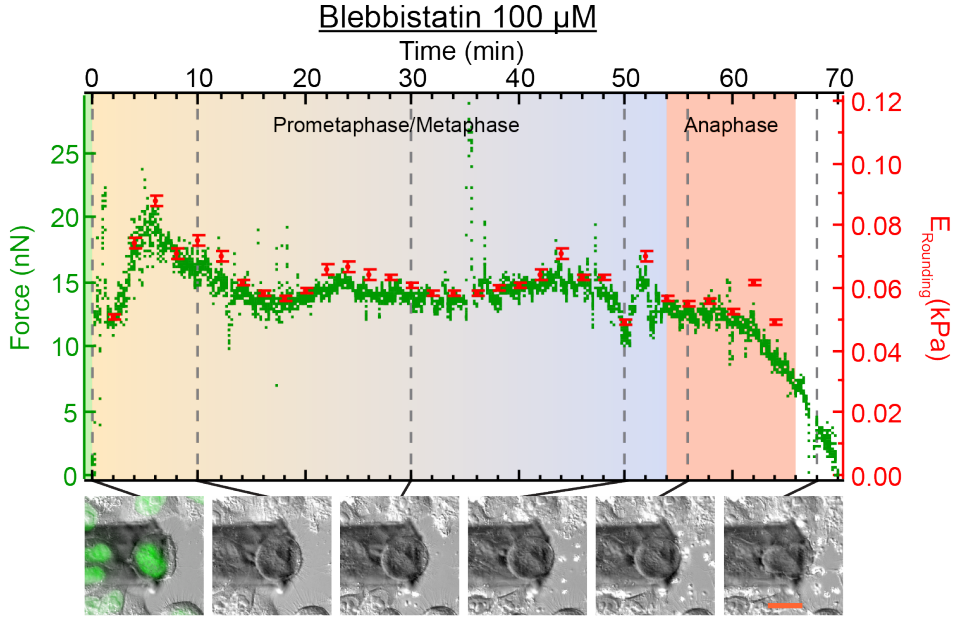
Blebbistatin 100 µM
Time (min)
0
10
20
30
40
50
60
70
Prometaphase/Metaphase
Anaphase
Force (nN)
0
5
10
15
20
25
E Rounding (kPa)
0.00
0.02
0.04
0.06
0.08
0.10
0.12

H

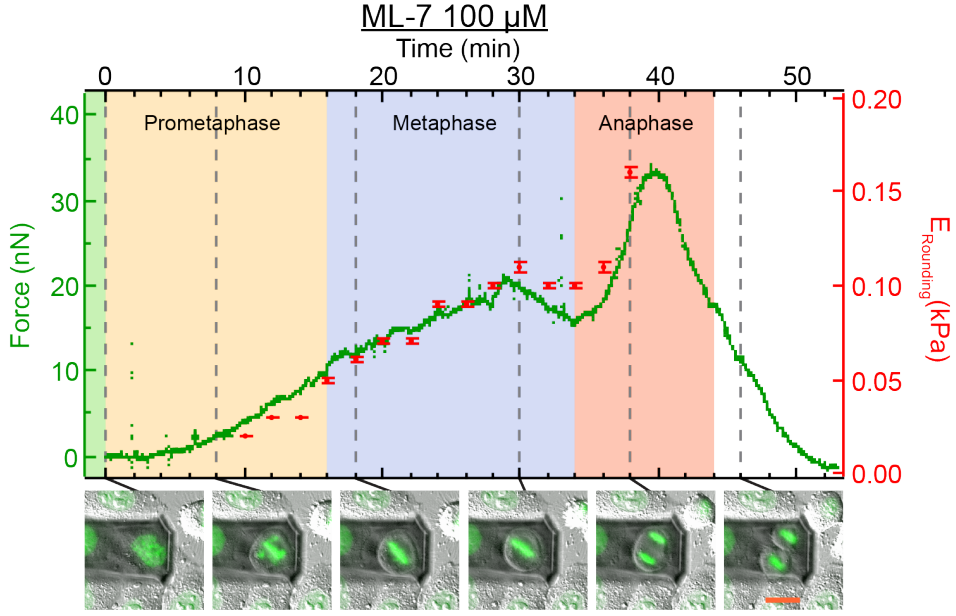
ML-7 100 µM
Time (min)
0
10
20
30
40
50
Prometaphase
Metaphase
Anaphase
Force (nN)
0
10
20
30
40
E Rounding (kPa)
0.00
0.05
0.10
0.15
0.20

I

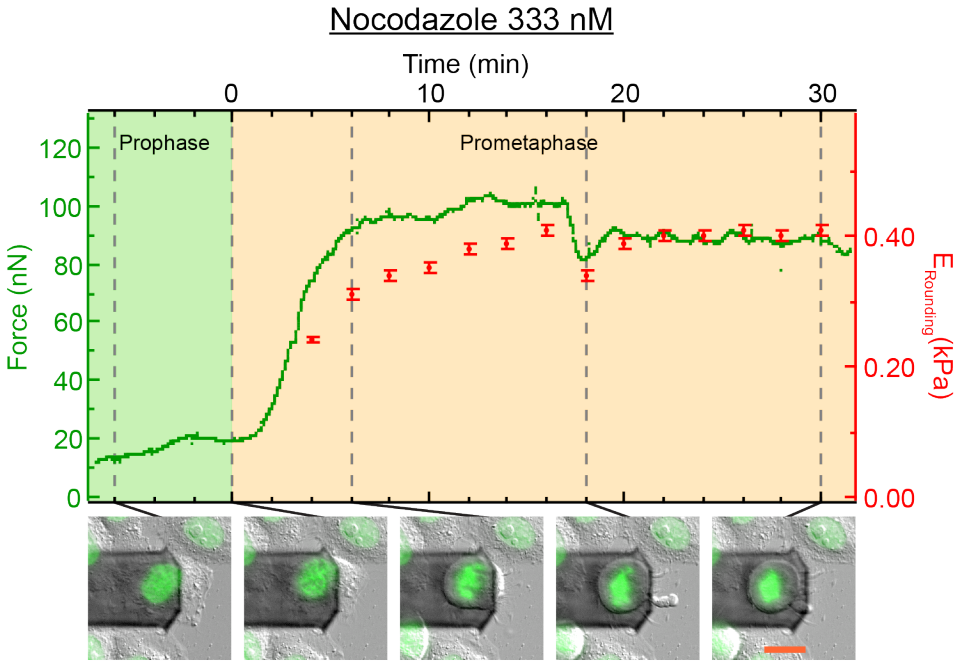
Nocodazole 333 nM
Time (min)
0
10
20
30
Prophase
Prometaphase
Force (nN)
120
100
80
60
40
20
0
0.40
0.20
0.00
E Rounding (kPa)

J

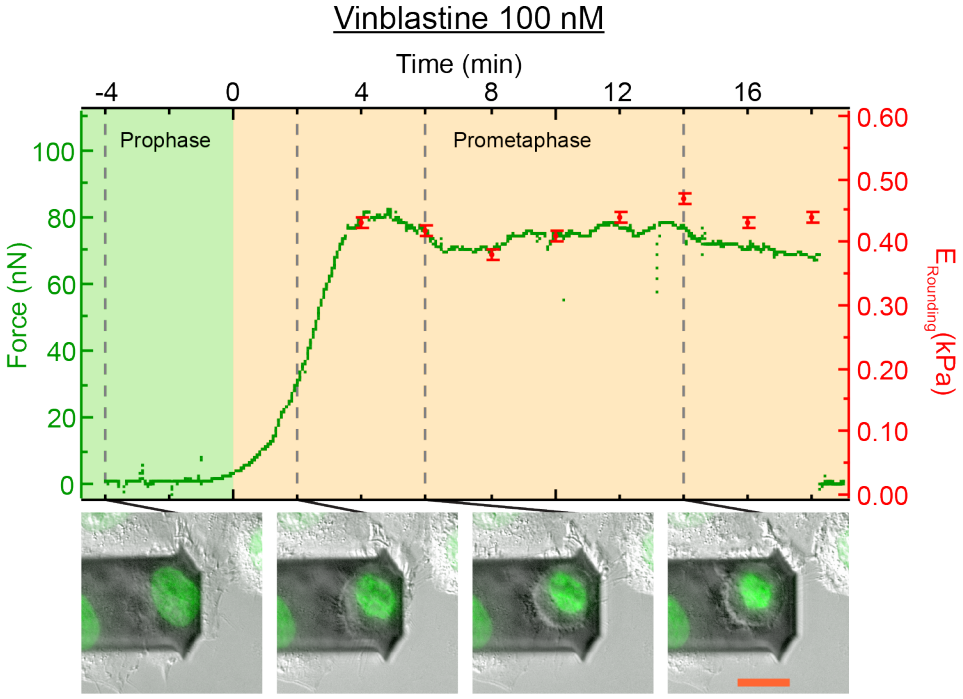
Vinblastine 100 nM
Time (min)
-4
0
4
8
12
16
Prophase
Prometaphase
Force (nN)
100
80
60
40
20
0
0.60
0.50
0.40
0.30
0.20
0.10
0.00
E Rounding (kPa)

K

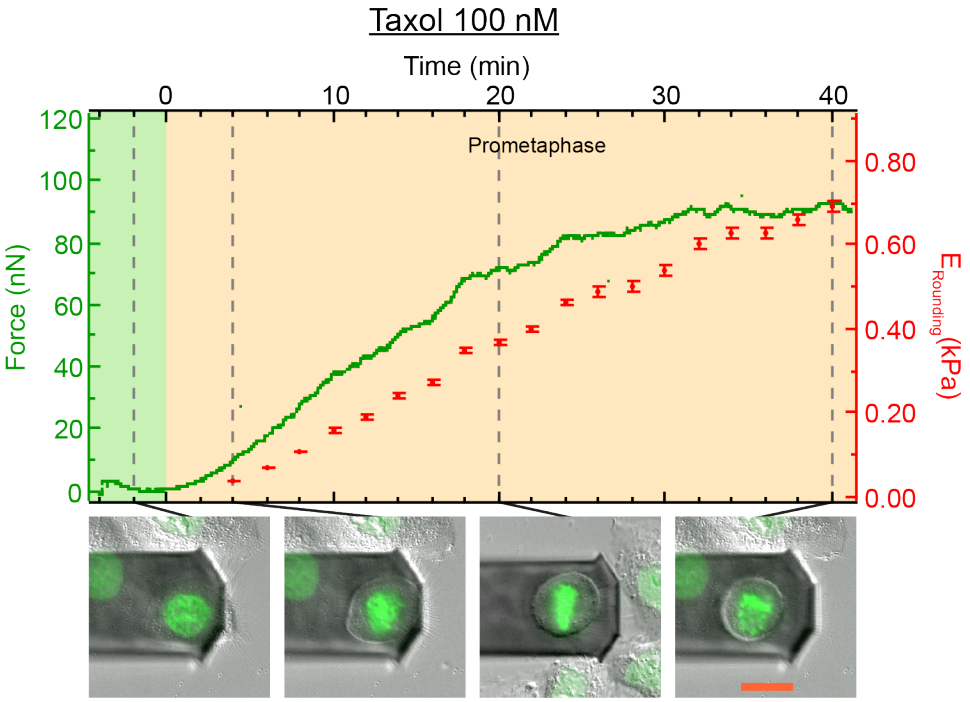
Taxol 100 nM
Time (min)
0
10
20
30
40
Prometaphase
Force (nN)
120
100
80
60
40
20
0
0.80
0.60
0.40
0.20
0.00
E Rounding (kPa)

L

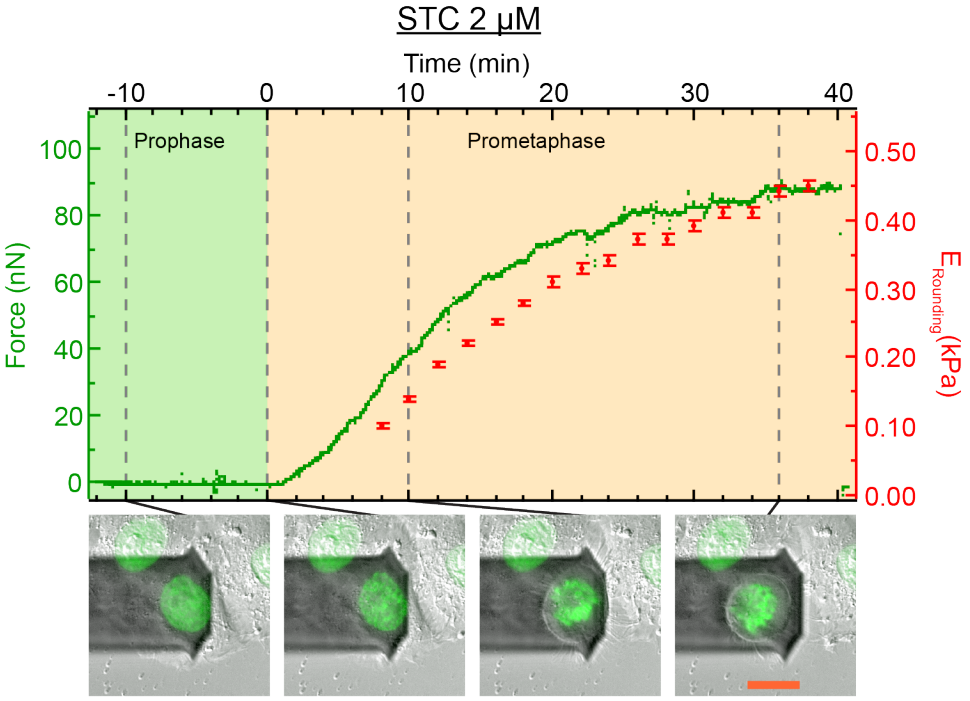
STC 2 µM
Time (min)
-10
0
10
20
30
40
Prophase
Prometaphase
Force (nN)
100
80
60
40
20
0
0.50
0.40
0.30
0.20
0.10
0.00
E Rounding (kPa)

M

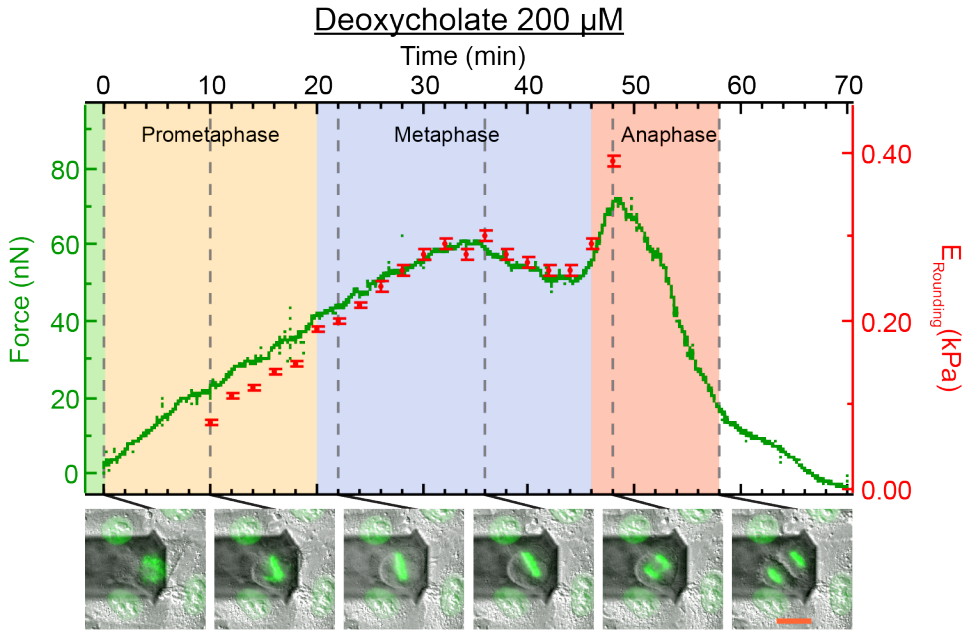
Deoxycholate 200 µM
Time (min)
0
10
20
30
40
50
60
70
Prometaphase
Metaphase
Anaphase
Force (nN)
0
20
40
60
80
0.00
0.20
0.40
E Rounding (kPa)

N

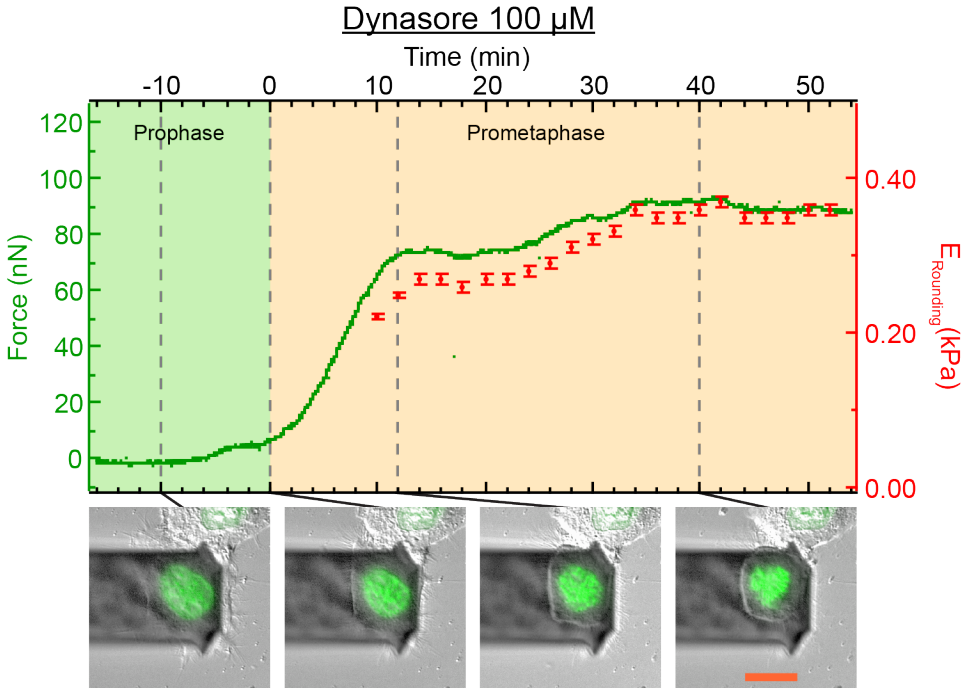
Dynasore 100 µM
Time (min)
-10
0
10
20
30
40
50
Prophase
Prometaphase
Force (nN)
0
20
40
60
80
100
120
0.00
0.20
0.40
E Rounding (kPa)

O

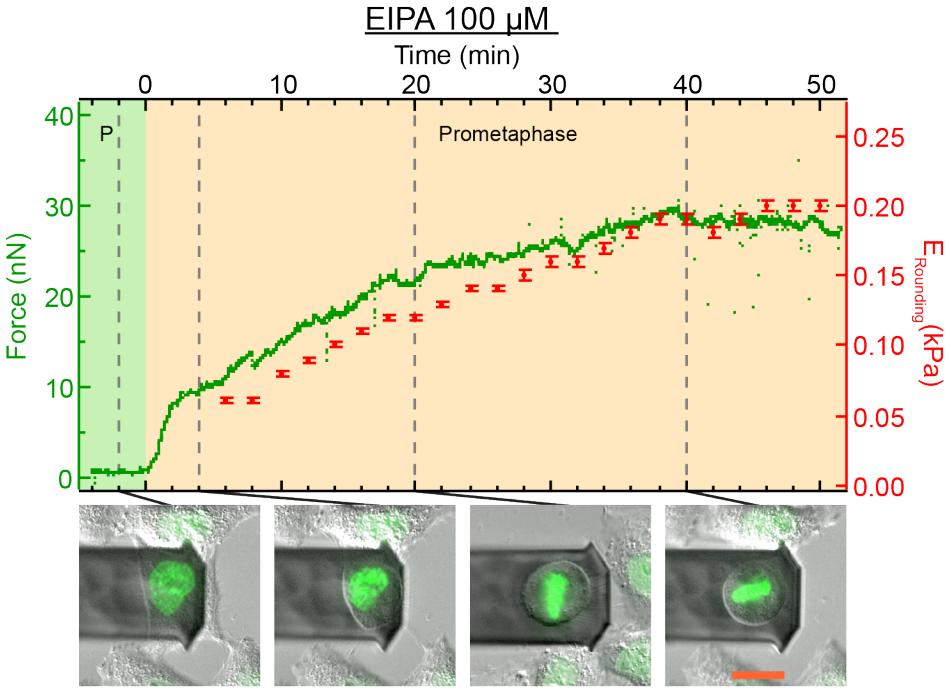
EIPA 100 µM
Time (min)
0
10
20
30
40
50
P
Prometaphase
Force (nN)
40
30
20
10
0
0.25
0.20
0.15
0.10
0.05
0.00
E Rounding (kPa)

P

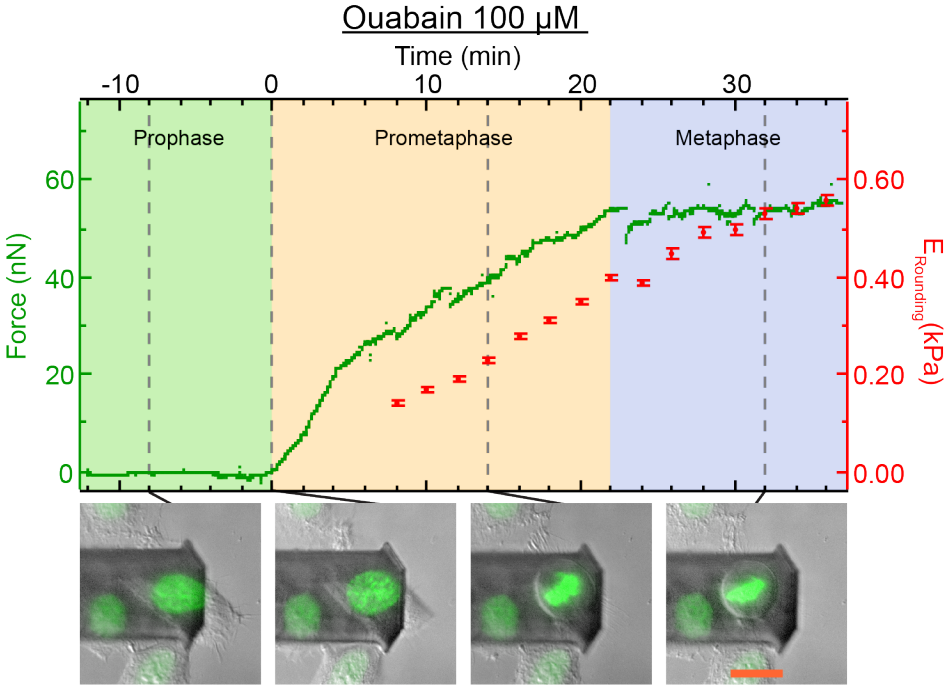
Ouabain 100 µM
Time (min)
-10
0
10
20
30
Prophase
Prometaphase
Metaphase
Force (nN)
60
40
20
0
0.60
0.40
0.20
0.00
E Rounding (kPa)

Q

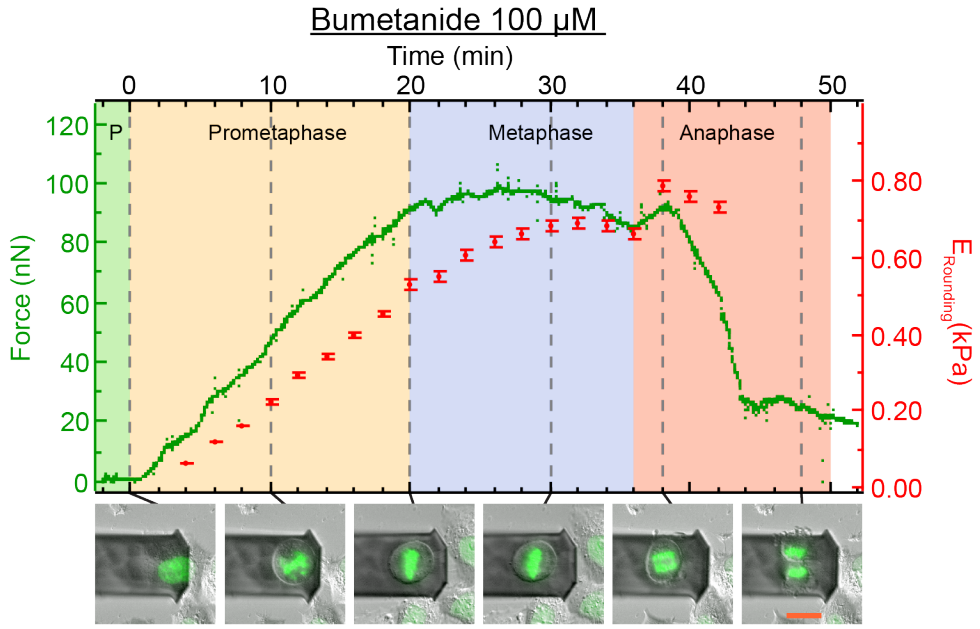
Bumetanide 100 µM
Time (min)
0
10
20
30
40
50
P
Prometaphase
Metaphase
Anaphase
Force (nN)
120
100
80
60
40
20
0
0.80
0.60
0.40
0.20
0.00
E Rounding (kPa)

R

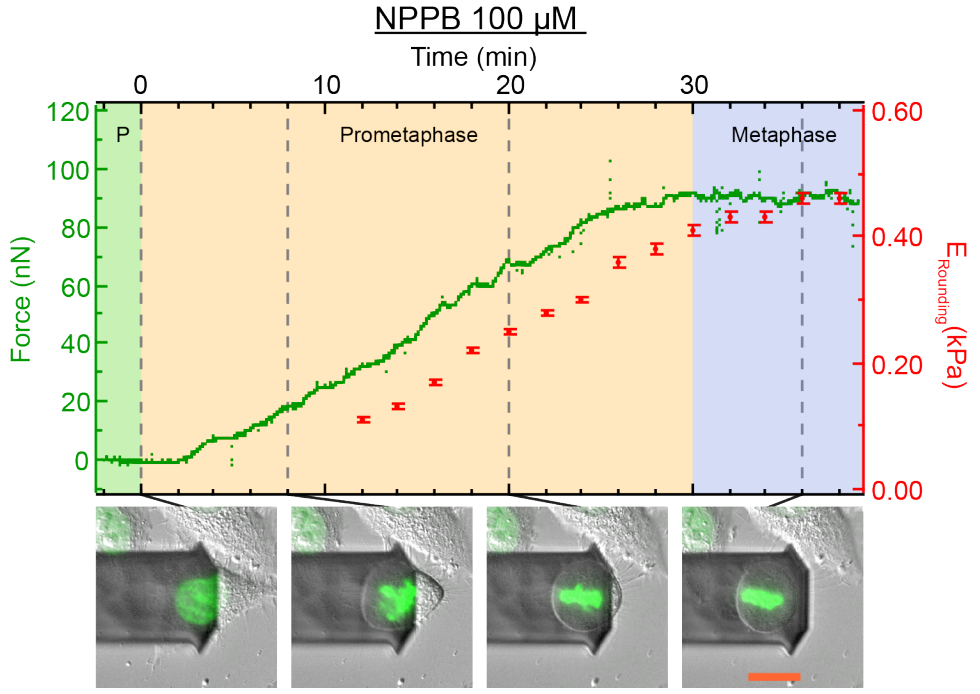
NPPB 100 µM
Time (min)
0
10
20
30
P
Prometaphase
Metaphase
Force (nN)
120
100
80
60
40
20
0
0.60
0.40
0.20
0.00
E Rounding (kPa)

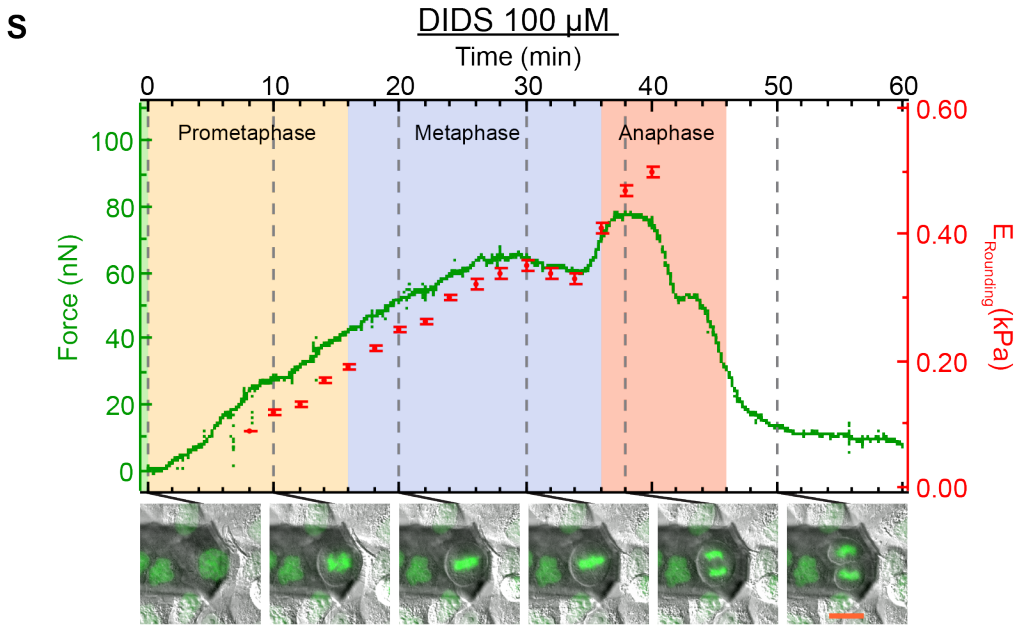

Figure 18: Probing the mechanics of mitotic cell rounding with the trans-mitotic CHA on single cells preincubated with the following perturbants: **A(i)** Latrunculin A, an actin monomer sequester, 40 nM, **(ii)** which caused cyclic blebbing upon arrival at a critical pressure (two characteristic cycles are shown), **B** and 200 nM, **C** Cytochalasin D, an actin barbed end capper, 500 nM, **D** Jasplakinolide, an F-actin stabilizer, 50 nM **E** and 100 nM, **F** Y-27632, a Rho kinase inhibitor, 100 µM, **G** Blebbistattin, a myosin II inhibitor, 100 µM, **H** ML-7, a Myosin light chain kinase inhibitor, 100 µM, **I** Nocodazole, a microtubule depolymerizer, 333 nM, **J** Vinblastine, a microtubule depolymerizer, 100 nM, **K** STC, a kinesin eg-5 inhibitor, 2 µM, **L** Taxol, a microtubule stabilizer, 100 nM, **M** Deoxycholate, a detergent used to lower membrane tension, 200 µM, **N** Dynasore, a dynamin inhibitor, 100 µM, **O** EIPA, an inhibitor of Na^+/H^+ exchange, 100 µM, **P** Ouabain, a Na^+/K^+ ATPase inhibitor, 100 µM, **Q** Bumetanide, an inhibitor of $K^+Na^+2Cl^-$ symport, 100 µM, **R** NPPB, an inhibitor of Cl^- transport, 100 µM, **S** and DIDS, an inhibitor of Cl^- transport, 100 µM. Cells were preincubated in perturbants for a minimum of 10 mins before commencement of experiments except in the case of **O** EIPA 100 µM and, **P** Ouabain 100 µM, which were added in mid-prophase because they otherwise prevented entry into mitosis[149, 150]. The following inhibitors arrested cells in prometaphase: **I** Nocodazole 333 nM, **J** Vinblastine 100 nM, **K** STC 2 µM, **L** Taxol 100 nM, **N** Dynasore 100 µM. Other inhibitors were frequently found to slow prometaphase/metaphase: **O** EIPA 100 µM, **P** Ouabain 100 µM, **R** NPPB 100 µM, **S** and DIDS 100 µM. H2B-GFP imaging was not used in the blebbistatin trans-mitotic CHAs **(G)** due to photoinactivation of blebbistatin by blue light[151, 152]. Instead one initial H2B-GFP image was used to indentify a candidate prophase cell then anaphase was assigned with DIC. Scale bars: 20 µm. See figures 9 and 10 for experimental details on the 8 µm trans-mitotic CHA.

Summary of Inhibitor Results

For each of the inhibitor experiments above (Fig 18A-S) the rounding force, pressure, modulus and volume were determined at the mitotic maximum for each cell tested (Fig 19).

In the case of the mechanical parameters (rounding force, pressure and modulus) all actomyosin inhibitors, except for the relatively non-specific ML-7[153], showed a clear dose-response decrease. In contrast, perturbing microtubule structure was not detrimental or even tended to augment mechanical response. Attempting to perturb membrane tension with dynasore or the detergent deoxycholate did not convincingly change mechanics. The statistically significant, but relatively minor effect of deoxycholate on rounding modulus may be due to the observed toxicity of this harsh agent on cells (altered morphology and accumulation of vacuoles were observed). Treatment with transport inhibitors established a role for Na^+/H^+ exchange in the mechanics of MCR. Results from the detachment agents exhibited lower forces due to sliding of cells along the cantilever (Figs 14 & 15). When the data was corrected for this effect with the rounding modulus parameter, there was no significant reduction. Indeed, there was even an increase observed for cells maintained in trypsin, probably due to activation of various pathways such as RhoA by protease-activated receptors[63, 102, 154].

The volume data is not as clear (Fig 19). Several doses of the actomyosin inhibitors showed statistically significant changes in volume out of step with the dose-response trends. This was more likely due to day-to-day variability in cell size and indicates that larger n-values are required to make solid conclusions on mitotic cell volume in HeLa cells. While taxol, ouabain, dynasore, and live trypsin caused statistically significant changes in mitotic cell volume, the meaning of these results remains unclear. For the case of taxol and trypsin, the concurrence of increased volume and rounding modulus may indicate a detectable increase in osmolyte accumulation but an obvious mechanism is unclear. To make stronger conclusions from the

equilibrium cell volume data would require further investigation and higher throughput methods to gather larger datasets.

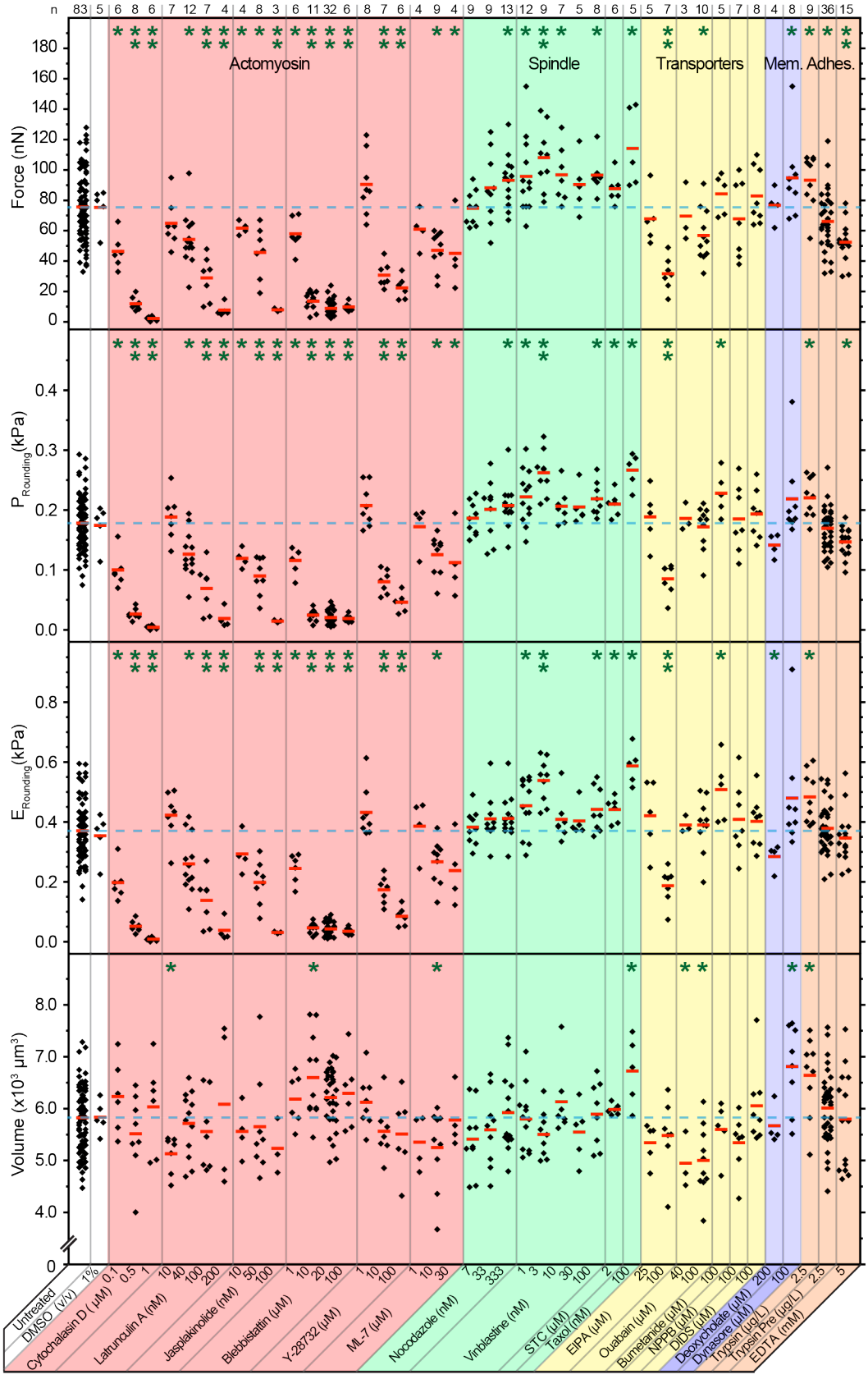

Figure 19: Rounding force, pressure, modulus, and volume at the mitotic maximum for cells preincubated with indicated perturbants and doses in 8 μm trans-mitotic CHAs. See Figs 10A,14,15,18 for example graphs of each condition and details on perturbants. Perturbant categories are actomyosin (red), spindle and microtubules (green), transporters implicated in volume regulation (yellow), membrane properties (blue), and adhesion (orange). p values (Mann-Whitney, two tailed) are designated *<0.05, ‡<0.001. The number of cells tested is given above each column. Horizontal, dashed blue lines show averages of the untreated condition.

Observations on Cell Rounding Rates with Inhibitors

In the course of the trans-mitotic CHA experiments it was noted that several treatments enhanced the post-NEBD force generation rate (Fig 20A). In particular, the microtubule destabilizing agents nocodazole and vinblastine exhibited a clear dose-response increase on force generation rate (Fig 20C). This may be because microtubule disassembly is known to augment RhoA-based actomyosin contractility via GEF-H1 signaling[56]. Acceleration of de-adhesion at mitotic entry could also be a contributing factor. Despite more rapid force generation rates at mitotic onset, the plateau forces attained were not significantly different (Fig 20C). This suggests that the effect of microtubule depolymerization on force generation may saturate at a threshold in mitosis. Notably, the nocadazole and vinblastine results were not generally related to the effects of prometaphase arrest because other agents that caused prometaphase arrest without microtubule depolymerization (STC, taxol, dynasore) did not promote accelerated rounding forces at mitotic onset.

Another interesting case of increased force generation rates occurred with the actin-stabilizing drug jasplakinolide. Although it retarded the plateau force attained in mitosis, it significantly increased immediate post-NEBD force rate when applied at intermediate concentrations. This suggests that incubation of mitotic cells with the drug may accelerate the stress fiber to cortex transition in the actomyosin cytoskeleton.

Overall, the observations on enhanced force generation rates reveal kinetics relating to the shift in the adherent to rounded shape transition at

mitotic onset. They also demonstrate the utility of the trans-mitotic CHA in tracking cellular mechanics phenomena at high temporal resolution.

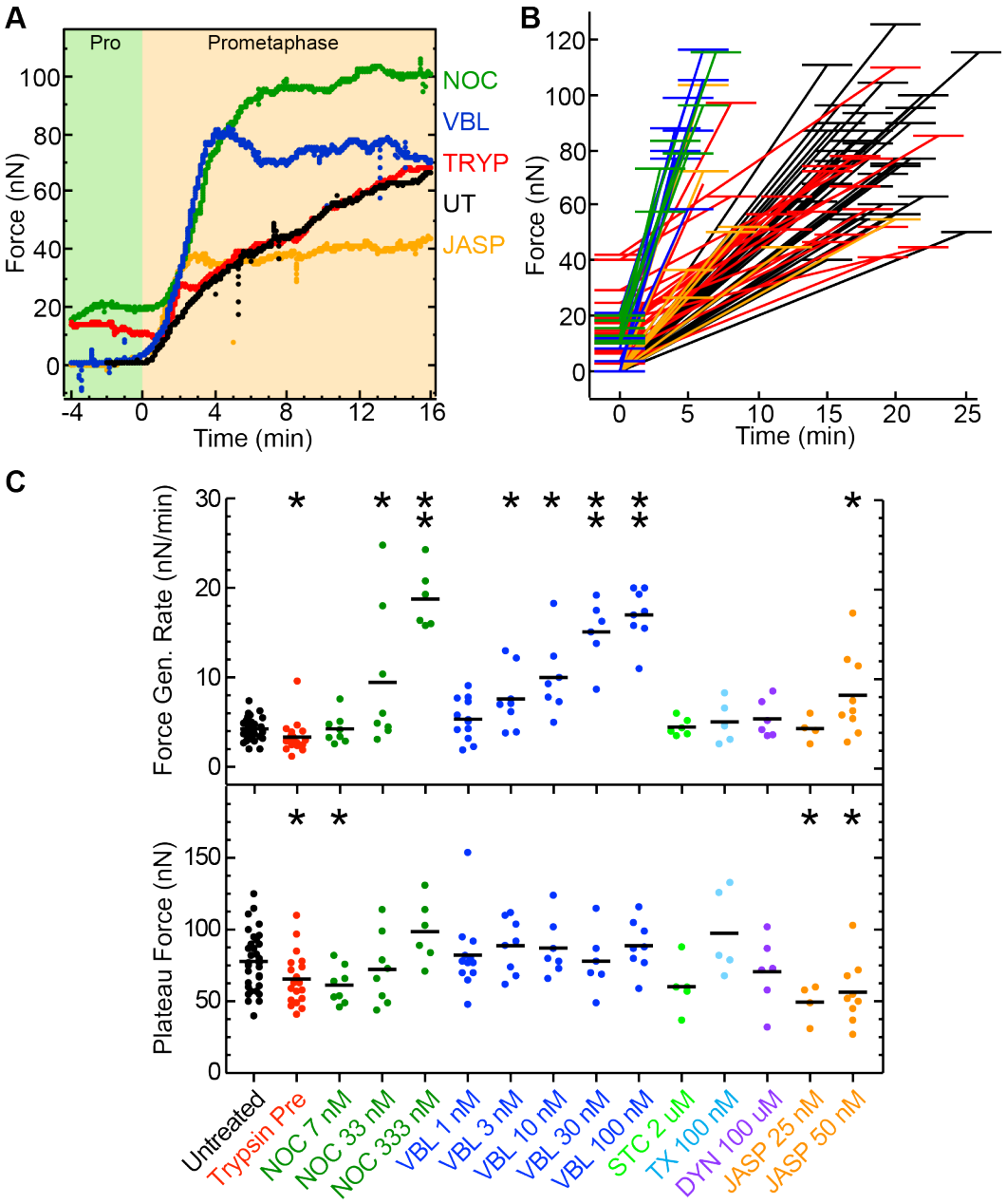

Figure 20: Post-NEBD force generation rates of cells treated with various perturbants in the 8 μm trans-mitotic CHA. **A** Examples of perturbants that alter post-NEBD force generation rates. Superimposed examples are UT (Untreated, black, Fig 10A), TRYP (Trypsin pre-rounded (2.5 μg/mL, then washout before experiment), red, Fig 14A), JASP (50 nM Jasplakinolide, orange, Fig 18D), NOC (333 nM Nocodazole, green, Fig 18I), VBL (100 nM Vinblastine, blue, Fig 18J). Cells were preincubated in perturbants for a minimum of 10 mins before commencement of experiments except in the case of trypsin, which was washed out and returned to normal medium. Mitotic phase assignment was based on the appearance of chromosomes (see methods). Time zero is aligned to prometaphase onset as defined by nuclear envelope breakdown (NEBD). See figures 9 and 10 for further experimental details on the 8 μm trans-mitotic CHA. **B** Force gradient trajectories for experiments with perturbants and colour schemes

shown in A. The flat marker at time zero represents the NEBD value while the corresponding marker represents the post-NEBD plateau value. Connecting lines indicate force gradient trajectories between the two points. At time zero, all Untreated (black) and Jasplakinolide (orange) examples start at zero while the majority of Nocodazole (green) and Vinblastine (blue) examples are more than 8 μm high as evidenced by measurement of non-zero forces. Trypsin treated cells (red) exhibit non-zero forces because they start pre-rounded. **C** Scatter plots of force gradients and plateau forces from trajectories in B. Perturbants are as above, as well as additional inhibitors that result in prometaphase arrest: STC (S-trityl-L-cysteine, light green, Fig 18K), TX (Taxol, blue, Fig 18L), and DYN (Dynasore, purple, Fig 18N). p values (Mann-Whitney, two tailed) are designated *<0.05, ⁑<0.001.

Observations on Cell Blebbing with Inhibitors

Blebs form when a section of membrane detaches from the actomyosin cortex[127] and retract when the actomyosin cortex reassembles underneath the membrane and pulls the bleb back into the main cell body[128]. In order for blebbing to occur cells must possess a critical amount of actomyosin cortex tension and intracellular pressure[92, 119]. Then, a bleb is thought to nucleate either because of a structural defect in the actomyosin cortex underlying the membrane or because of local detachment of the membrane from the cortex[155]. In the trans-membrane CHAs (Fig 18) blebbing in mitotic cells was observed with the actin perturbants latrunculin A, cytochalasin D, and jasplakinolide, and to a lesser extent by indirect actomyosin contractility stimulation with nocodazole, vinblastine, and trypsin. On the other hand, blockers of actomyosin contractility are known to suppress blebbing[119, 129, 155]. In accordance with this, Y-27632, blebbistatin, and ML-7 treated cells did not bleb in the 8 μm trans-mitotic CHA. Interestingly, inhibition of Na^+/H^+ exchange not only reduced the rounding pressure measured in the 8 μm CHA but additionally attenuated the polar blebbing characteristic of anaphase (Fig 21). This is consistent with a report from Mercer and Helenius which showed that EIPA and blebbistatin both reduced prevalence of blebbing[156]. These results further reinforce the idea that Na^+/H^+ exchange is involved in the control of intracellular pressure in mitosis.

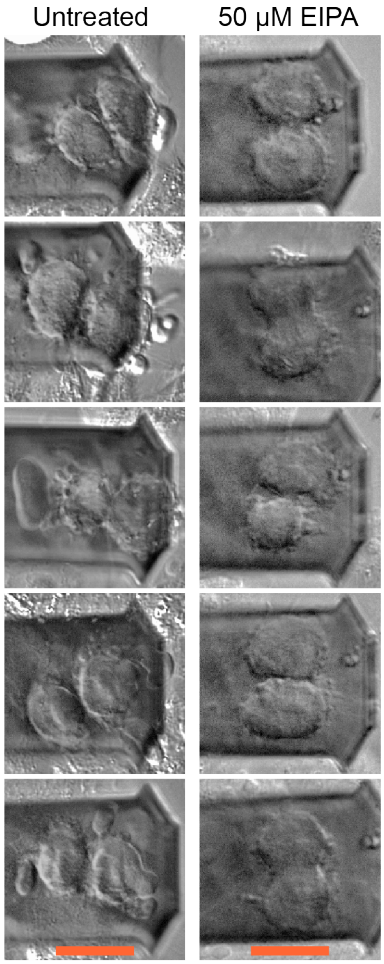

Figure 21: Suppression of characteristic cytokinetic polar blebbing with 50 µM EIPA, an inhibitor of Na^+/H^+ exchange. Images were acquired with DIC post-anaphase in a typical 8 µm trans-mitotic CHA. Scale bar 20 µm.

Dynamic perturbations

In the previous sections of this thesis mitotic cells were preincubated with inhibitors in the 8 µm trans-mitotic CHA or CFA to dissect the role of specific cellular processes in MCR. In accordance with the literature, those results demonstrated the indispensible nature of the actomyosin cortex in generating the driving forces that underlie many shape changes[30]. On the other hand, they also inferred a role for intracellular pressure changes that have been little emphasized by previous studies. To further understand and characterize this, an assay that measures both volume and pressure at high temporal resolution was required. Therefore, the 8 µm CHA was used for the comparison of rounding modulus and volume in single cells before, after and during recovery from real-time perturbations. The following section outlines

these experiments. Such experiments enabled the homeostatic regulation of pressure and volume to be tested in what will be henceforth termed “dynamic perturbation” experiments.

Tonic shocks

For mitotic cells in the CHA, the force on the cantilever could be a result of osmotic pressure. If the osmolarity is higher inside the cell than outside, water will flow into the cell and generate a hydrostatic pressure. To test this idea, the osmolarity of the medium was modulated in real-time. Introduction of hypotonic medium (-Δ100 mOsm) led to an immediate increase in the volume of metaphase cells (40±7%; n=9), indicating that water entered the cells (Fig 22A). This was accompanied by a concurrent increase in the measured rounding modulus (64±21%; n=9), presumably because the intracellular pressure increased. Within 5 minutes of changing the osmolarity, the cell volume and rounding pressure returned close to original levels. This is probably because, in response to increased osmotic pressure, regulatory volume decrease (RVD) causes cells to release ions[140]. Conversely, when hypertonic medium (+Δ200 mOsm) was introduced (Fig 22B) the changes in volume (-22±8%; n=9) and rounding modulus (-20±14%; n=9) were in the opposite direction. Again, the cells recovered the original rounding pressure and volume, presumably because regulatory volume increase (RVI) triggers the influx of osmolytes[140]. These experiments suggest that mitotic cells regulate setpoints in pressure and volume.

Actomyosin

To further probe the link between osmotic pressure and actomyosin contraction, experiments that spontaneously abolish or stimulate the actomyosin cortex were performed. If there is an intracellular pressure opposed by the actomyosin cortex, disruption of the cortex should result in dissipation of intracellular pressure and a small increase in cell volume. When the actomyosin cortex was dissolved with latrunculin A, cells erupted into a mess of irregularly shaped blebs, which made volume analysis impractical. Therefore mitotic cells were first preincubated with blebbistatin

to prevent myosin II related blebbing, and then with latrunculin A to depolymerize actin filaments. While this approach reduced the "starting" rounding modulus of cells by ~four-fold it successfully yielded a smooth cell shape with tractable volume analysis. Indeed, upon abolition of the cortex with latrunculin A, the volume of mitotic cells increased (7±4%; n=36) and the mitotic rounding modulus was completely abolished (Fig 22C). Conversely, the effects of instantaneous activation of the actomyosin cortex were examined. To do this blebbistatin's propensity to be inactivated by blue light[151, 152] was utilized. When blebbistatin was photoinactivated mitotic cells responded with an increase in rounding pressure (502±194% n=7) and decrease in volume (4±2% n=7) (Fig 22D(i)). These results emphasize the role of myosin II as a generator of contractile force in the actomyosin cortex, as opposed to one of a mere crosslinker[157]. Indeed, if myosin II were purely a crosslinker, it would be expected to stiffen the preexisting cell shape rather than contract and push up against the cantilever (Fig 22D(ii)). One can therefore conclude that stimulating contraction of the actomyosin cytoskeleton increases rounding pressure and decreases volume, while abolishing the actomyosin cortex reduces rounding pressure and increases volume.

Na^+/H^+ Exchange

Next, the source of the intracellular pressure that counteracts the actomyosin cortex was probed with dynamic perturbations affecting osmolyte transport processes. Since ion transporters at the plasma membrane increase intracellular osmotic pressure and restore volume of cells immediately after hypertonic challenge (Fig 22B), it is plausible that they might contribute to the increased rounding pressure seen in mitosis. In accordance with this notion, the Na^+/H^+ exchange inhibitor EIPA was previously observed to attenuate buildup of rounding modulus in cells transitioning into mitosis (Fig 18 O). Therefore it was hypothesized that addition of EIPA to metaphase cells in the CHA might lead to a decrease in pressure and/or volume. Metaphase cells in the CHA subject to an influx of 50 μM EIPA underwent a decrease in rounding modulus (-47±12%; n=19)

and volume (-8±2%; n=19; Fig 22E) over a ~5 minute period. Interestingly, after this initial change, cells were gradually able to recover rounding modulus (76±61%) without major changes in volume (3±4%). This suggests that alternative mechanisms may establish a new equilibrium and compensate for the loss of Na^+/H^+ exchange capacity. Indeed, redundancy is often observed as a fundamental principle in osmolyte regulation, as the cell selects the regulation mechanism with the least untoward impact on cellular function[140]. The EIPA perturbation experiments show that maintenance of Na^+/H^+ exchange is linked to mitotic cell mechanics.

Plasma Membrane Permeability

Another strategy to perturb osmolyte regulation is to alter the permeability of the plasma membrane. To this end the pore-forming toxin (PFT) *Staphylococcus aureus* α-toxin, which confers permeability to monovalent cations[158], was employed. Dose-response experiments showed that concentrations ≤ 20 μg/ml had no noticeable effect on cells, concentrations from 40-80 μg/ml were sublytic and caused a gradual reduction in volume and rounding modulus, and concentrations ≥ 100 μg/ml caused rapid lysis. In general, PFT induced lysis is purported to occur because of osmotic swelling that accompanies breakdown of the plasma membrane[159, 160], and is a ubiquitous phenomenom across many cell types. The novel result occurs in the sublytic concentration window, which caused a decrease in both volume (-41±5%; n=8) and rounding modulus (-79±12%; n=8; Fig 22F). Both of these parameters were found to decay over ~30 mins in a relationship resembling a negative exponential. Although such cell shrinkage has been previously observed (Sucharit Bhakdi private communication), there are presently no published reports on its mechanism in the literature. Therefore, the sublytic cell shrinkage phenomenon was studied further in the context of mitotic cells.

Actomyosin cortex contraction might contribute to α-toxin induced cell shrinkage by providing an inward directed hydrostatic pressure. In a cell with an unperturbed plasma membrane this actomyosin based hydrostatic pressure (in the range of 0.5 kPa) converts to an osmotic pressure[119].

However, in the case of a cell with an α-toxin perforated plasma membrane, the cytoplasm may not be capable of maintaining such an osmotic gradient, and perpetual shrinkage could result. To test this idea, the contractility and structure of the actomyosin cortex was disrupted with blebbistatin and latrunculin A respectively (as in Fig 22C), then α-toxin was introduced to the cell medium. Volume reduction again resembled a negative exponential decay profile over ~30 mins, but the magnitude was considerably decreased (-25±8%; n=10; Fig 22G). No change in rounding modulus occurred in this case because it was already zero before addition of the toxin. To demarcate the role of myosin II contraction on toxin-induced shrinkage, cells were preincubated exclusively with blebbistatin and then exposed to α-toxin in the same assay. Volume (-40±5%; n=8) and rounding modulus (-83±25%; n=5; Fig 22H) decreased to a similar extent as with untreated cells (Fig 22F). These results suggest that reducing cortical tension is not enough to prevent α-toxin induced cell shrinkage, but that a structurally intact actomyosin cortex does contribute.

To test the possibility that the effects of α-toxin were due to intracellular ATP leakage through α-toxin pores, experiments with cells additionally incubated in an exogenous source of ATP were conducted. 5 mM exogenous ATP did not substantially alter the response of mitotic cells to α-toxin (Fig 22I). The volume decrease (-45±5%; n=7) was not significantly different to untreated cells while the reduction in rounding modulus was also relatively standard (-70±23%; n=7). Therefore, it was concluded that the effects of α-toxin on cell volume were not due to leakage of ATP.

Another possible explanation for the α-toxin induced cell shrinkage could be the active transport of osmolytes out of the cell. The fact that the shrinkage occurs over tens of minutes lends support to the idea that an ongoing active process may drive the shrinkage. It was therefore hypothesized that the activity of the Na^+/K^+ ATPase might contribute to the phenomenon. To test for this, the ATPase was blocked with the specific inhibitor ouabain[142] before exposure of cells to α-toxin (Fig 22J). In contrast to other treatment combinations, the cell expanded and volume

increased (48±16%; n=4). Curiously, this was accompanied by a decrease in rounding modulus (-81±22%; n=4), as an influx of water might be expected to maintain or increase the rounding pressure against the cantilever if all other factors were held equal. This suggested that the actomyosin cortex was non-specifically compromised by the combination of ouabain and α-toxin because it could not encapsulate the pressure of osmolyte influx.

For the sake of comparison another pore-forming toxin, *E. coli* hemolysin A (HlyA), was assessed in the 8μm CHA. In contrast to α-toxin which only confers permeability to monovalent cations, HlyA renders the plasma membrane permeable to all cations[161]. Dose-response experiments showed that concentrations ≤1 μg/ml had no noticeable effect on cells, concentrations ~2 μg/ml were sublytic, and caused a reduction in volume, and concentrations ≥4 μg/ml caused rapid lysis. 2 μg/ml of HlyA applied to metaphase cells caused significant volume reduction (-16±5%; n=5) while rounding modulus was almost unchanged (-2±8%; n=5, Fig 22K). Skals et al. also found a 15-20% volume decrease as measured by forward scattering flow cytometry[162]. The difference in results from the PFTs HlyA and α-toxin are likely due to the difference in Ca^{2+} permeability. Because intracellular Ca^{2+} concentrations are about 10^4 fold lower than extracellular concentrations, Hlya treatment triggers large calcium influxes[161]. Since calcium is an important second messenger in many cellular signaling pathways (including, for example, actomyosin contraction and osmolyte flux), the different response of cells to the two PFTs is likely due to variations in calcium levels. Interestingly, many cell types are capable of rapid recovery from sublytic concentrations of HlyA[161] and in experiments on mitotic cells, volume and rounding modulus were often seen to dip and then recover (Fig 22K). It was therefore concluded that the physiology of the HlyA response is complicated by calcium signaling effects and the corresponding α-toxin shrinkage phenomena is not directly comparable.

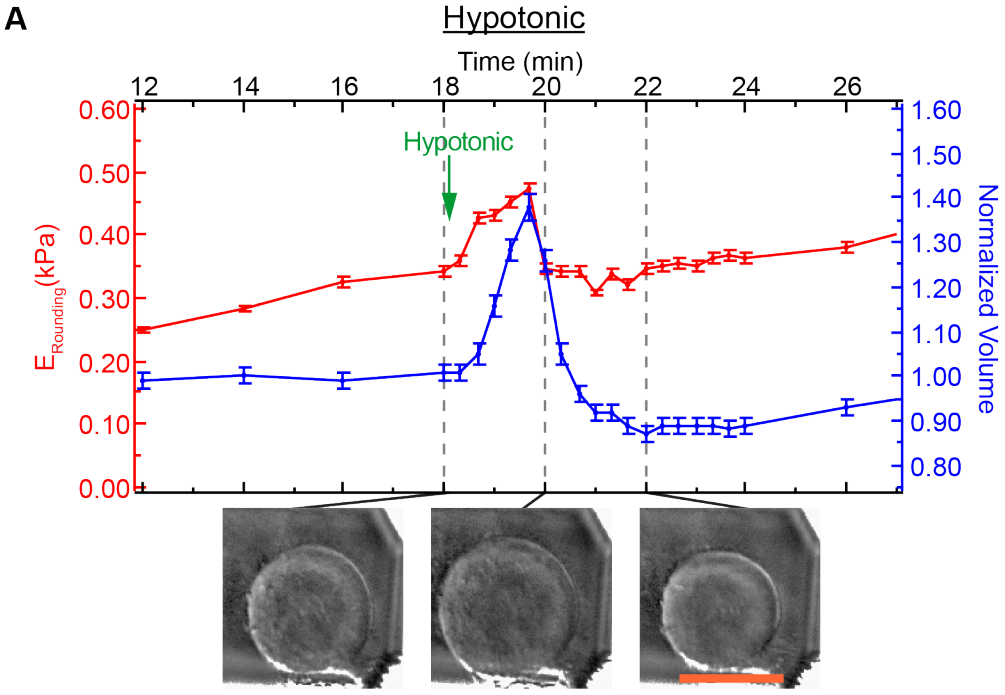
A
Hypotonic
Time (min)
12
14
16
18
20
22
24
26
Hypotonic
0.60
0.50
0.40
0.30
0.20
0.10
0.00
E_Rounding (kPa)
1.60
1.50
1.40
1.30
1.20
1.10
1.00
0.90
0.80
Normalized Volume

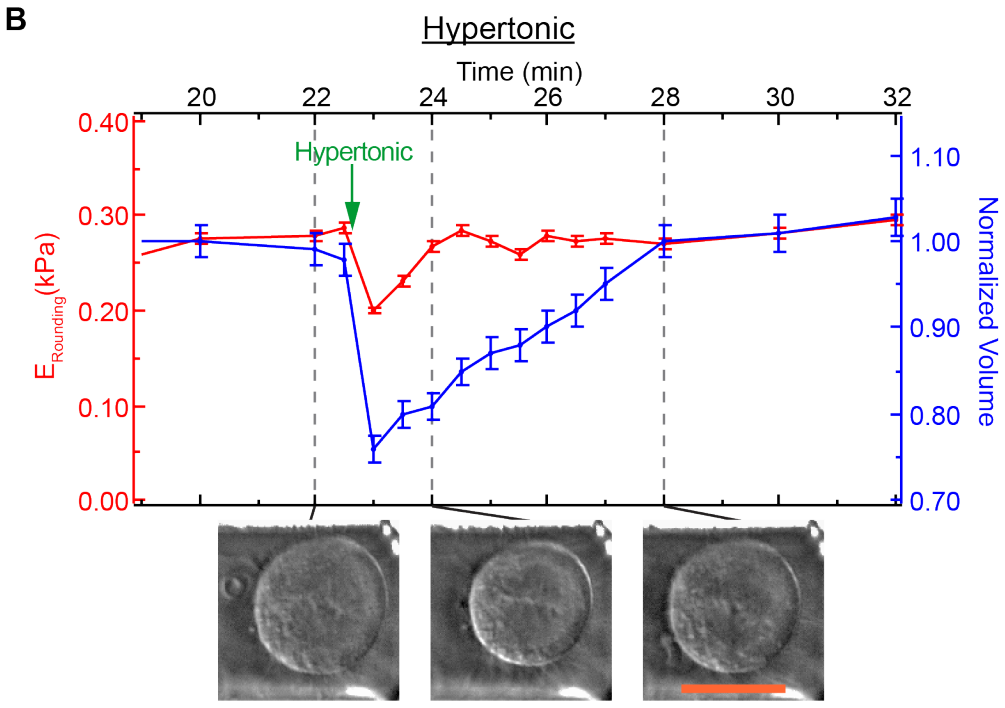
B
Hypertonic
Time (min)
20
22
24
26
28
30
32
Hypertonic
0.40
0.30
0.20
0.10
0.00
E_Rounding (kPa)
1.10
1.00
0.90
0.80
0.70
Normalized Volume

C

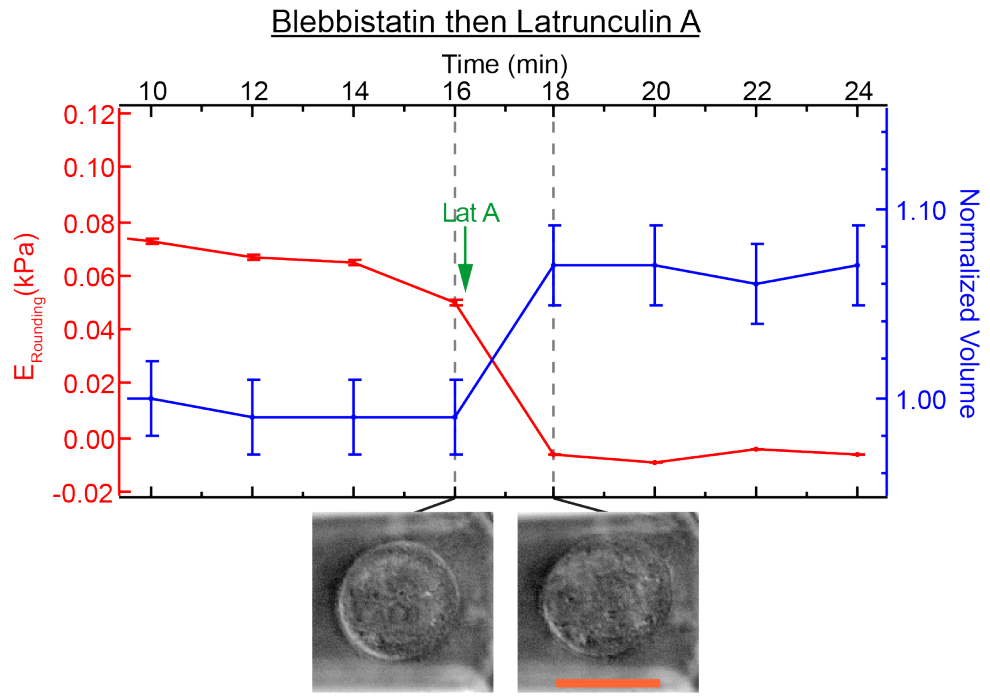
Blebbistatin then Latrunculin A
Time (min)
10
12
14
16
18
20
22
24
0.12
0.10
0.08
0.06
0.04
0.02
0.00
-0.02
E_Rounding (kPa)
Lat A
1.10
1.00
Normalized Volume

D (i)

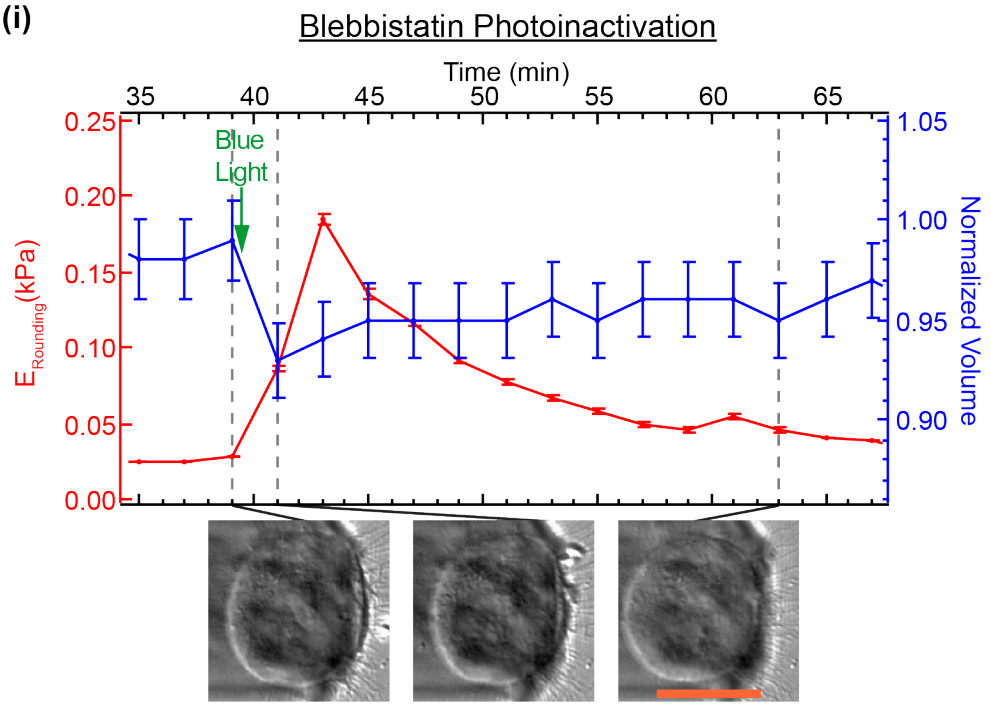
Blebbistatin Photoinactivation
Time (min)
35
40
45
50
55
60
65
0.25
0.20
0.15
0.10
0.05
0.00
E_Rounding (kPa)
Blue
Light
1.05
1.00
0.95
0.90
Normalized Volume

(ii)

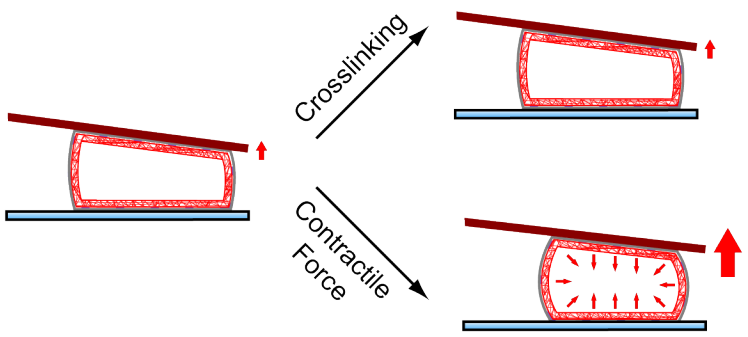
Crosslinking
Contractile
Force

E

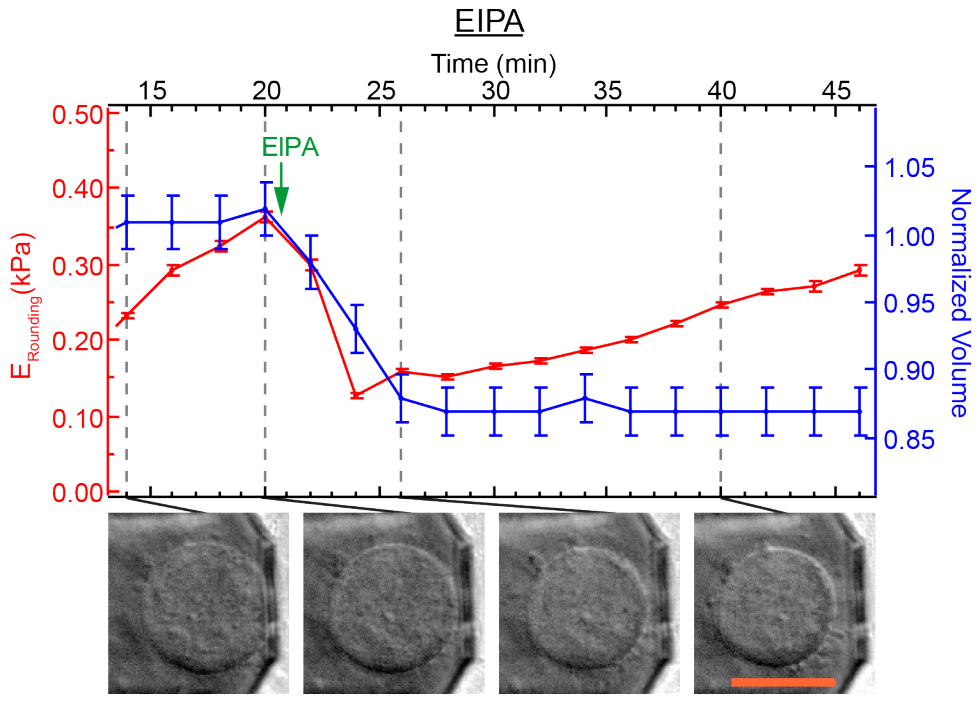
EIPA
Time (min)
15
20
25
30
35
40
45
EIPA
0.50
0.40
0.30
0.20
0.10
0.00
E Rounding (kPa)
1.05
1.00
0.95
0.90
0.85
Normalized Volume

F

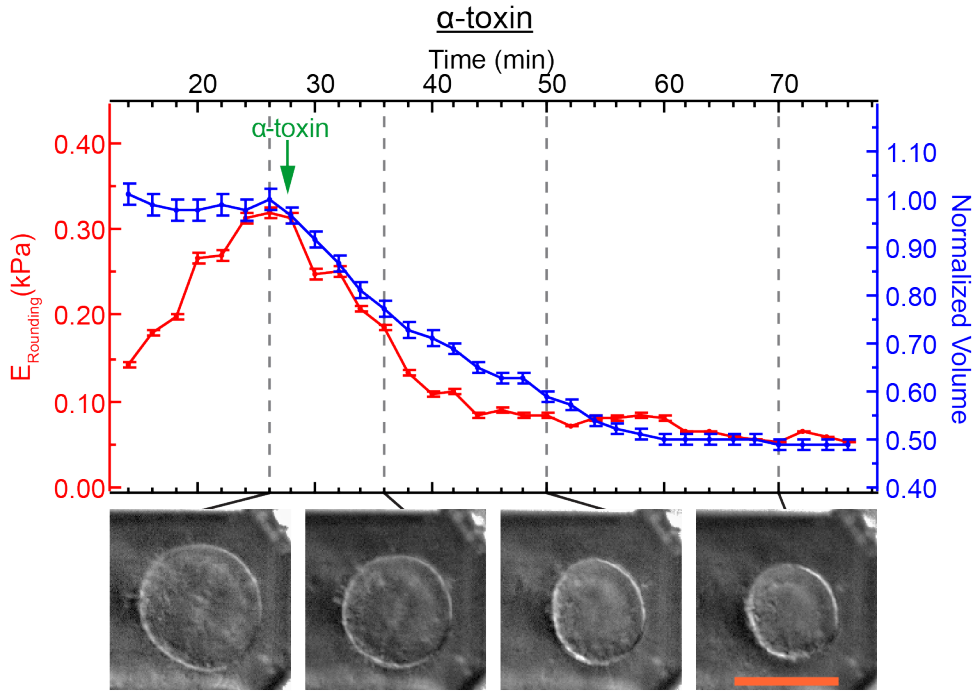
α-toxin
Time (min)
20
30
40
50
60
70
α-toxin
0.40
0.30
0.20
0.10
0.00
E Rounding (kPa)
1.10
1.00
0.90
0.80
0.70
0.60
0.50
0.40
Normalized Volume

G

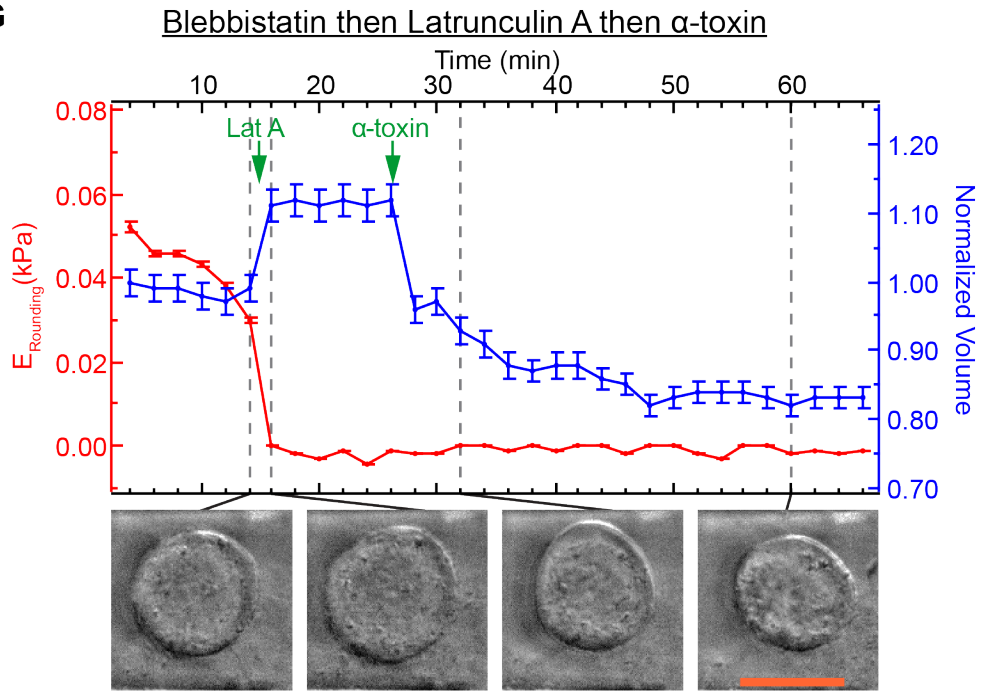
Blebbistatin then Latrunculin A then α-toxin
Time (min)
10
20
30
40
50
60
Lat A
α-toxin
0.08
0.06
0.04
0.02
0.00
E_Rounding (kPa)
1.20
1.10
1.00
0.90
0.80
0.70
Normalized Volume

H

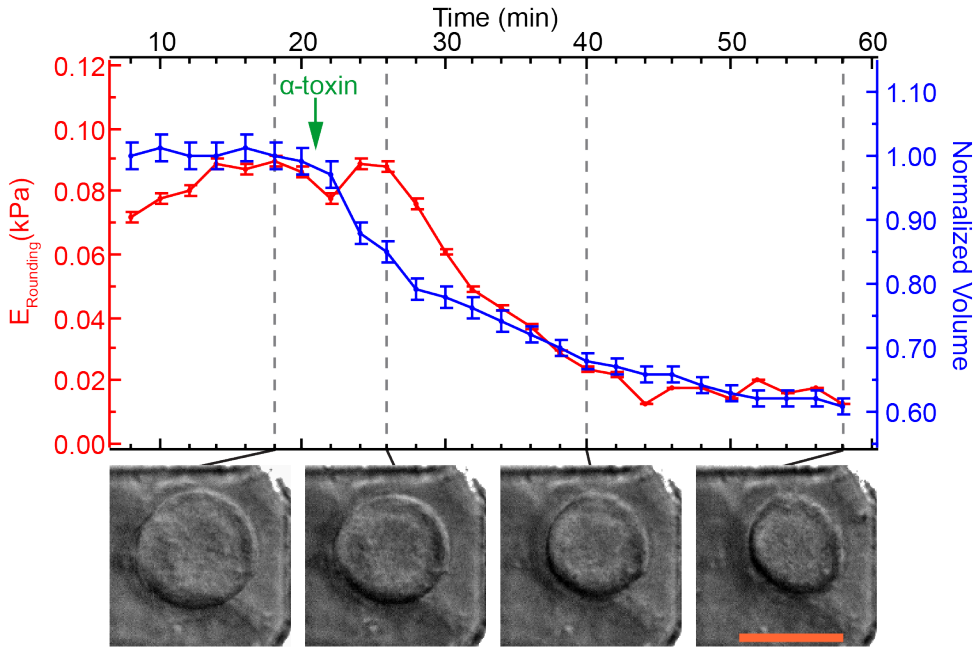
Blebbistatin then α-toxin
Time (min)
10
20
30
40
50
60
α-toxin
0.12
0.10
0.08
0.06
0.04
0.02
0.00
E_Rounding (kPa)
1.10
1.00
0.90
0.80
0.70
0.60
Normalized Volume

I

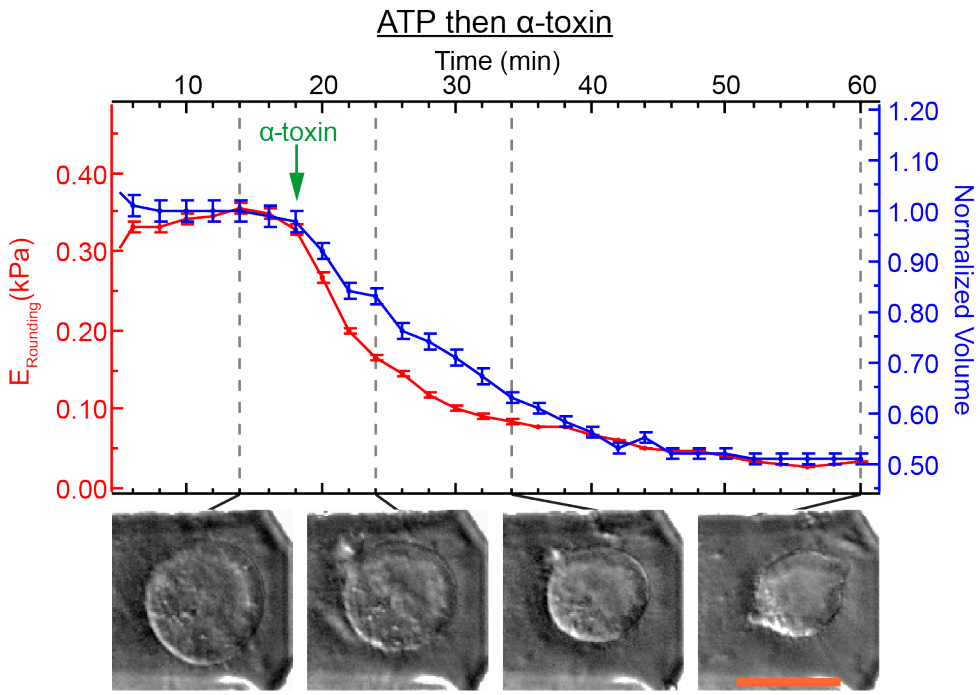
ATP then α-toxin
Time (min)
10
20
30
40
50
60
α-toxin
0.40
0.30
0.20
0.10
0.00
E Rounding (kPa)
1.20
1.10
1.00
0.90
0.80
0.70
0.60
0.50
Normalized Volume

J

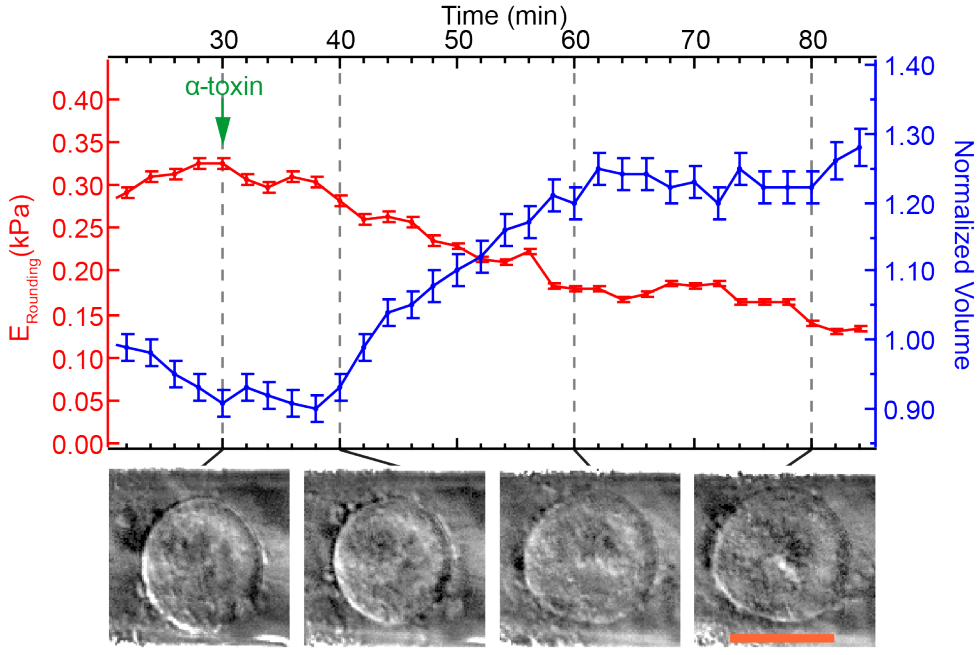
Ouabain then α-toxin
Time (min)
30
40
50
60
70
80
α-toxin
0.40
0.35
0.30
0.25
0.20
0.15
0.10
0.05
0.00
E Rounding (kPa)
1.40
1.30
1.20
1.10
1.00
0.90
Normalized Volume

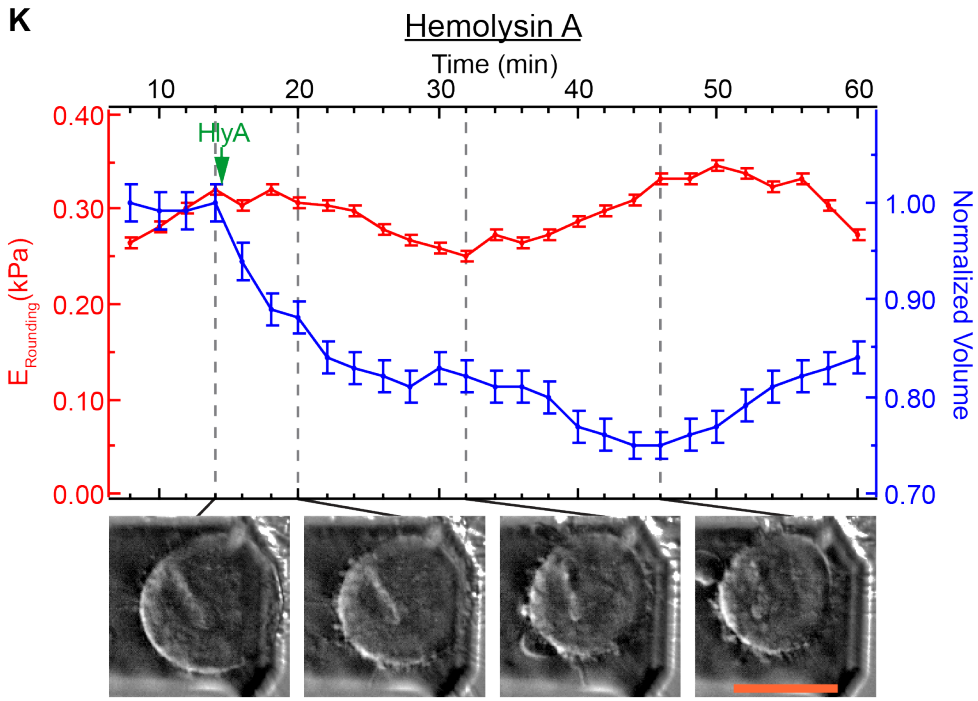

Figure 22: Probing the balance of mechanical forces in mitotic cell rounding with 8 µm CHAs and the following mid-experiment, instantaneous perturbations: **A** Hypotonic shock, n=9 (300 mOsm → 200 mOsm), **B** Hypertonic shock (300 mOsm → 500 mOsm), **C** 1 µM Latrunculin A (10 µM Blebbistatin, 2 µM STC, preincubation), **D** 10 mM Blebbstatin photoinactivated with blue light, **E** 50 µM EIPA, **F** 60 µg/mL α-toxin, **G** 1 µM Latrunculin A, then 60 µg/mL α-toxin (10 µM Blebbistatin, 2 µM STC preincubation), **H** 60 µg/mL α-toxin (10 µM Blebbistatin, 2 µM STC, preincubation), **I** 60 µg/mL α-toxin (5 mM ATP preincubation), **J** 60 µg/mL α-toxin (100 µM Ouabain preincubation), **K** 2 µg/mL Hemolysin A. Time zero defines the start of the experiment and is arbitrary relative to the cell cycle. H2B-GFP imaging was not performed in experiments featuring blebbistatin due to photoinactivation of blebbistatin by blue light[151, 152]. Instead one initial H2B-GFP image was used to check the cell cycle phase of candidate cells then they were monitored with DIC thereafter. Part **D(ii)** depicts a hypothesis of two possibilities upon blebbistatin photoinactivation. In the first, myosin II acts as a crosslinker and would stabilize the preexisting shape. In the second, myosin II represents an active contractile force generator and would lead to alterations in pressure and volume. $E_{rounding}$ and normalized volume error bars are ±2% (see Fig 9). Vertical gray dashed lines correspond with DIC images shown below each graph. See figures 9 and 10 for further experimental details on the 8 µm trans-mitotic CHA. Scale bars: 20 µm.

Summary of Dynamic Perturbation Results

The dynamic perturbation experiments show that perturbation of osmotic gradients, associated transporters and the actomyosin cortex caused changes in both volume and rounding pressure (see graph Fig 23A, diagram Fig 23B, and table 1). When osmotic pressure was reduced, rounding modulus and volume decreased (Fig 23, lower left quadrants). Conversely, if osmotic pressure was increased, rounding modulus and volume increased (Fig 23, upper right quadrants). When the actomyosin cytoskeleton was abolished, cell volume increased while rounding pressure decreased (Fig 23, lower right quadrants). However, stimulation of actomyosin cortex contraction triggered an increase in rounding modulus and volume decrease (Fig 23, upper left quadrants). In conclusion, these results reveal that the actomyosin cortex contracts against an opposing intracellular osmotic pressure.

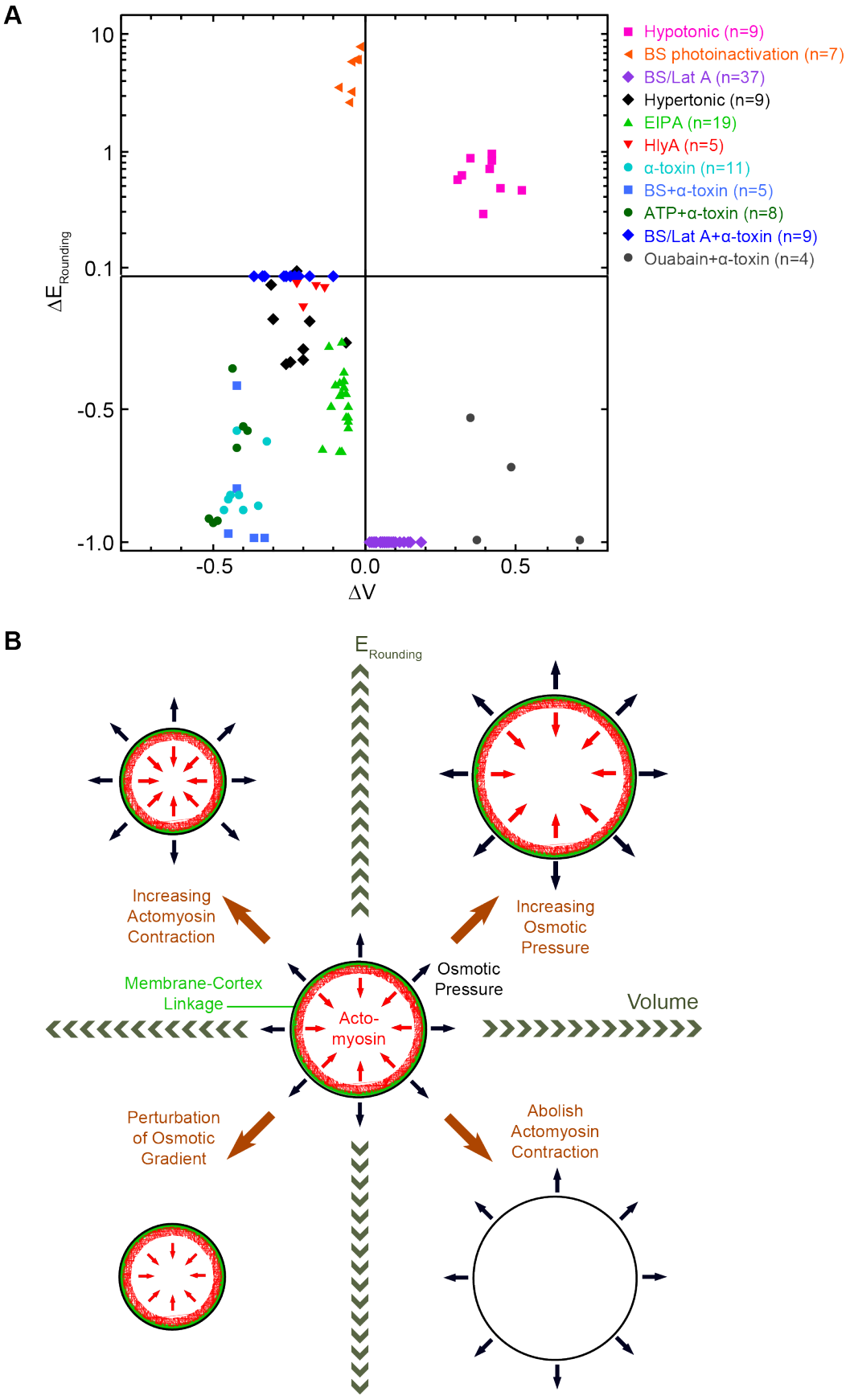

Figure 23: A Relative maximum changes in rounding modulus ($\Delta E_{Rounding}$) and normalized volume (ΔV) of mitotic cells subject to dynamic perturbations experiments. See figure 22 for individual examples of each treatment and

dosages used. The y-axis is log scale at $\Delta E_{Rounding} \geq 0.1$. n values are displayed in the key. **B** A uniform actomyosin contractile tension (red arrows) is balanced by an outward directed, intracellular osmotic pressure (black arrows). Various membrane-cortex linker proteins (green) are required to couple these two elements. The higher the tension and pressure the greater the rounding modulus, or rigidity. Imbalances between tension and osmotic pressure cause changes in cell volume and rounding force.

Treatment	Target/Action	Refs	Conc.	Equilibrium Mechanics	Dynamic Perturbation Pressure	Dynamic Perturbation Volume	Blebbing	Post-NEBD force rate	Mitotic arrest	Figures
Cytochalasin D	F-actin polymerization inhibitor	[78]	0.1-1 μM	⬇⬇⬇			⬆⬆		N	4, 5, 7, 18C, 19, 21
Y-27632	Rho kinase inhibitor	[79]	1-100 μM	⬇⬇			⬇		N	4, 5, 18F, 19
Trypsin	Protease - digests extracellular protein domains	[100, 101]	2.5 mg/L	⬆			⬆		Slight	13-16, 19, 20
EDTA	Sequesters Mg^{2+} and Ca^{2+} in cell medium	[100, 101]	5 mM	—			—		Slight	13-16, 19
Calyculin A	Phosphatase inhibitor	[104]	5-10 nM	⬆			⬆⬆		n/a	17
Latrunculin A	F-actin depolymerizer	[124]	10-1000 nM	⬇⬇⬇	⬇	⬆	⬆⬆		N	18A,B, 19, 22C,G, 23A
Jasplakinolide	F-actin stabilizer	[125]	10-100 nM	⬇⬇⬇			⬆	⬆	N	18D,E, 20, 19
Blebbistatin	Myosin II inhibitor	[129]	1-100 μM	⬇⬇			⬇⬇		N	18G, 19, 22C,D,G,H, 23A
ML-7	MLC kinase inhibitor	[130]	1-30 μM	⬇⬇			⬇		N	18H, 19
Nocodazole	Microtubule depolymerizer	[131]	7-333 nM	—			⬆	⬆⬆	Y, PM	18I, 19, 20
Vinblastine	Microtubule depolymerizer	[132]	1-100 nM	⬆			⬆	⬆⬆	Y, PM	18J, 19, 20
Taxol	Microtubule stabilizer	[133]	100 nM	⬆			—		Y, PM	18K, 19
STC	Kinesin eg-5 inhibitor	[134]	2 μM	—			—		Y, PM	18L, 19, 22C,G,H, 23A
Deoxycholate	Detergent - plasma membrane	[114]	200 μM	—			—		Slight	18M, 19
Dynasore	Dynamin inhibitor	[137]	100 μM	—			—		Y, PM	18N, 19
EIPA	Na^+/H^+ exchange inhibitor	[141]	25-100 μM	⬇⬇	⬇	⬇	⬇⬇		Y, P	18O, 19, 21, 22E, 23A
Ouabain	Na^+/K^+ ATPase inhibitor	[142]	40-100 μM	—			—		Y, P	18P, 19, 22J, 23A
Bumetanide	$Na^+K^+2Cl^-$ symport inhibitor	[143]	100 μM	—			—		N	18Q, 19
NPPB	Cl^- transport inhibitor	[144]	100 μM	—			—		Slight	18R, 19
DIDS	Cl^- transport inhibitor	[144]	100 μM	—			—		Slight	18S, 19
Hypotonic shock	Cell swelling	[140]	+200 mOsm	n/a	⬆	⬆	—		N	22A, 23A
Hypertonic shock	Cell shrinkage	[140]	-100 mOsm	n/a	⬇	⬇	—		N	22B, 23A
Blebbistatin photoinactivation	Blue light causes loss of myosin II inhibition	[151, 152]	10-20 μM	n/a	⬆	⬇	—		N	22D, 23A
S. Aureus α-toxin	Pores permeable to monovalent cations	[158]	40-100 μg/mL	n/a	⬇	⬇	⬇		Y	22F-J, 23A
ATP	Cellular chemical energy		5 mM	—			—		N	22I, 23A
E. Coli HlyA	Pores permeable to cations	[161]	2-4 μg/mL	n/a	⬇	⬇	⬆		Y	22K, 23A

Table 1: Index of inhibitors and perturbations used in single cell AFM experiments in order of figure appearance. A short description of the action or target of the treatment is given alongside seminal references. A summary of the experimental phenomena observed with application of the inhibitor is displayed column-wise. Downward arrows (⬇) represent decrease. Upward arrows (⬆) represent increase. Numbers of arrows rate the degree of the effect. Broad dashed lines indicate no substantial change. Empty cells indicate the experiment was not done or the phenomenon was not deemed worthy of analysis. Y = yes. N = no. n/a = not applicable. PM = prometaphase. P = Prophase.

Discussion

Physical Basis of MCR - Summary

The experiments in this thesis used AFM combined with optical microscopy to analyze the physical basis of cell shape trans-mitosis. The results from these experiments, in conjunction with the literature, suggest the following model for MCR (Fig 24). Rounding is triggered by the disassembly of stable focal adhesions[163-168] and rearrangement of actomyosin from an anisotropic distribution into a uniform contractile cortex[13, 17, 62, 63]. Hence, association of actin with focal adhesion complexes is diminished as membrane-bound linker proteins recruit actin to form a homogenous cortical layer beneath the plasma membrane. Because many extracellular adhesion domains still remain attached during mitosis, rounding causes the extrusion of retraction fibers and a reduction in cell-substrate grip[62, 66, 91]. Furthermore, the combination of actomyosin cortex assembly and increased contractile forces are responsible for a rise in surface tension, surface elasticity and whole-cell elastic modulus in M-phase (Fig 16 and[63, 64, 88, 89, 169-172]. Concomitantly, mitotic cells exhibit a substantial intracellular hydrostatic pressure related to the maintainence of osmotic gradients by ion transporters (Fig 23). Indeed, the trans-mitotic CHA (Fig 9) reveals the kinetics of intracellular pressure and surface tension trends as function of mitotic phase (Figs 15, 16). Thus, mitotic cell rounding is governed by a surface tension versus adhesion relationship (Fig 24). Diminished cell-substrate grip occurs by disassembly of focal adhesions while elevated cell surface tension is dependent on actomyosin contraction, linkage of actomyosin to the plasma membrane, and intracellular hydrostatic pressure. In congruence with the Young-Laplace principle, the forces of intracellular pressure and actomyosin contraction are balanced and opposed at steady state (Fig 23). The magnitudes of the cell surface tension and intracellular pressure determine apparent cell rigidity.

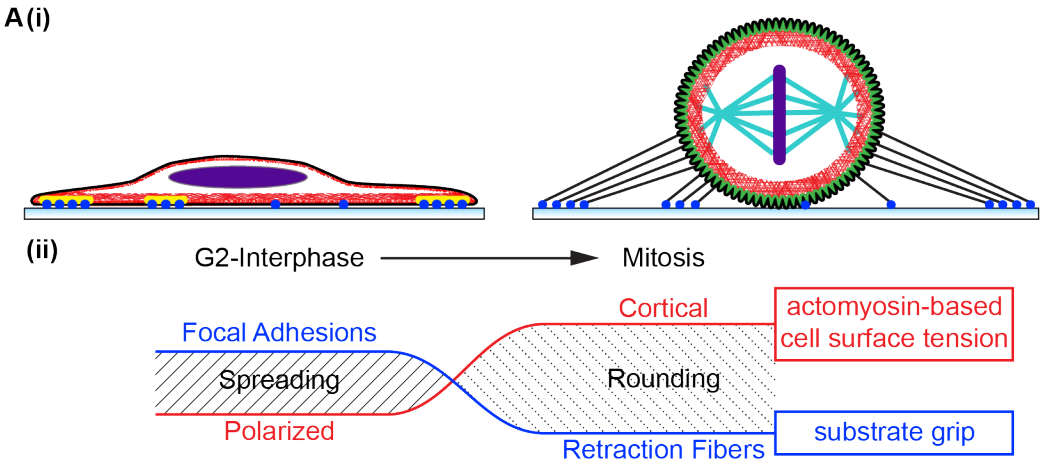

B

Cell cycle phase	interphase	mitosis
Cell morphology	flat, protracted	rounded
Actin morphology	polarized, inhomogenous	cortical, homogenous
Membrane-actin connection	mainly concentrated to adhesion sites	tight, homogenous
Substrate grip	via focal adhesions - strong	via retraction fibers - minimal
Elastic modulus	minimal	maximal
Surface tension	minimal	maximal
Intracellular pressure	minimal	maximal
Surface Area:Volume ratio	maximal	minimal
Membrane protrusion tendency	lamellipodia, filopodia, ruffles	blebs

Figure 24: Physical characteristics of cultured cells in interphase and mitosis. **A (i)** Schematic of cells in interphase and mitosis depicting integrin cell adhesion molecules (blue), focal adhesions (yellow), DNA (purple), microtubules (cyan), actomyosin (red), membrane (black), and plasma membrane-cortex linkers (green). MCR involves the rearrangement of polarized actomyosin into a contractile cortex that is uniformly linked to the plasma membrane. The actomyosin cortex determines cell surface area, as the plasma membrane is loose. Extrusion of retraction fibers is only possible because integrin adhesion molecules remain bound while focal adhesions disassemble. **(ii)** The balance between the forces of adhesion and actomyosin-based surface tension determines whether the cell is in a spreading or rounding regime. **B** Table of the physical characteristics relevant to interphase and mitotic cell shape.

Physical Basis of MCR - Details

Intracellular Pressure in Cell Mechanics

Surface Tension and Intracellular Pressure - the Liquid Drop Model

Because suspended cells tend to adopt a round shape, like water droplets, many researchers have adapted the liquid drop model to the context of cell mechanics. In liquid drops surface tension arises from the relative self-affinity of the liquid molecules, which collectively produce a net inward force across the surface and generate a hydrostatic pressure. The relationship between the radius, surface tension and hydrostatic pressure is given by the law of Young-Laplace. This relationship is also relevant to cells under appropriate conditions such as when in a non-adherent state.

Early Assessments of Intracellular Pressure in Sea Urchin Eggs

Sea urchin eggs are spherical ~100 μm diameter single cells. Early mechanical investigations of sea urchin eggs were probably the first to recognize the applicability of a liquid drop model to assess cell surface tension, intracellular pressure and deformability. Such models were used to interpret data from compression[172-175], micropipette[169, 171, 176], and centrifuge microscopy[177] experiments on single egg cells. A number of these studies analyzed the mechanics of the cell cycle and it was generally found that cells exhibited a significant surge in surface tension, intracellular pressure and stiffness in the period immediately preceding division. These effects appear to be a universal paradigm in the cell cycle of most animal cells (for a review see[139]).

Beyond Sea Urchin Eggs – Intracellular Pressure in Cultured Animal Cells

While spherical egg cells represent a straightforward application of the Young-Laplace law to determine surface tension and intracellular pressure, its implementation to cultured animal cells is only appropriate for those in a rounded or otherwise quasi-detached state with relatively uniform surface properties. The model is not applicable when a cell is among a cluster of cells or when significant adhesion or cortical anisotropies are present. Appropriate examples are noted in the literature[92, 139, 178-182].

Intracellular Pressure in MCR

In the case of rounded mitotic cells, the Young-Laplace model can be applied to isolated cells or those subject to parallel plate compression[174, 175] (Fig 25A). Due to lack of imaging capabilities, the analysis in this thesis assumes compressed cells adopt the shape of a barrel with uniform radius (Fig 9 and Fig 25A(ii)), but in reality the two principle radii of curvature are likely to be different and future efforts should employ more sensitive methods to attempt a more accurate measurement of the shape profile (Fig 25A(iii)). Nevertheless, rounding pressure as measured in the AFM CHA is related to the pressure difference across the plasma membrane[174, 175]. The average rounding pressure of untreated metaphase cells measured in this thesis was ~200 Pa. Taking into account the effects of adhesion, and anticipating a smaller contact area than assumed with the barrel-with-uniform-radius model might yield a more accurate estimate of intracellular pressure at ~ 400 Pa in mitosis and ~100 Pa in rounded interphase cells. Assuming a radius of 12 μm and inserting these numbers into the Young-Laplace equation gives a surface tension of approximately ~10 and ~2.5 nN/μm for mitosis and interphase, respectively. By comparison, Charras et al. calculated the intracellular pressure and cortical tension of nocodazole arrested metaphase HeLa cells to be ~100 Pa and ~0.5 nN/μm by analyzing images of blebbing cells[119]. Measured cortical tensions in other cells typically range from 0.1 to 10 nN/μm depending on cell type[139]. The mitotic increase in surface tension is dependent on the actomyosin cortex, which dominates cell surface tension when coupled to the membrane and the tension of the plasma membrane itself is comparatively negligible[92, 180]. The experiments in this thesis (overviews in Figs 19 and 23) and the research of others[62-64, 73, 75, 119] demonstrate how the various properties of the actomyosin cortex affect the maintenance of cell surface tension in MCR. These properties are shown in a schematic model (Fig 25B).

In cells the natural ability of water to flow across the plasma membrane is further accentuated by the presence of aquaporin water channels[183]. Thus, hydrostatic pressure in the cytoplasm almost immediately translates to an osmotic pressure, which is underpinned by an effective difference in

osmolyte concentration as specified by the van't Hoff law (Fig 25B). As discussed above, if mitotic HeLa cells are assumed to have an intracellular pressure of ~400 Pa, and if the van't Hoff factor is taken to be 1, this would render an effective osmolyte concentration difference of ~0.15 mOsm. However, there is little available information on the van't Hoff factor of common osmotic species in the cytoplasm. A crowded cytoplasm could reduce the van't Hoff factor of electrolytes[184]. For example, if only 1 of every 10 Na^+ ions were fully dissociated and osmotically active in the cytoplasm the van't Hoff factor of Na^+ would be 0.1. In such a case, an influx of 1.5 mM Na^+ would be required to elevate the intracellular osmolarity by 0.15 mOsm, which in turn would increase intracellular hydrostatic pressure by 400 Pa. Results of perturbation experiments with the NHE1 inhibitor, EIPA, indicate that exchange of H^+ for more osmotically active Na^+ in the cytoplasm is involved in the maintenance of mitotic cell volume and pressure (Fig 23). Moreover, although the ~0.15 mOsm gradient seems small, its maintenance might be associated with regulation of intracellular pressure and surface tension. For example, a possible consequence of gradient dissipation could be that contractile forces might be diverged from generating surface tension and instead channeled into driving cell shrinkage. Indeed, this is one explanation for the partial dependence of α-toxin shrinkage on the actomyosin cortex (Fig 23). The ~400 Pa intracellular pressure could exist passively and simply be dependent upon actomyosin cortex contraction and the semipermeable properties of the plasma membrane. Or it could be actively regulated and maintained by osmolyte transporters. But whether or not a cytoplasmic osmotic setpoint corresponding to a ~400 Pa would be regulated by the cell is unknown. The magnitude of the volume changes necessary to activate the volume-sensitive transporters appears to be no less than 3%[185, 186]. Perhaps transporters mediate coarse modulation of intracellular pressure while fine-tuning is actomyosin dependent.

It must be noted that many of the dynamic perturbation experiments (Fig 23) only adhere qualitatively to the relationships between steady-state tension, pressure and osmolyte concentration as dictated by the laws of

Young-Laplace and van't Hoff (Fig 25). For example, abolition of the actomyosin cortex with latrunculin A reduces the intracellular pressure from ~100 Pa to zero and causes an apparent volume increase of ~7% (Fig 22G). However, Δ100 Pa translates to an osmolyte concentration difference of 40 μOsm, which seems insufficient to drive such a volume change. Thus, while the qualitative trend makes sense, the quantitative relationship is not upheld. Possible explanations include:

1) Gross experimental errors,

2) Active response of the cell to rapidly switch on osmolyte transporters or regulate plasma membrane water permeability,

3) Peculiar cytoplasmic van't Hoff factors or possible changes to its value[184],

4) Feedback mechanisms that amplify or dampen certain perturbations,

5) The need for additional or unforeseen terms to adapt the classical theories to the cellular context[184],

6) A physical contribution of events away from the cell surface[184, 187] or not captured by the Young-Laplace model, or

7) Non-specific effects of the perturbations.

Future work will need to explore such issues in order to establish quantitative relationships that account for the active nature of cells in cytomechanics and volume control.

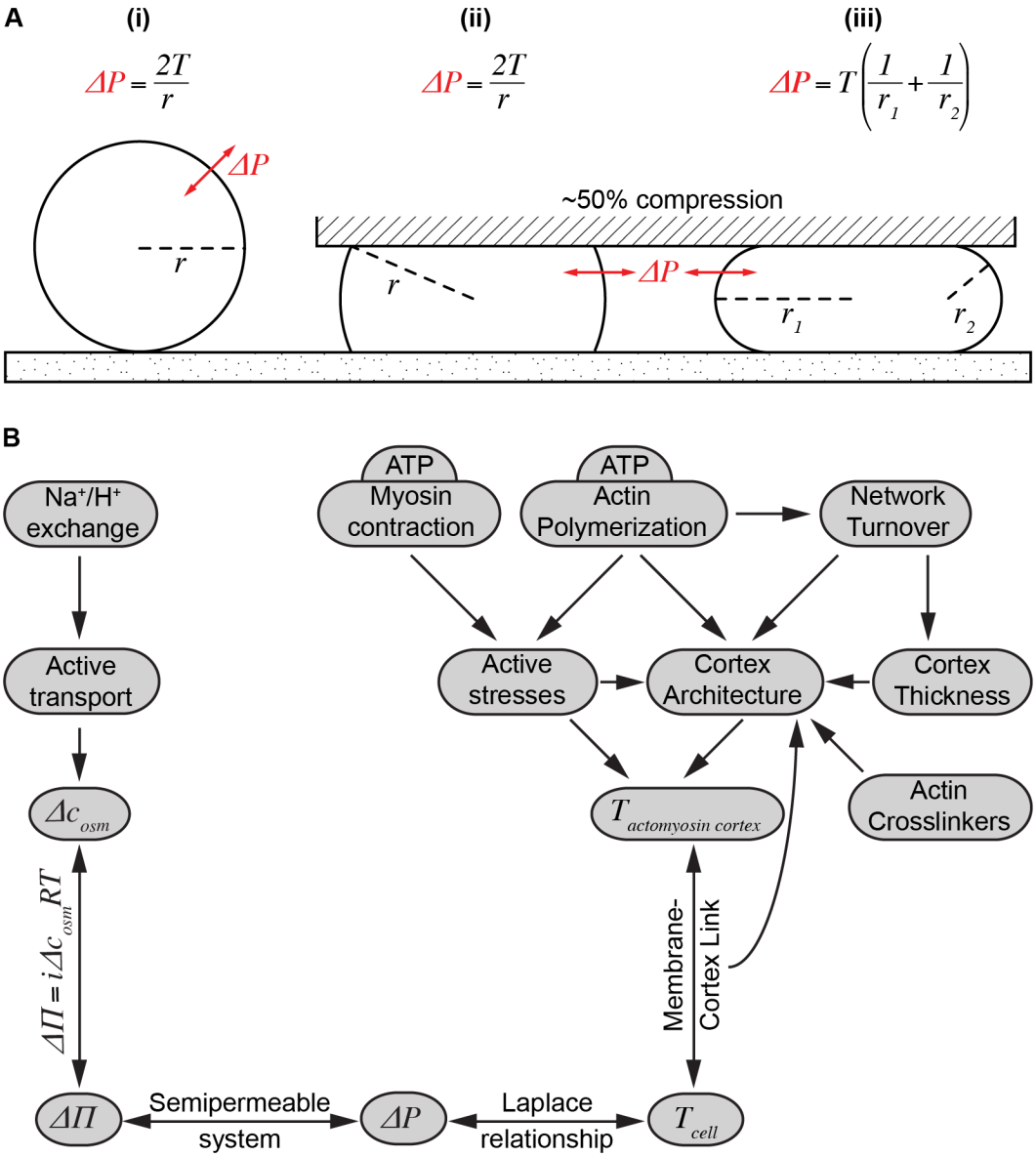

Figure 25: Relationship between actomyosin cortex properties, cell surface tension, intracellular pressure, and osmolyte gradients in mitotic or otherwise quasi-detached animal cells. **A** Application of the Young-Laplace equation to (i) an isolated round cell, (ii) a ~50% compressed cell assuming uniform radius, (iii) a ~50% compressed cell assuming distinct lateral (r_1) and vertical (r_2) side profiles. T: cell surface tension, ΔP: difference in hydrostatic pressure between cytosol and the extracellular milieu, r: principle radii. **B** A model of the relationship between actomyosin cortex properties, cell surface tension, hydrostatic pressure, and osmolyte gradients. Symbols are as in **A**. A complex system of biochemical and physical interactions governs the properties of the actomyosin cortex. Myosin motor proteins consume ATP to generate contractile stresses in the cortical network. Actin polymerization similarly consumes ATP and generates forces, guides actin architecture, and affects turnover. Actomyosin network turnover emerges from the balance between actin polymerization, depolymerization and stabilizing factors. Other factors such as cortex thickness, concentration of actin crosslinkers, and membrane-cortex linkage contribute to cortex organization and properties. The actomyosin parameters conspire to dictate cortex tension, $T_{actomyosin}$. Provided that the actomyosin cortex is tightly linked to the plasma membrane, $T_{actomyosin}$=T_{cell}. Total cell surface tension is related to intracellular hydrostic pressure through the Young-laplace equation. In a semipermeable

system such as the cell, hydrostatic pressure immediately converts to osmotic pressure ($\Delta\Pi$), and vice versa. Osmotic pressure across the cell membrane equates to a difference in effective osmolyte concentration (Δc_{osm}) via the van't Hoff law with i: van't Hoff factor, R: universal gas constant, T: temperature in kelvins. Active cellular transport mechanisms such as Na^+/H^+ exchange regulate cytoplasmic osmolyte concentrations. Perturbation of key properties distorts the homeostatic balance in cells and alters mechanics and volume as demonstrated in Fig 23.

Intracellular Pressure in Cell Shape and Movement

Increased intracellular pressure is clearly involved in MCR. By analogy, pressure gradients are known to govern shape in organisms with cell walls such as bacteria and plants[188, 189]. The experiments in this thesis support the idea that the actomyosin cortex behaves like an internal cell wall that channels outward osmotic force to control animal cell shape. By locally modulating actomyosin-cortex-dependent surface tension and globally regulating osmotic pressure, cells could control their volume, shape and mechanical properties. Indeed, similar ideas have been postulated to explain the mechanisms that drive cell motion and shape transformations[117, 118, 121, 155, 180, 190-193]. These ideas are expounded upon below.

The early researchers who studied intracellular pressure and surface tension in sea urchin eggs had almost no knowledge of the cytoskeleton and cortical actomyosin. Similarly, those who investigated blebbing cells recognized that hydrostatic pressure and cytoplasmic anisotropies must be at play but could only speculate on the identity of the molecules and structures[193-195]. The idea that actomyosin contractility might be linked to intracellular pressure came from later studies on blebbing and motility[117, 196-205]. In particular, one of these reports used an invasive method, the servo-null technique[206, 207], to directly measure the internal pressure of motile *Amoeba proteus*. Intracellular pressure was measured at ~500 Pa in rounded cells but dropped below 250 Pa with the formation of motile bleb-like psuedopods. These results indicate that hydrostatic pressure can be channeled into protrusive forces to drive amoeboidal blebbing-type motility[204]. Such findings are analogous to the release of MCR pressure by latrunculin A induced blebs as observed in this thesis (Fig 18A).

The notability of intracellular pressure in cell mechanics gained further attention after a series of reports demonstrated the biological importance of amoeboidal blebbing motion. Blaser et al. showed the prominence of myosin contractility, blebbing and associated cytoplasmic streaming in zebrafish primordial germ cell motility *in vivo*[190] while several cancer researchers also observed that amoeboidal/blebbing motility is an important mode of tumour cell invasion in tissues[208, 209]. Many more studies have since extended upon these results in a number of different cell types and biological contexts[155, 210-217]. In particular, the regulation of plasma membrane-cortex attachment has been observed to be a crucial factor controlling the cortical distribution and activity of actomyosin. For example, interfering with membrane-cortex linker proteins results in loss of directed migration in zebrafish germ layers *in vivo*[218]. As in MCR, the physical basis of amoeboidal motility appears to be the result of a tight coordination between the distribution and contractility of the actomyosin cortex, membrane-cortex attachment, intracellular pressure, and adhesion.

The idea that the opposing forces of actomyosin contraction and hydrostatic pressure govern cell mechanics is perhaps analogous to the once popular tensegrity model, which proposes that cytomechanics can be explained by opposing tensions in the cytoskeleton[219, 220]. As such, microtubules act as rigid beams to resist compression while actomyosin behaves as flexible rope-like elements to exert tensile stress. While the tensegrity model of the cytoskeleton has many flaws, it serves as a useful conceptual framework to motivate cell biologists to consider the balance of forces that govern cell shape.

Blebbing as a Window into Intracellular Hydraulics

Apart from being a central feature of amoeboidal motility, studies of cell blebbing have provided a window into some general principles in cell mechanics. For example, Dai and Sheetz used blebs to show that membrane-cortex attachment increases apparent membrane tension by comparing the membrane tension of normal plasma membrane with plasma membrane from blebs[180]. They also showed that actomyosin contractility generates

the pressure required to drive blebbing[180]. Other studies have lead to the idea that the cytoplasm might be “poroelastic”, and therefore able to facilitate pressure gradients that persist over tens of seconds and supra-micron length scales[119-121, 193, 221]. On the other hand, contradictory reports also used blebs as a probe to observe behavior inconsistent with the poroelastic effect[92]. Finally, in this thesis an understanding of cell blebbing aided the interpretation of the effects of key perturbations (Fig 18A and Fig 21). Blebbing has much to teach us about the physical properties of the cytoplasm, plasma membrane control, and the regulation of actomyosin dynamics, localization and contractility.

Volume Regulation

Cell volume control is integral to cell function. Cells utilize a host of mechanisms to manipulate intracellular osmolarity and the flow of osmotically obliged water. Activation of volume regulatory osmolyte transport is the primary mode of response to acute challenges of cell volume[140, 146, 147, 222]. In response to acute swelling, cell volume is regulated through the process of regulatory volume decrease (RVD), which is mediated by the efflux of K^+, Cl^-, and taurine. Conversely, in response to acute shrinkage, cell volume is regulated through the process of regulatory volume increase (RVI), which involves Na^+/H^+ exchange, Na^+-K^+-$2Cl^-$ co-transport, and Na^+ channels. This section integrates the results of this thesis with the current knowledge on volume regulation and its relationship to cell mechanics and the actomyosin cytoskeleton.

Osmotic Shock and the Actomyosin Cytoskeleton

The effect of osmotic stress is well characterized in non-adherent cells that feature a uniform actomyosin cortex where the geometry enables convenient imaging. In these cases, the actomyosin cortex appears to be disturbed and fragmented by hypotonic swelling[223-228] and enriched and reinforced by hypertonic shrinkage[223-225, 227, 229, 230]. Whether these effects are in part due to the mechanical stresses inherent to swelling or shrinkage is unclear, but most studies suggest that the rearrangements are mediated through biochemical signals[146, 222, 231, 232]. For example, PIP2

(phosphatidylinositol 4,5-bisphosphate) levels have been observed to increase with hypertonic shrinkage and decrease with hypotonic swelling[222]. High levels of PIP2 at the plasma membrane tend to boost membrane-cortex attachment, promote actin polymerization, and suppress actin severing[233].

In adherent cells osmotically induced changes in F-actin morphology are less dramatic but generally follow a similar trend to the non-adherent scenario[222, 231]. Hypotonic swelling causes dissolution of F-actin[234-237], which seems to be mediated by Cdc42, Rac1 and depletion of PIP2[222, 238]. Conversely, hyperosmotic shrinkage is commonly reported to result in a reduced number of stress fibers, redistribution of actin to the cell periphery and activation of myosin II[222, 231, 239]. These remodeling effects appear mostly due to the signaling response of the Rho-GTPases RhoA, Rac1, and Cdc42, activation of ERM proteins, and enhanced levels of PIP2 at the plasma membrane[222, 231]. In addition, hyperosmolarity confers an inhibitory phosphorylation to cofilin resulting in less actin severing and, by consequence, more actin polymerization[240]. Intriguingly, there appear to be striking similarities between the actomyosin signaling programs activated in mitosis (see table 2 and reference[139]) and those induced by hypertonic shock(see figure 7 in reference[222]).

The abovementioned studies show that the redistribution of the actomyosin cytoskeleton is a characteristic feature of osmotic shock. It has long been hypothesized that actomyosin might serve as a mechanosensor or transducer in cell volume regulation[146, 222, 231]. But, so far, research results are inconsistent and indicate cell type-specific involvement of actin in volume regulation: while actin disruption prevents RVI and RVD in some cells, its perturbation has no effect on others, or even stimulates electrolyte currents opposing volume regulation (for reviews see references[222, 231]). Past efforts have been overly reliant on non-specific inhibitors, possibly leading to spurious results. In contrast, one recent study used precise genetic methods to demonstrate the involvement of alpha-actinin isoform 4 (ACTN4), a protein best known for its implication in kidney diseases, in the

RVD response of a kidney cell line[241]. Future efforts will surely clarify the functions of the actomyosin cytoskeleton in volume regulation.

Osmotic Shock and Cell Mechanical Properties

As explained in the previous section, the general effect of osmotic shock is that hypotonic swelling compromises cortical actomyosin while hypertonic shrinkage reinforces it. Given that cortical actomyosin usually determines cell surface tension, it would be expected that swollen cells become softer and shrunken cells stiffer. Available mechanical measurements in the literature support this notion[226, 242-246]. In the case of extreme hypertonic conditions and shrinkage (>40% volume loss), Zhou et al. provide evidence that the cytoplasmic molecular crowding inherent to cell shrinkage dominates the mechanical response, and leads to an increase in stiffness and viscosity by analogy to colloids undergoing a glass transition[244].

Osmotic Shock and Mitotic Cells under the Cantilever

In this thesis mitotic cells in the 8 μm CHA were subject to hyper- and hypo-tonic shocks (Fig 22A-B). In both cases volume regulatory responses initiated rapidly and restored cell volume close to the initial setpoint within 3-5 minutes. A comparison with the literature on HeLa cells shows that there can be differential response times to hypo- and hyper-tonic shrinkage: RVD can take from ~5 minutes[247] to ~20 minutes[248], while RVI is more gradual and usually still not complete after 60+ minutes[249-251]. The speed of volume regulatory response can vary considerably between cell types[222]. For example, the typical time course of volume recovery is on the order of 2-4 minutes in EAT cells[222] and more than 40 minutes in rat cortical collecting duct cells[252]. These differences underscore the diversity of sensors, transducers, and effectors that are employed in cell volume regulation. Indeed, researchers have struggled to identify common mechanisms and pathways universal to the volume regulatory response[140, 146, 222, 231].

One possibility for the difference in volume recovery times in this thesis (3-5 minutes, Fig 22A-B) and the literature on HeLa cell volume regulation might be due to cell cycle state: cells might regulate their volume differently

in mitosis. Another possibility is that the stress and strain imposed by confinement under the cantilever alters volume regulation. Alternatively, the difference in cell attachment from flat (interphase) to round (mitosis) affects volume regulation. In some cell types integrin-mediated attachment is a major contributor to the hypo-osmotic volume response, as particular cell types behave differently in adherent or suspended states[253]. It is therefore of interest for future studies to analyze the contribution of cell cycle, mechanosensitive, and adhesion specific aspects of volume regulation.

As mentioned in the preceding section, osmotic shock can cause significant changes in cell mechanical properties. Hypotonic swelling usually causes disruption of actomyosin and cell softening while hypertonic shrinkage reinforces cortical actomyosin and induces cell stiffening. In contrast to this, the results on mitotic cells under the cantilever (Fig 22A-B) show that mechanical properties are bolstered by hypotonic swelling and compromised by hypertonic shrinkage. Because images of actin were unavailable, these results cannot be unequivocally related to the state of the actomyosin cortex. However, the lack of blebbing in response to hypotonic swelling and the apparent increase in surface tension would suggest that a disruption of actin does not occur (Fig 22A). This would indicate that the mitotic regulation of actomyosin cortex integrity overrides the usual disruptive effect of hypotonic swelling. On the other hand, an increase in actomyosin surface tension is not observed, as the literature might predict, for hypertonic shrinkage. This could be because the hypertonic stimulation of cortical actomyosin is redundant with the mitotic signaling program. Indeed, most of the pathways activated by hypertonic shock (see figure 7 in reference[222]) are already active in mitosis[139]. The small decrease in surface tension is concomitant with an efflux of osmolytes and recovers quickly with volume stabilization (Fig 22B). In future it will be interesting to examine these phenomena further with more precise measurements of intracellular pressure, cell surface tension, cell volume and actomyosin morphology.

Na^+/H^+ Exchange and the Physical Properties of Cells

Na^+/H^+ exchangers are transmembrane proteins that conduct the electroneutral export of a proton in exchange for the import of a Na^+ ion. In mammalian systems there are 9 known isoforms of Na^+/H^+ exchangers (NHE1-9). NHE1 (SLC9A1) is ubiquitously expressed in mammalian cells and is located at the plasma membrane, while NHE isoforms 2-9 are specific to distinct tissue, cell types or membrane compartments[254]. Because extracellular sodium concentrations are much higher than intracellular concentrations (~150 mM to ~15 mM), NHE exchangers at the plasma membrane do not require direct energy input to conduct transport. NHE1 is a major membrane transport mechanism in the regulation of intracellular pH and the restoration of volume in shrunken cells[145, 254]. It can also serve as a plasma membrane scaffold for actin through interactions with ERM proteins[255].

NHE1 activation increases the osmotic potential of the cytoplasm by increasing sodium concentration. Replacement of the extruded protons by dissociation of cytosolic weak acids results in a net gain of sodium with a comparatively minor alteration in proton concentration, and thus net osmotic gain[256]. This mechanism is an important avenue toward cell volume recovery post hypertonic shrinkage. That NHE1 is the primary mechanism driving RVI in many cell types has been confirmed by deletion experiments. Many cells lacking NHE1 fail to regain volume after imposed shrinkage[145, 222, 256]. The signals that trigger NHE1 activation are still incompletely understood, and attempts to elucidate them have failed to show that direct phosphorylation of NHE1 or the actin cytoskeleton-ERM interaction are involved in NHE1-mediated RVI[145, 222, 256]. More recent evidence suggests that the Akt kinase pathway might control NHE1 activity[251, 257].

Evidence exists that NHE1 can also regulate quiescent intracellular pressure. Na^+ influx has been linked to the induction of blebbing[258], and the propensity of cells to bleb is in proportion to the magnitude of intracellular pressure[119]. In congruence with this, blocking NHE1

frequently prevents blebbing[156, 259]. The experiments in this thesis also demonstrate a stark decrease in characteristic anaphase polar blebbing in the presence of 50 μM of the NHE1 inhibitor EIPA (Fig 21). Furthermore, the hormones aldosterone and 17beta-estradiol appear to stimulate Na^+/H^+ exchange and cause significant increases in cell volume and surface stiffness in cultured endothelial cells[260-262]. The effects of intracellular pressure at a single cell level may compound to influence tissue properties. For example, Na^+/H^+ blockade is known to reduce intraocular pressure and blood pressure in the cardiovascular system[145, 263].

Apart from regulating intracellular osmotic gradients through intracellular sodium concentrations, NHE1 also modulates cytoplasmic pH and can provide a plasma membrane anchor for the actin cytoskeleton. As a pH regulator it promotes intracellular alkalinization and, in some cases, localized extracellular acidification[264]. These functions have been linked to cell motility where NHE1 has been shown to be involved in migration of many cells types including human neutrophil granulocytes[265], human melanoma cells[266], keratinocytes[267], human breast cancer cells[268], NIH3T3 fibroblasts[269], and transformed MdCK cells[270]. NHE1 is often found enriched at the leading edge of migrating cells and co-localizes with ERMs, actin structures and focal adhesions[271, 272]. While the ERM-binding functionality of NHE1 affects cell shape and actin distribution, the ion translocating ability is required for directed cell migration[273-275].

In the past it has been difficult to untangle the contribution of intracellular osmotic pressure, pH regulation and cytoskeletal anchoring in NHE1's effects on actin morphology, cell motility and cell mechanics. Early work emphasized intracellular pressure as the motive force in cell movement[117, 267], but more recent research provides compelling evidence for pH modulation as the dominant factor[255, 257, 264, 268, 270, 272, 276-278]. Indeed, recent efforts by Barber and co-workers have highlighted the pH sensitivity of sub-membranous actin modulators such as Cdc42, cofilin, and talin[277-279].

Because NHE1 is highly stimulated at the G2/M transition[149], it is a candidate to contribute to the mechanical changes associated with MCR. Trans-mitotic CHAs where the NHE1 inhibitor EIPA was added at prophase showed that cells could not exert normal MCR forces (Figs 18 O, 19). Furthermore, addition of 50 μM EIPA to quasi-metaphase cells in the CHA triggered a reduction in both rounding modulus (-47±12%; n=19) and volume (-8±2%; n=19) over a ~5 minute period (Fig 22E). The -8±2% decrease in volume says that compressed mitotic cells could not maintain intracellular osmolyte concentrations without a sustained influx of sodium ions. This suggests the osmoregulatory function of NHE1 is required for mitotic homeostasis. While perturbation of intracellular pH is unlikely to cause changes in volume, it is unclear whether it contributes to the loss of rounding pressure and surface tension. Interestingly, after the initial perturbation, cells were able to gradually recover (~30 mins) normalized rounding pressure (76±61%; n=6) along with negligible alterations in volume (3±4%; n=6). This suggests that alternative mechanisms may partially compensate for the loss of Na^+/H^+ exchange capacity and fits well with the notion of widespread redundancy in cellular osmoregulation[140]. While the exact mechanisms are unclear, it can be concluded that activity of NHE1 is associated with the regulation of mitotic cell mechanics and volume.

Cell Volume and α-toxin Plasma Membrane Permeabilization

Treatment of mitotic cells with the pore former *S. Aureus* α-toxin leads to persistent cell shrinkage over ~30 mins (Fig 22F). While this shrinkage was partially dependent on an intact actomyosin cortex (Fig 22G), it was completely blocked by ouabain, an inhibitor of the Na^+/K^+ ATPase (Fig 22J). Others have observed that α-toxin exposure to human fibroblasts causes a decrease in K^+ and ATP concentrations[158, 280], suggesting that Na^+/K^+ ATPase might try to rescue K^+ gradients by consuming ATP. Indeed, it is known that the Na^+/K^+ ATPase is an important regulator of cell volume and membrane potential, and works by consuming one ATP molecule to export three Na^+ ions and import two K^+ ions, resulting in the net loss of one cation per cycle. In normal circumstances this serves to lower cell volume and

produce a negative membrane potential, which in turn helps to maintain intracellular chloride concentrations lower than that of the extracellular milieu[140]. These processes are essential to maintain intracellular cation concentrations at approximately 150 mM for K^+ and 15 mM for Na^+. When sublytic treatments of α-toxin cause monovalent cations to leak across the plasma membrane the cell must compensate by increasing the activity of the Na^+/K^+ ATPase. But due to the pump's $3Na^+:2K^+$ stoichiometry, the cell is 50% more efficient at transporting Na^+ outward than it is at bringing K^+ in. Therefore, while it may manage to keep Na^+ concentrations low, it fails to prevent the leakage of K^+. This loss of K^+ must represent a substantial loss of osmolytes and thereby lead to a decrease in cellular volume. Therefore, if the Na^+/K^+ ATPase pump is inactivated by ouabain the cell is unable to compensate for the flux of monovalent ions and they approach extracellular concentrations. Furthermore, from elementary cell physiology it is clear that these effects would trigger a breakdown in membrane polarization, influx of chloride, and subsequent swelling[140]. In line with this interpretation, it has been observed that α-toxin exposure to human fibroblasts causes a decrease in K^+ and ATP concentrations[158, 280]. Taken together, the α-toxin experiments indicate that sublytic shrinkage is primarily due to the activity of the Na^+/K^+ ATPase and its inherent stoichiometric imbalance, while the actomyosin cytoskeleton provides a secondary contribution. This is consistent with the principle that a decrease in cytoplasmic osmolarity leads to a drop in cell volume and rigidity.

Deformation and Cell Volume

It is clear that cells regulate their volume in response to osmotic challenge[140, 222]. But an interesting and largely unexplored aspect of volume regulation is whether cells regulate their volume in response to deformation. Cells sucked into micropipettes have been shown to exhibit equilibrium volumes 10-20% lower than undeformed cells[281]. The compression experiments in this thesis also indicate that a dynamic increase in compressive strain from 0.25 to 0.75 decreases mitotic HeLa cell volume by up to 15% (Fig 12). In materials science terms, the measure of how much

a sample changes volume with deformation is known as the Poisson's ratio. For example, a 15% volume reduction with 50% uniaxial strain corresponds to a Poisson's ratio of 0.35. In comparison, measurements on articular chondrocytes and osteoblasts have approximated the ratio to range from 0.3 to 0.4[282-286]. The volume loss associated with compression might simply be passive. On the other hand, cells might sense the compression and actively regulate volume accordingly. Such a scenario would give rise to the intriguing possibility that cells regulate their Poisson's ratio. This would add another dimension to the idea that cells can be modeled as active materials with material properties governed by the transduction of chemical energy into physical responses[287]. Therefore, it will be of interest for future studies to further address the relationship between cell volume and deformation.

Cell Volume Trans-Mitosis

The data in this thesis do not indicate that MCR involves obvious changes in cell volume (Fig 16A(ii)). This is in contrast with reports from Habela and Sontheimer in glioma cells[288, 289], and Boucrot and Kirchhausen in BSC1 monkey kidney epithelial cells[290] that report decreased cell volume on the order of 30-50% from G2 to metaphase. These measurements, however, are controversial and error-prone because they rely on microscopy techniques that are often poorly calibrated in the z-dimension. On the other hand, the CHA volume measurements (Fig 16A(ii)) are more reliable because AFM sets the z-dimension while light microscopy precisely measures x-y (Fig 9). Other researchers have not observed trans-mitotic changes in the diameter (and by relation volume) of suspended or otherwise quasi-detached cells. It seems that major changes in trans-mitotic cell volume are, at best, only specific to certain cell types of which the HeLa cells used in this thesis work cannot be included. The idea that major volume changes are a hallmark of mitosis is not supported by this thesis.

Plasma Membrane-Actomyosin Cortex Coupling

In mitotic or otherwise round cells actomyosin is usually localized immediately beneath the plasma membrane in a layer known as the actomyosin cortex. Because actomyosin assemblies are inherently contractile

they tend to collapse on themselves, and this behavior has been analyzed quantitatively in reconstituted systems[291]. In some reconstituted systems researchers have avoided collapse by linking actomyosin gels to apposing rigid supports[292]. In such cases, the active contractile forces produce a pronounced stiffening effect in the actomyosin network[292]. By analogy, cells prevent collapse of actomyosin assemblies by anchoring it to cellular structures such as the plasma membrane, focal adhesions, and organelles. Contractile forces between anchoring structures can either produce tension and stiffening or generate movements. In cells with a prominent contractile actin cortex linkage to the plasma membrane facilitates the buildup of a cortex with thicknesses ranging from several hundred nanometers to several microns depending on cell type[139]. Because the plasma membrane is not limiting[293], the properties of the actomyosin cortex govern cell surface tension and surface area in round cells[139]. Therefore, plasma membrane-actomyosin cortex attachment is a critical factor in the mechanical properties of cells.

Plasma membrane-actomyosin cortex attachment is achieved by specialized proteins that bind to both actin and to trans-membrane proteins or lipids[233]. The main lipids that facilitate membrane-to-cortex attachment are phosphoinositides, which feature a cytoplasm-facing inositol ring that regulates protein binding. The various proteins that can bind depend on phosphorylation state of the inositol ring (e.g. mono-, bi-, or tri-phosphorylated at different sites). The most common phosphoinositide implicated in membrane-cortex linkage is PIP2 (phosphatidylinositol 4,5-bisphosphate), which interacts with a number of actin-associated proteins at the plasma membrane[233, 294]. Proteins that can mediate lipid-actomyosin cortex association include the ERM (ezrin-radixin-moesin) family, merlin, protein 4.1, spectrins, MARCKS, myosin-I, anillin, annexins, and septins[233, 294-302]. Additionally, ERM proteins and filamins can link the actomyosin cortex to the intracellular domains of certain trans-membrane proteins[303, 304]. This is particularly interesting in the case of ERMs, which are capable of binding to the intracellular domain of the NHE1 antiporter[273]. This link represents an intriguing possibility for coordination of actomyosin

contractility and osmolyte gradients in the regulation of intracellular pressure and cell mechanical properties.

Several plasma membrane-actomyosin cortex linkers have been implicated in MCR. In *Drosophila,* which expresses the single ERM family member moesin, the round shape and increased stiffness characteristic of MCR was compromised by loss of active phospho-moesin[64, 73]. Depletion led to aberrant distributions of cortical actomyosin and subsequent instability in mitotic spindle orientation. These results reinforce the idea that cell shape and cortical cues are important for spindle morphogenesis[71, 72]. In mammalian systems ERMs have recently been demonstrated to modulate cortical mechanics in meiosis[305] and mitotis[70], but the respective contribution of ezrin, radixin, and moesin is yet to be determined. Evidence in *Drosophila* suggests that PIP2 may be the key lipid agent controlling the organization of ERMs and cortical actin in mitosis[306]. It will be interesting to see whether this also applies in mammalian mitosis and which proteins mediate the lipid-actin link. One possibility is a contribution from septins, which form scaffolds under the plasma membrane via PIP2 binding, and interact with actin and other cytoskeletal partners[302, 307]. Septins have recently been shown to prevent uncontrolled blebbing of mouse lymphocytes in mitosis, assist in coordination of the cortex during amoeboidal blebbing-based motility, and act at the cortex to affect proper volume cell control[308, 309].

Changes in Cell Surface Area During Cell Rounding

As discussed in the previous section the actomyosin cortex appears to dictate apparent cell surface area and surface tension when uniformly coupled to the plasma membrane. However, others have suggested that an active reduction in plasma membrane surface area might increase membrane tension and be a driving factor in MCR[114, 135, 136]. In this thesis, this possibility was tested by treating cells with deoxycholate, a non-specific detergent that acts to decrease membrane tension[114], and dynasore, an inhibitor of dynamin-mediated endocytosis, which has been purported to contribute to plasma membrane surface area decrease in mitosis[136].

Neither treatment drastically compromised the mechanical properties of mitotic cells in the trans-mitotic CHA (Fig 18N,M). Indeed, most reports in the literature indicate that plasma membrane surface is not taut and smooth in round cells. SEM images of round cells in interphase and mitosis show the plasma membrane as a continuum of micro-folds and invaginations[310-312]. Although the M-phase membrane does appear relatively smoother than interphase due to a general lack of blebs, microvilli, and filipodia, it by no means appears limiting[311]. Electrophysiological membrane capacitance measurements on spherical cells indicate that the cell membrane has sufficient reserve to allow for up to 5-fold volume increase without stretching the plasma membrane[313]. Studies of cell lysis by extreme hypotonic shock also indicate that spread cells with large surface areas can accommodate at least 2-fold increase in surface area before lysis[293]. These considerations lead to the conclusion that plasma membrane surface area is not limiting in mitotic or otherwise round cells, and therefore cannot be a major causative factor in cell rounding. Such notions are in agreement with the current theory in animal cell mechanics that the contributions of plasma membrane tension is negligible and that the surface mechanics of the cell are governed by the underlying actomyosin cortex when coupled appropriately to the plasma membrane[139].

Changes in Adhesion During Cell Rounding

It is commonly accepted that reduced adhesion accompanies MCR. A classic cell synchronization technique, the “mitotic shake-off”, enriches mitotic cells in the cell medium by shaking or tapping culture dishes to dislodge them from the surface[314]. Despite a general awareness of reduced adhesion in mitosis the concepts and terms used have failed to properly describe it. For example, it could entail a number of possibilities including:

1) Reduction in adhesion receptor affinity,

2) Proteolytic degradatation or truncation of adhesion proteins,

3) Endocytosis of trans-membrane adhesion proteins,

4) Displacement of adhesive bonds with extraneous ligands,

5) Lateral dispersion or de-clustering of trans-membrane adhesion proteins in the plasma membrane, and

6) Changes in focal adhesions or cytoskeletal anchoring structures that link to the intracellular domains of trans-membrane adhesion proteins.

A comprehensive analysis of the literature in conjunction with the data of this thesis suggests that possibilities number 5 and 6 are responsible for the alterations in cell attachment from interphase to mitosis. Because many cell adhesion molecules still remain attached during MCR, the reduction in cell surface area inherent to MCR causes the extrusion of retraction fibers[62]. In comparison to focal adhesions where adhesive bonds are clustered and stabilized, retraction fibers leave behind much smaller groups of bonds vulnerable to disruption[315]. Unlike in spread cells, rupture of this distal adhesion point leaves no possibility for recovery of the adhesion structure[315]. These events are sufficient to affect the reduction in substrate grip characteristic to cultured mitotic cells.

Characteristics of Retraction Fibers

Early studies using scanning electron- and light-microscopy to characterize rounded mitotic and trypsinized cells clearly revealed the presence of retraction fibers in many different types of cultured cells[66, 316-318]. The mitotic HeLa cells examined in this thesis similarly exhibit retraction fibers as seen by DIC and fluorescent imaging of the plasma membrane (Fig 7). Moreover, disruption of the actomyosin cortex with cytochalasin D causes sagging of round cells when retraction fibers were present, while fully detached cells subject to the same treatment remain round (Fig 7). This indicates that retraction fibers exert a significant downward force that requires actomyosin cortex tension to be overcome. Recent measurements of retraction fiber tension in HeLa cells come up with a force per retraction fiber of around 250 pN and put the total downward force exerted on a single cell at ~10 nN[91]. Retraction fibers are held in place by integrin-mediated bonds, suggesting they are extruded from disassembly of extracellular matrix (ECM) associated focal adhesions[91, 97, 319, 320]. They have also been reported to contain actin and motile nodules[62], but the

physiological importance of the nodules remains to be ascertained. Once retraction fibers have been extruded, mitotic cell shape depends on the balance between cell surface tension and the resisting forces exerted by retraction fibers.

Mechanisms of Focal Adhesion Disassembly

The exact mechanisms of focal adhesion disassembly in mitosis have not been clearly defined. There is significant evidence that several focal adhesion proteins dissociate from their binding partners, and a number of specific signaling pathways have been implicated in this process (see section: *Signaling Pathways and Proteins in MCR*). There may also be a contribution of actomyosin contractility, such as observed with keratinocyte motility in vitro where myosin II contributes to actin network disassembly and de-adhesion at the cell rear[35, 109]. Cells treated with the myosin II inhibitor blebbistatin certainly do struggle to retract the cell margin and extrude retraction fibers (general observation).

Interestingly, a number of focal adhesion components that disperse from the cell periphery at mitotic onset have been reported to relocate to the spindle, indicating dual roles for these proteins[321-325].

Differential Regulation of Cell-Cell and Cell-ECM Adhesion in MCR

Distinct adhesion molecules and regulatory pathways differentially govern cell-cell cohesion and cell-ECM adhesion. While cell-ECM adhesion in mitosis is weakened by the substitution of integrin-mediated focal adhesions for retraction fibers, most evidence suggests that cell-cell cohesion is maintained during mitosis. In this thesis AFM SCFS experiments[84] measuring the forces of cell-cell adhesion at short contact times (10 seconds) did not demonstrate a mitotic-specific decrease in affinity (Fig 8). Furthermore, other research featuring microscopy of cultured confluent epithelial monolayers demonstrates the retention of cell-cell adherens junctions in mitosis[86, 326, 327].

Role of Adhesion Retention in Mitosis

The selective retention of adhesion structures is an important feature of mitosis, particularly in the spatial control of cortical cues that guide spindle orientation and daughter cell positioning[315, 328, 329]. This was demonstrated by Thery et al. who used fibronectin-patterned substrates to control the spatial distribution of integrin-mediated retraction fibers in mitotic HeLa cells and showed that this geometry is transduced through the cell cortex to align the mitotic spindle[74, 97]. Follow-up studies have implicated the tensile force of retraction fibers in this process[91]. Similarly, on planar substrates Toyoshima and Nishida found that integrin-mediated adhesion is necessary to orient the spindle parallel to the substratum in an actin, myosin X, and EB1 dependent manner[320]. Moreover, in the case of confluent cultured epithelial monolayers, it has been observed that spindle orientation can be controlled by cadherin mediated cell-cell adhesion[327]. Together these studies show that adhesive cues can control spindle orientation in minimal *in vitro* systems.

Cell adhesion factors have also been analyzed in relation to spindle orientation in the three-dimensional tissues of living organisms. Lechler and Fuchs found that the asymmetric cell divisions necessary for proper embryonic mouse epidermis formation require both integrins and cadherins to align the spindle[85]. They found that the apical accumulation of LGN, a major spindle guidance factor, at the cell cortex determines spindle orientation and this process fails in β1-integrin and α-catenin knockout mice. In zebrafish Zigman et al. also observed the importance of cadherin/α-catenin-based adhesion foci in determining orientation planes in the developing neural keel[330]. Loss of specific cadherins or the proteins that regulate their clustering randomizes the division plane, which introduces defects in the tissue organization and compromises hindbrain morphogenesis. The abovementioned studies demonstrate that selective retention of adhesive structures in mitotic cells is not merely a side effect of mitosis, but serves as an important factor in spindle orientation and tissue organization in multicellular organisms.

Signaling Pathways and Proteins in MCR

Cdk1 and Mitosis

Cell cycle drivers are intrinsically linked to biochemical pathways controlling cell shape. Many of the pioneering mechanical investigations on sea urchins eggs revealed this even before the biochemical identity of cell cycle regulators was known[169, 171, 172, 174, 176, 177]. Indeed, these studies found that egg cells exhibited a significant surge in surface tension, intracellular pressure and stiffness in the period immediately preceding division. We now know progression through the cell cycle is stringently controlled by a core set of biochemical regulators called cyclins[61]. The master switch associated with entry into mitosis is CyclinB/cyclin-dependent kinase 1(Cdk1) complex, which drives the G2 to M phase transition. Although the details of many intermediate pathways still await elucidation, the CyclinB/Cdk1 complex must ultimately trigger signal cascades that initiate changes in cell shape and mechanical properties at mitotic onset.

That the CyclinB/Cdk1 complex is sufficient to induce rounding in cultured cells was first shown in rat embryonic fibroblasts injected with active Cdk1. Upon injection cells rounded up and exhibited a loss of actin stress fibers, enriched cortical actin, disrupted interphase microtubules, and condensed chromosomes[331]. More recently Pines and Gavet developed a FRET-based biosensor to measure Cdk1 activity in living mammalian cells as they transitioned into mitosis[332]. They found that threshold levels of Cdk1 activity correlate with nuclear envelope breakdown (NEBD) and cell rounding, which can be reversed by addition of a Cdk1 inhibitor. Indeed, the kinetics of Cdk1 activity in HeLa cells correlates remarkably with the mechanical profile of the trans-mitotic CHA (Fig 26). The following sections provide an overview of actomyosin, adhesion and cytoskeleton-related pathways likely to be involved in MCR. These pathways are summarized in table 2.

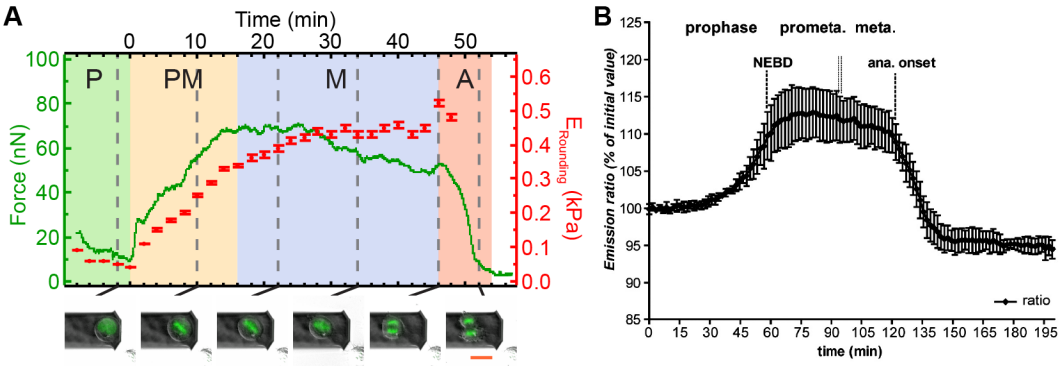

Figure 26: MCR and Cdk1 activity. **A** Cells pre-rounded with trypsin were characterized with the 8 µm trans-mitotic CHA (Fig 15A). Before experiments cells were allowed to round up in Dulbecco's Modified Eagle Media (DMEM) containing 2.5 mg/L trypsin without fetal calf serum (FCS). Medium was then exchanged back to standard DMEM with 10% FCS and cells incubated for at least 5 minutes before initiating an 8 µm CHA on a pre-rounded prophase cell. P, prophase; PM, prometaphase; M, metaphase; A, anaphase. The prophase to prometaphase transition is defined by nuclear envelope breakdown (NEBD). Scale bar: 20 µm. **B** Kinetic profile of Cdk1 activity in HeLa cells as derived with a FRET reporter. Figure B taken from reference[332].

Pathway	Upstream	Downstream	Description	Refs
Cdk1/CyclinB		ACTBL2, ACTG1, ACTN1, ACTN4, PDLIM7, FLNA, FLNB, FLNC, CORO1C, DBN1	Interactions reported but effects on actomyosin or cell mechanics yet to be explored.	[333, 334]
RhoA	Cdk1/CyclinB, GEFs, NEDD9	ROCK	ROCK activates myosin II and promotes actomyosin contractility. ROCK may also enrich cortical actin by reducing actin severing through the LIMK pathway. CyclinB/Cdk1 has been reported to activate ROCK directly.	[63, 333, 335]
ERM (ezrin-radixin-moesin) proteins	Sterile-20 kinases, PIP2	Actin	Facilitates plasma membrane to actin cytoskeleton attachment in mitotic *drosophila* cells. Promotes MCR and induces cortical stiffening. Required for proper cortex formation and MCR in mouse epidermis.	[64, 70, 73, 306, 336]
SRF		Transcription factor – actomyosin genes	Knockout causes MCR defects in mouse epidermis by interfering with expression of several actomyosin proteins including actin and myosin subunits, filamins, WDR1, GSN, CNN2, and PFN2.	[70]
WDR1 (AIP1)		ADF/cofilin, ERMs?	Actin severing protein. Synergistically acts with cofilin to sever actin and thereby regulate turnover. May also be involved in recruitment of ERMs to the cortex.	[70, 75, 337]
Caldesmon	Cdk1/CyclinB, PAKs, p38 MAPK, Calmodulin	Myosin II	Activates myosin II contraction leading to disassembly of stress fibers and formation of a prominent actomyosin cortex.	[338-341]
PAKs	Cdk1/CyclinB, Rac, CDC42, FLNa	Caldesmon, LIMK1, PLK1, myosin II, FLNa	Can upregulate myosin contractility by direct phosphorylation of myosin regulatory light chain or through the caldesmon pathway. May influence actin through the LIMK1/cofilin or filamin pathways.	[342-347]
LIMKs	PAKs, Aurora A kinase, ROCK	Cofilin, Aurora A kinase, TPPP, tubulin	Phosphorylates cofilin thereby inactivating its actin severing ability. Also reported to regulate mitotic microtubule and spindle dynamics.	[348-353]
PSK1&2 (TAOK1&2)	MAP kinases	Astral microtubules	Localizes to spindle poles, astral microtubules and the cortex in mitosis. Depletion retards MCR.	[354]
BCR-Abl	Cdk1/CyclinB	WAVE complex	Cdk1 phosphorylates Abi protein on serine 216 thereby attenuating the ability of BCR-Abl to tyrosine phosphorylate the WAVE complex	[355]
Src kinase	Cdk1/CyclinB	Unspecified focal adhesion partners	Mitotic specific phosphorylations occur on particular serine and threonine residues.	[356-359]
Sam68 (KHDRBS1)	Cdk1/CyclinB	Src	Associates with src in mitosis	[360]
TRASK (CDCP1)	Src family kinases	Integrins	Prevents integrin clustering without affecting integrin binding affinity. Antagonizes focal adhesion signaling.	[167, 361, 362]
Rap1	Cdk1/CyclinB, rap1GAP	RapL, Riam, AF6, vav2, Tiam, ARAP3, Rac, integrins	Inactivated during mitosis thereby effacing its usual function in promoting adhesion and spreading. RhoA and Rap1 reported to be mutually antagonistic.	[164, 363, 364]
α-parvin (actopaxin)	Cdk1/CyclinB	PINCH1, ILK, RhoA/ROCK	Deactivation leads to dissociation of the PINCH1/ILK/parvin focal adhesion complex and upregulation of RhoA/ROCK/myosin II contractility	[168, 365, 366]
FAK	Unspecified serine kinase	C-src, CAS, β-integrins	Serine phosphorylation of FAK in mitosis reduces its association with c-src, CAS and β-integrins	[166, 367]

Paxillin	Unspecified	Various focal adhesion partners	Paxillin is tyrosine dephosphorylated and subject to proteolytic degradation is mitosis	[165]
β1-integrin	CamKII	α-actinin	Phosphorylation at theonine-788 is purported to prevent association of the intracellular domain with α-actinin	[163]
Spectrin	Cdk1/CyclinB	n/a	Dissociates from the cell membrane to the cytoplasm	[333, 368]
Plectin	Cdk1/CyclinB	Intermediate filaments	Mitotic phosphorylation antagonizes plectin's bridging function between intermediate filaments and intracellular structures	[333, 369]
Vimentin	Cdk1/CyclinB, PKC, nestin, plk1, aurora B kinase, ROCK, plectin	n/a	Disassembled in mitosis, except in some cells lacking nestin	[333, 370-374]
Nestin	Cdk1/CyclinB	Vimentin	Disassembled in mitosis	[373, 375, 376]
Desmin	Cdk1/CyclinB	n/a	Disassembled in mitosis	[370, 371]

Table 2: A list of plausible and implicit signaling pathways involved in MCR.

Cdk1 Modulation of Actomyosin

The first studies to demonstrate the molecular link between Cdk1 and actomyosin proteins in mammalian cells were carried about by Yamashiro et al.[338, 339]. These studies showed that Cdk1 directly activates caldesmon, a protein that promotes myosin contractility when phosphorylated. Another pathway that leads to actomyosin contraction in mitosis is the RhoA/ROCK signaling cascade. Maddox and Burridge demonstrated that blockade of this pathway attenuates MCR[63]. Although a direct biochemical interaction between this pathway and Cdk1 was not demonstrated at that time, recent global mass spectrometry analysis of cyclins reveals that the Cdk1/CyclinB complex can directly interact with ROCK[333].

Cdk1-based modulation of mitotic actomyosin may also occur through intermediate pathways and accessory proteins that influence turnover and dynamics. Depletion of the actin severing protein WDR1 causes MCR defects in cultured cells[75] and in embryonic mouse epidermis[70]. WDR1 affects actin network turnover by severing actin in synergy with cofilin/ADF but observations in epidermal tissue suggest it might also serve to facilitate the cortical localization of ERM proteins[70]. The cofilin regulators LIM kinase 1 & 2 are also activated in mitosis and are thought to confer an inhibitory phosphorylation to cofilin, thereby retarding cofilin's actin severing function[348, 349]. However, inhibition of LIMKs does not seem to retard MCR, but rather interferes with spindle function, and more recent studies emphasize the microtubule and spindle regulating functions of LIMKs in mitosis[350-353]. In regard to the role of microtubules in MCR, the interplay between astral microtubules and actin may well be important. As such, the TAO kinases, which coordinate the interaction of astral microtubules with the cell cortex give significant MCR phenotypes in depletion experiments in HeLa cells[354]. Another example of the mitotic regulation of cytoskeletal dynamics occurs with the BCR-Abl complex where Cdk1 confers an inhibitory phosphorylation to the interactor Abi, which prevents the stimulation of WAVE, an actin polymerization factor typically involved in the extension of polymerized actin protrusions[355].

The p21-activated kinase (PAK) pathway can exert control over several of the abovementioned pathways including: LIMKs, caldesmon, myosin II (directly), and the actin crosslinking protein filamin[344-347]. Evidence exists for the activation of PAKs by Cdk1 in mitosis[342, 343]. Furthermore, an additional role in the governance of spindle regulator polo-like kinase emphasizes the complexity of PAK function in mitosis[343]. Despite this, a cytoskeletal or mechanical phenotype in mitotic cells has yet to be reported for the depletion or inhibition of PAKs.

In mitosis specialized proteins and lipids augment actomyosin cortex attachment to the plasma membrane (see section *Plasma Membrane-Actomyosin Cortex Coupling*). This is emphasized by studies in *Drosophila* that suggest this is accomplished through PIP2 phospholipids and phosphorylation (activation) of moesin, the lone ERM protein expressed in flies[64, 73, 295, 306, 336]. Experiments in mammalian systems also implicate ERM proteins in the cortical mechanics of meiosis and mitosis where their localization appears to enrich actomyosin[70, 305]. But the signals that govern these processes in mammalian systems and their relation to Cdk1 are still unclear.

Using mass spectrometry to conduct a time-resolved quantitative proteomics analysis of Cyclin/Cdk interactors, a significant step forward in the knowledge of how the CyclinB/Cdk1 complex governs actomyosin was achieved[333]. This global analysis confirmed several previously reported interactions and revealed new ones. Relevant cytoskeletal interactions reported include actin subunits (ACTBL2, ACTG1), α-actinin (ACTN1, ACTN4), rho kinase (ROCK1), filamins (FLNA, FLNB, FLNC), drebrin (DBN1), coronin (CORO1C), cortactin (CTTN), PDZ and LIM domain protein 7 (PDLIM7), LIM domain and actin binding protein-1 (LIMA1), actin filament associated protein 1 (AFAP1), smoothelin (SMTN), spectrin subunits (SPTAN1, SPTBN1), plectin (PLEC1), and vimentin (VIM)[333]. Such systems level protein-protein interaction data sets enable follow up studies on the mechanisms by which Cdk1 signaling controls the actomyosin cytoskeleton and other aspects of cell mechanics in mitosis.

Cdk1 Modulation of Cell Adhesion

Early studies on the c-src tyrosine kinase detected a dramatically different phosphorylation pattern in mitosis and subsequently identified Cdk1 as being responsible[356-358]. As major regulators of cellular signaling and adhesion, the src family kinases have known functions in cell shape control, but were also found to be required for cell cycle progression[377]. Consequently, the mechanical and non-mechanical functions of src kinases have been difficult to untangle in mitosis. A case in point is the mitosis specific c-src interactor sam68 ("src-associated in mitosis 68 kDa protein", gene name: KHDRBS1), which is known to be phosphorylated by Cdk1[360]. It functions as an RNA binding protein but its contribution to mitotic de-adhesion and cell architecture remains unclear. In contrast to sam68, one src-family interactor central to mitotic changes in adhesion is the recently characterized transmembrane glycoprotein TRASK (CDCP1), which undergoes specific phosphorylation by src kinases on its intracellular domain at mitotic entry[167]. Activation of TRASK triggers lateral dispersion of integrins without affecting integrin affinity state, and causes focal adhesion disassembly by antagonizing focal adhesion signaling[361, 362]. In interphase cells, constitutively active TRASK inhibits cell adhesion and spreading while TRASK knockdown boosts cell adhesion. TRASK therefore represents an active and mitotic-specific phosphotyrosine signaling program underlying the unanchored state.

Apart from the initiation of active de-adhesion programs such as TRASK, termination of pro-adhesion signaling pathways has been observed in mitosis. One example is Rap1, a small GTPase known to promote integrin- and Rac/Cdc42-based cell spreading[364]. Rap1 signaling is switched off in mitosis[164], probably through the antagonistic Rap1GAP, which undergoes Cdk1-dependent phosphorylation[363]. Constitutively active Rap1 inhibits the disassembly of premitotic focal adhesions and actin stress fibers while expression of dominant negative Rap1 mutant prevents post-mitotic spreading[164].

Focal adhesion components are not exempt from mitotic regulation. α-parvin, a member of the ILK/Pinch/α-parvin focal adhesion complex, is a substrate of Cdk1[168]. Not only does the dissociation of this complex contribute to the uncoupling of integrins to actin stress fibers by focal adhesion disassembly, but it also promotes myosin II contraction via stimulation of the RhoA/ROCK pathway[365, 366]. Other focal adhesion proteins such as FAK, paxillin, CAS, and β1-integrin are generally reported to undergo a mitosis specific decrease in tyrosine phosphorylation concomitant with an increase in serine/threonine phosphorylation[163, 165, 166, 367]. Such phosphorylations preclude the mutual interaction of these proteins, leading to the dissociation of focal adhesions. Moreover, while proteolytic degradation of some paxillin was observed in mitosis, interphase levels of FAK and surface expression of integrins are otherwise maintained in mitosis.

Cdk1 Modulation of Intermediate Filaments and Spectrin

While the mitotic functions of actomyosin and microtubules are somewhat clear, the possible roles of other cytoskeletal components like spectrins, septins, and intermediate filaments remain ambiguous in MCR. The membrane scaffolding protein spectrin has been observed to undergo phosphorylation, abandon the plasma membrane, and redistribute to the cytosol in mitosis[368]. Spectrin phosphorylation is likely mediated by Cdk1 directly as the interaction has been observed by mass spectrometry[333]. Similarly to spectrin, intermediate filaments are generally subject to mitotic dispersion through Cdk1-mediated phosphorylation[333, 369-376]. Plectin's function in connecting intermediate filaments to intracellular structures such as the nuclear envelope is abolished by mitotic phosphorylation[369]. Likewise, images of fluorescently marked vimentin, desmin and nestin usually show diffuse cytoplasmic localizations in mitosis[333, 369-376]. Cdk1 phosphorylated nestin assists in the disassembly of vimentin networks but mitotic vimentin filaments have been reported to persist in some cells types lacking nestin[373, 375]. In addition to their mechanical functions, intermediate filaments are also thought to act as physical scaffolds for a host

of biochemical pathways[46, 60]. Therefore, the mechanical implications of intermediate filament network disassembly in mitosis are unclear.

General Cell Rounding

The Adhesion versus Surface Tension Paradigm

Since the inception of *in vitro* cell culture, scientists have taken note of the various shapes that cells adopt on planar substrates. While some cells spread into protracted polygonal morphologies others remain more rounded. Early studies on the effect of viruses on cultured cells documented their ability to transform cells from a flat to rounded morphology[378]. Since then, the spreading versus rounding axis has been used as a gauge for many biological processes. It is therefore of fundamental importance to understand the physical basis of both cell rounding and cell spreading.

Cell shape on planar substrates can be thought of in terms of a balance between cell adhesion and cell surface tension, which is primarily governed by the actomyosin cortex[379]. Similarly, in tissue it has been proposed that actomyosin cortex tension counteracts cell-cell and cell-ECM adhesion to determine cell shape[38, 380]. Cell surface tension will also be related to intracellular pressure by the law of Laplace and the results of this thesis suggest that these parameters are influenced by both the actomyosin cotex and the modulation of osmotic gradients through the action of ion transporters (Fig 25). Throughout the following sections all further references to surface tension carry the connotion that changes in surface tension are intrinsically tied to changes in intracellular pressure.

A physical analysis of cell rounding yields the classification of four distinct modes (Fig 27). The first mode involves an increase in actomyosin cortex tension and a decrease in adhesion via focal adhesion disassembly (Fig 27B). This mode includes mitosis but has also been observed with interphase cells under specific circumstances. The second mode involves the weakening of adhesion through disruption of actin (Fig 27C). This is the subtlest form of cell rounding and is most easily understood as the inability of a cell to remain properly spread. The third mode of cell rounding results from the failure of

adhesion receptors to remain bound to their external ligands (Fig 27D). This can be caused by competing molecules or degradation of adhesion receptors. The fourth mode of cell rounding is through formation of an external surface coating (Fig 27E). The coating may exert its rounding effect through an imposed increase in surface tension and/or non-specific interference with adhesion receptors. These modes of cell rounding are not necessarily exclusive and it is possible for different modes to synergize and contribute to rounding. The details of these rounding modes along with the signaling pathways, proteins and mechanisms are summarized in table 3, and are expounded upon in the forthcoming sections.

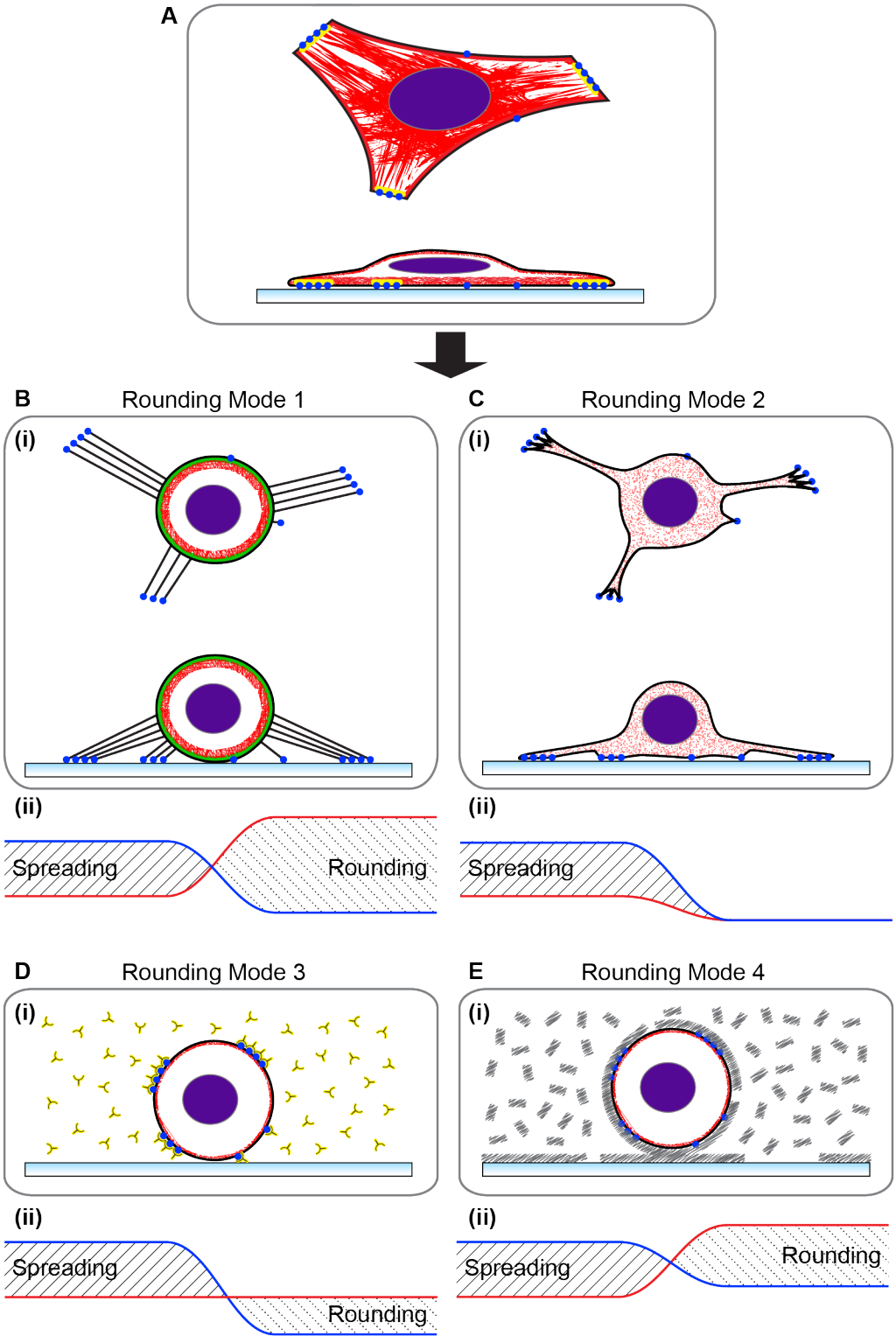

Figure 27: Cell Rounding Modes. A Illustration of a typical shape of a spread cell cultured on a flat substrate with cell adhesion molecules (blue), focal adhesions (yellow), the nucleus (purple), and actin (red). Top and side profiles are shown. **B (i)** Mode 1 cell rounding: cell adhesion points remain, focal adhesions disperse, and a uniform, contractile actomyosin cortex assembles with the aid of plasma membrane-actomyosin cortex linkers (green). Retraction fibers are drawn out and taut. **(ii)** A qualitative scheme of forces for adhesion (blue) and cell surface tension (red). The transition from spread to round occurs because

net surface tension becomes greater than collective adhesion forces. **C (i)** Mode 2 cell rounding: disruption of the actin cytoskeleton and/or focal adhesions causes an arborized type of cell rounding. **(ii)** A qualitative scheme of forces leading to the loss of a spread morphology. **D (i)** Mode 3 cell rounding: addition of soluble molecules that block cell adhesion (yellow/black) prevent interaction with the substrate. **(ii)** A qualitative scheme of forces illustrating that ablation of adhesion is sufficient to cause rounding even without changes in surface tension. **E (i)** Mode 4 cell rounding: addition of soluble lectins (grey) leads to the formation of an extracellular coat around cells. **(ii)** A qualitative scheme of forces illustrating that coat formation increases cell surface tension and interferes with adhesion to trigger rounding. Note that changes in cell surface tension are related to changes in intracellular pressure through the law of Laplace (Fig 25).

Mode	Mediator	Upstream	Downstream	Description	Refs
1	**Cdk1/CyclinB**		Mitotic cell rounding	See table 2	
1	**Rho kinase (ROCK)**	RhoA, PTPN11	Myosin II	In combination with focal adhesion disassembly, actomyosin contractility promotes rounding. Activates LIM kinase, which confers an inhibitory phosphorylation to cofilin thereby blocking its actin-depolymerizing activity.	[381-384]
1	**ARHGAP18**		RhoA	A GTPase activating protein (GAP) that confers inhibition to RhoA. Depletion can cause rounding by excessive stimulation of the RhoA/ROCK/myosin II pathway.	[385]
1	**ARHGAP24**		Rac1, Cdc42, FLNa	A GTPase activating protein (GAP) that confers inhibition to Rac1. Overexpression suppresses Rac1, which tilts the signaling balance towards the RhoA/ROCK pathway and causes cell rounding.	[386, 387]
1	**ARHGEF25**	Bves	Rac1	A guanine nucleotide exchange factor (GEF) that promotes Rac1 activity. Depletion suppresses Rac1, which tilts the signaling balance towards the RhoA/ROCK pathway and causes cell rounding.	[388]
1	**LPA receptors (LPARs)**	Lyosophosphatidic acid (LPA)	Gα12/13, RhoA, ROCK, myosin II	LPARs 1,2,4 and 5 are GPCRs that cause cell rounding through RhoA/ROCK/myosin II pathway. LPAR3 does not activate this pathway or initiate cell rounding.	[381, 389-392]
1	**Protease-activated-receptors (PAR1-4)**	Thrombin, trypsin, other proteases	Gα12/13, RhoGEFs, Rho-GTPases, RhoA, ROCK, myosin II	GPCRs that activate the RhoA/ROCK/myosin II pathway	[102, 154, 389, 393-401]
1	**Eicosanoid receptors EP1, EP3, F2α, TPr**	Eicosanoids	Gα12/13, RhoA, Ca^{2+} influx	GPCRs that activate RhoA/ROCK/myosin II pathway and calcium influx while inhibiting cAMP/PKA	[402-408]
1	**Dopamine receptors (D1-5)**	Dopamine	RhoA, Rac1, Cdc42	Dopamine receptors are GPCRs that can cause cell rounding by activating the RhoA/ROCK/myosin II pathway and downregulating Rac1 and Cdc42	[409-411]
1	**Plexin receptors**	Semaphorins	RhoA, Rac1, CDC42, Rap1	Cell surface receptors that cause cell rounding through signal cascades that activate RhoA and inhibit Rac1, CDC42, and Rap1.	[412-417]
1	**Ephrin receptors (A1-10, B1-6)**	Ephrin ligands	RhoA, Rap1, Rac1, Pak1, NCK2, Abl, CRK	Receptor tyrosine kinases that upregulate RhoA/ROCK/myosin II signaling and downregulate adhesion/spreading by suppressing Rap1, Rac1, Pak1, NCK2, Abl and CRK.	[418-424]
1	**Prolactin receptors**	Prolactin	Rac1, Pak1	Cytokine receptors that downregulate Rac1 and tilt the Rho-GTPase signaling balance towards the RhoA/ROCK/myosin II pathway in certain cell types	[425-427]
1	**Nitric oxide**	Cannabinoid receptors, opiates, morphine	RhoA, protein kinase G	Relaxant of vascular cell types but has been reported to cause contraction and rounding through the RhoA/ROCK/myosin II pathway in neural and other cell types	[428-431]
1	**IpaA**		RhoA, talin	*Shigella* protein that heavily stimulates the RhoA/ROCK/myosin II pathway and reduces β1-integrin affinity via interference with talin	[432]
1	**PAKs**	Rac, Cdc42	Caldesmon, LIMK, myosin, GEF-H1, paxillin, filamins, others	Certain PAKs can directly phosphorylate myosin II and lead to cell contraction. Other PAKs can contribute to cell rounding through the LIMK/cofilin pathway or by influencing the RhoA/ROCK pathway through GEF-H1.	[344, 345, 433-436]
1	**Calyculin A**	n/a	Phosphatases	Global serine/threonine phosphatase inhibitor thought to cause cell rounding through constitutively active myosin contractility and focal adhesion disassembly	[105-107]
1 or 2	**EGF receptor (EGFR)**	Epidermal growth factor (EGF)	Various Ras and Rho family GTPases, MAPK signaling	Receptor tyrosine kinases that activate various combinations of Rho-GTPase signaling programs and can cause rounding (via mode 1 or 2) or promote spreading depending on cell type.	[29, 437-443]

2	**Cytochalasins**		F-actin	Potent F-actin barbed end cappers that disrupt actin network architecture	[10-12, 444-449]
2	**Latrunculins**		F-actin	Actin monomer sequesters that cause rounding by disrupting F-actin	[450]
2	**Focal adhesion disassembly**	Perturbants of focal adhesion components		Chemical or genetic perturbations against focal adhesion components can cause rounding. Examples include α-actinin, src family kinases, FAK, PYK2, and TRASK.	[167, 451-455]
2	**RND1-3**		RhoA, F-actin	Rho family GTPases so named because they cause rounding in many cell types by antagonizing RhoA, reducing F-actin content, and diminishing focal adhesions	[456-458]
2	**ARAP1 & 3**	PIP3	RhoA, Arf	Membrane localized GTPases activating proteins (GAPs) that confer inhibition to RhoA and Arf. Overexpression causes loss of stress fibers and cell rounding.	[459, 460]
2	**Mevalonate pathway**	Statins	Rho GTPases	Suppression of the mevalonate pathway prevents proper prenylation of Rho-GTPases, retarding their coordination at the plasma membrane	[461-464]
2	**PKA**	cAMP, forskolin	RhoA, paxillin, Rap1, Epac	Triggers an arborized/stellate cell morphology by retarding RhoA activity to reduce actomyosin contractility and stress fibers. Additionally, mediates tyrosine dephosphorylation of paxillin to cause focal adhesion disassembly/turnover.	[465-467]
2	**ACTH receptor**	Adrenocorticotropic hormone (ACTH)	cAMP, PKA	As above, see PKA	[12, 468-470]
2	**FSH receptor**	Follicle stimulating hormone (FSH)	cAMP, PKA	As above, see PKA	[471, 472]
2	**β2-Adrenergic receptor**	Isoproterenol, other agonists	cAMP, PKA	As above, see PKA	[473, 474]
2	**Trifluoperazine**		Dopamine receptors, calmodulin	An antipsychotic drug that can cause cell rounding, probably through its proposed functions as an antagonist of dopamine receptors and/or inhibitor of calmodulin	[475, 476]
2	***Clostridium difficile* toxins A and B**		Rho family GTPases	Inactivates Rho-GTPases through glucosylation	[477, 478]
2	***Clostridium botulinum* C3 toxin**		RhoA, RhoB, RhoC	Inactivates RhoA, B and C through ADP-ribosylation	[479]
2	***Chlamydia trachomatis* protein CT166**		Rac1	Inactivates Rac1 through glucosylation	[480]
2	**AexT, ExoT, ExoS, YopE,**		Rho family GTPases	Exogenous GTPase activating proteins (GAPs) that inhibit Rho family GTPases. ExoT and AexT also ADP-ribosylate CRK focal adhesion proteins and actin, respectively.	[481-488]
2	**Vibrio VopS**		Rho family GTPases	Inactivates rho-GTPases through AMPylation	[489]
2	**EspH**		Rho GEFs	Binds to and inhibits Rho GEFs	[490]
2	**RTX toxin**		G-actin	Inhibits actin polymerization by covalently crosslinking G-actin	[491-493]
1 or 2	**Rous sarcoma virus**		v-src, vinculin, cofilin	v-src displaces endogenous c-src and targets proteins such as vinculin and cofilin to disrupt focal adhesions and actin turnover	[378]
1 or 2	**Herpes simplex virus**		US3 viral kinase, Rho family GTPases, PAKs	US3 viral kinase manipulates the function of Rho family GTPases and PAKs to induce stress fiber dissolution and cell rounding	[494-499]
2	**Vaccinia virus**		F11L, RhoA	Viral protein F11L interferes with RhoA function	[500-504]

2	**Cytomegalovirus**		Paxillin, α-actinin, Hic-5	Causes rounding by downregulating listed focal adhesion proteins	[505, 506]
1 & 3	**Trypsin**		CAM proteolysis, PARs, G-Proteins, RhoA, Caldesmon, TRASK	Trypsin is believed to cleave adhesion receptors on the cell surface. Additionally, trypsin engages protease-activated receptors (PARs) 2 and 4, which trigger the RhoA/ROCK/myosin II pathway. Trypsin rounding is attenuated if the RhoA pathway is inhibited or when TRASK and caldesmon are depleted, suggesting those pathways play a role in rounding.	[63, 101, 154, 362, 507, 508]
3	**Disintegrins**		Integrins	Cause cell detachment by blocking integrins, usually by exploiting the specific integrin binding peptide sequence RGD. Include natural and synthetic compounds such as contortrostatin, saxatilin, cilengitide.	[509-513]
3	**Integrin antibodies**		Integrins	Cause cell detachment by blocking integrins	[514]
3	**Ebola virus**		β-integrins	Ebola viral glycoprotein downregulates surface expression of β-integrins	[515, 516]
2 & 3	**EDTA/EGTA**		Ca^{2+} and Mg^{2+} dependent cell adhesion molecules	Agents that chelate extracellular Ca^{2+} and Mg^{2+} can interfere with the function of cell adhesion molecules and cause rounding. Unclear whether the main effect is on binding affinity or CAM clustering/organization.	[13, 100, 101, 517]
2 & 3	**Tenascin-C**		Integrins	Acts as an intermediary between integrin cell adhesion molecules and the ECM Also reported to trigger outside-in signaling programs that downmodulate focal adhesions	[518-522]
2 & 3	**SPARC/osteonectin**		Integrins	Acts as an intermediary between integrin cell adhesion molecules and the ECM. Also reported to trigger outside-in signaling programs that downmodulate focal adhesions.	[523-527]
3	**Galectins**		β-galactosides	Act as intermediaries between the cell surface and the ECM. Can serve to boost or reduce cell adhesion depending on concentration, ECM composition and cell type	[528, 529]
3 & 4	**Plumieribetin**		Mannose residues, integrins	Fish lectin with mannose crosslinking and integrin binding capabilities	[530]
4	**Concanavalin A (ConA)**		Mannose residues	Lectin from jackbean that crosslinks mannose residues on the plasma membrane and increases cell surface tension	[531-534]
4	**Wheat germ agglutinin (WGA)**		GlcNAc residues	Lectin from wheat germ that crosslinks N-acetylglucosamine (GlcNAc) cell surface residues and rigidifies plasma membrane	[531, 535]
4	***Helix pomatia* lectin (HPL)**		GalNAc residues	Lectin from snails that crosslinks N-acetylgalactosamine (GalNAc) cell surface residues	[536]
4	***Xerocomus chrysenteron* lectin (XCL)**		GalNAc residues, galactose residues	Fungal lectin that crosslinks galactose and N-acetylgalactosamine (GalNAc) cell surface residues	[537]
4	**Spacemaker (SPAM)**		Prominin	Binds to the extracellular domains of prominin and forms a protective coat around drosophila cells	[538]
?	**GH receptor**	Human growth hormone (GH)	unknown	unknown	[427, 539]

Table 3: Signaling pathways, proteins, and mechanisms involved in the various modes of cell rounding.

Rounding Mode 1 – Actomyosin Surface Tension

Rounding mode 1 involves an increase in cell surface tension via actomyosin cortex contraction and a decrease in adhesion by controlled disassembly of focal adhesions (Fig 27B). Focal adhesion disassembly is mediated by the regulated dissociation of structural components but actomyosin contractility may also contribute. This rounding mode yields smooth rounded cells, often with retraction fibers that are held in place by adhesion molecules at their distal termini. Mitosis is the most prominent example of rounding mode 1 but it has also been observed with interphase cells under specific circumstances.

Cell Rounding by the RhoA Pathway

Actomyosin dynamics are largely governed by small Rho-family GTPases. There are more than 20 known Rho-GTPases but the three considered most prominent are RhoA, Rac1 and Cdc42[30]. While Rac1 and Cdc42 generally promote cell elongation and surface protrusions through actin polymerization and actomyosin relaxation, RhoA stimulates actin polymerization and actomyosin contraction[31]. RhoA does this by activating ROCK, which in turn promotes myosin II activity and contraction[381]. ROCK also phosphorylates LIM kinase, which in turn phosphorylates cofilin, inhibiting its actin-depolymerizing activity[384]. Furthermore, RhoA can mediate actin polymerization through the mDia pathway[31]. On a whole-cell scale, RhoA-based actomyosin contractility can do two things to cell shape. Firstly, in combination with stable focal adhesions it results in the development of stress fibers, which promotes cell anchorage[29]. In this case the contractile forces of actomyosin are distributed between basal adhesion zones. Alternatively, in the absence of focal adhesions, RhoA-based actomyosin contractility is transduced into increased cell surface tension, intracellular pressure, and cell rounding. This occurs in MCR[63] and several other forms of cell rounding[381, 382, 399]. Whether RhoA-based contractile tension is channeled into substrate grip or cell rounding depends on the regulation of focal adhesions.

RhoA stimulated actomyosin contractility is not only involved in managing the balance between cell rounding and spreading, but also in motility. Amoeboidal/blebbing motility is powered by RhoA signaling because actomyosin contractility generates the cytosolic pressure required to drive protruding blebs[208]. In the case of lamellipodial motility on surfaces, which involves active cycles of protrusion and retraction at the leading edge, a distinct spatiotemporal pool of active RhoA controls the retraction cycle[540]. RhoA-based contractility also appears to facilitate the detachment of the trailing edge in many modes of cell migration[35, 541]. Indeed different spatiotemporal pools of active RhoA have been observed to correlate with cell polarization, movement, and the generation of different shapes[540]. In all of these cases, RhoA signaling generates centripetal forces in the cell through actomyosin contraction.

Signals Inducing Cell Rounding by the RhoA Pathway

Upstream regulators of Rho-GTPases include guanine nucleotide exchange factors (GEFs) and guanine dissociation inhibitors (GDIs), which stimulate GTPases, and the GTPase activating proteins (GAPs), which catalyze a transition to the inactive state. Most GEFs possess pleckstrin homology domains that localize them to membranes where they regulate actomyosin through Rho-GTPases[542]. Currently, over 70 GEFs, more than 80 GAPs and 3 GDIs have been identified for the Rho-GTPases, of which more than 20 exist[231, 542-544]. These regulators control the balance of activity in their downstream effectors[31]. Because of the apparent antagonism between RhoA, which tends to cause contraction and Rac1, which to tends to promote protrusion and relaxation[545, 546], factors that inhibit Rac1 can potentiate RhoA signaling and vice versa. Therefore extreme RhoA activation can, in effect, be similar to extreme Rac1 suppression, and both have been reported to induce cell rounding. Examples that cause cell rounding include depletion of ARHGAP18, a GAP that inhibits RhoA[385]; overexpression of ARHGAP24, which confers inhibition to Rac1[386, 387]; and depletion of ARHGEF25, a GEF that promotes Rac1 activity[388].

The activation of the RhoA/ROCK pathway is mediated by a variety of factors. In mitosis it occurs through signals originating from the Cdk1/CyclinB complex[63, 333]. In other situations it arises from extracellular signals carried through cell surface receptors, specific secondary messengers, or pathogenic effector proteins. Examples include activation of lysophosphatidic acid receptors (LPARs), protease-activated receptors (PARs), plexin receptors, ephrin receptors, various eicosanoid receptors, dopamine receptors, prolactin receptors, epidermal growth factor receptors (EGFRs), nitric oxide signaling, and the *Shigella* toxin IpaA. The following sections discuss these examples.

Lysophosphatidic acid (LPA) induces neurite retraction and cell rounding in a variety of neural cells via RhoA signaling and assembly of cortical actin[390, 391]. It does this by binding to lysophosphatidic acid receptors (LPARs) 1,2,4 and 5, which are G-protein coupled receptors (GPCRs) that signal through the G-proteins $G\alpha_{12/13}$ to activate RhoA[391, 392].

Several sets of receptors are known to cause cell rounding by tilting the balance of Rho-GTPase signaling towards RhoA and away from Rac1. These include the GPCR sub-family of dopamine receptors (D1-5)[409-411], the type I cytokine receptors of prolactin[425-427], and plexin(receptor)-semaphorin(ligand) signaling[412-417]. Furthermore, certain agents like cannabinoid receptors that serve to increase nitric oxide can cause RhoA-based cell rounding in neural and other cell types[428-431].

Cell Rounding by Eicosanoids

Eicosanoids are signaling molecules that are synthesized from the oxidation of twenty-carbon essential fatty acids. They serve pivotal functions in inflammatory and immune processes such as platelet aggregation and the balance between vasoconstriction and vasorelaxation. Eicosanoids consist of four sub-families: prostaglandins, prostacyclins, thromboxanes, and leukotrienes; and they all act by stimulating various GPCRs. The effects of the various prostaglandins are often tissue specific. For example, prostaglandin E2, which is known to interact with the four GPCRs EP-1, -2, -3, and -4, can have differential or opposing effects depending on which receptors are

stimulated[402, 405]. Stimulation of the receptors EP1 and EP3 causes contraction via Ca^{2+} influx, RhoA signaling and cAMP inhibition[405]. In cultured cells these signals cause individual cells to contract and round up[404, 406, 547]. On the other hand EP2 and EP4 stimulation promote cell spreading, migration, and relaxation via cyclic AMP(cAMP)/protein kinase A(PKA) signaling[405, 548]. Another prostaglandin, F2-α, a known promoter of tissue contraction, triggers rounding in cultured cells through FP-receptor mediated RhoA signaling[403, 408]. The thromboxane-prostanoid receptor (TPr) also mediates a strong RhoA/ROCK-based contractile response in vascular smooth muscle cells[407]. In many of these cases, the emergent theme is that large-scale tissue contractions *in vivo* correspond with rounding of cultured cells *in vitro*.

Cell Rounding by Ephrins

Ephrin signaling serves as a repulsive cue to keep cells apart. This is important in physiological contexts such as the maintenance of tissue boundaries and axon pathfinding[424, 549]. The ephrin system consists of a first cell presenting ephrin ligands and a second that harbors ephrin receptors, which are receptor tyrosine kinases. Upon ligand-receptor binding, bidirectional signals trigger cellular retraction via actomyosin contraction and down-regulation of adhesion. The signals involved include activation of the RhoA/ROCK signaling, attenuation of the Rac1/Cdc42 and Rap1 pathways, and regulation of adhesion proteins paxillin, Nck2 and Crk[418, 419, 421-423]. In cultured cells activation of these signaling pathways translates into a shape transition from spread to round.

Cell Rounding by Protease-Activated Receptors: Thrombin & Trypsin

Thrombin is a protease capable of inducing cell rounding in various cultured cells[389, 394-398]. Thrombin specifically activates protease-activated receptors PAR-1 and PAR-4[400, 401], which, like all PARs, are activated by irreversible and specific proteolytic cleavage of their extracellular N-termini. As with LPA and eicosanoid receptors, PARs are GPCRs, and PAR-1, -2 and -4 are known to signal through G-proteins $G\alpha_{12/13}$ to activate RhoGEFs upstream of the RhoA/ROCK pathway[399-401].

Thrombin also shares similarities with nocodazole in that both contribute to microtubule disassembly and stimulate RhoA activity through GEF-H1[550]. Interestingly, Cuerrier et al. observed that endothelial cells stimulated with thrombin exhibit an almost two-fold increase in actomyosin-dependent cell surface stiffness as measured by AFM[551]. Thus, thrombin-induced rounding appears to be mostly driven by the RhoA pathway and subsequent changes in the actomyosin cytoskeleton.

Trypsin, another protease that is functionally similar to thrombin, is commonly used as a cell dissociation agent in tissue and cell culture applications. Its mode of action is commonly attributed to non-specific cleavage of cell adhesion molecules (wikipedia, April 2012, trypsin article). However, trypsin specifically cleaves and activates PAR-2 and PAR-4, both of which signal to the RhoA/ROCK pathway through G-proteins $G\alpha_{12/13}$[102, 154, 393, 400, 401]. It is therefore plausible that PAR-mediated biochemical signaling and the resultant actomyosin contraction might be responsible for cell rounding. Indeed, a number of early reports detailing the response of cells to trypsin proposed similar ideas. SEM and optical phase images show that a number of different cell types retain retraction fibers post-trypsinization and thus demonstrate that trypsin does not necessarily degrade attachment points[66, 99, 100, 317]. Because of this, one of these authors, Kathryn Vogel, suggested, *"Proteolysis of specific membrane proteins (not necessarily adhesive proteins) could trigger contraction of the cell"*[100]. Another study tested the competence of cells treated with different proteases to spread on fibronectin-coated substrates immediately post treatment. It was found that trypsinized cells rapidly spread and re-adhered while their pronase-treated counterparts could not[552]. Flow cytometry studies also indicate that a Trypsin/EDTA combination causes only minimal depletion of nine cell surface markers[553]. Badley et al. imaged the actin cytoskeleton with fluorescent markers and observed that trypsin treatment causes dispersion of stress fibers in advance of the shape change[13]. Another report showed that trypsin and EDTA treatments do not mediate a decrease in polymerized F-actin, suggesting that stress fiber dispersion occurs through the redistribution of actin into a contractile cortex rather than filament

destruction[554]. In congruence with this notion, cells pretreated with the myosin II inhibitor blebbistatin round up more slowly in response to trypsin[507]. Moreover, cells expressing a constitutively active version of the myosin II activator caldesmon produce faster rounding rates[508]. Furthermore, the data in this very thesis measured the steady state rounding modulus of trypsinized interphase cells in the CHA at 0.24 ±0.08 kPa and less than 0.1 kPa for interphase and prophase cells without trypsin (Fig 16A). Peak round moduli values in mitosis were 0.48 ±0.08 kPa (n=8) for cells maintained in trypsin and 0.37 ±0.09 kPa (n=83) for those in normal media (Fig 16A). These results show that trypsin increases the surface tension, intracellular pressure and mechanical rigidity of already round cells regardless of cell cycle phase. Evidence also exists that trypsin activation of PARs may trigger signals that result in the disassembly of focal adhesions in spread cells. For example, cells deficient in the focal adhesion-dispersing protein TRASK are resistant to trypsin rounding[362]. Interestingly, many of the signaling pathways implicated in trypsin rounding overlap with those involved in MCR (Fig 28). This suggests that, like MCR, trypsin-mediated cell rounding might occur through a combination of increased actomyosin-dependent cell surface tension and regulated focal adhesion disassembly. This is not accounted for in current models that emphasize proteolytic degradation of cell adhesion receptors as the reason for cell detachment. In future, further work will need to be done to characterize the relative contribution of these possibilities. Given the widespread use of trypsin in tissue culture and biotechnology, this remains a pertinent question.

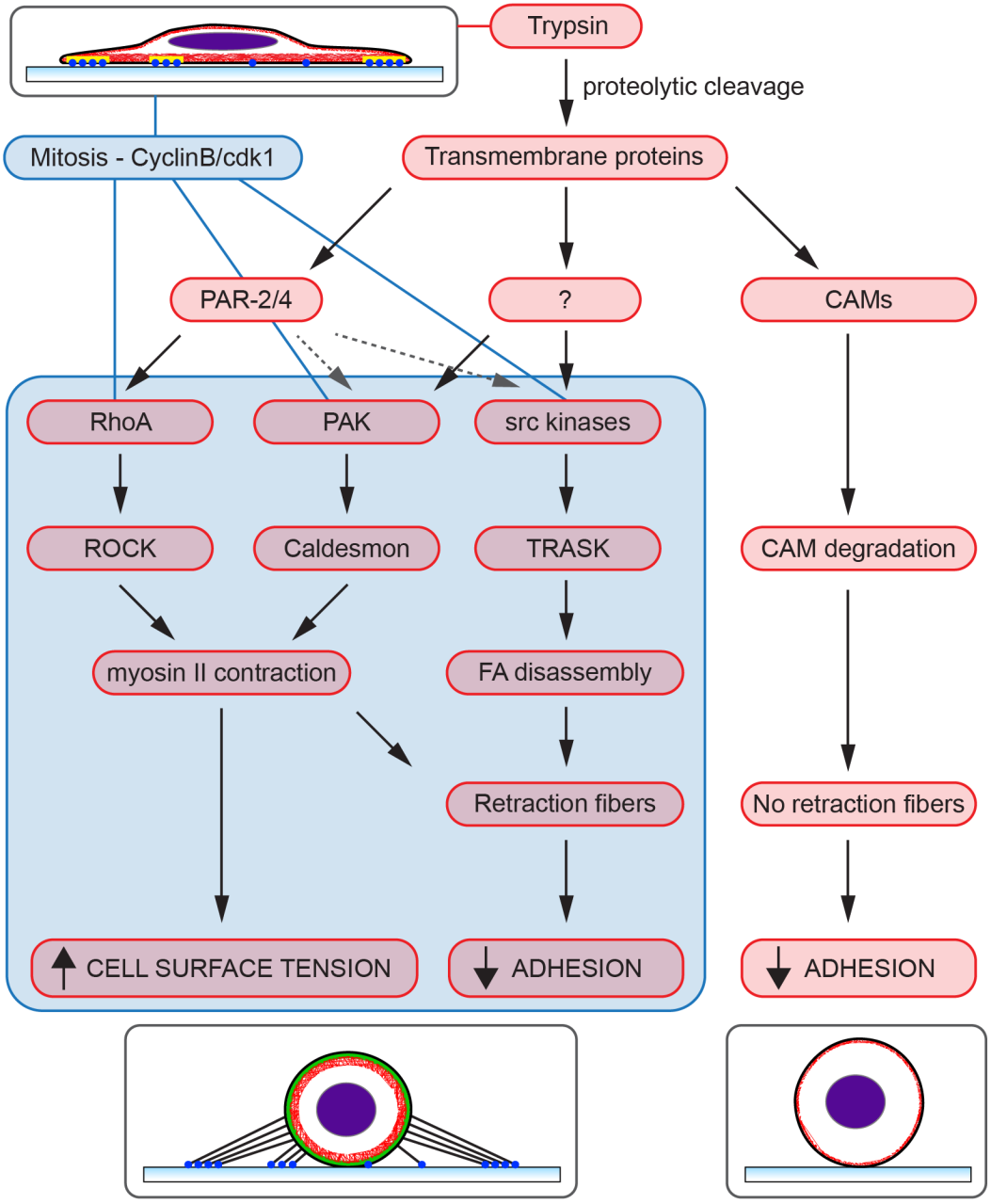

Figure 28: Pathways implicated in trypsin-mediated cell rounding and their overlap with mitotic cell rounding. Black arrows denote direct or indirect stimulation as suggested in the literature while dashed arrows represent speculative links. The blue lines from CyclinB/cdk1 are links suggested in the literature (see table 2). A model based on degradation of cell adhesion molecules (CAMs) would lead to the cell shape depicted on the lower right. A model based on biochemical signaling and rounding induced by actomyosin contraction and retraction fibers is depicted on the lower left. The blue overlap represents relationships also implicated in mitotic cell rounding.

Cell Rounding by the PAK Pathway

p21-activated kinases (PAKs) have been reported to induce cell rounding in certain cases. PAKs are classified into group I PAKs (PAKs 1-3), and group

II PAKs (PAKs 4-6). Many PAKs remodel actin by regulating cytoskeletal interactors such as Rho-family GTPases, the crosslinking protein filamin, the LIMK/cofilin pathway, caldesmon, and various focal adhesion component proteins[435, 436, 555].

Group I PAKs can cause actomyosin contraction by direct activation of myosin II or through the caldesmon pathway[556]. Introduction of constitutively active group I PAKs into cultured cells causes cell rounding via direct phosphorylation of myosin light chain[344, 345]. The downstream effector caldesmon has also been shown to contribute to cell rounding in mitosis[338, 341, 557] and in response to trypsin[508]. Moreover, overexpression of caldesmon in endothelial cells triggers formation of an actomyosin cortex, rounding, and reduced cell migration[558, 559]. Along with PAKs, caldesmon activation may also be mediated by p38 MAPK signaling[559-561].

Less is known about group II PAKs, but the best-studied example, PAK4, has been observed to mediate cell rounding in certain cases. The shape change is reported to occur through PAK4's interaction with GEFs upstream of RhoA and regulation of focal adhesion turnover via paxillin[433, 434, 562].

Cell Rounding by Phosphatase Inhibition

Calyculin A, an inhibitor of serine/threonine phosphatases 1 and 2A[104], has been observed to trigger cell rounding[64, 105-107]. Although general phosphatase inhibition is highly non-specific, the mechanism of shape change is believed to be because it produces a population of constitutively phosphorylated cytoskeletal proteins[105, 108]. This, in turn, causes increased actomyosin contractility and promotes cytoskeletal reorganization. Some studies have gone so far as to employ calyculin A as a means to constitutively activate myosin contractility[109, 110].

Rounding Mode 2 – Weakening of Internal Structures

Rounding mode 2 involves the weakening of adhesion through disruption or dissolution of internal structures required to maintain a spread morphology (Fig 27C). This is perhaps the least striking form of cell

rounding. Terms used to describe it include a “stellate” or “arborized” morphology, a star-like shape characterized by a rounded central body and disorganized extensions held in place by adhesion nodes. Rounding mode 2 occurs mostly through exogenous perturbations but can, to a lesser extent, be the result of endogenous regulation.

Cell Rounding by Perturbation of Actin and Focal Adhesions

One well-characterized example of rounding mode 2 occurs with agents that perturb F-actin, the latrunculins (marine sponge toxins)[450] and cytochalasins (fungal metabolites)[10-12, 444-450]. The disruption of F-actin results in the inability of protracted cells to remain properly spread. Bundles of F-actin cables support the webbed edges of adherent cells[563, 564], and without these actin cables, cells tend to collapse into an arborized morphology. Another reason for cell rounding via actin perturbation is that F-actin forms an integral part of focal adhesions. Its dispersion therefore compromises adhesion structures[36].

Perturbation of focal adhesions can also cause mode 2 cell rounding. Examples include genetic interventions that interfere with src family or focal adhesion kinases[451, 454, 455], microinjection or overexpression of negative regulators of focal adhesion formation[167, 453], and artificially synthesized inhibitors of key focal adhesion proteins[452].

Cell Rounding by Upstream Regulators of Actin and Focal Adhesions

On the level of upstream regulators, Rho family GTPase signaling is capable of inducing mode 2 cell rounding. Rnd1, -2, and -3 are a subset of Rho family proteins so called because they induce cell rounding in a number of cell types. When strongly activated they tend to antagonize RhoA/ROCK signaling and mediate disassembly of actin and focal adhesions[456-458]. Another example is ARAP1 and ARAP3, which are plasma membrane localized GAPs that confer inhibition to RhoA and Arf GTPases. When overexpressed they can cause loss of stress fibers and cell rounding[459, 460]. Similarly, cell rounding occurs with high concentrations (greater than 10μM) of statins, the widely prescribed HMG-CoA reductase inhibitors used to reduce patient cholesterol levels. Statins inhibit the mevalonate pathway,

which is responsible for the synthesis of cholesterol and a variety of other lipids. One result of this inhibition is that Rho-GTPases undergo diminished prenylation and therefore fail to anchor to the plasma membrane and regulate actin at the cell periphery, which can ultimately cause cell rounding[461-464, 565]. The statin results indicate that the spatiotemporal localization of Rho-GTPases to the plasma membrane is key to the coordination of actomyosin at cell membranes and this notion is in accordance with currently held views in the field[540].

Another major physiological pathway involved in cell shape changes and tissue relaxation is the cyclic AMP(cAMP)/protein kinase A(PKA) signaling program. Early studies in cell physiology linked elevated cAMP to an arborized mode of cell rounding[12, 470, 566, 567]. The activity of PKA is directly related to the concentration of cAMP in the cytosol, and PKA is a master regulator of many cellular processes including actomyosin and focal adhesion dynamics. When active PKA suppresses signaling through a number of Rho GTPases[568], particularly attenuating RhoA-based actomyosin contractility[466, 569-573]. PKA signaling also weakens focal adhesions by conferring an inhibitory phosphorylation to paxillin[465, 467, 468]. These signals converge to bring about a decrease in stress fibers, focal adhesions, and actomyosin contractility and can ultimately induce arborized cell rounding. A variety of diverse signals lead to cAMP/PKA-mediated rounding such as the cAMP-elevating agents forskolin or isobutylmethylxanthine, and agonists of receptors such as the adrenocorticotropic hormone receptor[12, 468-470], follicle stimulating hormone receptor[471, 472], and β2-adrenergic receptor[473].

Cell Rounding by Pathogenic Disruption of Actin and Focal Adhesions

A common strategy of pathogenic processes is to manipulate the properties of host cells through subversion of the actomyosin cytoskeleton[378, 574]. Such perturbations reconfigure the host cell machinery to the pathogen's advantage by facilitating processes ranging from virus entry to breakdown of tissue barriers for bacterial invasion. These

manipulations may occur at the level of upstream regulators, such as Rho-GTPases, or by direct perturbation of actin, myosin and focal adhesion molecules. Studies on the effect of bacteria and viruses in cultured cells have identified a variety of effector molecules that induce cell rounding. The following section outlines multiple pertinent examples.

Bacterial toxins reported to cause cell rounding by distorting the activity of Rho-GTPases include *Clostridium difficile* toxins A and B, which universally disable small Rho-family proteins via glucosylation[477, 478, 575], *Clostridium botulinum* C3 transferase toxin, which inactivates RhoA, RhoB, and RhoC via ADP-ribosylation[479], *Chlamydia trachomatis* protein CT166, which inactivates Rac1 through glucosylation[480], the functionally similar bacterial proteins AexT, ExoT, ExoS, and YopE, which act as GAPs to inhibit Rho-family GTPases[481-488], *Vibrio* VopS, which inactivates Rho-family GTPases through AMPylation[489], and a prototype conserved bacterial protein, EspH, which binds to and nullifies Rho-GEFs[490]. *Vibrio cholerae* uses a different strategy to cause rounding by secreting an effector called RTX toxin that covalently crosslinks G-actin and, like latrunculin A, renders it unresponsive to endogenous regulation[491-493].

Apart from bacterial effectors, viral manipulation of cellular processes can also mediate cell rounding. Viral rounding is unrelated to apoptosis, as viral transformation typically down-modulates apoptotic pathways. Historically, studies of transforming viruses provided the first appreciation that viral infection alters the host cytoskeleton. The most prominent changes in transformed cells include the rounded cell shape, motile blebs, bulging pseudopodia, loss of contact inhibition and lack of stress fibers[378]. For example, the Rous sarcoma virus (RSV) viral src (v-src) gene product is known to be responsible for the actin filament reorganization, altered surface topography, and rounding observed during infection[378]. It works by displacing the endogenous c-src protein, disrupting focal adhesions and dissolving stress fibers, and subverts actin to produce competing structures called invadapodia. Targets that are phosphorylated by v-src in these processes include vinculin and cofilin.

Herpes simplex virus also produces cell rounding through the action of a powerful effector, the US3 viral kinase. In the latter stages of the herpes virus replication cycle, when US3 is highly expressed, host cells undergo disassembly of stress fibers and rounding concomitant with the formation of actin-rich cell projections[496, 497, 499]. This occurs through US3 kinase manipulation of the activity of Rho family GTPases and PAKs[495, 497, 498].

Early studies on vaccinia virus demonstrated that infection can trigger cell rounding within a matter of hours[500, 501]. More recent studies attribute these results to the effector protein F11L, which inhibits RhoA[502-504, 576]. Indeed, vaccinia-induced cell rounding causes an arborized morphology characteristic of rounding mode 2 and apparently promotes host cell motility by reducing stable anchorage.

Cells infected with cytomegalovirus undergo decreased gene expression of focal adhesion proteins paxillin, Hic-5, and α-actinin[505]. These changes explain the cell rounding phenotype seen with ongoing infection[505, 506].

Rounding Mode 3 – Interference with External Adhesion Receptors

Cell Rounding by Interference with Integrins

Rounding mode 3 results from the failure of adhesion receptors to remain bound to their external ligands (Fig 27D). In cultured cells on a planar surface, the maintenance of adhesion is mostly dependent on integrins, which are transmembrane glycoproteins that form heterodimers from α and β subunits. The specificity of integrins for the various ECM ligands depends on the heterodimer combinations. For example, the $\alpha_5\beta_1$ combination binds to fibronectin but not collagen or laminin. The anchorage and clustering of integrins is required for the formation of basal focal adhesions and associated actin structures[28, 577]. Thus, it is not surprising that the debilitation of integrin function causes cell rounding and surface detachment. This has been demonstrated with antibodies against integrins[514] and disintegrins[509], molecules that contain specific peptide sequence motifs, such as RGD or KGD that specifically bind to integrins and displace competing ligands. Disintegrins reported to induce cell rounding include the naturally

occurring snake venom components contortrostatin[510] and saxatilin[511], and the synthetic cyclic-RGD containing compound cilengitide[512, 513]. Ebola virus glycoprotein also causes cell rounding by down regulation of cell surface levels of integrins[515, 516].

Several types of cell adhesion molecules, including integrins and cadherins, are dependent on divalent cations for their function. The Mg^{2+} and Ca^{2+} chelating agents EDTA and EGTA interfere with cell adhesion and are commonly employed as cell dissociation agents in tissue culture. However, it is still unclear whether divalent cation deprivation primarily affects the binding affinity of adhesion receptors, triggers internal rearrangements, or both. For one, retraction fibers are often observed with EDTA/EGTA-mediated cell rounding, indicating that many bonds remain in place (references[100, 517] and personal observations). Furthermore, a dependence on active and cytoskeletal processes has been observed[13, 101]. These observations support the idea that internal rearrangements in focal adhesions and the cytoskeleton may contribute to EDTA/EGTA-mediated cell rounding[100]. Culture agitation would then lead to rupture of isolated bonds[517].

Cell Rounding via the Action of Cell-Matrix Modulators

In high enough concentrations, certain endogenously secreted proteins can cause cell rounding through interactions with the extracellular domain of integrins. The anti-adhesive glycoprotein SPARC is expressed by the endothelium in response to injury and induces cell rounding, formation of intercellular gaps and an increase in endothelial barrier permeability[523, 524, 526]. The exact rounding mechanism is unclear but it is believed that SPARC modulates extracellular adhesion by mediating cell-matrix interactions. Residues identified for cell binding, inhibition of adhesion, and curtailment of focal adhesions sit on one face of the protein, whereas collagen-binding regions lie opposite[524]. These features suggest a molecular mechanism by which its potent anti-adhesive effects occur. It is also possible that SPARC initiates signaling events that affect cell attachment through effectors such as integrin-linked kinase[525, 527].

Tenascins are another group of counter-adhesive ECM ligands that are similar to SPARC and can induce rounding[522]. The tenascin family consists of four members, the best studied of which is tenascin-C, a protein reported to block the binding sites between cell surface proteins such as syndecan-4 and the ECM ligand fibronectin[521]. Evidence suggests that tenascin-C down-modulates the activity of $\alpha_5\beta_1$ integrins. It may also signal through integrins to suppress FAK-induced focal adhesion formation, and attenuate RhoA and tropomyosin-1 signaling[518-520]. Other members of the family, tenascins-R, and –X, also share the capability to down-modulate adhesion, although the exact mechanisms await characterization[522].

Cell rounding has sometimes been observed with high extracellular concentrations of galectins, a family of soluble glycan binding proteins[528]. Galectins have been observed to exert both anti- and pro-adhesive effects depending on concentration, ECM composition, and cell type[528, 529]. One commonly accepted model proposes that low concentrations of galectins promote adhesion by bridging cell-ECM interactions while higher concentrations weaken adhesion through dissociation effects[528].

Rounding Mode 4 – Surface Coating

Cell Rounding by Lectins

Rounding mode 4 occurs through formation of an external cell surface coating. This type of cell rounding is seen with lectins, multivalent proteins that bind each other and the carbohydrate moieties present in cell surface glycoproteins and glycolipids (Fig 29). They act like a bio-glue to crosslink cell surface residues and form a sticky coating around the cell, which can ultimately increase cell surface stiffness and non-specifically displace receptor-ligand bonds[534, 535]. In a multicellular scenario lectins tend to cause agglutination of cells. In the context of cell shape and mechanics, the most well studied lectins are concanavalin A (ConA), which binds mannose residues, and wheat germ agglutinin (WGA), which binds N-acetylgalactosamine (GalNAc) residues. Addition of these lectins in soluble form has been observed to cause rounding of cells in both culture[532] and live tissue environments[531, 533]. The reported timescales for lectin-

induced cell rounding span from 30 minutes to more than 6 hours. Suspended cells coated with lectins also fail to spread[537]. Notably, treatments that disrupt actin tend to lessen the degree of lectin-induced cell rounding[532, 536, 566] and cell surface stiffness[534], indicating distinct contributions of the lectin coat and the actomyosin cortex. Thus lectin coatings would seem to act synergistically with the actomyosin cortex. Because lectins behave as a non-specific type of glue, the geometry of their presentation is critical. While addition of soluble lectins causes rounding, cells seeded on lectin-functionalized surfaces can stick and spread, particularly if they exhibit low cortex tensions[536, 578, 579]. In extreme cases lectins can "glue" cells to the surface and make them resistant to trypsin and EDTA[579]. Interestingly, a fish lectin called plumieribetin seems to inhibit adhesion by a hybrid mechanism: in addition to mannose-binding capabilities like ConA, it has been reported to specifically block the integrin $\alpha_1\beta_1$-collagen interaction[530]. Taken together, these studies on lectin-induced cell rounding reinforce the idea that cell rounding is governed by an adhesion versus surface tension paradigm (Fig 29). Furthermore, given their importance in biotechnology, it is surprising so few studies have been conducted to characterize the effects of lectins on cell shape and mechanics.

Another protein reported to form an extracellular shield around cells is the drosophila protein spam. It binds to the trans-membrane protein prominin to produce a coating that endows cells with up to ten times increased stiffness, and an improved ability to resist chemically- and mechanically-induced deformations[538]. While not yet tested for cell rounding *per se*, spam fulfils the requirements of an agent that could be expected to induce cell rounding.

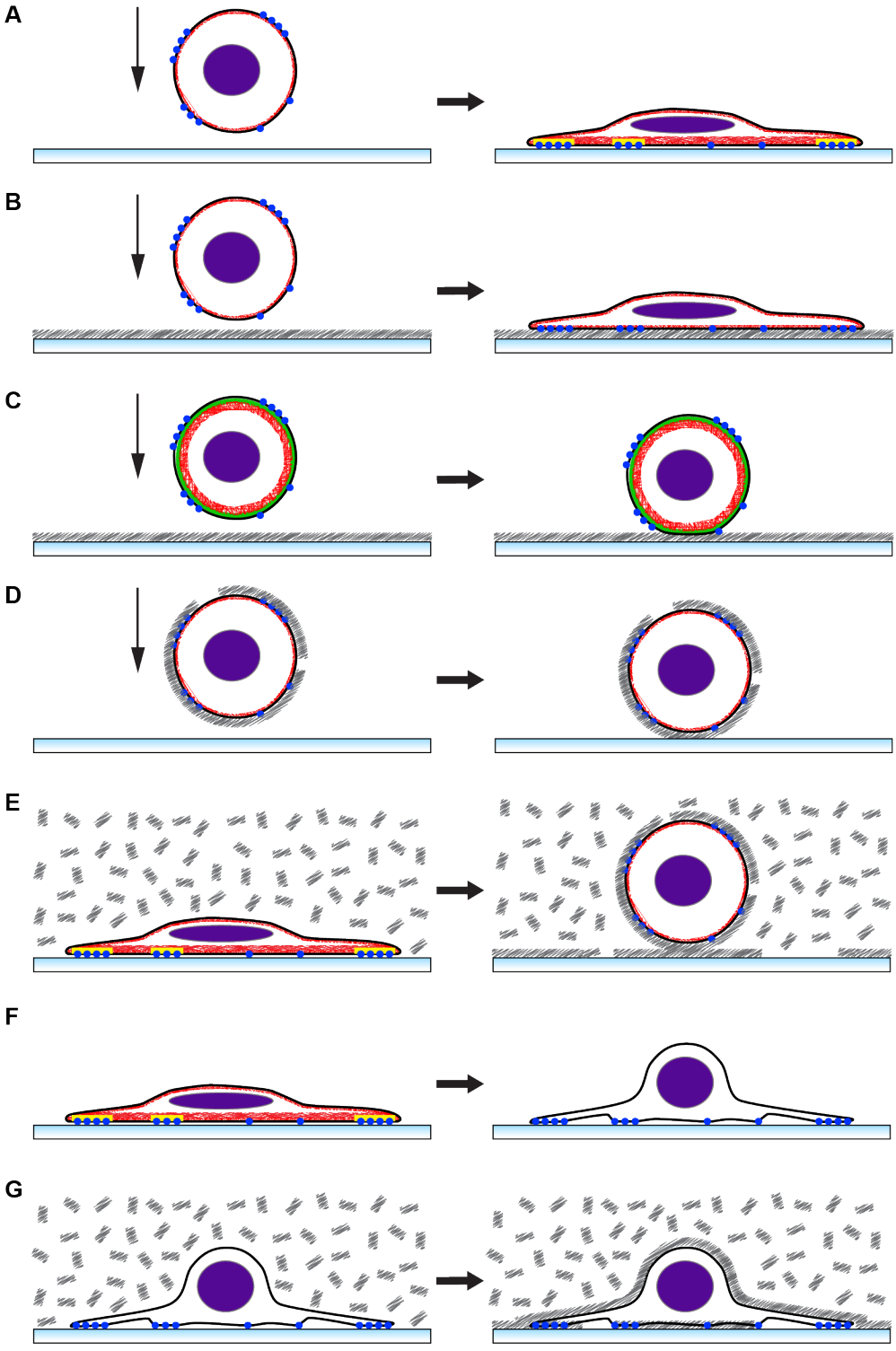

Figure 29: Lectins and Cell Shape. A Illustration of a suspended cell spreading on a substrate under normal conditions. **B** Scenario of a cell with low surface tension (thin actomyosin cortex) spreading on a lectin-coated substrate. **C** Scenario of a cell with high surface tension (thick actomyosin cortex) and prominent plasma-membrane-actomyosin cortex linkage remaining round on a lectin-coated substrate. **D** Failure of a lectin-coated cell to spread on a substrate. **E** Cell rounding by addition of soluble lectins to spread cells. **F** Weakening of actin and focal adhesions causes rounding mode 2 (see corresponding section). **G** Addition of soluble lectins to cells with weakened actin does not induce further rounding in many cases. Colours refer to actomyosin (red), integrins (blue) focal

adhesions (yellow) DNA (purple), lectins (grey), and plasma-membrane-actomyosin cortex linkage (green).

The Adhesion versus Surface Tension Paradigm in Tissue Barriers

Important tissue barriers in mammalian physiology include the cardiovascular endothelium[580], the blood-brain barrier[581], the gastrointestinal lumen[582], lung epithelia[583], and the kidney glomerular filtration barrier[584]. In each case, a single layer of cells forms a physical barrier to tightly control the movement of ions, molecules, and cells between apposing tissue spaces[585, 586]. In endothelium, increased barrier penetrance is a vital part of the acute inflammatory response to injury or infection. For example, inflammatory mediators facilitate the opening of gaps in the endothelial layer to allow leukocyte extravasation. This is particularly important in infected tissue where the infiltration of blood plasma and professional phagocytes work to combat bacteria. On the other hand, unchecked or chronic inflammation can lead to tissue degradation and problems like excessive scar tissue formation, abscesses, ulcers, and edema. Tissue barrier permeability is thus controlled by a finely-tuned set of biophysical and biochemical parameters.

The mechanical behavior and shape of constituent cells affects tissue barrier permeability. The principles that characterize the cell rounding versus spreading paradigm are also applicable to cells in tissue barriers. Increased tissue barrier permeability tends to occur through decreased cell-cell cohesion, increased actomyosin contractility, and reinforced basal adhesion[580, 587, 588](Fig 30). While the first two factors suggest cell rounding and the opening of paracellular gaps, reinforced basal adhesion prevents dissociation of cells from the layer through the fortification of underlying focal adhesions and stress fibers[580, 588, 589]. In comparison, MCR also involves an increase in actomyosin contraction but the opposite regulation of adhesion. Indeed, mitotic cells in tissue barriers downregulate basal ECM adhesion[163-168, 367] while retaining neighboring tight adherens junctions[86, 326, 327](Fig 30). In this way dissociation of mitotic

cells from the tissue layer or loss of barrier integrity is mitigated. Thus, the mechanics of contractile cell rounding (rounding mode 1) bear similarities to the mechanics of barrier permeability regulation. Furthermore, barrier tightening exhibits parallels with cell spreading, since both rely on actomyosin relaxation and an increase in adhesion[580, 588, 589]. Mechanical measurements also support this notion as barrier disruptive agonists were found to increase cell stiffness through actomyosin contraction while barrier protective agents induce cell relaxation[590].

On a biomolecular level, the biochemical interactions and pathways involved in rounding mode 1 (see Table 3) overlap significantly with those that promote tissue barrier permeability. Agents that mediate increased tissue barrier permeability include LPA, thrombin, calyculin A, angiotensin II, TGF-β1, TNF-α, microtubule disruption/GEF-H1, PKC activators, p38 activators, and TRP channels/calcium influx[580, 589, 591-599]. Many of these agents are inflammatory mediators that activate actomyosin contraction through the RhoA/ROCK/myosin II pathway[600, 601]. On the other hand, agents and pathways implicated in barrier tightening are related to actomyosin relaxation and cell spreading. These include: cAMP/PKA, Epac, Rap1, Rac1, microtubule stabilization, sphingosine-1-phosphate, fibroblast growth factor, vasodilator-stimulated phosphoprotein, and resveratrol[580, 601-607].

Modulation of tissue barrier permeability is a critical aspect of animal physiology and health. Because tissue barriers present a major obstacle to invasion, a number of pathogens employ strategies to break down or manipulate monolayer barrier integrity, often through subversion of the actin cytoskeleton and adhesion[608-610]. One strategy involves the ectopic and excessive activation of actomyosin contraction to generate para-cellular gaps for bacterial invasion. This has been reported to occur with type III group B streptococcus, which opens up the blood-brain barrier by manipulating RhoA and Rac1 signaling[611]. Moreover, extreme cases of cell contraction in tissue layers can induce a form of cell detachment known as “cell shedding”, further compromising tissue integrity[612-614]. Cell

shedding *in vivo* is analogous to cell rounding *in vitro*. Other bacteria break down tissue barriers by disrupting actomyosin in a manner analogous to rounding mode 2 (Fig 27C). *Clostridium difficile* toxin A exerts this type of effect through a global inhibition of Rho-family GTPases[575]. Similarly, *Clostridium sordellii* lethal toxin interferes with various small GTPases, including the Rac proteins to disrupt the actin cytoskeleton of endothelial cells, which eventually kills host mice by inducing a major increase in lung vascular permeability[615]. *Staphylococcus aureus* toxin C3stau inhibits RhoA, B, and C through ADP-ribosylation and this dysfunction results in the generation of para-cellular passages for bacterial transit[616]. Taken together, these and other research reports support the idea that tissue barrier integrity emerges from the effects of adhesion forces and contractile actomyosin tension at the cellular scale. Better insight into the physical basis of cellular mechanics is thus required for a more complete understanding of tissue physiology, particularly in regards to the ability to resist bacterial invasion.

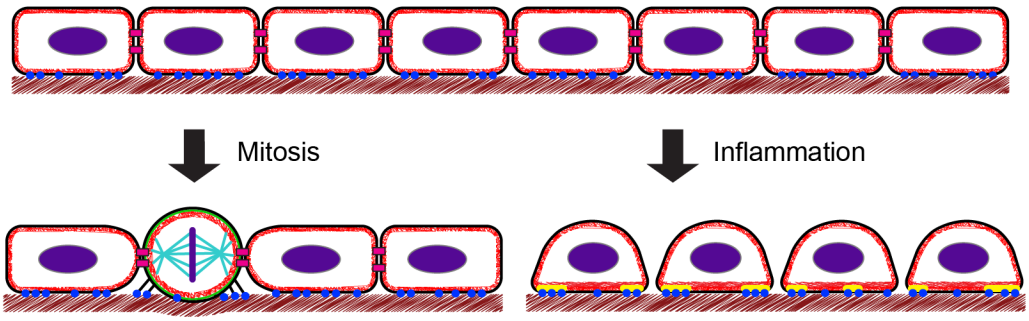

Figure 30: The adhesion versus contractile tension paradigm in tissue barrier monolayers. The schematic shows a quiescent monolayer of cells anchored to basal ECM (brown scribble). Depicted features include actomyosin (red), DNA (purple), cell-ECM adhesion molecules (blue), cell-cell adhesion junctions (pink), focal adhesions (yellow), mitotic microtubules (cyan), and prominent cortex-plasma membrane linkers (green). Mitotic cells round up through actomyosin cortex contraction and diminution of extracellular matrix adhesion but retain cell-cell junctions. Inflammatory signals lead to partial rounding of cells and an increase in tissue barrier permeability. This is mediated through actomyosin contraction, down-modulation of cell-cell contacts and increased cell-ECM basal adhesion.

Discussion Summary

The physical basis of MCR involves an increase in intracellular pressure and surface tension, and a decrease in adhesion (Fig 24). The experiments of this thesis focussed on the origin of increased mitotic rounding pressure and found it to be dependent on the actomyosin cortex and transmembrane osmolyte gradients (Fig 23-25). An analysis of the literature reveals that mitotic deadhesion is mediated by disassembly of focal adhesions and reorganization of actomyosin[13, 17, 62, 63, 163-168].

The biological basis of MCR originates from the activity of the Cdk1-CyclinB complex, which drives mitotic entry (Fig 26). A summary of candidate biochemical pathways that culminate to drive the physical changes characteristic of MCR is presented table 2.

A comprehensive synthesis of the literature on cell rounding (approx. 750 pubmed search hits on "cell rounding" as of April 2012) reveals that the spread-to-round transition can be explained by considering the balance between surface tension/intracellular pressure and adhesion ([38, 139] and Fig 27). With such a paradigm, cell rounding can be physically categorized into four distinct modes (Fig 27), of which one is an MCR-like mode (rounding mode 1). The diversity of biochemical signals, biophysical mechanisms and pathophysiological strategies that underly these rounding transitions are presented in table 3. This analysis highlights the idea that cell rounding *in vitro* is indicative of changes in tissue properties *in vivo*. As an example, the biophysical paradigms evident from studies of cell rounding can be applied to describe the physiology of tissue barrier permeability (Fig 30). Thus, much can be learnt about the organization of cells and tissues by thinking about MCR and other types of cell rounding in terms of their physiological and biological contexts.

Outlook

MCR as a Model Problem in Cell Mechanics

While cell adhesion and spreading on surfaces have been thoroughly studied, cell rounding has received comparatively little attention. But given the wide range of biological contexts it is implicated in (see discussion section *General Cell Rounding*), striving towards a better understanding of cell rounding is a worthwhile endeavour. The mechanics of rounded cells may even be more physiologically relevant than the classic, but somewhat artificial, spread shape of cultured cells on planar substrates since cells in tissues are generally more globular. Furthermore, much can be learned about how cell adhesion works by studying the reciprocal process of rounding. For example, MCR reveals that cells can markedly decrease their substrate grip without necessarily having to alter the affinity of external adhesion receptors (see discussion section C*hanges in Adhesion During Rounding*). As has been demonstrated in this thesis, rounded cells are also a suitable system to investigate the general relationship between the actomyosin cortex, cell surface tension, intracellular pressure and whole-cell stiffness (Fig 25).

The tools and approaches developed in this thesis have been used to gain insight into both induced and mitotic cell rounding. Indeed, MCR represents a model problem that can be leveraged to elucidate both general and cell cycle specific principles that govern cell shape, size and mechanical properties.

The Mechanics of Cell Rounding Beyond Mitosis

Cell rounding has been observed with microscopy for many years and the role of a number of biological pathways and pathophysiological processes involved have been catalogued (Table 3). However, very little mechanical analysis has been performed until now and thus the physical basis of the various types of cell rounding remains poorly understood. The optical microscopy-AFM setup and subsequent assays developed in this thesis to probe MCR can similarly be applied to the full diversity of problems in cell rounding. For example, the precise quantification of changes in surface

tension and intracellular pressure of single endothelial cells in response to inflammatory mediators should pave the way for a better understanding of tissue barrier permeability and the physiology of inflammation (Fig 30). Such studies would help to reveal how core biochemical pathways modulate the physical properties of cells and tissues.

Improved Cell Mechanics Methodology

Parallel plate compression experiments such as the AFM CHA measure the force response of a given cell in response to deformation. In the case of the AFM CHA, one major improvement would be to correct for the 10 degree tilt of the cantilever. This could be done by functionalizing the end of the cantilever with a wedge. Tilt-corrected cantilevers would enable proper parallel plate mechanics and simplify the geometrical analysis. They would also prevent sliding of cells, an advancement that would allow the application of larger forces and deformations, and mean the utilization of the somewhat clumsy "rounding modulus" would no longer be necessary to normalize pressure to changes in deformation throughout an experiment. Indeed, moving away from force and rounding modulus toward more standard parameters like pressure and tension should be a goal for future studies.

In order to calculate the pressure difference across the cell membrane in a CHA one needs to know the force and the contact area. Surface tension can then be calculated from the pressure and radii of curvature through the law of Young-Laplace[175]. Due to limitations with imaging, the analysis in this thesis simply assumes that compressed cells take on the shape of a barrel with uniform radius (Fig 25A). In future, better determination of cell shape should enable proper evaluation of the intracellular pressure and cell surface tension. Furthermore, the uniform surface tension of rounded cells should allow residual cell-substrate adhesion to be approximated. As a result of adhesion, the shape of the rounded cell will deviate from the theoretical non-adhered shape (Young-Laplace model). The extent of this deviation could be used to qualitatively assess adhesion.

True parallel plate mechanics would also facilitate the application of the large forces and deformations necessary to probe the link between rounding

and mitotic progression (Fig 5). Indeed, it remains to be determined to what extent cell shape is related to mitotic progression across different cell types.

Understanding Cell Compression

Surprisingly little is known about the passive and active response of cells to compression. Parameters of interest include changes in intracellular pressure, surface tension, surface area, volume, and viscoelastic relaxation dynamics. In response to tensile deformation, many cell types have been observed to exhibit nonlinear elasticity, with reports of both strain-hardening[617] and strain-softening[618] behavior. However, it is currently unknown whether nonlinear elasticity occurs with compression. A related question is whether intracellular pressure and surface tension change with compression. One might expect these effects to be intrinsically linked to the geometrical consequence of the deformation itself. For example, a sphere-to-barrel shape transition, such as is assumed to occur in the compression of mitotic cells (Fig 9), is indicative of an increase in surface area. If the total amount of actomyosin were limiting, this would cause a "dilution" of actin and myosin over an increased surface area or, in other words, a thinning of the cortical layer and a reduction in myosin motor protein density per unit area. On short timescales the elasticity of the actomyosin cortex would likely resist such an increase in surface area. But on timescales ranging from tens of seconds to several minutes it would lose any shape-memory linking it to the uncompressed state, because actomyosin networks in cells are gel-like, dynamic, and exhibit high turnover rates[619-622]. Therefore, MCR might serve as a mechanism to concentrate a limited amount of actin and myosin into a minimum surface area, thereby maximizing actomyosin cortex tension for a given cell.

Another intriguing aspect of cell compression is to what extent changes in volume or surface area occur. Poisson's ratios of 0.3 to 0.4 have been reported in articular chondrocytes subject to compression (see section *Deformation and Cell Volume*). The results achieved with HeLa cells in this thesis (Fig 12), imply a Poisson's ratio of 0.35. In future, it will be interesting to see how Poisson's ratio varies among cell types and whether the cell

regulates this property. If so, it would constitute a largely unexplored form of volume regulation.

This thesis primarily dealt with equilibrium mechanical properties of cells. Trans-mitotic CFA and CHA experiments looked at the sustained response of cells to constant forces and deformations. However, an example of a dynamic experiment is demonstrated with the CHA-via-compression on already round cells, where initially high forces relax to equilibrium over a characteristic timescale (Fig 11A). By addressing the dynamic aspects of cell mechanics, insight into the origins of cellular viscoelasticity can be made[90] and this should be a point of active interest in future. A proper understanding of the response of rounded cells to compression would be a significant step forward in cell mechanics.

Ongoing AFM-based Screening for MCR Pathways

This thesis explored the physical basis of MCR, but many of the individual genes and proteins involved in MCR remain to be identified. In order to improve our understanding of MCR, future efforts must link the mechanical phenomena to molecular pathways and attempt to build a parts list of molecular assemblies and mesoscale components that govern cellular force generation and mechanical properties. One way to systematically determine the function of proteins in a cellular process is large-scale chemical or genetic screening[122, 623]. To date, no screens have been conducted to catalogue mechanical phenotypes, probably due to a lack of suitable assays.

To test the technical feasibility and scientific value of mechanical phenotyping, the 8 μm CHA-via-compression (Fig 11A, Fig 31A) was used to perform a pilot RNAi screen on 93 gene products previously shown to localize to the periphery of mitotic cells([624] and observations from Yusuke Toyoda). With the 8 μm CHA-via-compression it was possible to harvest one force-relaxation curve per cell every ~5 minutes. For each esiRNA knockdown approximately ten force relaxation curves were gathered in an hour. This work rate enabled the mitotic mechanical phenotypes of the 93 gene products to be screened in about two weeks. Force-relaxation data shows that compressed mitotic cells typically reach an equilibrium force

after about 80-120 seconds (Fig 31B). Normalizing the equilibrium force to a rounding modulus reveals significant differences between the various esiRNA knockdown treatments (Fig 31C). Out of the 93 genes tested, 9 came up as being significantly different compared to negative controls (Fig 31D). Expected hits such as myosin II subunits (MRLC2, MYH9), Rho kinases (ROCK1, ROCK2), and a Rho GEF known to be highly active in mitosis (ECT2)[625] were detected. In addition, Park7, UACA, CDC37, and alpha-actinin isoform 4 (ACTN4) yielded novel mechanical phenotypes. These results demonstrate the technical feasibility and scientific value of mechanical phenotyping with AFM. Such approaches should pave the way for a systematic identification of genes and proteins involved in MCR and cell mechanics.

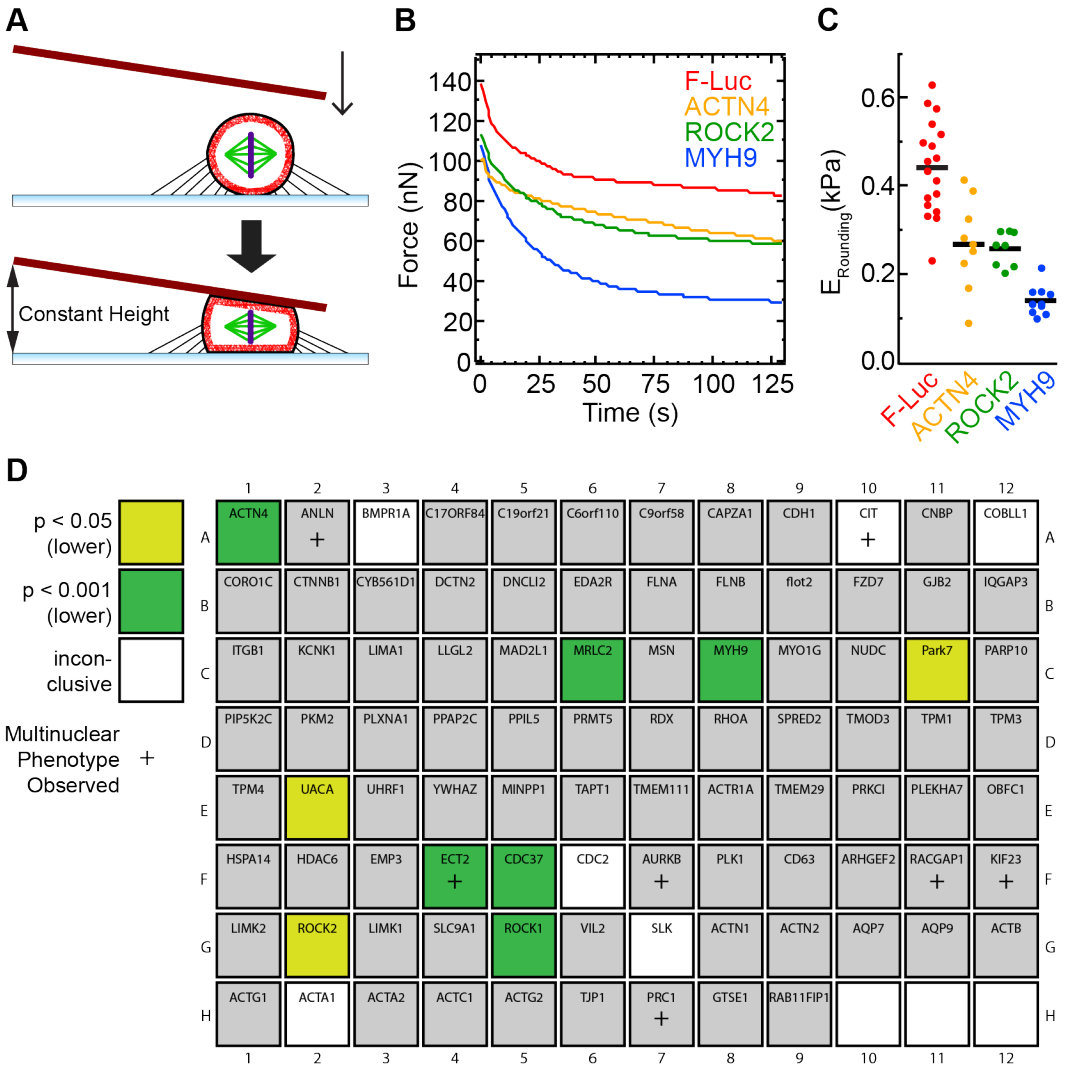

Figure 31: A An 8 µm compression-initiated CHA on an already round cell as shown in figure 11A. **B** Averaged force-relaxation curves for esiRNA knockdowns

of Firefly luciferase (negative control, F-luc, red, n=17), α-actinin isoform 4 (ACTN4, yellow, n=10), Rho kinase 2 (ROCK2, green, n=10), and non-muscle myosin heavy chain IIA (MYH9, blue, n=9) in transgenic H2B-GFP mCherry-CAAX HeLa cells. **C** Scatter plots of equilibrium (plateau) rounding moduli ($E_{Rounding}$) for indicated esiRNA conditions in B. **D** Mitotic mechanical phenotyping of 93 genes previously observed to exhibit cortex localization in mitosis ([624] and Yusuke Toyoda experimental data) with esiRNA expression knockdowns and the 8 μm compression-initiated CHA (A, Fig 11A). Mitotic cells were arrested with 2 μM STC. p values determined with students t-tests (Excel) in comparison to F-Luc negative controls are colored as indicated. Multinucleate phenotypes (+) indicate cell division failure phenotypes.

Conclusions

To facilitate rounding in a dense environment, mitotic cells must produce an active outward force against external impediments. An AFM-based assay that uses flat tipless cantilevers, the constant height assay (CHA), was developed and deployed to measure these forces. Mitotic cells uniaxially confined to ~50% of their spherical height produce forces of up to 100 nN, which corresponds to internal pressures of at least 200 Pascals and surface tensions of up to 10 nN/μm. The balance between actomyosin cortex contraction and intracellular osmotic potential sets the surface tension and volume of cells. Moreover, the results of this thesis suggest that the actomyosin cortex can serve in an analogous manner to the cell wall of plants and microorganisms to facilitate the buildup of significant hydrostatic pressure in animal cells.

The shape change inherent to MCR involves an increase in cell surface tension and a decrease in cell-substrate adhesion. The actomyosin cortex and intracellular osmotic potential set cell surface tension. Decreased adhesion is mediated by focal adhesion disassembly and reorganization of the cytoskeleton, and thus does not require diminution in the affinity of external adhesion receptors.

The adhesion versus surface tension paradigm in cell mechanics is central to cell shape control in a wide variety of biological contexts beyond mitosis. As such, MCR can be leveraged as a model problem to uncover general and cell cycle specific principles that govern the mechanics, morphology, and physiology of cells and the tissues they form. The combined AFM-optical microscopy approaches developed in this thesis will provide a useful foundation for future investigations in these topics.

Methods

Outlined is an equipment list, details of reagent setup, and protocols for setup of the AFM and calibration, CFAs and CHAs, and mid-experiment introduction of perturbants.

Equipment

• Nanowizard AFM system (JPK, Berlin). Accessories such as petridish holders or the JPK biocell were used to host live cells in medium on the microscope stage.

• Axiovision/Cell Observer inverted optical microscope (Zeiss, Germany). Included were capabilities for differential interference contrast (DIC) microscopy, which enables improved imaging through the silicon cantilever, and fluorescence microscopy to image fluorescently tagged proteins in cells. Images were acquired with an Apochromat 20x/0.8 NA objective lens.

• "The cube and box" incubation system (LIS, Switzerland). A custom setup was designed to enclose the whole microscope. The setup was switched on at least 4 hours before experiments to allow the system to thermally equilibrate.

• Tipless silicon AFM cantilevers NSC-12 series (Mikromasch, Estonia), featuring six different cantilevers per chip, labeled A-F. NSC-12 cantilevers D-F were used, and are 250-350 μm long, 35 μm wide, 2 μm thick and made of pure silicon. Unless the cantilevers were new, they were cleaned by cyclical rinsing with 2% helmanex and pure water. Ultrasonic cleaning in 2% helmanex at 50-60°C for 5 minutes is useful in particularly resistant cases.

▲ **CRITICAL** Cantilever material choice is a critical parameter in these experiments. Pure silicon or silicon nitride cantilevers were used as metal-coated cantilevers often suffer from extensive drift due to the difference between the thermal expansion coefficients of bulk cantilever material and the metal layer.

▲ **CRITICAL** HeLa cells under significant deformations (≥50%) can be expected to produce resistance forces of up to 100 nN. For this reason, mikromasch cantilevers D, E or F (nominal k≈0.35, 0.3, 0.65 N/m,

respectively) were selected. First, a cantilever that is too soft will deflect the laser beam beyond the range detectable by the AFM optics. Second, a stiffer cantilever is better at maintaining the cell under a state of constant deformation. For example, a cantilever with k≈0.3 N/m bends ≈333 nm at 100 nN.

• Twin Aladdin push-pull pump setup (WPI, Berlin) along with syringes and tubings for media exchange.

Reagent Setup

HeLa cell culture. HeLa cells were maintained in DMEM (Invitrogen, cat. no. 31966-021) supplemented with 10% fetal bovine serum (FBS; Gibco, cat. no. 10270) and 1% penicillin-streptomycin (100×; Gibco, cat. no. 15140). To prepare cells for AFM experiments, HeLa cells were seeded onto substrates compatible with mounting on the microscope stage. The goal was to achieve between 25% to 75% confluency at the time of AFM experiments. This ensured sufficient cells while also providing enough spaces to reference the height of the substrate.

▲ **CRITICAL** To visualize chromatin appearance and assess mitotic phase a H2B-GFP transgenic cell line was used. Such a cell line can be produced as outlined by Kanda et al.[77]. Alternatively, Hoechst33342 (100 ng/ml) may be used to visualize chromatin for a short time[76].

CO_2 independent DMEM for AFM experiments. A sachet of DMEM powder (Invitrogen, cat. no. 12800-017) makes one liter of medium, as indicated by instructions on packet. Because the AFM setup was not enclosed in a 5% CO_2 environment, CO_2 independent medium was used. DMEM can be made CO_2 independent by altering the recipe to include only 4 mM (350 mg) $NaHCO_3$ (Sigma, cat. no. S6014) and adding 20 mM (4.77 g) HEPES (Sigma, cat. no. H3375). After sterile filtering, medium can be kept for several months at 4°C. Before experiments, 10% FBS was added. 1% penicillin-streptomycin is optional.

Inhibitors. Inhibitors (see table 1 for a list) were ordered from Sigma-Aldrich, Merck, or Tocris. Inhibitors were made up in stock solutions with

DMSO and concentrations were selected to yield no more than 1% DMSO when diluted in cell medium.

EDTA and Trypsin for induced rounding experiments. EDTA was simply added to experimental cell medium at the concentrations indicated. Because DMEM contains 1.8 mM calcium and 0.8 mM magnesium, at least 3 mM EDTA was generally required to induce cell rounding. For trypsin-induced cell rounding, experimental medium was supplemented with 10% NuSerum (BD Biosciences, NJ, USA), a low protein alternative to FBS. NuSerum was selected to increase the efficiency of the 2.5 mg/L (1x) trypsin (Gibco cat. no. 15090-046) treatment.

Tonic shocks. For hypotonic shocks, experimental medium was diluted in water to 190 mOsm/kg. For hypertonic shocks, osmolarity of experimental medium was elevated to 490 mOsm/kg with xylose (Sigma, cat. no. 95729), which increases osmolarity by approximately ~70 mOsm per 1% w/v added.

Pore-forming toxins. *Staphylococcus aureus* α-toxin and *Escherichia Coli* hemolysin (HlyA) were obtained from Sucharit Bhakdi (Johannes Gutenberg-University, Mainz). α-toxin stock was made at 2 mg/ml in PBS. Due to limited amounts of α-toxin stock, 100 µl of a 5x concentrate was added to 400 µl of experimental medium to arrive at the final concentration. The effect of α-toxin seemed to be related to confluency, therefore the cell confluency was carefully controlled at 40-50% for toxin experiments. Concentrations at and below 20 µg/ml had no noticeable effect on cells while dosages of 40-80 µg/ml caused effects such as those seen in figure 22F. HlyA stock was made up at 910 µg/ml in 8 M guanine HCl solution. Again, due to limited amount of toxin stock the 5x concentrate addition method was used as described for α-toxin. A final concentration of 1 µg/ml had little effect on cells. However, 2-4 µg/ml yielded results as seen in figure 22K.

▲ **CRITICAL** In experiments where mid-experiment addition of perturbants or medium exchange occur (see table 1, dynamic perturbations) it is essential to match the refractive index (RI) of perturbant media to the standard experimental medium. This is because introduction of a second liquid with a different RI causes spurious disturbances in the laser-based

AFM measurements (Fig 32). Ficoll (Sigma, cat. no. F2637), a neutral, inert, high mass, and hydrophilic polysaccharide that has negligible effect on osmolarity can be added to the hypotonic solution until the RI is matched. Addition of 1% w/v ficoll increases RI by +0.0013. RI may be checked with a refractometer. When using inhibitors dissolved in DMSO, one must consider that addition of DMSO changes RI by +0.0015 per 1% v/v.

▲ **CRITICAL** In cases where the perturbant mixture and standard experimental medium exhibit an unintended mismatch in osmolarity, xylose can be used to raise the osmolarity of the lower solution. 1% w/v xylose increases osmolarity by ~70 mOsm but also increases RI by 0.0013. In such cases, ficoll can be additionally employed to match RI. In all cases, ficoll and xylose never exceeded 3% w/v and did not retard progression through mitosis or adversely influence the mechanical properties of cells.

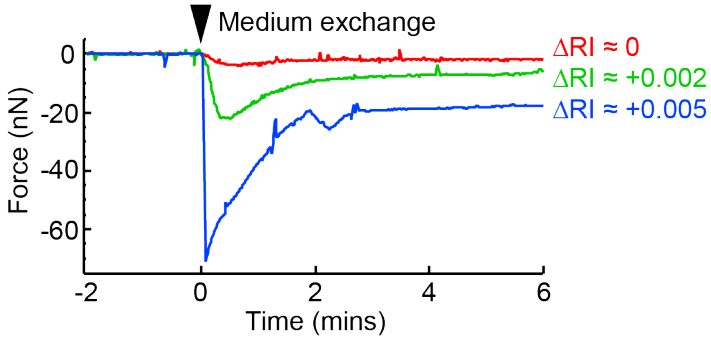

Figure 32: Examples of spurious disturbance in force recorded by the AFM setup during exchange of medium with different refractive indices. At time t = 2 min, 2,000 µl medium is exchanged at a flow rate of 2,500 µl/min while the AFM cantilever hovers ~10 µm above the substrate surface. Spurious disturbance in force can be minimized to a negligible level by reducing the difference in refractive index, ΔRI, between incoming and extant medium.

Protocols

Setting up AFM, Optical Microscope and Cantilever Calibration

1| AFM controller, optical microscope and camera are turned on. The AFM control and optical microscopy software programs are opened.

2| A clean NSC-12 cantilever is mounted onto the transparent AFM cantilever holding block supplied with the AFM. The longer cantilevers (D, E and F) are positioned to face out.

3| The cantilever holding block is inserted and locked into the AFM head. The AFM head is placed on the microscope stage and the cantilever is positioned within the field of view of the optical microscope, focused on, and checked to be in suitable condition. The height of the cantilever is noted by checking the z-focus in the microscopy software. The AFM head is removed and put aside. The appropriate liquid container is mounted on the microscope stage. The substrate of the liquid container positioned lower than the height of the cantilever by comparing the z-focus in microscopy software and making adjustment in the AFM head height if necessary. The AFM head is then reinstated on the stage ensuring that the cantilever is submerged in liquid.

4| The cantilever is focused on with optical microscopy software. The AFM laser signal is switched on and made visible by selecting the appropriate filters that allow the camera to detect the laser. The microscopy software is then used to acquire a live image and camera exposure reduced until the laser spot can be clearly seen. The laser spot is aligned on the end of the cantilever and the photodiode signal adjusted according to the guidelines of the AFM manufacturer.

5| To begin calibrating the cantilever, the cantilever is positioned over a blank region on the substrate and the approach program in the AFM software used to bring the cantilever within the vicinity of the surface. Then, extension-retraction cycles are performed against the glass surface and the cantilever sensitivity is subsequently determined according to the routines incorporated in the AFM control software.

▲ **CRITICAL** The factor used to convert the volts measured in the AFM photodiode to nanometers of cantilever deflection is usually referred to as sensitivity. It depends on many parameters, including the type of cantilever and how it is mounted. Thus, sensitivity must be determined each time a cantilever is mounted or remounted. To determine sensitivity, an extension retraction cycle is performed against the hard surface of the glass coverslip. The subsequent force-distance data is used to analyze the deflection of the cantilever when in contact with the glass surface. In this contact region, the

deflection of the cantilever is equal to the vertical movement of the AFM piezo element.

6| To complete the calibration process, a cantilever spring constant (k) must be provided. The AFM software is used to perform a thermal noise calibration. To avoid surface induced artifacts, the cantilever must be withdrawn at least 100 μm from the glass coverslip.

▲ **CRITICAL** The parameters established in cantilever calibration are necessary to convert the measured photodiode voltage into a force. Firstly voltage (V) is multiplied by sensitivity (nm/V) to yield deflection distance (nm), which is in turn multiplied by the spring constant (N/m) to calculate the force (N). Most manufacturers supply a nominal spring constant for a given cantilever. The spring constant can be estimated from the dimensions of the cantilever and the properties of the constituent material. However, true spring constants of cantilevers frequently differ from the nominal values by a factor up to 3. Most AFM software packages enable the measurement of the spring constant of a cantilever using the thermal noise method, which records the thermal fluctuations of the cantilever and uses this data in conjunction with the equipartition theorem to calculate the cantilever spring constant[626]. Essentially, the theorem equates the thermal energy at a given temperature with the energy within the oscillation of the cantilever. The thermal noise method is the most versatile and implementable method of cantilever calibration[627]. A high estimate of the method's error is 20%[627]. It can be argued that other calibration methods are more accurate, but the extra effort required to apply these with the numerous cantilevers used in this thesis make them unfeasible.

Performing an AFM Constant Force/Height Assay

1| The blank liquid container used for setup and calibration is replaced with cultured cells (see *REAGENT SETUP*). Cells are then submerged in CO_2 independent experimental medium (see *REAGENT SETUP*) and maintained at 37°C with the appropriate incubation equipment.

2| A cell of interest is identified with optical microscopy. The fluorescence H2B-GFP signal can be used to determine mitotic phase according to the scheme shown in figure 33.

3| The cantilever is approached to a blank site on the substrate adjacent the cell of interest and height of the substrate is determined.

4| The end of the cantilever is positioned over the cell.

A: For an 8 μm CHA, the AFM software is used to extend the cantilever down to a height 8 μm above the substrate and this position is held. The cell is thus confined to an 8 μm height. The AFM software is set to record force versus time into a data file.

B: For the CFA, the AFM software is used to extend the cantilever down until the selected force is reached and maintained by feedback loops. The cell is thus subject to a constant force. The AFM software is set to record height versus time into a data file. The cell height under the applied force is the recorded height minus the height of the substrate determined in step 3.

5| Optical microscopy software is used to acquire DIC and fluorescence images of the cell at 2 minute intervals or as dictated by the requirements of the experiment. In the case of the CHA, these images are then analyzed and used in conjunction with the force data to calculate the volume, rounding pressure and rounding modulus (Fig 9).

6| After a CHA or CFA, the height of the substrate was re-measured to assess mechanical drift. If significant, substrate drift data was linearized and integrated into the calculation of height for each time point. Cantilever deflection drift was usually <2 nN per hour and was considered negligible when taking into account the magnitude of forces measured (CHA) or applied (CFA).

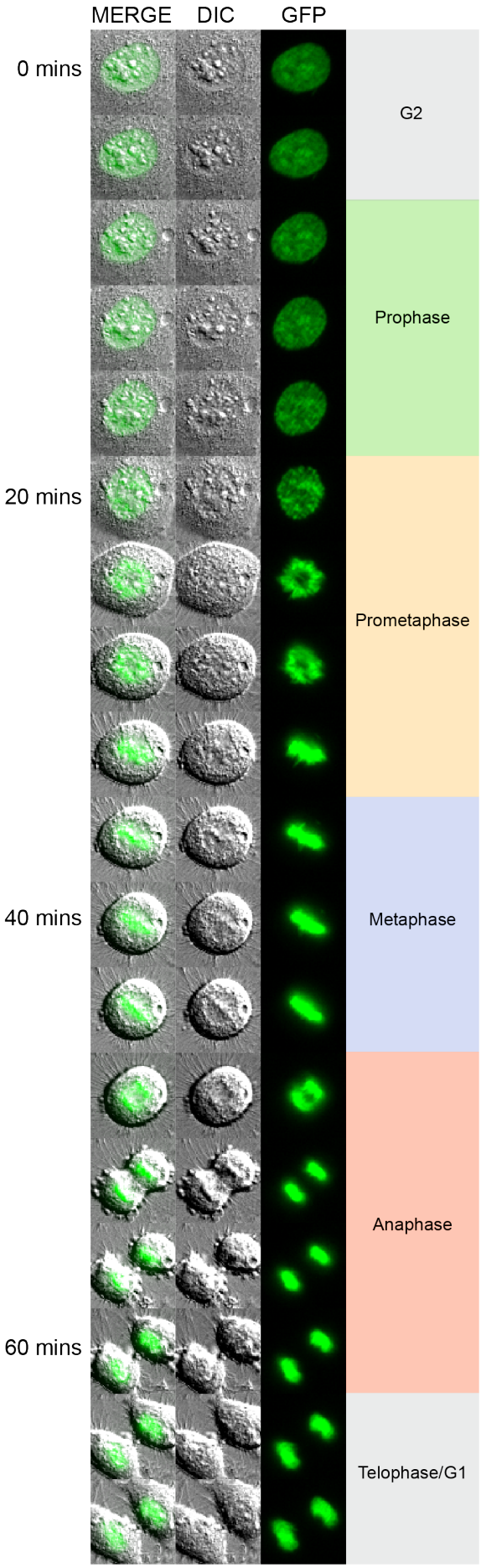
MERGE
DIC
GFP
0 mins
20 mins
40 mins
60 mins
G2
Prophase
Prometaphase
Metaphase
Anaphase
Telophase/G1

Figure 33: Example of a transgenic HeLa cell expressing H2B-GFP going from G2 through to the end of mitosis. DIC and GFP images are shown every 4 minutes. The phases and designated colour schemes are shown on the right. GFP-H2B images were used to determine the phase of mitosis according to the following criteria: prophase cells contain condensed chromosomes surrounded by an intact nuclear envelope; prometaphase starts with nuclear envelope breakdown; metaphase is when chromosomes align to form the metaphase plate; anaphase starts when the chromosomes begin to separate; telophase commences when chromosomes de-condense.

Mid-Experiment Dynamic Perturbations

1| As indicated in *REAGENT SETUP*, the refractive index of a perturbant mixture is first checked to be matched with the standard experimental medium.

2| Two methods were used to introduce perturbants:

A) Addition of a concentrate. A micro-syringe connected to plastic tubing is used to inject agents into the experimental media as a concentrate at the appropriate volume ratio. For example, by injecting 100 µl of a 5x concentrate into 400 µl medium, as was done with the pore-forming toxins. This option is useful when dealing with limited amounts of reagents.

B) Medium exchange. Twin syringes (>3 ml) are used in conjunction with push-pull syringe pumps (See *EQUIPMENT*) to exchange the full volume. The full volume of the experimental container is exchanged 5 times at maximum pumping speed, such that tonic shock or other medium exchange will occur as rapidly as possible (within less than a minute in the case of experiments in figure 22).

▲ **CRITICAL** To prevent bubbles being pumped into the experimental chamber, no more than 95% of a given syringe's volume was pumped out.

A schematic of the setup for medium exchange during an AFM CHA is shown in figure 34.

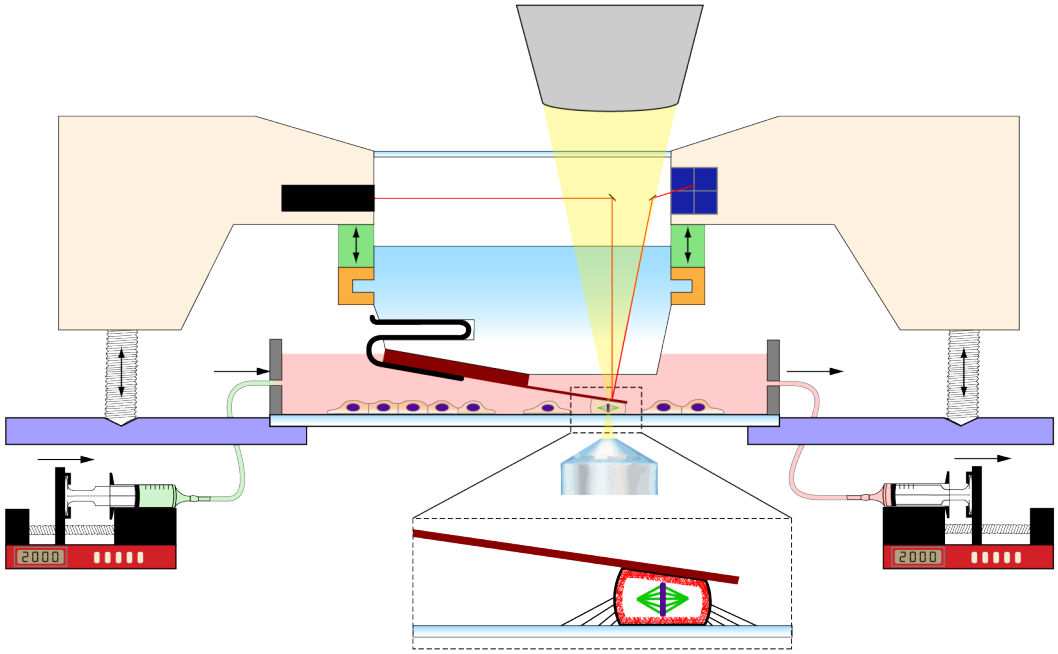

Figure 34: Experimental setup: a schematic of the AFM setup and a mitotic HeLa cell as it is confined under a flat tipless AFM cantilever. Cantilever deflection is measured with the AFM laser-based optical lever principle and converted to a force via parameters established through standard calibration procedures. The cantilever is held in place flush with the 10° angle of the glass block using a metal spring clip (black). The glass block is secured into the AFM head below the piezoelectric actuator with a twist-lock system (orange). A window within the AFM head facilitates transmission light microscopy. Coarse motors (screw legs) vertically position the AFM head within range of the substrate. Fine piezoelectric movements (green element) control the movement of the glass block and cantilever chip combination during AFM experiments. Push-pull pump setups can be used to exchange media during live cell experiments, and therefore expose the cell to various perturbations. A zoomed diagram of the confined cell and cantilever is shown in the dashed box.

Methods Discussion

Methods in Cell Mechanics

Advancement in the field of cell mechanics has been driven by the development and optimization of techniques to measure and apply forces and displacements with piconewton and nanometer sensitivity in combination with enhanced live cell microscopy[628]. Methods currently in use can be roughly split into two categories. The first involves active imposition of force or deformation on the cell and this category includes micropipette aspiration[179], parallel plate devices[629, 630], magnetic twisting cytometry[631, 632], active microrheology[633], optical tweezers[634-636], optical cell stretching[637], cell-populated substrate or

gel deformation devices[638, 639], fluid shear stress[640, 641], microfluidics[642, 643], micro-electro-mechanical systems (MEMS)[644, 645], and various modes of atomic force microscopy (AFM)[646-651]. The second category of methods instead tease out mechanical information from optical or acoustic data and includes passive microrheology by tracking probe particles[633] or subcellular components[652, 653], analysis of contractile release dynamics[507, 654, 655], acoustic microscopy[656, 657], laser ablation of subcellular structures[658], optical mapping of intracellular force distribution[659], and traction force microscopy in 2D using deformable substrates[660, 661] and flexible micropillar arrays[662, 663] or in 3D with elastic gel matrices containing embedded fiduciary markers[664, 665]. In general, the first category of techniques is more straightforward and involves fewer assumptions while the second category involves substantial computational and data analysis but has a better capability to probe beyond the surface.

AFM in Cell Mechanics

Of the abovementioned techniques one of the most versatile is AFM, which provides a multifaceted platform to study forces and mechanics in cell biology. Commercial AFMs designed for biological research are becoming increasingly adaptable and include cell-friendly options such as temperature control, liquid perfusion and compatibility with high-end light microscopes. Moreover, the experimental procedure can be tailored to probe local or global mechanical properties of cells over a wide range of forces from picoNewtons to microNewtons, at nanometer precision, and high temporal resolution ranging from microseconds to hours. The cantilever can be made to perform rapid indentations, long-timescale deformations, or oscillations over various frequencies to extract rheological moduli. For example, mechanical measurements can be made locally by using pyramidal or spherical tips to indent the cell[39, 646, 666, 667] or subjecting it to oscillations of varying frequency[647, 649-651]. Alternatively, global cell measurements can be made by using flat cantilevers to perform whole cell compression[648, 668], stretching[648], or oscillatory deformation[669]

experiments. Apart from traditional mechanics, other innovative AFM methods have been developed to quantify, for example, cell adhesion forces down to single receptor level[83, 84] and the forces of cell motility[670]. Moreover, AFM is also a valuable tool to probe the nanomechanics of biomolecules, such as individual proteins, that may be important in cellular mechanics[628, 671, 672]. Notwithstanding these benefits, disadvantages of most AFM-based methods in cell mechanics include the time consuming and low throughput nature of single-cell experiments and the inability to probe beyond the cell surface.

The AFM Constant Height Assay to Analyze Cell Mechanics and Volume

The main assay used to analyze cell mechanics and volume in this thesis was the 8μm CHA, where a round cell is vertically deformed ≈50% by a flat tipless cantilever while the AFM records the response force in real time. This is essentially a stress-relaxation assay in materials science terms: a constant deformation is imposed on a material sample and the response stress is monitored as a function of time[90]. Simultaneously, transmission and/or fluorescence optical microscopy are used to measure cell dimensions (Fig 9). From this one can calculate cell volume, response stress or "rounding pressure", and a normalized version of rounding pressure termed "rounding modulus" (Fig 9). In the context of mitotic cells the response stress is referred to as rounding pressure because these forces must drive mitotic cell rounding in a tight packed tissue environment. If cell deformation is close to constant, then the measured pressure (force/area) is essentially proportional to elastic modulus, a convenient mechanical boundary condition for this protocol. To prevent the CHA from changing height too much and also to measure larger forces (greater than 100 nN), stiff cantilevers (at least 300 mN/m) are used. Furthermore, large cellular deformations (greater than 50%) are helpful in experiments where significant volume changes are anticipated. This is demonstrated in figure 35 with the case of a round cell that changes volume by 20%. With a CHA that vertically deforms the cell height by 10%, a 20% volume decrease or increase causes vertical deformation to become 3% or 15.3%, respectively (Fig 35A(i)). However,

with a 50% cell height deformation, the same volume alterations cause vertical deformation to become 46.1% and 52.9% respectively (Fig 35A(ii)). Therefore, a CHA with a larger initial deformation is better at holding deformation at a constant value during cell volume changes. In future, an integrated system that calculates cell deformation in real time might be able to provide a true "deformation clamp". Compared with 10% deformation, the 50% vertical deformation condition also increases the sensitivity of volume change detection with light microscopy, because more of the volume change will be translated into changes in the horizontal dimensions (Fig 35A). For these reasons it is preferable to produce a larger original deformation (≈50%) in an experiment where the researcher anticipates a volume change or expects intrinsic volume change during a cellular process. Importantly, a ≈50% deformation (cell height:width ratio of 0.5) does not inhibit cells from proceeding through mitosis in normal time (Fig 5). Moreover, cells in real tissue are not mechanically isolated like in *in vitro* cell culture, and therefore, this method represents a way to simulate the constraints of real tissue or examine the effect of various imposed forces and deformations. While this protocol is demonstrated on round mitotic cells, it should be amenable to study most globular-shaped cells, such as those maintained in non-adherent environments[191, 636, 637, 643, 667], intrinsically non-adherent cells[181, 182, 535, 667, 673], cells extracted from widely-studied developmental systems such as zebrafish and C. elegans[39, 658], and egg cells[169, 171-177]. Notably, investigations on single globular cells have been carried out with parallel plate setups featuring geometry similar to the CHA[172, 174, 629, 630, 648, 668, 674].

Other AFM Methods to Analyze Cell Mechanics and Volume

In the early nineteen nineties researchers began using AFM to analyze the mechanics of soft biological samples. They did this by indenting samples with commonly available pyramidal tip cantilevers[675] and interpreting mechanical properties by exploiting Hertzian mechanics[676] with Sneddon's modifications[677]. These advancements were then adapted to live cells in physiological medium[678]. The high spatial resolution attainable

with pointed AFM tips enabled force-volume measurements that probe the cell surface with vertical force-distance indentations (Fig 35B), thereby generating cell height and stiffness values for each point sampled[679, 680]. The cell height at each point can be summed up to determine cell volume and a spatial map of cell surface stiffness. However, it was found that pyramidal tips that indent the cell surface (up to several μm) induce mechanical artifacts and overestimate stiffness due to uncertainties in contact point, contact area, strain estimations and dubious assumptions regarding cell properties including material homogeneity, Poisson's ratio and tip-sample interaction[666, 681]. Some of these problems were alleviated by switching to spherical tips (Fig 35C), which have now become the standard[39, 667, 681, 682]. Nonetheless, local indentation techniques do offer enhanced spatial resolution even though they struggle to describe the dynamic and heterogeneous complexity of the entire cell. This contrasts with approaches such as the CHA that achieve a whole cell read-out of force or stress without the aid of sophisticated models and equivocal assumptions. Regardless of the approach it must be kept in mind that all AFM techniques must impose significant cellular deformations to adequately probe mechanical properties of the entire cell (and not only of the cell surface or plasma membrane).

The features of AFM-based methods for analyzing cell mechanics and volume of different cell shapes are shown in table 4. While others have used flat tipless cantilevers to measure whole cell mechanics[648, 668], this thesis represents the first attempt to simultaneously measure mechanics and volume in a parallel plate setup. Due to the tipless cantilever geometry, such measurements extract quantitative data preferably from globular or round cells (Fig 35). However, qualitative assessment of spread cells can also yield worthwhile biological insights and presents advantages such as speed and simplicity[192]. In contrast, pyramidal tips perform poorly in cell mechanical measurements[666, 681] but are capable of mapping cell volume if cells are flat enough and scan speeds sufficiently slow (a few tens of minutes) to generate clean data (Fig 35B)[244, 679, 680]. Applied to round cells, pyramidal tips can only access a limited portion of the top surface (Fig 35B). Spherical tips perform better in local mechanical analysis, but do away with

the resolution needed for precision surface scanning and volume maps, and so only qualitative assessments of cell volume can be made (Fig 35C)[242, 245, 682]. Both these local indentation techniques are limited to probing flat parts of cells because non-perpendicular loading is beyond the considerations of the models used to interpret the data (Fig 35). Importantly, all these AFM techniques are strong in measuring dimensions in the vertical axis where light microscopy has traditionally been weak. Therefore, AFM in any mode can be applied to rounded cells in conjunction with light microscopy to determine cell volume at high temporal resolution (such as in Fig 7). Finally, in both volume and mechanics measurements, the same AFM instrument with a different cantilever and experimental procedure can potentially be used in complimentary manner to (at least qualitatively) control and confirm observations.

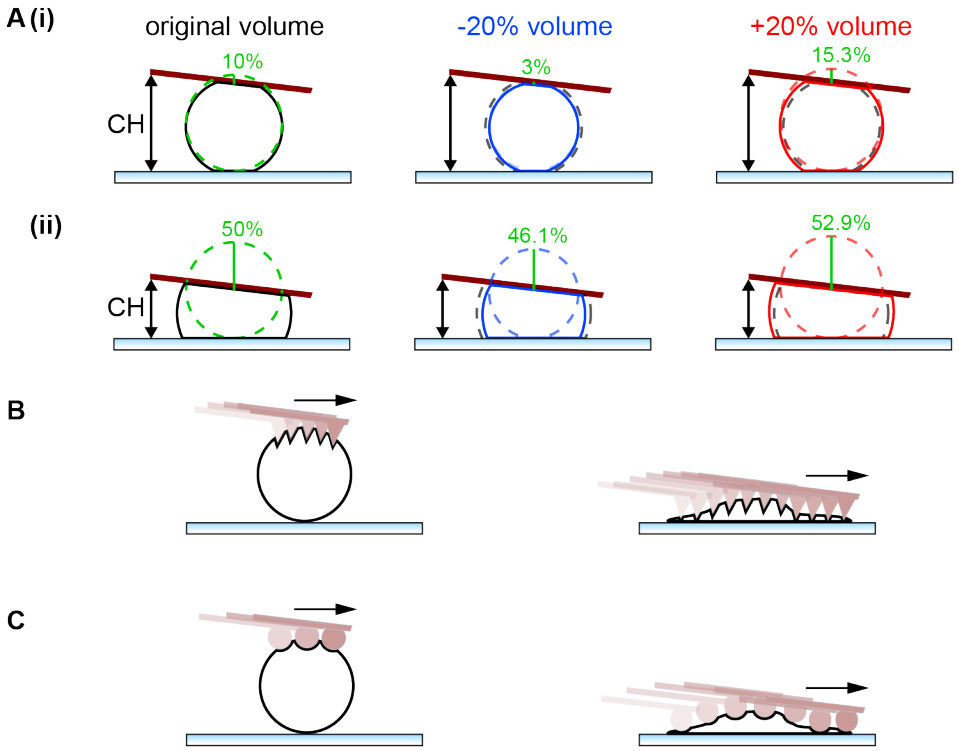

Figure 35: AFM-based techniques for cellular mechanics and volume measurements. **A** A schematic of cells in a CHA throughout the course of a volume change. Dashed black cell outlines depict cell size if no volume change had occurred. Blue and red represent 20% volume decrease and increase, respectively. Dashed coloured cell outlines depict cell shape if no cantilever compression or adhesion were present. The vertical deformation is related to the would-be spherical cell height (coloured dashed) and compressed cell height (solid lines) according to the formula $d_{vert}(\%)=(1-z_{spher}/z_{compr})x100$. With volume decrease and increase of 20% respectively an initial vertical deformation (green line) of (i) 10% becomes 3% and 15.3% and (ii) 50% becomes 46.1% and 52.9%.

B Schematic of a pyramidal tip probing a round and a flat cell. **C** Schematic of a spherical tip probing a round and a flat cell.

Cantilever Geometry	Cell Shape	Volume Measurement	Mechanics Measurement	Refs
Flat tipless	Globular	AFM (height), OM (width). Fast measurements (seconds)	Probing the whole cell. Analysis using force, height and contact area.	[648, 668]
	Spread	*Qualitative*	*Qualitative*	[192]
Pyramidal tip	Globular	AFM topography. Slow measurements (minutes)	Local indentation of cell surface. Analysis using liquid drop and Hertz models.	[64, 667]
	Spread	AFM topography. Slow measurements (minutes)	Local indentation of cell surface. Analysis using Hertz model.	[244, 679, 680]
Spherical tip	Globular	AFM topography. Slow measurements (minutes)	Local indentation of cell surface. Analysis using liquid drop and Hertz models.	[39, 667]
	Spread	*Qualitative*	Local indentation of cell surface. Analysis using Hertz model.	[242, 245, 682]

Table 4: Features of AFM-based methods for analyzing cell mechanics and volume. OM = Optical microscopy.

Outlook for Methods in Cytomechanics and "Systems Physiology"

This thesis shows that the combination of AFM and optical microscopy is well suited to accurately analyze cell mechanics and volume and demonstrates these measurements can be used to gain insight into pertinent biological problems, such as the physical basis of MCR. However, while presently one of the best options available, AFM is an expensive, time-consuming, and grossly over-engineered solution. In future one can envisage lab-on-chip, microfluidic[683] and MEMS[644, 645, 684-687] devices that feature parallel plate mechanical setups capable of performing CHAs and CFAs in a similar manner to AFM. The development of minimalist, user-friendly, fast, and cheap micromechanical assays that can be mounted on the stage of a standard microscope for cell analysis is a worthwhile future

endeavor. Such breakthroughs will be especially pertinent for high throughput mechanical screening of cells[688], molecular aggregates[689] and tissue explants. These possibilities will enable a new systems-based approach to physiology, which should drive discovery at the junction of cell biophysics, physiology and systems biology (Fig 36).

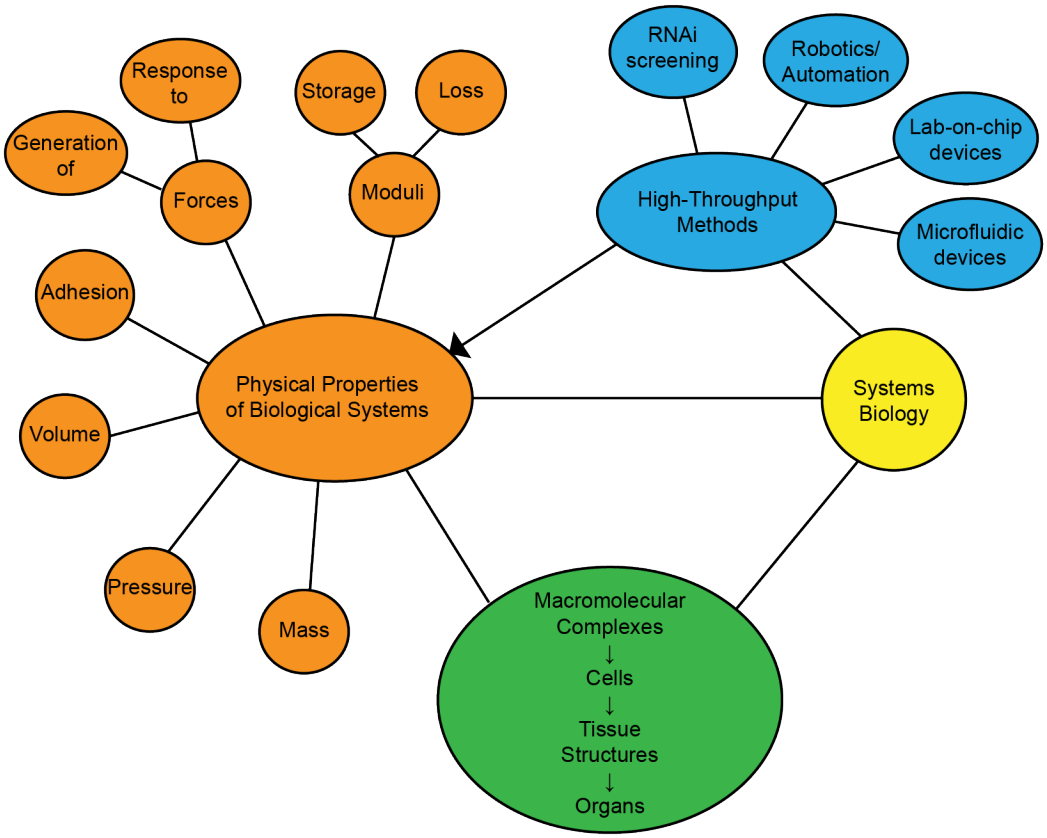

Figure 36: Proposed rationale for generating discoveries in "systems physiology". Assessing physical properties across the diverse length scales of biological architecture by leveraging high throughput technologies in combination with perturbation methods in molecular biology will yield insights into physiological principles at a systems level.

Terms and Abbreviations

AFM: atomic force microscopy

IF: Intermediate filament

MCR: mitotic cell rounding

CFA: constant force assay

CHA: constant height assay

DIC: differential interference microscopy

H2B-GFP: histone-H2B green fluorescent protein

NEBD: nuclear envelope breakdown

SCFS: single cell force spectroscopy

$P_{Rounding}$: Rounding pressure (see Fig 9E)

$E_{Rounding}$: Rounding modulus (see Fig 9E)

DMEM: Dulbecco's modified Eagle medium

FCS: fetal calf serum

RI: refractive index

EDTA: ethylene diamine tetraacetic acid

EGTA: ethylene glycol tetraacetic acid

EIPA: 5-(N-ethyl-N-isopropyl)-amiloride

ERM: ezrin-radixin-moesin

Cdk1: cyclin-dependent kinase 1

ECM: extracellular matrix

PIP2: phosphatidylinositol 4,5-bisphosphate

STC: s-trityl-L-cysteine

ECM: extracellular matrix

RVI: Regulatory volume increase

RVD: Regulatory volume decrease

List of Publications

Stewart, M. P., Helenius, J., Toyoda, Y., Ramanathan, S. P., Muller, D. J. & Hyman, A. A.
Hydrostatic pressure and the actomyosin cortex drive mitotic cell rounding. *Nature* **469**, 226-230, (2011).

Stewart, M. P., Toyoda, Y., Hyman, A. A. & Muller, D. J.
Force probing cell shape changes to molecular resolution. *Trends in Biochemical Science* **36**, 444-450, (2011).

Toyoda, Y., Stewart, M. P., Hyman, A. A. & Muller, D. J.
Atomic Force Microscopy to Study Mechanics of Living Mitotic Mammalian Cells. *Jpn J Appl Phys* **50**, 08LA01, (2011).

Stewart, M. P., Toyoda, Y., Hyman, A. A. & Muller, D. J.
Tracking mechanics and volume of globular cells with atomic force microscopy using a constant-height clamp. *Nature Protocols* **7**, 143-154, (2012).

Acknowledgements

Daniel Müller, Tony Hyman - for primary scientific guidance.

Francis Stewart, Michelle Meredyth-Stewart and family - for their patience, support, and encouragement during the Dresden leg of my PhD.

Yusuke Toyoda, Jonne Helenius, Subramanian Ramanathan, Michael Krieg, Jens Friedrichs, Anna Taubenberger, Clemens Franz, Isabel Richter, Karin Krell, Eugene Petrov, JC Olaya, Pete Pitrone, Cédric Cattin, Philip Germann - for help in the lab, technical assistance and fruitful scientific interactions.

Joe Howard, Eva Paluch, Zoltan Maliga, Stephan Grille, Cliff Brangwynne - for stimulating discussions and advice.

Sucharit Bhakdi - for gifts of reagents and advice on their use.

The TU Dresden Graduiertenkolleg on “bio- and nano-technology for electronic packaging” - for having the flexibility and open-mindedness to accommodate this project within the framework of their program.

References

1. Paluch, E. and C.P. Heisenberg, *Biology and Physics of Cell Shape Changes in Development.* Current Biology, 2009. **19**(17): p. R790-R799.
2. Fletcher, D.A. and D. Mullins, *Cell mechanics and the cytoskeleton.* Nature, 2010. **463**(7280): p. 485-492.
3. Strangeways, T.S.P., *Observations on the changes seen in living cells during growth and division.* Proceedings of the Royal Society of London Series B-Containing Papers of a Biological Character, 1922. **94**(658): p. 137-141.
4. Mcconnell, C.H., *The Mitosis Found in Hydra.* Science, 1930. **72**(1859): p. 170.
5. Ohnishi, T., *Extraction of Actin- and Myosin-Like Proteins from Liver Mitochondria.* Journal of Biochemistry, 1962. **52**(3): p. 230-&.
6. Ishikawa.H, R. Bischoff, and H. Holtzer, *Formation of Arrowhead Complexes with Heavy Meromyosin in a Variety of Cell Types.* Journal of Cell Biology, 1969. **43**(2P1): p. 312-&.
7. Wells, W.A., *The discovery of tubulin.* The Journal of Cell Biology, 2005. **169**(4): p. 552.
8. Ishikawa, H., R. Bischoff, and H. Holtzer, *Mitosis and Intermediate-Sized Filaments in Developing Skeletal Muscle.* Journal of Cell Biology, 1968. **38**(3): p. 538-&.
9. Eriksson, A. and L.E. Thornell, *Intermediate (Skeletin) Filaments in Heart Purkinje-Fibers - Correlative Morphological and Biochemical Identification with Evidence of a Cytoskeletal Function.* Journal of Cell Biology, 1979. **80**(2): p. 231-247.
10. Yahara, I., et al., *Correlation between Effects of 24 Different Cytochalasins on Cellular Structures and Cellular Events and Those on Actin Invitro.* Journal of Cell Biology, 1982. **92**(1): p. 69-78.
11. Jones, J.L., et al., *The effect of cytochalasin B on the endosteal lining cells of mammalian bone. A scanning electron microscopic study.* Calcif Tissue Res, 1977. **24**(1): p. 1-10.
12. Cortese, F. and J. Wolff, *Cytochalasin-Stimulated Steroidogenesis from High-Density Lipoproteins.* Journal of Cell Biology, 1978. **77**(2): p. 507-516.
13. Badley, R.A., et al., *Cytoskeleton changes in fibroblast adhesion and detachment.* Journal of Cell Science, 1980. **43**: p. 379-90.
14. Pollard, T.D. and R.R. Weihing, *Actin and myosin and cell movement.* CRC Crit Rev Biochem, 1974. **2**(1): p. 1-65.
15. Schroeder, T.E., *Actin in dividing cells: contractile ring filaments bind heavy meromyosin.* Proc Natl Acad Sci U S A, 1973. **70**(6): p. 1688-92.
16. Sanger, J.W., *Changing patterns of actin localization during cell division.* Proc Natl Acad Sci U S A, 1975. **72**(5): p. 1913-6.
17. Sanger, J.W. and J.M. Sanger, *Surface and Shape Changes during Cell-Division.* Cell and Tissue Research, 1980. **209**(2): p. 177-186.
18. Beck, J.S., J.T. Saari, and A.W.L. Jay, *Effects of Cytochalasin-B on Osmotic Fragility and Deformability of Human Erythrocytes.* Canadian Journal of Physiology and Pharmacology, 1972. **50**(7): p. 684-&.
19. Erickson, C.A., *The Deformability of Bhk Cells and Polyoma Virus-Transformed Bhk Cells in Relation to Locomotory Behavior.* Journal of Cell Science, 1980. **44**(Aug): p. 187-200.
20. Mazur, M.T. and J.R. Williamson, *Macrophage Deformability and Phagocytosis.* Journal of Cell Biology, 1977. **75**(1): p. 185-199.
21. Petersen, N.O., W.B. Mcconnaughey, and E.L. Elson, *Dependence of Locally Measured Cellular Deformability on Position on the Cell, Temperature, and Cytochalasin-B.* Proceedings of the National Academy of Sciences of the United States of America-Biological Sciences, 1982. **79**(17): p. 5327-5331.
22. Lazarides, E. and K. Burridge, *Alpha-Actinin - Immunofluorescent Localization of a Muscle Structural Protein in Nonmuscle Cells.* Cell, 1975. **6**(3): p. 289-298.
23. Geiger, B., et al., *Vinculin, an Intracellular Protein Localized at Specialized Sites Where Microfilament Bundles Terminate at Cell-Membranes.* Proceedings of the National Academy of Sciences of the United States of America-Biological Sciences, 1980. **77**(7): p. 4127-4131.
24. Burridge, K. and P. Mangeat, *An Interaction between Vinculin and Talin.* Nature, 1984. **308**(5961): p. 744-746.
25. Turner, C.E., J.R. Glenney, and K. Burridge, *Paxillin - a New Vinculin-Binding Protein Present in Focal Adhesions.* Journal of Cell Biology, 1990. **111**(3): p. 1059-1068.
26. Buck, C.A., et al., *Integrin (the Csat Antigen) - Functionality Requires Oligomeric Integrity.* Journal of Cell Biology, 1986. **103**(6): p. 2421-2428.
27. Tamkun, J.W., et al., *Structure of Integrin, a Glycoprotein Involved in the Transmembrane Linkage between Fibronectin and Actin.* Cell, 1986. **46**(2): p. 271-282.
28. Buck, C.A. and A.F. Horwitz, *Integrin, a Transmembrane Glycoprotein Complex Mediating Cell Substratum Adhesion.* Journal of Cell Science, 1987: p. 231-250.
29. Ridley, A.J. and A. Hall, *The Small Gtp-Binding Protein Rho Regulates the Assembly of Focal Adhesions and Actin Stress Fibers in Response to Growth-Factors.* Cell, 1992. **70**(3): p. 389-399.
30. Ridley, A.J., *Life at the leading edge.* Cell, 2011. **145**(7): p. 1012-22.
31. Hall, A., *Rho GTPases and the control of cell behaviour.* Biochemical Society Transactions, 2005. **33**: p. 891-895.
32. Rohn, J.L., et al., *Comparative RNAi screening identifies a conserved core metazoan actinome by phenotype.* Journal of Cell Biology, 2011. **194**(5): p. 789-805.
33. Pollard, T.D. and G.G. Borisy, *Cellular motility driven by assembly and disassembly of actin filaments.* Cell, 2003. **112**(4): p. 453-65.

34. Rafelski, S.M. and J.A. Theriot, *Crawling toward a unified model of cell mobility: spatial and temporal regulation of actin dynamics.* Annual Review of Biochemistry, 2004. **73**: p. 209-39.
35. Wilson, C.A., et al., *Myosin II contributes to cell-scale actin network treadmilling through network disassembly.* Nature, 2010. **465**(7296): p. 373-U137.
36. Gardel, M.L., et al., *Mechanical integration of actin and adhesion dynamics in cell migration.* Annu Rev Cell Dev Biol, 2010. **26**: p. 315-33.
37. Eggert, U.S., T.J. Mitchison, and C.M. Field, *Animal cytokinesis: From parts list to mechanisms.* Annual Review of Biochemistry, 2006. **75**: p. 543-566.
38. Lecuit, T. and P.F. Lenne, *Cell surface mechanics and the control of cell shape, tissue patterns and morphogenesis.* Nature Reviews Molecular Cell Biology, 2007. **8**(8): p. 633-644.
39. Krieg, M., et al., *Tensile forces govern germ-layer organization in zebrafish.* Nat Cell Biol, 2008. **10**(4): p. 429-36.
40. Discher, D.E., D.J. Mooney, and P.W. Zandstra, *Growth factors, matrices, and forces combine and control stem cells.* Science, 2009. **324**(5935): p. 1673-7.
41. de Forges, H.l.n., A.Ø. Bouissou, and F. Perez, *Interplay between microtubule dynamics and intracellular organization.* The International Journal of Biochemistry & Cell Biology, 2012. **44**(2): p. 266-274.
42. Welte, M.A., *Bidirectional transport along microtubules.* Current Biology, 2004. **14**(13): p. R525-R537.
43. Kline-Smith, S.L. and C.E. Walczak, *Mitotic spindle assembly and chromosome segregation: Refocusing on microtubule dynamics.* Molecular Cell, 2004. **15**(3): p. 317-327.
44. Linck, R.W., *Cilia and Flagella*, in *eLS*2001, John Wiley & Sons, Ltd.
45. Goldman, R.D., et al., *Intermediate filaments: versatile building blocks of cell structure.* Current Opinion in Cell Biology, 2008. **20**(1): p. 28-34.
46. Eriksson, J.E., et al., *Introducing intermediate filaments: from discovery to disease.* Journal of Clinical Investigation, 2009. **119**(7): p. 1763-1771.
47. Cheng, J., et al., *The Genetic-Basis of Epidermolytic Hyperkeratosis - a Disorder of Differentiation-Specific Epidermal Keratin Genes.* Cell, 1992. **70**(5): p. 811-819.
48. Shimi, T., et al., *Nuclear lamins in cell regulation and disease.* Cold Spring Harb Symp Quant Biol, 2010. **75**: p. 525-31.
49. Herrmann, H., et al., *Intermediate filaments: from cell architecture to nanomechanics.* Nature Reviews Molecular Cell Biology, 2007. **8**(7): p. 562-573.
50. Kreplak, L., et al., *Exploring the mechanical behavior of single intermediate filaments.* Journal of Molecular Biology, 2005. **354**(3): p. 569-577.
51. Godsel, L.M., R.P. Hobbs, and K.J. Green, *Intermediate filament assembly: dynamics to disease.* Trends in Cell Biology, 2008. **18**(1): p. 28-37.
52. Alberts, B., *Cell Biology: The Endless Frontier.* Molecular Biology of the Cell, 2010. **21**(22): p. 3785-3785.
53. Madreperla, S.A. and R. Adler, *Opposing Microtubule-Dependent and Actin-Dependent Forces in the Development and Maintenance of Structural Polarity in Retinal Photoreceptors.* Developmental Biology, 1989. **131**(1): p. 149-160.
54. Dennerll, T.J., et al., *Tension and Compression in the Cytoskeleton of Pc-12 Neurites Ii - Quantitative Measurements.* Journal of Cell Biology, 1988. **107**(2): p. 665-674.
55. Ingber, D.E., *Cellular Tensegrity - Defining New Rules of Biological Design That Govern the Cytoskeleton.* Journal of Cell Science, 1993. **104**: p. 613-627.
56. Chang, Y.C., et al., *GEF-H1 couples nocodazole-induced microtubule disassembly to cell contractility via RhoA.* Molecular Biology of the Cell, 2008. **19**(5): p. 2147-53.
57. Zhou, J.A., et al., *Macroscopic stiffening of embryonic tissues via microtubules, RhoGEF and the assembly of contractile bundles of actomyosin.* Development, 2010. **137**(16): p. 2785-2794.
58. Waterman-Storer, C.M., et al., *Microtubule growth activates Rac1 to promote lamellipodial protrusion in fibroblasts.* Nature Cell Biology, 1999. **1**(1): p. 45-50.
59. Kasza, K.E., et al., *The cell as a material.* Current Opinion in Cell Biology, 2007. **19**(1): p. 101-107.
60. Kim, S. and P.A. Coulombe, *Intermediate filament scaffolds fulfill mechanical, organizational, and signaling functions in the cytoplasm.* Genes & Development, 2007. **21**(13): p. 1581-1597.
61. Nurse, P., *Regulation of the eukaryotic cell cycle.* European Journal of Cancer, 1997. **33**(7): p. 1002-1004.
62. Cramer, L.P. and T.J. Mitchison, *Investigation of the mechanism of retraction of the cell margin and rearward flow of nodules during mitotic cell rounding.* Mol. Biol. Cell, 1997. **8**(1): p. 109-19.
63. Maddox, A.S. and K. Burridge, *RhoA is required for cortical retraction and rigidity during mitotic cell rounding.* J. Cell Biol., 2003. **160**(2): p. 255-65.
64. Kunda, P., et al., *Moesin controls cortical rigidity, cell rounding, and spindle morphogenesis during mitosis.* Curr. Biol., 2008. **18**(2): p. 91-101.
65. Picone, R., et al., *A polarised population of dynamic microtubules mediates homeostatic length control in animal cells.* Plos Biology, 2010. **8**(11): p. e1000542.
66. Harris, A., *Location of cellular adhesions to solid substrata.* Dev. Biol., 1973. **35**(1): p. 97-114.
67. Dard, N., S. Louvet-Vallee, and B. Maro, *Orientation of Mitotic Spindles during the 8-to 16-Cell Stage Transition in Mouse Embryos.* PLoS One, 2009. **4**(12).
68. Gibson, M.C., et al., *The emergence of geometric order in proliferating metazoan epithelia.* Nature, 2006. **442**(7106): p. 1038-1041.
69. Meyer, E.J., A. Ikmi, and M.C. Gibson, *Interkinetic Nuclear Migration Is a Broadly Conserved Feature of Cell Division in Pseudostratified Epithelia.* Current Biology, 2011. **21**(6): p. 485-491.
70. Luxenburg, C., et al., *Developmental roles for Srf, cortical cytoskeleton and cell shape in epidermal spindle orientation.* Nature Cell Biology, 2011. **13**(3): p. 203-U51.
71. Kunda, P. and B. Baum, *The actin cytoskeleton in spindle assembly and positioning.* Trends Cell Biol., 2009. **19**(4): p. 174-9.

72. Thery, M. and M. Bornens, *Get round and stiff for mitosis.* Hfsp Journal, 2008. **2**(2): p. 65-71.
73. Carreno, S., et al., *Moesin and its activating kinase Slik are required for cortical stability and microtubule organization in mitotic cells.* Journal of Cell Biology, 2008. **180**(4): p. 739-746.
74. Thery, M., et al., *Experimental and theoretical study of mitotic spindle orientation.* Nature, 2007. **447**(7143): p. 493-6.
75. Fujibuchi, T., et al., *AIP1/WDR1 supports mitotic cell rounding.* Biochem. Biophys. Res. Commun., 2005. **327**(1): p. 268-75.
76. Haraguchi, T., T. Kaneda, and Y. Hiraoka, *Dynamics of chromosomes and microtubules visualized by multiple-wavelength fluorescence imaging in living mammalian cells: Effects of mitotic inhibitors on cell cycle progression.* Genes to Cells, 1997. **2**(6): p. 369-380.
77. Kanda, T., K.F. Sullivan, and G.M. Wahl, *Histone-GFP fusion protein enables sensitive analysis of chromosome dynamics in living mammalian cells.* Current Biology, 1998. **8**(7): p. 377-385.
78. Casella, J.F., M.D. Flanagan, and S. Lin, *Cytochalasin D inhibits actin polymerization and induces depolymerization of actin filaments formed during platelet shape change.* Nature, 1981. **293**(5830): p. 302-5.
79. Uehata, M., et al., *Calcium sensitization of smooth muscle mediated by a Rho-associated protein kinase in hypertension.* Nature, 1997. **389**(6654): p. 990-4.
80. Sauer, F.C., *Mitosis in the neural tube.* Journal of Comparative Neurology, 1935. **62**(2): p. 377-405.
81. Norden, C., et al., *Actomyosin is the main driver of interkinetic nuclear migration in the retina.* Cell, 2009. **138**(6): p. 1195-208.
82. Rappaport, R., *Experiments concerning the cleavage stimulus in sand dollar eggs.* Journal of Experimental Zoology, 1961. **148**: p. 81-9.
83. Friedrichs, J., J. Helenius, and D.J. Muller, *Quantifying cellular adhesion to extracellular matrix components by single-cell force spectroscopy.* Nature Protocols, 2010. **5**(7): p. 1353-1361.
84. Helenius, J., et al., *Single-cell force spectroscopy.* Journal of Cell Science, 2008. **121**(11): p. 1785-1791.
85. Lechler, T. and E. Fuchs, *Asymmetric cell divisions promote stratification and differentiation of mammalian skin.* Nature, 2005. **437**(7056): p. 275-280.
86. Baker, J. and D. Garrod, *Epithelial-Cells Retain Junctions during Mitosis.* Journal of Cell Science, 1993. **104**: p. 415-425.
87. Callister, W.D., *Materials Science and Engineering*2010, New York: Wiley.
88. Matzke, R., K. Jacobson, and M. Radmacher, *Direct, high-resolution measurement of furrow stiffening during division of adherent cells.* Nat. Cell Biol., 2001. **3**(6): p. 607-10.
89. Dvorak, J.A. and E. Nagao, *Kinetic analysis of the mitotic cycle of living vertebrate cells by atomic force microscopy.* Experimental Cell Research, 1998. **242**(1): p. 69-74.
90. Janmey, P.A., P.C. Georges, and S. Hvidt, *Basic rheology for biologists.* Methods Cell Biol, 2007. **83**: p. 3-27.
91. Fink, J., et al., *External forces control mitotic spindle positioning.* Nature Cell Biology, 2011. **13**(7): p. 771-U401.
92. Tinevez, J.Y., et al., *Role of cortical tension in bleb growth.* Proc Natl Acad Sci U S A, 2009. **106**(44): p. 18581-6.
93. Delanoe-Ayari, H., J.P. Rieu, and M. Sano, *4D Traction Force Microscopy Reveals Asymmetric Cortical Forces in Migrating Dictyostelium Cells.* Physical Review Letters, 2010. **105**(24).
94. Wang, N., et al., *Cell prestress. I. Stiffness and prestress are closely associated in adherent contractile cells.* American Journal of Physiology-Cell Physiology, 2002. **282**(3): p. C606-C616.
95. Griffin, M.A., et al., *Patterning, prestress, and peeling dynamics of myocytes.* Biophysical Journal, 2004. **86**(2): p. 1209-1222.
96. Griffin, M.A., et al., *Adhesion-contractile balance in myocyte differentiation.* Journal of Cell Science, 2004. **117**(24): p. 5855-5863.
97. Thery, M., et al., *The extracellular matrix guides the orientation of the cell division axis.* Nat. Cell Biol., 2005. **7**(10): p. 947-53.
98. Mitchison, T.J., *Actin Based Motility on Retraction Fibers in Mitotic Ptk2 Cells.* Cell Motility and the Cytoskeleton, 1992. **22**(2): p. 135-151.
99. Revel, J.P., P. Hoch, and D. Ho, *Adhesion of Culture Cells to Their Substratum.* Experimental Cell Research, 1974. **84**(1-2): p. 207-218.
100. Vogel, K.G., *Effects of Hyaluronidase, Trypsin, and Edta on Surface Composition and Topography during Detachment of Cells in Culture.* Experimental Cell Research, 1978. **113**(2): p. 345-357.
101. Britch, M. and T.D. Allen, *Modulation of Cellular Contractility and Adhesion by Trypsin and Egta.* Experimental Cell Research, 1980. **125**(1): p. 221-231.
102. Cottrell, G.S., et al., *Protease-activated receptor 2: activation, signalling and function.* Biochemical Society Transactions, 2003. **31**: p. 1191-1197.
103. Bengrine, A., et al., *Indirect activation of the epithelial Na+ channel by trypsin.* J Biol Chem, 2007. **282**(37): p. 26884-96.
104. Ishihara, H., et al., *Calyculin-a and Okadaic Acid - Inhibitors of Protein Phosphatase-Activity.* Biochemical and Biophysical Research Communications, 1989. **159**(3): p. 871-877.
105. Hosoya, N., et al., *Changes in the Cytoskeletal Structure of Cultured Smooth-Muscle Cells Induced by Calyculin-A.* Journal of Cell Science, 1993. **105**: p. 883-890.
106. Marushige, K. and Y. Marushige, *Modulation of cell rounding and apoptosis in trigeminal neurinoma cells by protein phosphatase inhibitors.* Anticancer Research, 1998. **18**(1A): p. 295-300.
107. Leung, Y.M., et al., *Calyculin A-induced endothelial cell shape changes are independent of [Ca2+](i) elevation and may involve actin polymerization.* Biochimica Et Biophysica Acta-Molecular Cell Research, 2002. **1589**(2): p. 93-103.
108. Hishiya, A., et al., *Protein phosphatase 2C inactivates F-actin binding of human platelet moesin.* J Biol Chem, 1999. **274**(38): p. 26705-12.
109. Yam, P.T., et al., *Actin-myosin network reorganization breaks symmetry at the cell rear to*

spontaneously initiate polarized cell motility. Journal of Cell Biology, 2007. **178**(7): p. 1207-1221.
110. Fabian, L., J. Troscianczuk, and A. Forer, *Calyculin A, an enhancer of myosin, speeds up anaphase chromosome movement.* Cell Chromosome, 2007. **6**: p. 1.
111. Tosuji, H., et al., *Calyculin-a Induces Contractile Ring-Like Apparatus Formation and Condensation of Chromosomes in Unfertilized Sea-Urchin Eggs.* Proceedings of the National Academy of Sciences of the United States of America, 1992. **89**(22): p. 10613-10617.
112. Medema, R.H. and A. Lindqvist, *Boosting and suppressing mitotic phosphorylation.* Trends in Biochemical Sciences, 2011. **36**(11): p. 578-584.
113. Gompper, G. and M. Schick, *Soft Matter: Lipid bilayers and red blood cells*2008: Wiley-VCH.
114. Raucher, D. and M.P. Sheetz, *Membrane expansion increases endocytosis rate during mitosis.* Journal of Cell Biology, 1999. **144**(3): p. 497-506.
115. Marenduzzo, D., K. Finan, and P.R. Cook, *The depletion attraction: an underappreciated force driving cellular organization.* Journal of Cell Biology, 2006. **175**(5): p. 681-686.
116. Valentine, M.T., et al., *Mechanical properties of Xenopus egg cytoplasmic extracts.* Biophysical Journal, 2005. **88**(1): p. 680-689.
117. Bereiter-Hahn, J., *Mechanics of crawling cells.* Medical Engineering & Physics, 2005. **27**(9): p. 743-753.
118. Keren, K., et al., *Intracellular fluid flow in rapidly moving cells.* Nature Cell Biology, 2009. **11**(10): p. 1219-U137.
119. Charras, G.T., et al., *Life and times of a cellular bleb.* Biophys. J., 2008. **94**(5): p. 1836-53.
120. Charras, G.T., T.J. Mitchison, and L. Mahadevan, *Animal cell hydraulics.* Journal of Cell Science, 2009. **122**(18): p. 3233-3241.
121. Mitchison, T.J., G.T. Charras, and L. Mahadevan, *Implications of a poroelastic cytoplasm for the dynamics of animal cell shape.* Seminars in Cell & Developmental Biology, 2008. **19**(3): p. 215-223.
122. Stockwell, B.R., *Chemical genetics: Ligand-based discovery of gene function.* Nature Reviews Genetics, 2000. **1**(2): p. 116-125.
123. Coue, M., et al., *Inhibition of Actin Polymerization by Latrunculin-A.* Febs Letters, 1987. **213**(2): p. 316-318.
124. Spector, I., et al., *Latrunculins: novel marine toxins that disrupt microfilament organization in cultured cells.* Science, 1983. **219**(4584): p. 493-5.
125. Bubb, M.R., et al., *Jasplakinolide, a cytotoxic natural product, induces actin polymerization and competitively inhibits the binding of phalloidin to F-actin.* J. Biol. Chem., 1994. **269**(21): p. 14869-71.
126. Spector, I., et al., *New anti-actin drugs in the study of the organization and function of the actin cytoskeleton.* Microscopy Research and Technique, 1999. **47**(1): p. 18-37.
127. Cunningham, C.C., *Actin Polymerization and Intracellular Solvent Flow in Cell-Surface Blebbing.* Journal of Cell Biology, 1995. **129**(6): p. 1589-1599.
128. Charras, G.T., et al., *Reassembly of contractile actin cortex in cell blebs.* Journal of Cell Biology, 2006. **175**(3): p. 477-490.
129. Straight, A.F., et al., *Dissecting temporal and spatial control of cytokinesis with a myosin II Inhibitor.* Science, 2003. **299**(5613): p. 1743-7.
130. Makishima, M., et al., *Induction of differentiation of human leukemia cells by inhibitors of myosin light chain kinase.* FEBS Lett., 1991. **287**(1-2): p. 175-7.
131. De Brabander, M.J., et al., *The Effects of Methyl [5-(2-Thienylcarbonyl)-1H-benzimidazol-2-yl]carbamate, (R 17934; NSC 238159), a New Synthetic Antitumoral Drug Interfering with Microtubules, on Mammalian Cells Cultured in Vitro.* Can. Res., 1976. **36**(3): p. 905-916.
132. Malawista, S.E., H. Sato, and K.G. Bensch, *Vinblastine and Griseofulvin Reversibly Disrupt the Living Mitotic Spindle.* Science, 1968. **160**(3829): p. 770-772.
133. Schiff, P.B., J. Fant, and S.B. Horwitz, *Promotion of microtubule assembly in vitro by taxol.* Nature, 1979. **277**(5698): p. 665-7.
134. Skoufias, D.A., et al., *S-trityl-L-cysteine is a reversible, tight binding inhibitor of the human kinesin Eg5 that specifically blocks mitotic progression.* J. Biol. Chem., 2006. **281**(26): p. 17559-69.
135. Sheetz, M.P., *Cell control by membrane-cytoskeleton adhesion.* Nature Reviews Molecular Cell Biology, 2001. **2**(5): p. 392-396.
136. Boucrot, E. and T. Kirchhausen, *Endosomal recycling controls plasma membrane area during mitosis.* Proc. Natl. Acad. Sci. U S A, 2007. **104**(19): p. 7939-44.
137. Macia, E., et al., *Dynasore, a cell-permeable inhibitor of dynamin.* Dev. Cell., 2006. **10**(6): p. 839-50.
138. Montagnac, G., A. Echard, and P. Chavrier, *Endocytic traffic in animal cell cytokinesis.* Current Opinion in Cell Biology, 2008. **20**(4): p. 454-61.
139. Clark, A.G. and E. Paluch, *Mechanics and regulation of cell shape during the cell cycle.* Results Probl Cell Differ, 2011. **53**: p. 31-73.
140. Lang, F., *Mechanisms and Significance of Cell Volume Regulation*2006, Basel, Switzerland: Karger. 276.
141. Vigne, P., et al., *Ethylisopropyl-amiloride: a new and highly potent derivative of amiloride for the inhibition of the Na+/H+ exchange system in various cell types.* Biochem. Biophys. Res. Commun., 1983. **116**(1): p. 86-90.
142. Charnock, J.S. and R.L. Post, *Evidence of the Mechanism of Ouabain Inhibition of Cation-Activated Adenosine Triphosphate.* Nature, 1963. **199**: p. 910-1.
143. Haas, M. and T.J. McManus, *Bumetanide inhibits (Na + K + 2Cl) co-transport at a chloride site.* Am. J. Physiol., 1983. **245**(3): p. C235-40.
144. Strange, K., F. Emma, and P.S. Jackson, *Cellular and molecular physiology of volume-sensitive anion channels.* American Journal of Physiology, 1996. **270**(3 Pt 1): p. C711-30.
145. Alexander, R.T. and S. Grinstein, *Na+/H+ exchangers and the regulation of volume.* Acta Physiologica, 2006. **187**(1-2): p. 159-167.
146. Koivusalo, M., A. Kapus, and S. Grinstein, *Sensors, Transducers, and Effectors That Regulate Cell Size and Shape.* Journal of Biological Chemistry, 2009. **284**(11): p. 6595-6599.

147. Wehner, F., et al., *Cell volume regulation: osmolytes, osmolyte transport, and signal transduction.* Rev. Physiol. Biochem. Pharmacol., 2003. **148**: p. 1-80.
148. Johnson, J.D. and D. Epel, *Intracellular pH and activation of sea urchin eggs after fertilisation.* Nature, 1976. **262**(5570): p. 661-4.
149. Putney, L.K. and D.L. Barber, *Na-H exchange-dependent increase in intracellular pH times G2/M entry and transition.* J. Biol. Chem., 2003. **278**(45): p. 44645-9.
150. Verheye-Dua, F.A. and L. Bohm, *Influence of ouabain on cell inactivation by irradiation.* Strahlenther Onkol, 1996. **172**(3): p. 156-61.
151. Kolega, J., *Phototoxicity and photoinactivation of blebbistatin in UV and visible light.* Biochem. Biophys. Res. Commun., 2004. **320**(3): p. 1020-5.
152. Sakamoto, T., et al., *Blebbistatin, a myosin II inhibitor, is photoinactivated by blue light.* Biochemistry, 2005. **44**(2): p. 584-8.
153. Bain, J., et al., *The specificities of protein kinase inhibitors: an update.* Biochemical Journal, 2003. **371**(Pt 1): p. 199-204.
154. Greenberg, D.L., G.J. Mize, and T.K. Takayama, *Protease-activated receptor mediated RhoA signaling and cytoskeletal reorganization in LNCaP cells.* Biochemistry, 2003. **42**(3): p. 702-709.
155. Charras, G. and E. Paluch, *Blebs lead the way: how to migrate without lamellipodia.* Nature Reviews Molecular Cell Biology, 2008. **9**(9): p. 730-736.
156. Mercer, J. and A. Helenius, *Vaccinia virus uses macropinocytosis and apoptotic mimicry to enter host cells.* Science, 2008. **320**(5875): p. 531-535.
157. Laevsky, G. and D.A. Knecht, *Cross-linking of actin filaments by myosin II is a major contributor to cortical integrity and cell motility in restrictive environments.* Journal of Cell Science, 2003. **116**(18): p. 3761-3770.
158. Valeva, A., et al., *Staphylococcal alpha-toxin: repair of a calcium-impermeable pore in the target cell membrane.* Molecular Microbiology, 2000. **36**(2): p. 467-476.
159. Freer, J.H., *Cytolytic Toxins and Surface-Activity.* Toxicon, 1982. **20**(1): p. 217-221.
160. Bhakdi, S., M. Muhly, and R. Fussle, *Correlation between Toxin Binding and Hemolytic-Activity in Membrane Damage by Staphylococcal Alpha-Toxin.* Infection and Immunity, 1984. **46**(2): p. 318-323.
161. Koschinski, A., et al., *Why Escherichia coli alpha-hemolysin induces calcium oscillations in mammalian cells - the pore is on its own.* Faseb Journal, 2006. **20**(7): p. 973-+.
162. Skals, M., et al., *Escherichia coli alpha-hemolysin triggers shrinkage of erythrocytes via K(Ca)3.1 and TMEM16A channels with subsequent phosphatidylserine exposure.* J Biol Chem, 2010. **285**(20): p. 15557-65.
163. Suzuki, K. and K. Takahashi, *Reduced cell adhesion during mitosis by threonine phosphorylation of beta1 integrin.* J Cell Physiol, 2003. **197**(2): p. 297-305.
164. Dao, V.T., et al., *Dynamic changes in Rap1 activity are required for cell retraction and spreading during mitosis.* Journal of Cell Science, 2009. **122**(16): p. 2996-3004.
165. Yamaguchi, R., et al., *Mitosis specific serine phosphorylation and downregulation of one of the focal adhesion protein, paxillin.* Oncogene, 1997. **15**(15): p. 1753-61.
166. Yamakita, Y., et al., *Dissociation of FAK/p130(CAS)/c-Src complex during mitosis: role of mitosis-specific serine phosphorylation of FAK.* Journal of Cell Biology, 1999. **144**(2): p. 315-24.
167. Bhatt, A.S., et al., *Adhesion signaling by a novel mitotic substrate of src kinases.* Oncogene, 2005. **24**(34): p. 5333-5343.
168. Curtis, M., S.N. Nikolopoulos, and C.E. Turner, *Actopaxin is phosphorylated during mitosis and is a substrate for cyclin B1/cdc2 kinase.* Biochemical Journal, 2002. **363**: p. 233-242.
169. Mitchison, J.M. and M.M. Swann, *The Mechanical Properties of the Cell Surface .3. The Sea-Urchin Egg from Fertilization to Cleavage.* Journal of Experimental Biology, 1955. **32**(4): p. 734-750.
170. Hiramoto, Y., *Mechanical Properties of Sea Urchin Eggs. Ii. Changes in Mechanical Properties from Fertilization to Cleavage.* Experimental Cell Research, 1963. **32**: p. 76-89.
171. Wolpert, L., *Mechanical Properties of Membrane of Sea Urchin Egg during Cleavage.* Experimental Cell Research, 1966. **41**(2): p. 385.
172. Yoneda, M. and K. Dan, *Tension at the surface of the dividing sea-urchin egg.* J Exp Biol, 1972. **57**(3): p. 575-87.
173. Cole, K.S., *Surface forces of the arbacia egg.* J Cell Comp Physiol, 1932. **1**(1): p. 1-9.
174. Hiramoto, Y., *Mechanical Properties of Sea Urchin Eggs. I. Surface Force and Elastic Modulus of the Cell Membrane.* Experimental Cell Research, 1963. **32**: p. 59-75.
175. Yoneda, M., *Tension at the Surface of Sea-Urchin Egg: A Critical Examination of Cole's Experiment.* J Exp Biol, 1964. **41**: p. 893-906.
176. Mitchison, J.M. and M.M. Swann, *The Mechanical Properties of the Cell Surface .1. The Cell Elastimeter.* Journal of Experimental Biology, 1954. **31**(3): p. 443-&.
177. Hiramoto, Y., *Observations and Measurements of Sea Urchin Eggs with a Centrifuge Microscope.* J Cell Physiol, 1967. **69**(2): p. 219.
178. Rand, R.P. and A.C. Burton, *Mechanical Properties of the Red Cell Membrane. I. Membrane Stiffness and Intracellular Pressure.* Biophysical Journal, 1964. **4**: p. 115-35.
179. Hochmuth, R.M., *Micropipette aspiration of living cells.* J Biomech, 2000. **33**(1): p. 15-22.
180. Dai, J.W. and M.P. Sheetz, *Membrane tether formation from blebbing cells.* Biophysical Journal, 1999. **77**(6): p. 3363-3370.
181. Evans, E. and A. Yeung, *Apparent Viscosity and Cortical Tension of Blood Granulocytes Determined by Micropipet Aspiration.* Biophysical Journal, 1989. **56**(1): p. 151-160.
182. Yeung, A. and E. Evans, *Cortical Shell-Liquid Core Model for Passive Flow of Liquid-Like Spherical Cells into Micropipets.* Biophysical Journal, 1989. **56**(1): p. 139-149.
183. Preston, G.M., et al., *Appearance of Water Channels in Xenopus Oocytes Expressing Red-Cell Chip28 Protein.* Science, 1992. **256**(5055): p. 385-387.

184. Shepherd, V.A., *The cytomatrix as a cooperative system of macromolecular and water networks.* Current Topics in Developmental Biology, Vol 75, 2006. **75**: p. 171-223.
185. Hoffman, B.D. and J.C. Crocker, *Cell mechanics: dissecting the physical responses of cells to force.* Annu Rev Biomed Eng, 2009. **11**: p. 259-88.
186. Grunnet, M., et al., *KCNQ1 channels sense small changes in cell volume.* Journal of Physiology-London, 2003. **549**(2): p. 419-427.
187. Fels, J., S.N. Orlov, and R. Grygorczyk, *The Hydrogel Nature of Mammalian Cytoplasm Contributes to Osmosensing and Extracellular pH Sensing.* Biophysical Journal, 2009. **96**(10): p. 4276-4285.
188. Zonia, L. and T. Munnik, *Life under pressure: hydrostatic pressure in cell growth and function.* Trends in Plant Science, 2007. **12**(3): p. 90-97.
189. Harold, F.M., *To Shape a Cell - an Inquiry into the Causes of Morphogenesis of Microorganisms.* Microbiological Reviews, 1990. **54**(4): p. 381-431.
190. Blaser, H., et al., *Migration of zebrafish primordial germ cells: A role for myosin contraction and cytoplasmic flow.* Developmental Cell, 2006. **11**(5): p. 613-627.
191. Salbreux, G., et al., *Shape oscillations of non-adhering fibroblast cells.* Physical Biology, 2007. **4**(4): p. 268-284.
192. Lulevich, V., et al., *Single-cell mechanics provides a sensitive and quantitative means for probing amyloid-beta peptide and neuronal cell interactions.* Proceedings of the National Academy of Sciences of the United States of America, 2010. **107**(31): p. 13872-13877.
193. Albrecht-Buehler, G., *Does Blebbing Reveal the Convulsive Flow of Liquid and Solutes through the Cytoplasmic Meshwork.* Cold Spring Harbor Symposia on Quantitative Biology, 1981. **46**: p. 45-49.
194. Trinkaus, J.P., *Surface-Activity and Locomotion of Fundulus Deep Cells during Blastula and Gastrula Stages.* Developmental Biology, 1973. **30**(1): p. 68-103.
195. Trinkaus, J.P. and C.A. Erickson, *Protrusive Activity, Mode and Rate of Locomotion, and Pattern of Adhesion of Fundulus Deep Cells during Gastrulation.* Journal of Experimental Zoology, 1983. **228**(1): p. 41-70.
196. Oster, G.F. and A.S. Perelson, *The physics of cell motility.* J. Cell. Sci. Suppl., 1987. **8**: p. 35-54.
197. Strohmeier, R. and J. Bereiterhahn, *Hydrostatic-Pressure in Epidermal-Cells Is Dependent on Ca-Mediated Contractions.* Journal of Cell Science, 1987. **88**: p. 631-640.
198. Keller, H.U., *Locomoting blebbing cells: A new model to test whether formation of protrusions is primarily due to hydrostatic pressure or to actin elongation.* Biomechanics of Active Movement and Division of Cells, 1994. **84**: p. 431-435

578.

199. Fedier, A. and H.U. Keller, *Suppression of bleb formation, locomotion, and polarity of Walker carcinosarcoma cells by hypertonic media correlates with cell volume reduction but not with changes in the F-actin content.* Cell Motility and the Cytoskeleton, 1997. **37**(4): p. 326-337.
200. Keller, H. and P. Eggli, *Protrusive activity, cytoplasmic compartmentalization, and restriction rings in locomoting blebbing Walker carcinosarcoma cells are related to detachment of cortical actin from the plasma membrane.* Cell Motility and the Cytoskeleton, 1998. **41**(2): p. 181-193.
201. Schutz, K. and H. Keller, *Protrusion, contraction and segregation of membrane components associated with passive deformation and shape recovery of Walker carcinosarcoma cells.* European Journal of Cell Biology, 1998. **77**(2): p. 100-110.
202. Rentsch, P.S. and H. Keller, *Suction pressure can induce uncoupling of the plasma membrane from cortical actin.* European Journal of Cell Biology, 2000. **79**(12): p. 975-981.
203. Keller, H., P. Rentsch, and J. Hagmann, *Differences in cortical actin structure and dynamics document that different types of blebs are formed by distinct mechanisms.* Experimental Cell Research, 2002. **277**(2): p. 161-172.
204. Yanai, M., et al., *Intracellular pressure is a motive force for cell motion in Amoeba proteus.* Cell Motility and the Cytoskeleton, 1996. **33**(1): p. 22-29.
205. Dong, C., S. Aznavoorian, and L.A. Liotta, *2 Phases of Pseudopod Protrusion in Tumor-Cells Revealed by a Micropipette.* Microvascular Research, 1994. **47**(1): p. 55-67.
206. Kelly, S.M. and P.T. Macklem, *Direct Measurement of Intracellular Pressure.* American Journal of Physiology, 1991. **260**(3): p. C652-C657.
207. Kelly, S.M., J.P. Butler, and P.T. Macklem, *Control of Cell-Volume in Oocytes and Eggs from Xenopus-Laevis.* Comparative Biochemistry and Physiology a-Physiology, 1995. **111**(4): p. 681-691.
208. Sahai, E. and C.J. Marshall, *Differing modes of tumour cell invasion have distinct requirements for Rho/ROCK signalling and extracellular proteolysis.* Nature Cell Biology, 2003. **5**(8): p. 711-719.
209. Friedl, P. and K. Wolf, *Proteolytic and non-proteolytic migration of tumour cells and leucocytes.* Proteases and the Regulation of Biological Processes, 2003. **70**: p. 277-285.
210. Langridye, P.D. and R.R. Kay, *Blebbing of Dictyostelium cells in response to chemoattractant.* Experimental Cell Research, 2006. **312**(11): p. 2009-2017.
211. Yoshida, K. and T. Soldati, *Dissection of amoeboid movement into two mechanically distinct modes.* Journal of Cell Science, 2006. **119**(18): p. 3833-3844.
212. Madsen, C.D. and E. Sahai, *Cancer Dissemination-Lessons from Leukocytes.* Developmental Cell, 2010. **19**(1): p. 13-26.
213. Maugis, B., et al., *Dynamic instability of the intracellular pressure drives bleb-based motility.* Journal of Cell Science, 2010. **123**(22): p. 3884-3892.
214. Lammermann, T. and M. Sixt, *Mechanical modes of 'amoeboid' cell migration.* Curr Opin Cell Biol, 2009. **21**(5): p. 636-44.
215. Guck, J., et al., *Critical review: cellular mechanobiology and amoeboid migration.* Integr Biol (Camb), 2010. **2**(11-12): p. 575-83.
216. Lorentzen, A., et al., *An ezrin-rich, rigid uropod-like structure directs movement of amoeboid blebbing cells.* Journal of Cell Science, 2011. **124**(8): p. 1256-1267.

217. Fackler, O.T. and R. Grosse, *Cell motility through plasma membrane blebbing.* Journal of Cell Biology, 2008. **181**(6): p. 879-884.
218. Diz-Munoz, A., et al., *Control of directed cell migration in vivo by membrane-to-cortex attachment.* Plos Biology, 2010. **8**(11): p. e1000544.
219. Ingber, D.E., *Tensegrity II. How structural networks influence cellular information processing networks.* Journal of Cell Science, 2003. **116**(8): p. 1397-1408.
220. Ingber, D.E., *Tensegrity I. Cell structure and hierarchical systems biology.* Journal of Cell Science, 2003. **116**(7): p. 1157-1173.
221. Charras, G.T., et al., *Non-equilibration of hydrostatic pressure in blebbing cells.* Nature, 2005. **435**(7040): p. 365-369.
222. Hoffmann, E.K., I.H. Lambert, and S.F. Pedersen, *Physiology of cell volume regulation in vertebrates.* Physiol Rev, 2009. **89**(1): p. 193-277.
223. Ebner, H.L., et al., *Importance of cytoskeletal elements in volume regulatory responses of trout hepatocytes.* American Journal of Physiology-Regulatory Integrative and Comparative Physiology, 2005. **289**(3): p. R877-R890.
224. Hallows, K.R., et al., *Changes in cytoskeletal actin content, F-actin distribution, and surface morphology during HL-60 cell volume regulation.* Journal of Cellular Physiology, 1996. **167**(1): p. 60-71.
225. Pedersen, S.F., J.W. Mills, and E.K. Hoffmann, *Role of the F-actin cytoskeleton in the RVD and RVI processes in Ehrlich ascites tumor cells.* Experimental Cell Research, 1999. **252**(1): p. 63-74.
226. Guilak, F., G.R. Erickson, and H.P. Ting-Beall, *The effects of osmotic stress on the viscoelastic and physical properties of articular chondrocytes.* Biophysical Journal, 2002. **82**(2): p. 720-727.
227. Hoffmann, E.K. and S.F. Pedersen, *Sensors and signal transduction pathways in vertebrate cell volume regulation.* Mechanisms and Significance of Cell Volume Regulation, 2006. **152**: p. 54-104.
228. Piao, L., et al., *Mechanosensitivity of voltage-gated K+ currents in rat trigeminal ganglion neurons.* Journal of Neuroscience Research, 2006. **83**(7): p. 1373-1380.
229. Levitan, I., et al., *Modulation of a Volume-Regulated Chloride Current by F-Actin.* Journal of Membrane Biology, 1995. **147**(3): p. 283-294.
230. Rizoli, S.B., et al., *Hypertonic inhibition of exocytosis in neutrophils: central role for osmotic actin skeleton remodeling.* American Journal of Physiology-Cell Physiology, 2000. **279**(3): p. C619-C633.
231. Di Ciano-Oliveira, C., et al., *Osmotic stress and the cytoskeleton: the R(h)ole of Rho GTPases.* Acta Physiologica, 2006. **187**(1-2): p. 257-272.
232. Erickson, G.R., D.L. Northrup, and F. Guilak, *Hypo-osmotic stress induces calcium-dependent actin reorganization in articular chondrocytes.* Osteoarthritis and Cartilage, 2003. **11**(3): p. 187-197.
233. Sheetz, M.P., J.E. Sable, and H.G. Dobereiner, *Continuous membrane-cytoskeleton adhesion requires continuous accommodation to lipid and cytoskeleton dynamics.* Annual Review of Biophysics and Biomolecular Structure, 2006. **35**: p. 417-434.
234. Mountian, I., et al., *Changes in actin cytoskeleton during volume regulation in C6 glial cells.* European Journal of Cell Biology, 1998. **77**(3): p. 196-204.
235. Tamma, G., et al., *Hypotonicity causes actin reorganization and recruitment of the actin-binding ERM protein moesin in membrane protrusions in collecting duct principal cells.* American Journal of Physiology-Cell Physiology, 2007. **292**(4): p. C1476-C1484.
236. Jorgensen, N.K., et al., *Cell swelling activates cloned Ca2+-activated K+ channels: a role for the F-actin cytoskeleton.* Biochimica Et Biophysica Acta-Biomembranes, 2003. **1615**(1-2): p. 115-125.
237. Cornet, M., Y. Isobe, and L.F. Lemanski, *Effects of Anisosmotic Conditions on the Cytoskeletal Architecture of Cultured Pc12 Cells.* Journal of Morphology, 1994. **222**(3): p. 269-286.
238. Carton, I., D. Hermans, and J. Eggermont, *Hypotonicity induces membrane protrusions and actin remodeling via activation of small GTPases Rac and Cdc42 in Rat-1 fibroblasts.* American Journal of Physiology-Cell Physiology, 2003. **285**(4): p. C935-C944.
239. Kuwayama, H., et al., *Protection against osmotic stress by cGMP-mediated myosin phosphorylation.* Science, 1996. **271**(5246): p. 207-209.
240. Thirone, A.C.P., et al., *Hyperosmotic stress induces Rho/Rho kinase/LIM kinase-mediated cofilin phosphorylation in tubular cells: key role in the osmotically triggered F-actin response.* American Journal of Physiology-Cell Physiology, 2009. **296**(3): p. C463-C475.
241. Ando-Akatsuka, Y., et al., *Involvements of the ABC protein ABCF2 and alpha-actinin-4 in regulation of cell volume and anion channels in human epithelial cells.* J Cell Physiol, 2012.
242. Steltenkamp, S., et al., *Membrane stiffness of animal cells challenged by osmotic stress.* Small, 2006. **2**(8-9): p. 1016-1020.
243. Roos, K.P. and A.J. Brady, *Osmotic Compression and Stiffness Changes in Relaxed Skinned Cardiac Myocytes in Pvp-40 and Dextran T-500.* Biophysical Journal, 1990. **58**(5): p. 1273-1283.
244. Zhou, E.H., et al., *Universal behavior of the osmotically compressed cell and its analogy to the colloidal glass transition.* Proceedings of the National Academy of Sciences of the United States of America, 2009. **106**(26): p. 10632-10637.
245. Spagnoli, C., et al., *Atomic force microscopy analysis of cell volume regulation.* Physical Review E, 2008. **78**(3): p. -.
246. Tan, Y.H., et al., *Mechanical Characterization of Human Red Blood Cells Under Different Osmotic Conditions by Robotic Manipulation With Optical Tweezers.* Ieee Transactions on Biomedical Engineering, 2010. **57**(7): p. 1816-1825.
247. Hermoso, M., et al., *ClC-3 is a fundamental molecular component of volume-sensitive outwardly rectifying Cl- channels and volume regulation in HeLa cells and Xenopus laevis oocytes.* Journal of Biological Chemistry, 2002. **277**(42): p. 40066-40074.
248. Numata, T., T. Shimizu, and Y. Okada, *TRPM7 is a stretch- and swelling-activated cation channel involved in volume regulation in human epithelial*

cells. American Journal of Physiology-Cell Physiology, 2007. **292**(1): p. C460-C467.
249. Wehner, F., et al., *Signalling events employed in the hypertonic activation of cation channels in HeLa cells.* Cellular Physiology and Biochemistry, 2007. **20**(1-4): p. 75-82.
250. Numata, T., et al., *Hypertonicity-induced cation channels rescue cells from staurosporine-elicited apoptosis.* Apoptosis, 2008. **13**(7): p. 895-903.
251. Subramanyam, M., et al., *Inhibition of Protein Kinase Akt1 by Apoptosis Signal-regulating Kinase-1 (ASK1) Is Involved in Apoptotic Inhibition of Regulatory Volume Increase.* Journal of Biological Chemistry, 2010. **285**(9): p. 6109-6117.
252. Ford, P., et al., *Volume regulation in cortical collecting duct cells: role of AQP2.* Biology of the Cell, 2005. **97**(9): p. 687-697.
253. Schliess, F. and D. Haussinger, *Osmosensing and signaling in the regulation of liver function.* Mechanisms and Significance of Cell Volume Regulation, 2006. **152**: p. 198-209.
254. Malo, M.E. and L. Fliegel, *Physiological role and regulation of the Na+/H+ exchanger.* Canadian Journal of Physiology and Pharmacology, 2006. **84**(11): p. 1081-1095.
255. Meima, M.E., J.R. Mackley, and D.L. Barber, *Beyond ion translocation: structural functions of the sodium-hydrogen exchanger isoform-1.* Current Opinion in Nephrology and Hypertension, 2007. **16**(4): p. 365-372.
256. Alexander, R.T. and S. Grinstein, *Activation of kinases upon volume changes: Role in cellular homeostasis.* Mechanisms and Significance of Cell Volume Regulation, 2006. **152**: p. 105-124.
257. Meima, M.E., et al., *The sodium-hydrogen exchanger NHE1 is an Akt substrate necessary for actin filament reorganization by growth factors.* J Biol Chem, 2009. **284**(39): p. 26666-75.
258. Shi, X.R., P.G. Gillespie, and A.L. Nuttall, *Na+ influx triggers bleb formation on inner hair cells.* American Journal of Physiology-Cell Physiology, 2005. **288**(6): p. C1332-C1341.
259. Yi, Y.-H., et al., *Integrin-mediated Membrane Blebbing is Dependent on Sodium-Proton Exchanger 1 and Sodium-Calcium Exchanger 1 Activity.* Journal of Biological Chemistry, 2012.
260. Schneider, S.W., et al., *Rapid aldosterone-induced cell volume increase of endothelial cells measured by the atomic force microscope.* Cell Biol Int, 1997. **21**(11): p. 759-68.
261. Hillebrand, U., et al., *17beta-estradiol increases volume, apical surface and elasticity of human endothelium mediated by Na+/H+ exchange.* Cardiovasc Res, 2006. **69**(4): p. 916-24.
262. Oberleithner, H., et al., *Endothelial cell swelling by aldosterone.* J Membr Biol, 2003. **196**(3): p. 163-72.
263. Avila, M., et al., *Inhibitors of NHE-1 Na+/H+ exchange reduce mouse intraocular pressure.* Investigative Ophthalmology & Visual Science, 2002. **43**: p. U1166-U1166.
264. Busco, G., et al., *NHE1 promotes invadopodial ECM proteolysis through acidification of the peri-invadopodial space.* Faseb Journal, 2010. **24**(10): p. 3903-3915.
265. Ritter, M., et al., *Effect of inhibitors of Na(+)/H(+)-exchange and gastric H(+)/K(+) ATPase on cell volume, intracellular pH and migration of human polymorphonuclear leucocytes.* British Journal of Pharmacology, 1998. **124**(4): p. 627-638.
266. Stock, C., et al., *Migration of human melanoma cells depends on extracellular pH and Na+/H+ exchange.* Journal of Physiology-London, 2005. **567**(1): p. 225-238.
267. Bereiter-Hahn, J. and M. Voth, *Ionic Control of Locomotion and Shape of Epithelial-Cells .2. Role of Mono-Valent Cations.* Cell Motility and the Cytoskeleton, 1988. **10**(4): p. 528-536.
268. Cardone, R.A., V. Casavola, and S.J. Reshkin, *The role of disturbed pH dynamics and the Na+/H+ exchanger in metastasis.* Nature Reviews Cancer, 2005. **5**(10): p. 786-795.
269. Schneider, L., et al., *The Na(+)/H(+) exchanger NHE1 is required for directional migration stimulated via PDGFR-alpha in the primary cilium.* Journal of Cell Biology, 2009. **185**(1): p. 163-176.
270. Lagana, A., et al., *Regulation of the formation of tumor cell pseudopodia by the Na+/H+ exchanger NHE1.* Journal of Cell Science, 2000. **113**(20): p. 3649-3662.
271. Grinstein, S., et al., *Focal Localization of the Nhe-1 Isoform of the Na+/H+ Antiport - Assessment of Effects on Intracellular Ph.* Embo Journal, 1993. **12**(13): p. 5209-5218.
272. Stock, C. and A. Schwab, *Role of the Na+/H+ exchanger NHE1 in cell migration.* Acta Physiologica, 2006. **187**(1-2): p. 149-157.
273. Denker, S.P., et al., *Direct binding of the Na-H exchanger NHE1 to ERM proteins regulates the cortical cytoskeleton and cell shape independently of H+ translocation.* Molecular Cell, 2000. **6**(6): p. 1425-1436.
274. Denker, S.P. and D.L. Barber, *Cell migration requires both ion translocation and cytoskeletal anchoring by the Na-H exchanger NHE1.* Journal of Cell Biology, 2002. **159**(6): p. 1087-1096.
275. Denker, S.P. and D.L. Barber, *Ion transport proteins anchor and regulate the cytoskeleton.* Current Opinion in Cell Biology, 2002. **14**(2): p. 214-220.
276. Martin, C., et al., *Intracellular pH gradients in migrating cells.* American Journal of Physiology-Cell Physiology, 2011. **300**(3): p. C490-C495.
277. Frantz, C., et al., *Cofilin is a pH sensor for actin free barbed end formation: role of phosphoinositide binding.* Journal of Cell Biology, 2008. **183**(5): p. 865-879.
278. Srivastava, J., et al., *Structural model and functional significance of pH-dependent talin-actin binding for focal adhesion remodeling.* Proc Natl Acad Sci U S A, 2008. **105**(38): p. 14436-41.
279. Frantz, C., et al., *Positive feedback between Cdc42 activity and H+ efflux by the Na-H exchanger NHE1 for polarity of migrating cells.* Journal of Cell Biology, 2007. **179**(3): p. 403-410.
280. Walev, I., et al., *Recovery of Human Fibroblasts from Attack by the Pore-Forming Alpha-Toxin of Staphylococcus-Aureus.* Microbial Pathogenesis, 1994. **17**(3): p. 187-201.
281. Jones, W.R., et al., *Alterations in the Young's modulus and volumetric properties of chondrocytes isolated from normal and osteoarthritic human cartilage.* Journal of Biomechanics, 1999. **32**(2): p. 119-127.

282. Trickey, W.R., et al., *Determination of the Poisson's ratio of the cell: recovery properties of chondrocytes after release from complete micropipette aspiration.* Journal of Biomechanics, 2006. **39**(1): p. 78-87.
283. Freeman, P.M., et al., *Chondrocyte Cells Respond Mechanically to Compressive Loads.* Journal of Orthopaedic Research, 1994. **12**(3): p. 311-320.
284. Ofek, G., D.C. Wiltz, and K.A. Athanasiou, *Contribution of the Cytoskeleton to the Compressive Properties and Recovery Behavior of Single Cells.* Biophysical Journal, 2009. **97**(7): p. 1873-1882.
285. Shieh, A.C., E.J. Koay, and K.A. Athanasiou, *Strain-dependent recovery behavior of single chondrocytes.* Biomechanics and Modeling in Mechanobiology, 2006. **5**(2-3): p. 172-179.
286. Shin, D. and K. Athanasiou, *Cytoindentation for obtaining cell biomechanical properties.* Journal of Orthopaedic Research, 1999. **17**(6): p. 880-890.
287. MacKintosh, F.C. and C.F. Schmidt, *Active cellular materials.* Current Opinion in Cell Biology, 2010. **22**(1): p. 29-35.
288. Habela, C.W. and H. Sontheimer, *Cytoplasmic volume condensation is an integral part of mitosis.* Cell Cycle, 2007. **6**(13): p. 1613-1620.
289. Cuddapah, V.A., et al., *Kinase activation of ClC-3 accelerates cytoplasmic condensation during mitotic cell rounding.* Am J Physiol Cell Physiol, 2011.
290. Boucrot, E. and T. Kirchhausen, *Mammalian cells change volume during mitosis.* PLoS ONE, 2008. **3**(1): p. e1477.
291. Bendix, P.M., et al., *A quantitative analysis of contractility in active cytoskeletal protein networks.* Biophysical Journal, 2008. **94**(8): p. 3126-36.
292. Mizuno, D., et al., *Nonequilibrium mechanics of active cytoskeletal networks.* Science, 2007. **315**(5810): p. 370-3.
293. Groulx, N., et al., *Membrane reserves and hypotonic cell swelling.* Journal of Membrane Biology, 2006. **214**(1-2): p. 43-56.
294. Saarikangas, J., H.X. Zhao, and P. Lappalainen, *Regulation of the Actin Cytoskeleton-Plasma Membrane Interplay by Phosphoinositides.* Physiological Reviews, 2010. **90**(1): p. 259-289.
295. Roch, F., et al., *Differential roles of PtdIns(4,5)P(2) and phosphorylation in moesin activation during Drosophila development.* Journal of Cell Science, 2010. **123**(12): p. 2057-2066.
296. Pyrpassopoulos, S., H. Shuman, and E.M. Ostap, *Single-Molecule Adhesion Forces and Attachment Lifetimes of Myosin-I Phosphoinositide Interactions.* Biophysical Journal, 2010. **99**(12): p. 3916-3922.
297. McConnell, R.E. and M.J. Tyska, *Leveraging the membrane - cytoskeleton interface with myosin-1.* Trends in Cell Biology, 2010. **20**(7): p. 418-426.
298. Mani, T., et al., *FERM Domain Phosphoinositide Binding Targets Merlin to the Membrane and Is Essential for Its Growth-Suppressive Function.* Molecular and Cellular Biology, 2011. **31**(10): p. 1983-1996.
299. Siripala, A.D. and M.D. Welch, *SnapShot: Actin regulators II.* Cell, 2007. **128**(5): p. 1014-1014.
300. Liu, J., et al., *Cleavage furrow organization requires PIP(2)-mediated recruitment of anillin.* Curr Biol, 2012. **22**(1): p. 64-9.
301. Rescher, U., et al., *Annexin 2 is a phosphatidylinositol (4,5)-bisphosphate binding protein recruited to actin assembly sites at cellular membranes.* Journal of Cell Science, 2004. **117**(16): p. 3473-3480.
302. Gilden, J. and M.F. Krummel, *Control of Cortical Rigidity by the Cytoskeleton: Emerging Roles for Septins.* Cytoskeleton, 2010. **67**(8): p. 477-486.
303. Fehon, R.G., A.I. McClatchey, and A. Bretscher, *Organizing the cell cortex: the role of ERM proteins.* Nature Reviews Molecular Cell Biology, 2010. **11**(4): p. 276-287.
304. Popowicz, G.M., et al., *Filamins: promiscuous organizers of the cytoskeleton.* Trends in Biochemical Sciences, 2006. **31**(7): p. 411-419.
305. Larson, S.M., et al., *Cortical Mechanics and Meiosis II Completion in Mammalian Oocytes Are Mediated by Myosin-II and Ezrin-Radixin-Moesin (ERM) Proteins.* Molecular Biology of the Cell, 2010. **21**(18): p. 3182-3192.
306. Roubinet, C., et al., *Molecular networks linked by Moesin drive remodeling of the cell cortex during mitosis.* Journal of Cell Biology, 2011. **195**(1): p. 99-112.
307. Estey, M.P., M.S. Kim, and W.S. Trimble, *Septins.* Current Biology, 2011. **21**(10): p. R384-R387.
308. Tooley, A.J., et al., *Amoeboid T lymphocytes require the septin cytoskeleton for cortical integrity and persistent motility.* Nature Cell Biology, 2009. **11**(1): p. 17-U37.
309. Gilden, J.K., et al., *The septin cytoskeleton facilitates membrane retraction during motility and blebbing.* Journal of Cell Biology, 2012. **196**(1): p. 103-14.
310. Erickson, C.A. and J.P. Trinkaus, *Microvilli and blebs as sources of reserve surface membrane during cell spreading.* Experimental Cell Research, 1976. **99**(2): p. 375-84.
311. Knutton, S., M.C.B. Sumner, and C.A. Pasternak, *Role of Microvilli in Surface Changes of Synchronized P815y Mastocytoma-Cells.* Journal of Cell Biology, 1975. **66**(3): p. 568-576.
312. Thyberg, J. and S. Moskalewski, *Influence of Proteolytic-Enzymes and Calcium-Binding Agents on Nuclear and Cell-Surface Topography.* Cell and Tissue Research, 1984. **237**(3): p. 587-593.
313. Okada, Y., *Volume expansion-sensing outward-rectifier Cl- channel: Fresh start to the molecular identity and volume sensor.* American Journal of Physiology-Cell Physiology, 1997. **273**(3): p. C755-C789.
314. Terasima, T. and L.J. Tolmach, *Growth and Nucleic Acid Synthesis in Synchronously Dividing Populations of Hela Cells.* Experimental Cell Research, 1963. **30**(2): p. 344-&.
315. Thery, M. and M. Bornens, *Cell shape and cell division.* Curr. Opin. Cell Biol., 2006. **18**(6): p. 648-57.
316. Dalen, H. and P. Scheie, *Microextensions on Changs Liver Cells as Observed Throughout Their Division Cycle.* Experimental Cell Research, 1969. **57**(2-3): p. 351-&.
317. Dalen, H. and P.W. Todd, *Surface Morphology of Trypsinized Human Cells in-Vitro.* Experimental Cell Research, 1971. **66**(2): p. 353-&.
318. Wetzel, B., et al., *A systematic scanning electron microscope analysis of mitotic cell populations in monolayer culture.* Scanning Electron Microscopy, 1978(2): p. 1-10.

319. Geuijen, C.A. and A. Sonnenberg, *Dynamics of the alpha6beta4 integrin in keratinocytes.* Molecular Biology of the Cell, 2002. **13**(11): p. 3845-58.
320. Toyoshima, F. and E. Nishida, *Integrin-mediated adhesion orients the spindle parallel to the substratum in an EB1-and myosin X-dependent manner.* Embo Journal, 2007. **26**(6): p. 1487-1498.
321. Herreros, L., et al., *Paxillin localizes to the lymphocyte microtubule organizing center and associates with the microtubule cytoskeleton.* J Biol Chem, 2000. **275**(34): p. 26436-40.
322. Hirota, T., et al., *Zyxin, a regulator of actin filament assembly, targets the mitotic apparatus by interacting with h-warts/LATS1 tumor suppressor.* Journal of Cell Biology, 2000. **149**(5): p. 1073-1086.
323. Law, S.F., et al., *Cell cycle-regulated processing of HEF1 to multiple protein forms differentially targeted to multiple subcellular compartments.* Molecular and Cellular Biology, 1998. **18**(6): p. 3540-3551.
324. Fielding, A.B., et al., *Integrin-linked kinase localizes to the centrosome and regulates mitotic spindle organization.* Journal of Cell Biology, 2008. **180**(4): p. 681-689.
325. Pugacheva, E.N. and E.A. Golemis, *The focal adhesion scaffolding protein HEF1 regulates activation of the Aurora-A and Nek2 kinases at the centrosome.* Nature Cell Biology, 2005. **7**(10): p. 937-U18.
326. Reinsch, S. and E. Karsenti, *Orientation of Spindle Axis and Distribution of Plasma-Membrane Proteins during Cell-Division in Polarized Mdckii Cells.* Journal of Cell Biology, 1994. **126**(6): p. 1509-1526.
327. den Elzen, N., et al., *Cadherin Adhesion Receptors Orient the Mitotic Spindle during Symmetric Cell Division in Mammalian Epithelia.* Molecular Biology of the Cell, 2009. **20**(16): p. 3740-3750.
328. Marthiens, V., et al., *Adhesion molecules in the stem cell niche - more than just staying in shape?* Journal of Cell Science, 2010. **123**(10): p. 1613-1622.
329. Castanon, I. and M. Gonzalez-Gaitan, *Oriented cell division in vertebrate embryogenesis.* Current Opinion in Cell Biology, 2011. **23**(6): p. 697-704.
330. Zigman, M., et al., *Zebrafish Neural Tube Morphogenesis Requires Scribble-Dependent Oriented Cell Divisions.* Current Biology, 2011. **21**(1): p. 79-86.
331. Lamb, N.J., et al., *Microinjection of p34cdc2 kinase induces marked changes in cell shape, cytoskeletal organization, and chromatin structure in mammalian fibroblasts.* Cell, 1990. **60**(1): p. 151-65.
332. Gavet, O. and J. Pines, *Progressive Activation of CyclinB1-Cdk1 Coordinates Entry to Mitosis.* Developmental Cell, 2010. **18**(4): p. 533-543.
333. Pagliuca, F.W., et al., *Quantitative Proteomics Reveals the Basis for the Biochemical Specificity of the Cell-Cycle Machinery.* Molecular Cell, 2011. **43**(3): p. 406-417.
334. Cukier, I.H., Y. Li, and J.M. Lee, *Cyclin B1/Cdk1 binds and phosphorylates Filamin A and regulates its ability to cross-link actin.* Febs Letters, 2007. **581**(8): p. 1661-72.
335. Dadke, D., et al., *Deregulation of HEF1 impairs M-phase progression by disrupting the RhoA activation cycle.* Molecular Biology of the Cell, 2006. **17**(3): p. 1204-1217.
336. Kunda, P., et al., *PP1-Mediated Moesin Dephosphorylation Couples Polar Relaxation to Mitotic Exit.* Current Biology, 2012. **22**(3): p. 231-236.
337. Kato, A., et al., *Critical roles of actin-interacting protein 1 in cytokinesis and chemotactic migration of mammalian cells.* Biochemical Journal, 2008. **414**: p. 261-270.
338. Yamashiro, S., et al., *Mitosis-Specific Phosphorylation Causes 83k Nonmuscle Caldesmon to Dissociate from Microfilaments.* Nature, 1990. **344**(6267): p. 675-678.
339. Yamashiro, S. and F. Matsumura, *Mitosis-Specific Phosphorylation of Caldesmon - Possible Molecular Mechanism of Cell Rounding during Mitosis.* Bioessays, 1991. **13**(11): p. 563-568.
340. Yamashiro, S., et al., *Mutant Caldesmon lacking cdc2 phosphorylation sites delays M-phase entry and inhibits cytokinesis.* Molecular Biology of the Cell, 2001. **12**(1): p. 239-50.
341. Kordowska, J., et al., *Phosphorylated 1-caldesmon is involved in disassembly of actin stress fibers and postmitotic spreading.* Experimental Cell Research, 2005. **312**(2): p. 95-110.
342. Thiel, D.A., et al., *Cell cycle-regulated phosphorylation of p21-activated kinase 1.* Current Biology, 2002. **12**(14): p. 1227-1232.
343. Maroto, B., et al., *P21-activated kinase is required for mitotic progression and regulates Plk1.* Oncogene, 2008. **27**(36): p. 4900-4908.
344. Zeng, Q., et al., *Endothelial cell retraction is induced by PAK2 monophosphorylation of myosin II.* Journal of Cell Science, 2000. **113**(3): p. 471-482.
345. Szczepanowska, J., E.D. Korn, and H. Brzeska, *Activation of myosin in HeLa cells causes redistribution of focal adhesions and F-actin from cell center to cell periphery.* Cell Motility and the Cytoskeleton, 2006. **63**(6): p. 356-374.
346. Bernstein, B.W. and J.R. Bamburg, *ADF/cofilin: a functional node in cell biology.* Trends in Cell Biology, 2010. **20**(4): p. 187-95.
347. Vadlamudi, R.K., et al., *Filamin is essential in actin cytoskeletal assembly mediated by p21-activated kinase 1.* Nature Cell Biology, 2002. **4**(9): p. 681-690.
348. Amano, T., et al., *Mitosis-specific activation of LIM motif-containing protein kinase and roles of cofilin phosphorylation and dephosphorylation in mitosis.* J Biol Chem, 2002. **277**(24): p. 22093-102.
349. Kaji, N., A. Muramoto, and K. Mizuno, *LIM kinase-mediated cofilin phosphorylation during mitosis is required for precise spindle positioning.* Journal of Biological Chemistry, 2008. **283**(8): p. 4983-4992.
350. Ritchey, L., et al., *A functional cooperativity between Aurora A kinase and LIM kinase1: Implication in the mitotic process.* Cell Cycle, 2012. **11**(2): p. 296-309.
351. Heng, Y.W., et al., *TPPP acts downstream of RhoA-ROCK-LIMK2 to regulate astral microtubule organization and spindle orientation.* Journal of Cell Science, 2012.
352. Gorovoy, M., et al., *LIM kinase 1 coordinates microtubule stability and actin polymerization in human endothelial cells.* Journal of Biological Chemistry, 2005. **280**(28): p. 26533-26542.
353. Acevedo, K., et al., *The phosphorylation of p25/TPPP by LIM kinase 1 inhibits its ability to assemble*

microtubules. Experimental Cell Research, 2007. **313**(20): p. 4091-4106.
354. Wojtala, R.L., et al., *Prostate-derived Sterile 20-like Kinases (PSKs/TAOKs) Are Activated in Mitosis and Contribute to Mitotic Cell Rounding and Spindle Positioning.* Journal of Biological Chemistry, 2011. **286**(34): p. 30161-30170.
355. Zhuang, C.M., et al., *CDK1-mediated Phosphorylation of Abi1 Attenuates Bcr-Abl-induced F-actin Assembly and Tyrosine Phosphorylation of WAVE Complex during Mitosis.* Journal of Biological Chemistry, 2011. **286**(44): p. 38614-38626.
356. Chackalaparampil, I. and D. Shalloway, *Altered Phosphorylation and Activation of Pp60c-Src during Fibroblast Mitosis.* Cell, 1988. **52**(6): p. 801-810.
357. Morgan, D.O., et al., *Mitosis-Specific Phosphorylation of P60c-Src by P34cdc2-Associated Protein-Kinase.* Cell, 1989. **57**(5): p. 775-786.
358. Shenoy, S., et al., *Purified Maturation Promoting Factor Phosphorylates Pp60c-Src at the Sites Phosphorylated during Fibroblast Mitosis.* Cell, 1989. **57**(5): p. 763-774.
359. Kato, G. and S. Maeda, *Novel Phosphorylation at a Mitotic Site, Serine-75, in Human Pp60(C-Src) from Unsynchronized Human Tumor-Cells Having a Spherical Morphology.* Biochemical and Biophysical Research Communications, 1995. **216**(2): p. 619-629.
360. Resnick, R.J., et al., *Phosphorylation of the Src substrate Sam68 by Cdc2 during mitosis.* Oncogene, 1997. **15**(11): p. 1247-1253.
361. Spassov, D.S., C.H. Wong, and M.M. Moasser, *Trask phosphorylation defines the reverse mode of a phosphotyrosine signaling switch that underlies cell anchorage state.* Cell Cycle, 2011. **10**(8): p. 1225-1232.
362. Spassov, D.S., et al., *Phosphorylation of Trask by Src Kinases Inhibits Integrin Clustering and Functions in Exclusion with Focal Adhesion Signaling.* Molecular and Cellular Biology, 2011. **31**(4): p. 766-782.
363. Janoueixlerosey, I., et al., *Phosphorylation of Rap1gap during the Cell-Cycle.* Biochemical and Biophysical Research Communications, 1994. **202**(2): p. 967-975.
364. Bos, J.L., *Linking Rap to cell adhesion.* Current Opinion in Cell Biology, 2005. **17**(2): p. 123-128.
365. Montanez, E., et al., *alpha-parvin controls vascular mural cell recruitment to vessel wall by regulating RhoA/ROCK signalling.* Embo Journal, 2009. **28**(20): p. 3132-3144.
366. Wickstrom, S.A., et al., *The ILK/PINCH/parvin complex: the kinase is dead, long live the pseudokinase!* Embo Journal, 2010. **29**(2): p. 281-291.
367. Ma, A., et al., *Serine phosphorylation of focal adhesion kinase in interphase and mitosis: A possible role in modulating binding to p130(Cas).* Molecular Biology of the Cell, 2001. **12**(1): p. 1-12.
368. Fowler, V.M. and E.J.H. Adam, *Spectrin Redistributes to the Cytosol and Is Phosphorylated during Mitosis in Cultured-Cells.* Journal of Cell Biology, 1992. **119**(6): p. 1559-1572.
369. Foisner, R., et al., *M-phase-specific phosphorylation and structural rearrangement of the cytoplasmic cross-linking protein plectin involve p34(cdc2) kinase.* Molecular Biology of the Cell, 1996. **7**(2): p. 273-288.
370. Chou, Y.H., E. Rosevear, and R.D. Goldman, *Phosphorylation and Disassembly of Intermediate Filaments in Mitotic Cells.* Proceedings of the National Academy of Sciences of the United States of America, 1989. **86**(6): p. 1885-1889.
371. Chou, Y.H., et al., *Intermediate Filament Reorganization during Mitosis Is Mediated by P34cdc2 Phosphorylation of Vimentin.* Cell, 1990. **62**(6): p. 1063-1071.
372. Takai, Y., et al., *Mitosis-specific phosphorylation of vimentin by protein kinase C coupled with reorganization of intracellular membranes.* Journal of Cell Biology, 1996. **133**(1): p. 141-149.
373. Chou, Y.H., et al., *Nestin promotes the phosphorylation-dependent disassembly of vimentin intermediate filaments during mitosis.* Molecular Biology of the Cell, 2003. **14**(4): p. 1468-1478.
374. Yamaguchi, T., et al., *Phosphorylation by Cdk1 induces Plk1-mediated vimentin phosphorylation during mitosis.* Journal of Cell Biology, 2005. **171**(3): p. 431-436.
375. Sahlgren, C.M., et al., *Mitotic reorganization of the intermediate filament protein nestin involves phosphorylation by cdc2 kinase.* Journal of Biological Chemistry, 2001. **276**(19): p. 16456-16463.
376. Veselska, R., et al., *Nestin expression in the cell lines derived from glioblastoma multiforme.* Bmc Cancer, 2006. **6**.
377. Laird, A.D. and D. Shalloway, *Oncoprotein signalling and mitosis.* Cellular Signalling, 1997. **9**(3-4): p. 249-255.
378. Taylor, M.P., O.O. Koyuncu, and L.W. Enquist, *Subversion of the actin cytoskeleton during viral infection.* Nature Reviews Microbiology, 2011. **9**(6): p. 427-439.
379. Cuvelier, D., et al., *The universal dynamics of cell spreading.* Current Biology, 2007. **17**(8): p. 694-699.
380. Montell, D.J., *Morphogenetic Cell Movements: Diversity from Modular Mechanical Properties.* Science, 2008. **322**(5907): p. 1502-1505.
381. Hirose, M., et al., *Molecular dissection of the Rho-associated protein kinase (p160ROCK)-regulated neurite remodeling in neuroblastoma N1E-115 cells.* Journal of Cell Biology, 1998. **141**(7): p. 1625-1636.
382. Chen, B.H., et al., *Roles of Rho-associated kinase and myosin light chain kinase in morphological and migratory defects of focal adhesion kinase-null cells.* J Biol Chem, 2002. **277**(37): p. 33857-63.
383. Lee, H.H. and Z.F. Chang, *Regulation of RhoA-dependent ROCKII activation by Shp2.* Journal of Cell Biology, 2008. **181**(6): p. 999-1012.
384. Maekawa, M., et al., *Signaling from rho to the actin cytoskeleton through protein kinases ROCK and LIM-kinase.* Science, 1999. **285**(5429): p. 895-898.
385. Maeda, M., et al., *ARHGAP18, a GTPase-activating protein for RhoA, controls cell shape, spreading, and motility.* Molecular Biology of the Cell, 2011. **22**(20): p. 3840-52.
386. Lavelin, I. and B. Geiger, *Characterization of a novel GTPase-activating protein associated with focal adhesions and the actin cytoskeleton.* Journal of Biological Chemistry, 2005. **280**(8): p. 7178-7185.

387. Ohta, Y., J.H. Hartwig, and T.P. Stossel, *FilGAP, a Rho- and ROCK-regulated GAP for Rac binds filamin A to control actin remodelling.* Nature Cell Biology, 2006. **8**(8): p. 803-U35.
388. Smith, T.K., et al., *Bves directly interacts with GEFT, and controls cell shape and movement through regulation of Rac1/Cdc42 activity.* Proceedings of the National Academy of Sciences of the United States of America, 2008. **105**(24): p. 8298-8303.
389. Jalink, K., et al., *Inhibition of Lysophosphatidate-Induced and Thrombin-Induced Neurite Retraction and Neuronal Cell Rounding by Adp-Ribosylation of the Small Gtp-Binding Protein-Rho.* Journal of Cell Biology, 1994. **126**(3): p. 801-810.
390. Kranenburg, O., et al., *Dissociation of LPA-induced cytoskeletal contraction from stress fiber formation by differential localization of RhoA.* Journal of Cell Science, 1997. **110**: p. 2417-2427.
391. Noguchi, K., et al., *Lysophosphatidic acid (LPA) and its receptors.* Current Opinion in Pharmacology, 2009. **9**(1): p. 15-23.
392. Choi, J.W., et al., *LPA Receptors: Subtypes and Biological Actions.* Annual Review of Pharmacology and Toxicology, 2010. **50**: p. 157-186.
393. Mccoy, K.L., S.F. Traynelis, and J.R. Hepler, *PAR1 and PAR2 Couple to Overlapping and Distinct Sets of G Proteins and Linked Signaling Pathways to Differentially Regulate Cell Physiology.* Molecular Pharmacology, 2010. **77**(6): p. 1005-1015.
394. Jalink, K. and W.H. Moolenaar, *Thrombin Receptor Activation Causes Rapid Neural Cell Rounding and Neurite Retraction Independent of Classic 2nd Messengers.* Journal of Cell Biology, 1992. **118**(2): p. 411-419.
395. Vouret-Craviari, V., et al., *Regulation of the actin cytoskeleton by thrombin in human endothelial cells: Role of Rho proteins in endothelial barrier function.* Molecular Biology of the Cell, 1998. **9**(9): p. 2639-2653.
396. Vouret-Craviari, V., D. Grall, and E. Van Obberghen-Schilling, *Modulation of Rho GTPase activity in endothelial cells by selective proteinase-activated receptor (PAR) agonists.* Journal of Thrombosis and Haemostasis, 2003. **1**(5): p. 1103-1111.
397. Majumdar, M., et al., *Requirement for Rho-mediated myosin light chain phosphorylation in thrombin-stimulated cell rounding and its dissociation from mitogenesis.* J Biol Chem, 1998. **273**(17): p. 10099-106.
398. Majumdar, M., et al., *A Rho exchange factor mediates thrombin and G alpha(12)-induced cytoskeletal responses.* Journal of Biological Chemistry, 1999. **274**(38): p. 26815-26821.
399. Sandquist, J.C., et al., *Rho kinase differentially regulates phosphorylation of nonmuscle myosin II isoforms A and B during cell rounding and migration.* J Biol Chem, 2006. **281**(47): p. 35873-83.
400. Adams, M.N., et al., *Structure, function and pathophysiology of protease activated receptors.* Pharmacology & Therapeutics, 2011. **130**(3): p. 248-282.
401. Soh, U.J.K., et al., *Signal transduction by protease-activated receptors.* British Journal of Pharmacology, 2010. **160**(2): p. 191-203.
402. Hirata, T. and S. Narumiya, *Prostanoid Receptors.* Chemical Reviews, 2011. **111**(10): p. 6209-6230.
403. Pierce, K.L., et al., *Activation of FP prostanoid receptor isoforms leads to Rho-mediated changes in cell morphology and in the cell cytoskeleton.* Journal of Biological Chemistry, 1999. **274**(50): p. 35944-35949.
404. Shum, W.W.C., et al., *Involvement of Rho-kinase in contraction of guinea-pig aorta induced by prostanoid EP3 receptor agonists.* British Journal of Pharmacology, 2003. **139**(8): p. 1449-1461.
405. Sugimoto, Y. and S. Narumiya, *Prostaglandin E receptors.* Journal of Biological Chemistry, 2007. **282**(16): p. 11613-11617.
406. Macias-Perez, I.M., et al., *Mouse EP3 alpha, beta, and gamma receptor variants reduce tumor cell proliferation and tumorigenesis in vivo.* Journal of Biological Chemistry, 2008. **283**(18): p. 12538-12545.
407. Denniss, S.G., A.J. Jeffery, and J.W.E. Rush, *RhoA-Rho kinase signaling mediates endothelium- and endoperoxide-dependent contractile activities characteristic of hypertensive vascular dysfunction.* American Journal of Physiology-Heart and Circulatory Physiology, 2010. **298**(5): p. H1391-H1405.
408. Goupil, E., et al., *A Novel Biased Allosteric Compound Inhibitor of Parturition Selectively Impedes the Prostaglandin F2 alpha-mediated Rho/ROCK Signaling Pathway.* Journal of Biological Chemistry, 2010. **285**(33): p. 25624-25636.
409. Vitale, M.L. and M.E. Carbajal, *Involvement of myosin II in dopamine-induced reorganization of the lactotroph cell's actin cytoskeleton.* Journal of Histochemistry & Cytochemistry, 2004. **52**(4): p. 517-527.
410. Ho, G.Y., et al., *Activation of serum response element by D2 dopamine receptor is governed by G beta gamma-mediated MAPK and Rho pathways and regulated by RGS proteins.* Pharmacology, 2007. **79**(2): p. 114-121.
411. Everett, P.B. and S.E. Senogles, *D(3) dopamine receptor signals to activation of phospholipase D through a complex with Rho.* Journal of Neurochemistry, 2010. **112**(4): p. 963-971.
412. Hu, H., T.F. Marton, and C.S. Goodman, *Plexin B mediates axon guidance in Drosophila by simultaneously inhibiting active Rac and enhancing RhoA signaling.* Neuron, 2001. **32**(1): p. 39-51.
413. Barberis, D., et al., *Plexin signaling hampers integrin-based adhesion, leading to Rho-kinase independent cell rounding, and inhibiting lamellipodia extension and cell motility.* Faseb Journal, 2004. **18**(1): p. 592-+.
414. Negishi, M., I. Oinuma, and H. Katoh, *Plexins: axon guidance and signal transduction.* Cell Mol Life Sci, 2005. **62**(12): p. 1363-71.
415. Li, X.H. and A.Y.W. Lee, *Semaphorin 5A and Plexin-B3 Inhibit Human Glioma Cell Motility through RhoGDI alpha- mediated Inactivation of Rac1 GTPase.* Journal of Biological Chemistry, 2010. **285**(42): p. 32436-32445.
416. Roney, K.E., et al., *Plexin-B2 Negatively Regulates Macrophage Motility, Rac, and Cdc42 Activation.* PLoS One, 2011. **6**(9).
417. Wang, Y., et al., *Plexins Are GTPase-Activating Proteins for Rap and Are Activated by Induced Dimerization.* Sci Signal, 2012. **5**(207): p. ra6.

418. Cowan, C.A. and M. Henkemeyer, *The SH2/SH3 adaptor Grb4 transduces B-ephrin reverse signals.* Nature, 2001. **413**(6852): p. 174-179.
419. Lawrenson, I.D., et al., *Ephrin-A5 induces rounding, blebbing and de-adhesion of EphA3-expressing 293T and melanoma cells by CrkII and Rho-mediated signalling.* Journal of Cell Science, 2002. **115**(Pt 5): p. 1059-72.
420. Deroanne, C., et al., *EphrinA1 inactivates integrin-mediated vascular smooth muscle cell spreading via the Rac/PAK pathway.* Journal of Cell Science, 2003. **116**(7): p. 1367-1376.
421. Miao, H., et al., *Inhibition of integrin-mediated cell adhesion but not directional cell migration requires catalytic activity of EphB3 receptor tyrosine kinase. Role of Rho family small GTPases.* J Biol Chem, 2005. **280**(2): p. 923-32.
422. Riedl, J.A., et al., *Down-regulation of Rap1 activity is involved in ephrinB1-induced cell contraction.* Biochemical Journal, 2005. **389**: p. 465-469.
423. Huang, X.D., et al., *Induction of cell retraction by the combined actions of Abl-CrkII and Rho-ROCK1 signaling.* Journal of Cell Biology, 2008. **183**(4): p. 711-723.
424. Rohani, N., et al., *EphrinB/EphB Signaling Controls Embryonic Germ Layer Separation by Contact-Induced Cell Detachment.* Plos Biology, 2011. **9**(3).
425. Fleenor, D., et al., *Constitutive expression of placental lactogen in pancreatic beta cells: Effects on cell morphology, growth, and gene expression.* Pediatric Research, 2000. **47**(1): p. 136-142.
426. Lee, S.H., et al., *16-kDa prolactin inhibits endothelial cell migration by down-regulating the Ras-Tiam1-Rac1-Pak1 signaling pathway.* Cancer Research, 2007. **67**(22): p. 11045-11053.
427. Shiu, R.P.C. and J.A. Paterson, *Alteration of Cell-Shape, Adhesion, and Lipid-Accumulation in Human-Breast Cancer-Cells (T-47d) by Human-Prolactin and Growth-Hormone.* Cancer Research, 1984. **44**(3): p. 1178-1186.
428. Kumar, A. and Z.H. Song, *CB1 cannabinoid receptor-mediated changes of trabecular meshwork cellular properties.* Molecular Vision, 2006. **12**(31): p. 290-297.
429. Magazine, H.I., et al., *Morphine-induced conformational changes in human monocytes, granulocytes, and endothelial cells and in invertebrate immunocytes and microglia are mediated by nitric oxide.* Journal of Immunology, 1996. **156**(12): p. 4845-4850.
430. Stefano, G.B., Y. Liu, and M.S. Goligorsky, *Cannabinoid receptors are coupled to nitric oxide release in invertebrate immunocytes, microglia, and human monocytes.* Journal of Biological Chemistry, 1996. **271**(32): p. 19238-19242.
431. Sunico, C.R., et al., *Nitric Oxide Induces Pathological Synapse Loss by a Protein Kinase G-, Rho Kinase-Dependent Mechanism Preceded by Myosin Light Chain Phosphorylation.* Journal of Neuroscience, 2010. **30**(3): p. 973-984.
432. DeMali, K.A., A.L. Jue, and K. Burridge, *IpaA targets beta 1 integrins and Rho to promote actin cytoskeleton rearrangements necessary for Shigella entry.* Journal of Biological Chemistry, 2006. **281**(51): p. 39534-39541.
433. Wells, C.M., A. Abo, and A.J. Ridley, *PAK4 is activated via PI3K in HGF-stimulated epithelial cells.* Journal of Cell Science, 2002. **115**(20): p. 3947-3956.
434. Wells, C.M. and G.E. Jones, *The emerging importance of group II PAKs.* Biochemical Journal, 2010. **425**: p. 465-473.
435. Arias-Romero, L.E. and J. Chernoff, *A tale of two Paks.* Biology of the Cell, 2008. **100**(2): p. 97-108.
436. Whale, A., et al., *Signalling to cancer cell invasion through PAK family kinases.* Frontiers in Bioscience-Landmark, 2011. **16**: p. 849-864.
437. Li, J., et al., *Integrin-mediated migration of murine B82L fibroblasts is dependent on the expression of an intact epidermal growth factor receptor.* Journal of Biological Chemistry, 1999. **274**(16): p. 11209-11219.
438. Tu, S., et al., *Epidermal growth factor-dependent regulation of Cdc42 is mediated by the Src tyrosine kinase.* Journal of Biological Chemistry, 2003. **278**(49): p. 49293-49300.
439. Yip, S.C., et al., *The distinct roles of Ras and Rac in PI3-kinase-dependent protrusion during EGF-stimulated cell migration.* Journal of Cell Science, 2007. **120**(17): p. 3138-3146.
440. Kakiashvili, E., et al., *The Epidermal Growth Factor Receptor Mediates Tumor Necrosis Factor-alpha-induced Activation of the ERK/GEF-H1/RhoA Pathway in Tubular Epithelium.* Journal of Biological Chemistry, 2011. **286**(11): p. 9268-9279.
441. Chinkers, M., J.A. Mckanna, and S. Cohen, *Rapid Rounding of Human Epidermoid Carcinoma-Cells a-431 Induced by Epidermal Growth-Factor.* Journal of Cell Biology, 1981. **88**(2): p. 422-429.
442. Jackowski, M.M., et al., *Morphologic Changes in Human Carcinoma-Cells (a-431) Stimulated by Epidermal Growth-Factor - Effect of Cholesterol and Low-Density Lipoproteins on the Ruffling Response.* Journal of Cellular Physiology, 1990. **142**(3): p. 458-468.
443. Samson, T., *Endogenous RhoG is rapidly activated after epidermal growth factor stimulation through multiple guanine-nucleotide exchange factors (vol 21, pg 1629, 2010).* Molecular Biology of the Cell, 2011. **22**(14): p. 2659-2659.
444. Miranda, A.F., et al., *Action of Cytochalasin D on Cells of Established Lines .1. Early Events.* Journal of Cell Biology, 1974. **61**(2): p. 481-500.
445. Miranda, A.F., G.C. Godman, and Tanenbau.Sw, *Action of Cytochalasin-D on Cells of Established Lines .2. Cortex and Microfilaments.* Journal of Cell Biology, 1974. **62**(2): p. 406-423.
446. Godman, G.C., et al., *Action of Cytochalasin-D on Cells of Established Lines .3. Zeiosis and Movements at Cell-Surface.* Journal of Cell Biology, 1975. **64**(3): p. 644-667.
447. Schliwa, M., *Action of Cytochalasin-D on Cytoskeletal Networks.* Journal of Cell Biology, 1982. **92**(1): p. 79-91.
448. Newman, P. and F.M. Watt, *Influence of Cytochalasin D-Induced Changes in Cell-Shape on Proteoglycan Synthesis by Cultured Articular Chondrocytes.* Experimental Cell Research, 1988. **178**(2): p. 199-210.
449. Higgins, P.J., M.P. Ryan, and A. Ahmed, *Cell-Shape-Associated Transcriptional Activation of the P52(Pai-*

1) Gene in Rat-Kidney Cells. Biochemical Journal, 1992. **288**: p. 1017-1024.
450. Spector, I., et al., *Latrunculins - Novel Marine Macrolides That Disrupt Microfilament Organization and Affect Cell-Growth .1. Comparison with Cytochalasin-D.* Cell Motility and the Cytoskeleton, 1989. **13**(3): p. 127-144.
451. Smith, C.S., et al., *Effect of focal adhesion kinase (FAK) downregulation with FAK antisense oligonucleotides and 5-fluorouracil on the viability of melanoma cell lines.* Melanoma Research, 2005. **15**(5): p. 357-362.
452. Trulsson, M., et al., *HAMLET binding to alpha-actinin facilitates tumor cell detachment.* PLoS One, 2011. **6**(3): p. e17179.
453. Du, Q.S., et al., *Inhibition of PYK2-induced actin cytoskeleton reorganization, PYK2 autophosphorylation and focal adhesion targeting by FAK.* Journal of Cell Science, 2001. **114**(16): p. 2977-2987.
454. Li, L., M. Okura, and A. Imamoto, *Focal adhesions require catalytic activity of Src family kinases to mediate integrin-matrix adhesion.* Molecular and Cellular Biology, 2002. **22**(4): p. 1203-17.
455. Golubovskaya, V.M., et al., *The direct effect of Focal Adhesion Kinase (FAK), dominant-negative FAK, FAK-CD and FAK siRNA on gene expression and human MCF-7 breast cancer cell tumorigenesis.* Bmc Cancer, 2009. **9**.
456. Nobes, C.D., et al., *A new member of the Rho family, Rnd1, promotes disassembly of actin filament structures and loss of cell adhesion.* Journal of Cell Biology, 1998. **141**(1): p. 187-197.
457. Chardin, P., *Function and regulation of Rnd proteins.* Nature Reviews Molecular Cell Biology, 2006. **7**(1): p. 54-62.
458. Lartey, J., et al., *Expression of RND proteins in human myometrium.* Biology of Reproduction, 2006. **75**(3): p. 452-461.
459. Miura, K., et al., *ARAP1: A point of convergence for Arf and Rho signaling.* Molecular Cell, 2002. **9**(1): p. 109-119.
460. Stacey, T.T.I., et al., *ARAP3 is transiently tyrosine phosphorylated in cells attaching to fibronectin and inhibits cell spreading in a RhoGAP-dependent manner.* Journal of Cell Science, 2004. **117**(25): p. 6071-6084.
461. Danesh, F.R., et al., *3-hydroxy-3-methylglutaryl CoA reductase inhibitors prevent high glucose-induced proliferation of mesangial cells via modulation of Rho GTPase/p21 signaling pathway: Implications for diabetic nephropathy.* Proceedings of the National Academy of Sciences of the United States of America, 2002. **99**(12): p. 8301-8305.
462. Heusinger-Ribeiro, J., B. Fischer, and M. Goppelt-Struebe, *Differential effects of simvastatin on mesangial cells.* Kidney International, 2004. **66**(1): p. 187-195.
463. Song, J., et al., *Effects of cholesterol-lowering statins on the aqueous humor outflow pathway.* Investigative Ophthalmology & Visual Science, 2005. **46**(7): p. 2424-2432.
464. Yin, H., Y. Gui, and X.L. Zheng, *2-Methoxyestradiol Inhibits Atorvastatin-Induced Rounding of Human Vascular Smooth Muscle Cells.* Journal of Cellular Physiology, 2010. **222**(3): p. 556-564.
465. Han, J.D. and C.S. Rubin, *Regulation of cytoskeleton organization and paxillin dephosphorylation by cAMP - Studies on murine Y1 adrenal cells.* Journal of Biological Chemistry, 1996. **271**(46): p. 29211-29215.
466. Ramakers, G.J.A. and W.H. Moolenaar, *Regulation of astrocyte morphology by RhoA and lysophosphatidic acid.* Experimental Cell Research, 1998. **245**(2): p. 252-262.
467. Whitehouse, B.J., et al., *Interdependence of steroidogenesis and shape changes in Y1 adrenocortical cells: studies with inhibitors of phosphoprotein phosphatases.* Journal of Endocrinology, 2002. **172**(3): p. 583-593.
468. Rocchi, S., et al., *Adrenocorticotrophic hormone stimulates phosphotyrosine phosphatase SHP2 in bovine adrenocortical cells: phosphorylation and activation by cAMP-dependent protein kinase.* Biochemical Journal, 2000. **352**: p. 483-490.
469. Vilgrain, I., et al., *Hormonal regulation of focal adhesions in bovine adrenocortical cells: induction of paxillin dephosphorylation by adrenocorticotropic hormone.* Biochemical Journal, 1998. **332**: p. 533-540.
470. Cuprak, L.J., C.J. Lammi, and R.C. Bayer, *Scanning Electron-Microscopy of Induced Cell Rounding of Mouse Adrenal-Cortex Tumor-Cells in Culture.* Tissue & Cell, 1977. **9**(4): p. 667-680.
471. Maizels, E.T., et al., *Follicle stimulating hormone (FSH) activates the p38 mitogen-activated protein kinase pathway, inducing small heat shock protein phosphorylation and cell rounding in immature rat ovarian granulosa cells.* Endocrinology, 1998. **139**(7): p. 3353-3356.
472. Lawrence, T.S., et al., *Hormonally Induced Cell-Shape Changes in Cultured Rat Ovarian Granulosa-Cells.* Journal of Cell Biology, 1979. **80**(1): p. 21-36.
473. Smith, J.B., *Beta-Adrenergic Stimulation Inhibits Calcium Efflux and Alters the Morphology of Cultured Arterial Muscle-Cells.* Journal of Cellular Physiology, 1984. **121**(2): p. 375-382.
474. Gebhardt, T., et al., *beta 2-adrenoceptor-mediated suppression of human intestinal mast cell functions is caused by disruption of filamentous actin dynamics.* European Journal of Immunology, 2005. **35**(4): p. 1124-1132.
475. Connor, C.G., R.C. Brady, and B.L. Brownstein, *Trifluoperazine Inhibits Spreading and Migration of Cells in Culture.* Journal of Cellular Physiology, 1981. **108**(3): p. 299-307.
476. Dudani, A.K. and R.S. Gupta, *Effect of Chlorpromazine and Trifluoperazine on Cytoskeletal Components and Mitochondria in Cultured-Mammalian-Cells.* Tissue & Cell, 1987. **19**(2): p. 183-196.
477. Wedel, N., et al., *Ultrastructural Effects of Clostridium-Difficile Toxin-B on Smooth-Muscle Cells and Fibroblasts.* Experimental Cell Research, 1983. **148**(2): p. 413-422.
478. Just, I., et al., *Glucosylation of Rho-Proteins by Clostridium-Difficile Toxin-B.* Nature, 1995. **375**(6531): p. 500-503.
479. Paterson, H.F., et al., *Microinjection of Recombinant-P21rho Induces Rapid Changes in Cell Morphology.* Journal of Cell Biology, 1990. **111**(3): p. 1001-1007.

480. Thalmann, J., et al., *Actin re-organization induced by Chlamydia trachomatis serovar D--evidence for a critical role of the effector protein CT166 targeting Rac.* PLoS One, 2010. **5**(3): p. e9887.
481. Kazmierczak, B.I. and J.N. Engel, *Pseudomonas aeruginosa ExoT acts in vivo as a GTPase-activating protein for RhoA, Rac1, and Cdc42.* Infection and Immunity, 2002. **70**(4): p. 2198-2205.
482. Deng, Q., J. Sun, and J.T. Barbieri, *Uncoupling Crk signal transduction by Pseudomonas exoenzyme T.* J Biol Chem, 2005. **280**(43): p. 35953-60.
483. Goehring, U.M., et al., *The N-terminal domain of Pseudomonas aeruginosa exoenzyme S is a GTPase-activating protein for Rho GTPases.* Journal of Biological Chemistry, 1999. **274**(51): p. 36369-36372.
484. Black, D.S. and J.B. Bliska, *The RhoGAP activity of the Yersinia pseudotuberculosis cytotoxin YopE is required for antiphagocytic function and virulence.* Molecular Microbiology, 2000. **37**(3): p. 515-527.
485. Pederson, K.J., et al., *Intracellular localization and processing of Pseudomonas aeruginosa ExoS in eukaryotic cells.* Molecular Microbiology, 2000. **37**(2): p. 287-99.
486. Sun, J. and J.T. Barbieri, *ExoS Rho GTPase-activating protein activity stimulates reorganization of the actin cytoskeleton through Rho GTPase guanine nucleotide disassociation inhibitor.* J Biol Chem, 2004. **279**(41): p. 42936-44.
487. Fehr, D., et al., *Aeromonas exoenzyme T of Aeromonas salmonicida is a bifunctional protein that targets the host cytoskeleton.* Journal of Biological Chemistry, 2007. **282**(39): p. 28843-28852.
488. Litvak, Y. and Z. Selinger, *Aeromonas salmonicida toxin AexT has a Rho family GTPase-activating protein domain.* Journal of Bacteriology, 2007. **189**(6): p. 2558-2560.
489. Yarbrough, M.L., et al., *AMPylation of Rho GTPases by Vibrio VopS Disrupts Effector Binding and Downstream Signaling.* Science, 2009. **323**(5911): p. 269-272.
490. Dong, N., L.P. Liu, and F. Shao, *A bacterial effector targets host DH-PH domain RhoGEFs and antagonizes macrophage phagocytosis.* Embo Journal, 2010. **29**(8): p. 1363-1376.
491. Fullner, K.J. and J.J. Mekalanos, *In vivo covalent cross-linking of cellular actin by the Vibrio cholerae RTX toxin.* Embo Journal, 2000. **19**(20): p. 5315-5323.
492. Sheahan, K.L., C.L. Cordero, and K.J.F. Satchell, *Identification of a domain within the multifunctional Vibrio cholerae RTX toxin that covalently cross-links actin.* Proceedings of the National Academy of Sciences of the United States of America, 2004. **101**(26): p. 9798-9803.
493. Kudryashov, D.S., et al., *Characterization of the enzymatic activity of the actin cross-linking domain from the Vibrio cholerae MARTX(Vc) toxin.* Journal of Biological Chemistry, 2008. **283**(1): p. 445-452.
494. Schlehofer, J.R., H. Hampl, and K.O. Habermehl, *Differences in the Morphology of Herpes-Simplex Virus-Infected Cells .1. Comparative Scanning and Transmission Electron-Microscopic Studies on Hsv-1 Infected Hep-2 and Chick-Embryo Fibroblast Cells.* Journal of General Virology, 1979. **44**(Aug): p. 433-442.
495. Murata, T., et al., *Expression of herpes simplex virus type 2 US3 affects the Cdc42/Rac pathway and attenuates c-Jun N-terminal kinase activation.* Genes to Cells, 2000. **5**(12): p. 1017-1027.
496. Favoreel, H.W., et al., *Cytoskeletal rearrangements and cell extensions induced by the US3 kinase of an alphaherpesvirus are associated with enhanced spread.* Proceedings of the National Academy of Sciences of the United States of America, 2005. **102**(25): p. 8990-8995.
497. Favoreel, H.W., L.W. Enquist, and B. Feierbach, *Actin and Rho GTPases in herpesvirus biology.* Trends in Microbiology, 2007. **15**(9): p. 426-433.
498. Van den Broeke, C., et al., *Alphaherpesvirus US3-mediated reorganization of the actin cytoskeleton is mediated by group A p21-activated kinases.* Proceedings of the National Academy of Sciences of the United States of America, 2009. **106**(21): p. 8707-8712.
499. Ladelfa, M.F., et al., *Effect of the US3 protein of bovine herpesvirus 5 on the actin cytoskeleton and apoptosis.* Veterinary Microbiology, 2011. **153**(3-4): p. 361-366.
500. Gamliel, H., A. Polliack, and I. Sarov, *Surface Features of Vaccinia Virus-Infected Human Embryonic Cells as Studied by Scanning Electron-Microscopy.* Virology, 1977. **83**(1): p. 195-203.
501. Bablanian, R., et al., *Studies on the mechanisms of vaccinia virus cytopathic effects. II. Early cell rounding is associated with virus polypeptide synthesis.* Journal of General Virology, 1978. **39**(3): p. 403-13.
502. Valderrama, F., et al., *Vaccinia virus-induced cell motility requires F11L-mediated inhibition of RhoA signaling.* Science, 2006. **311**(5759): p. 377-381.
503. Arakawa, Y., J.V. Cordeiro, and M. Way, *F11L-mediated inhibition of RhoA-mDia signaling stimulates microtubule dynamics during Vaccinia virus infection.* Cell Host & Microbe, 2007. **1**(3): p. 213-226.
504. Morales, I., et al., *The vaccinia virus F11L gene product facilitates cell detachment and promotes migration.* Traffic, 2008. **9**(8): p. 1283-1298.
505. Stanton, R.J., et al., *Cytomegalovirus destruction of focal adhesions revealed in a high-throughput western blot analysis of cellular protein expression.* Journal of Virology, 2007. **81**(15): p. 7860-7872.
506. Furukawa, T., A. Fioretti, and S. Plotkin, *Growth Characteristics of Cytomegalovirus in Human Fibroblasts with Demonstration of Protein-Synthesis Early in Viral Replication.* Journal of Virology, 1973. **11**(6): p. 991-997.
507. Sen, S. and S. Kumar, *Cell-Matrix De-Adhesion Dynamics Reflect Contractile Mechanics.* Cell Mol Bioeng, 2009. **2**(2): p. 218-230.
508. Jiang, Q.F., et al., *Caldesmon regulates the motility of vascular smooth muscle cells by modulating the actin cytoskeleton stability.* Journal of Biomedical Science, 2010. **17**.
509. McLane, M.A., et al., *Disintegrins.* Curr Drug Targets Cardiovasc Haematol Disord, 2004. **4**(4): p. 327-55.
510. Schmitmeier, S., et al., *Potent mimicry of fibronectin-induced intracellular signaling in glioma cells by the homodimer snake venom disintegrin*

contortrostatin. Neurosurgery, 2005. **57**(1): p. 141-153.
511. Sohn, Y.D., et al., *Suppressive effect and mechanism of saxatilin, a disintegrin from Korean snake (Gloydius saxatilis), in vascular smooth muscle cells.* Toxicon, 2008. **52**(3): p. 474-80.
512. Oliveira-Ferrer, L., et al., *Cilengitide induces cellular detachment and apoptosis in endothelial and glioma cells mediated by inhibition of FAK/src/AKT pathway.* J Exp Clin Cancer Res, 2008. **27**: p. 86.
513. Maurer, G.D., et al., *Cilengitide modulates attachment and viability of human glioma cells, but not sensitivity to irradiation or temozolomide in vitro.* Neuro Oncol, 2009. **11**(6): p. 747-56.
514. Gamble, J.R., et al., *Regulation of in vitro capillary tube formation by anti-integrin antibodies.* Journal of Cell Biology, 1993. **121**(4): p. 931-43.
515. Takada, A., et al., *Downregulation of beta 1 integrins by Ebola virus glycoprotein: Implication for virus entry.* Virology, 2000. **278**(1): p. 20-26.
516. Francica, J.R., M.K. Matukonis, and P. Bates, *Requirements for cell rounding and surface protein down-regulation by Ebola virus glycoprotein.* Virology, 2009. **383**(2): p. 237-247.
517. Culp, L.A., B.A. Murray, and B.J. Rollins, *Fibronectin and Proteoglycans as Determinants of Cell-Substratum Adhesion.* Journal of Supramolecular Structure, 1979. **11**(3): p. 401-427.
518. Wenk, M.B., K.S. Midwood, and J.E. Schwarzbauer, *Tenascin-C suppresses Rho activation.* Journal of Cell Biology, 2000. **150**(4): p. 913-919.
519. Midwood, K.S. and J.E. Schwarzbauer, *Tenascin-C modulates matrix contraction via focal adhesion kinase- and Rho-mediated signaling pathways.* Molecular Biology of the Cell, 2002. **13**(10): p. 3601-3613.
520. Lange, K., et al., *Endothelin receptor type B counteracts tenascin-C-induced endothelin receptor type A-dependent focal adhesion and actin stress fiber disorganization.* Cancer Research, 2007. **67**(13): p. 6163-6173.
521. Midwood, K.S. and G. Orend, *The role of tenascin-C in tissue injury and tumorigenesis.* J Cell Commun Signal, 2009. **3**(3-4): p. 287-310.
522. Chiquet-Ehrismann, R. and R.P. Tucker, *Tenascins and the Importance of Adhesion Modulation.* Cold Spring Harbor Perspectives in Biology, 2011. **3**(5).
523. Goldblum, S.E., et al., *Sparc (Secreted Protein Acidic and Rich in Cysteine) Regulates Endothelial-Cell Shape and Barrier Function.* Proceedings of the National Academy of Sciences of the United States of America, 1994. **91**(8): p. 3448-3452.
524. Bornstein, P. and E.H. Sage, *Matricellular proteins: extracellular modulators of cell function.* Current Opinion in Cell Biology, 2002. **14**(5): p. 608-616.
525. Barker, T.H., et al., *SPARC regulates extracellular matrix organization through its modulation of integrin-linked kinase activity.* Journal of Biological Chemistry, 2005. **280**(43): p. 36483-36493.
526. Hudson, A.E., et al., *Spreading of embryologically distinct urothelial cells is inhibited by SPARC.* Journal of Cellular Physiology, 2005. **202**(2): p. 453-463.
527. Weaver, M.S., G. Workman, and E.H. Sage, *The copper binding domain of SPARC mediates cell survival in vitro via interaction with integrin beta 1 and activation of integrin-linked kinase.* Journal of Biological Chemistry, 2008. **283**(33): p. 22826-22837.
528. Elola, M.T., et al., *Galectins: matricellular glycan-binding proteins linking cell adhesion, migration, and survival.* Cellular and Molecular Life Sciences, 2007. **64**(13): p. 1679-1700.
529. Friedrichs, J., et al., *Galectin-3 Regulates Integrin alpha(2)beta(1)-mediated Adhesion to Collagen-I and -IV.* Journal of Biological Chemistry, 2008. **283**(47): p. 32264-32272.
530. Evangelista, K.D., et al., *Plumieribetin, a Fish Lectin Homologous to Mannose-binding B-type Lectins, Inhibits the Collagen-binding alpha 1 beta 1 Integrin.* Journal of Biological Chemistry, 2009. **284**(50): p. 34747-34759.
531. Lee, H., N. Karasanyi, and R.G. Nagele, Jr., *The role of the cell surface in the migration of primordial germ cells in early chick embryos: effects of concanavalin A.* J Embryol Exp Morphol, 1978. **46**: p. 5-20.
532. Storrie, B., *Antagonism by Dibutryl Adenosine Cyclic 3',5'-Monophosphate and Testololactone of Concanavalin-a Capping.* Journal of Cell Biology, 1975. **66**(2): p. 392-403.
533. Moran, D., *Fluorescent Observations on the Stress Fiber System of Neural Crest Cells after Con-a Treatment - a Simple, Quick, Fluorescent Method.* Journal of Experimental Zoology, 1981. **217**(2): p. 297-301.
534. Pasternak, C. and E.L. Elson, *Lymphocyte Mechanical Response Triggered by Cross-Linking Surface-Receptors.* Journal of Cell Biology, 1985. **100**(3): p. 860-872.
535. Evans, E. and A. Leung, *Adhesivity and Rigidity of Erythrocyte-Membrane in Relation to Wheat-Germ-Agglutinin Binding.* Journal of Cell Biology, 1984. **98**(4): p. 1201-1208.
536. Glatz, R., et al., *Lectin-induced haemocyte inactivation in insects.* Journal of Insect Physiology, 2004. **50**(10): p. 955-963.
537. Marty-Detraves, C., et al., *Inhibitory action of a new lectin from Xerocomus chrysenteron on cell-substrate adhesion.* Molecular and Cellular Biochemistry, 2004. **258**(1-2): p. 49-55.
538. Cook, B., et al., *Preserving cell shape under environmental stress.* Nature, 2008. **452**(7185): p. 361-4.
539. Guller, S., et al., *Growth Hormone-Induced Alteration of Morphology and Tubulin Expression in 3t3 Preadipose Cells.* Biochemical and Biophysical Research Communications, 1989. **163**(2): p. 895-901.
540. Pertz, O., *Spatio-temporal Rho GTPase signaling - where are we now?* Journal of Cell Science, 2010. **123**(11): p. 1841-1850.
541. Alblas, J., et al., *Activation of RhoA and ROCK are essential for detachment of migrating Leukocytes.* Molecular Biology of the Cell, 2001. **12**(7): p. 2137-2145.
542. Rossman, K.L., C.J. Der, and J. Sondek, *GEF means go: Turning on Rho GTPases with guanine nucleotide-exchange factors.* Nature Reviews Molecular Cell Biology, 2005. **6**(2): p. 167-180.
543. Jaffe, A.B. and A. Hall, *Rho GTPases: Biochemistry and biology.* Annual Review of Cell and Developmental Biology, 2005. **21**: p. 247-269.

544. Garcia-Mata, R., E. Boulter, and K. Burridge, *The 'invisible hand': regulation of RHO GTPases by RHOGDIs.* Nature Reviews Molecular Cell Biology, 2011. **12**(8): p. 493-504.
545. vanLeeuwen, F.N., et al., *The guanine nucleotide exchange factor Tiam1 affects neuronal morphology; Opposing roles for the small GTPases Rac and Rho.* Journal of Cell Biology, 1997. **139**(3): p. 797-807.
546. van Leeuwen, F.N., et al., *Rac regulates phosphorylation of the myosin-II heavy chain, actinomyosin disassembly and cell spreading.* Nature Cell Biology, 1999. **1**(4): p. 242-248.
547. Katoh, H., M. Negishi, and A. Ichikawa, *Prostaglandin E receptor EP3 subtype induces neurite retraction via small GTPase Rho.* J Biol Chem, 1996. **271**(47): p. 29780-4.
548. Kojima, F., et al., *Prostaglandin E2 activates Rap1 via EP2/EP4 receptors and cAMP-signaling in rheumatoid synovial fibroblasts: involvement of Epac1 and PKA.* Prostaglandins Other Lipid Mediat, 2009. **89**(1-2): p. 26-33.
549. Hattori, M., M. Osterfield, and J.G. Flanagan, *Regulated cleavage of a contact-mediated axon repellent.* Science, 2000. **289**(5483): p. 1360-1365.
550. Birukova, A.A., et al., *GEF-H1 is involved in agonist-induced human pulmonary endothelial barrier dysfunction.* American Journal of Physiology-Lung Cellular and Molecular Physiology, 2006. **290**(3): p. L540-L548.
551. Cuerrier, C.M., et al., *Effect of thrombin and bradykinin on endothelial cell mechanical properties monitored through membrane deformation.* Journal of Molecular Recognition, 2009. **22**(5): p. 389-396.
552. Tarone, G., et al., *Cell-Surface Molecules and Fibronectin-Mediated Cell-Adhesion - Effect of Proteolytic Digestion of Membrane-Proteins.* Journal of Cell Biology, 1982. **94**(1): p. 179-186.
553. Corver, W.E., et al., *Limited Loss of 9 Tumor-Associated Surface Antigenic Determinants after Tryptic Cell-Dissociation.* Cytometry, 1995. **19**(3): p. 267-272.
554. Blikstad, I. and L. Carlsson, *On the dynamics of the microfilament system in HeLa cells.* Journal of Cell Biology, 1982. **93**(1): p. 122-8.
555. Manser, E., et al., *Expression of constitutively active alpha-PAK reveals effects of the kinase on actin and focal complexes.* Molecular and Cellular Biology, 1997. **17**(3): p. 1129-1143.
556. Foster, D.B., et al., *Phosphorylation of caldesmon by p21-activated kinase - Implications for the Ca2+ sensitivity of smooth muscle contraction.* Journal of Biological Chemistry, 2000. **275**(3): p. 1959-1965.
557. Yamashiro, S., et al., *Phosphorylation of Nonmuscle Caldesmon by P34cdc2 Kinase during Mitosis.* Nature, 1991. **349**(6305): p. 169-172.
558. Numaguchi, Y., et al., *Caldesmon-dependent switching between capillary endothelial cell growth and apoptosis through modulation of cell shape and contractility.* Angiogenesis, 2003. **6**(1): p. 55-64.
559. Mirzapoiazova, T., et al., *The role of caldesmon in the regulation of endothelial cytoskeleton and migration.* Journal of Cellular Physiology, 2005. **203**(3): p. 520-528.
560. Borbiev, T., et al., *p38 MAP kinase-dependent regulation of endothelial cell permeability.* American Journal of Physiology-Lung Cellular and Molecular Physiology, 2004. **287**(5): p. L911-L918.
561. Chu, Z.G., et al., *P38 Map Kinase Mediates Burn Serum-Induced Endothelial Barrier Dysfunction: Involvement of F-Actin Rearrangement and L-Caldesmon Phosphorylation.* Shock, 2010. **34**(3): p. 222-228.
562. Wells, C.M., et al., *PAK4: a pluripotent kinase that regulates prostate cancer cell adhesion.* Journal of Cell Science, 2010. **123**(10): p. 1663-1673.
563. Zand, M.S. and G. Albrechtbuehler, *What Structures, Besides Adhesions, Prevent Spread Cells from Rounding Up.* Cell Motility and the Cytoskeleton, 1989. **13**(3): p. 195-211.
564. Zand, M.S. and G. Albrechtbuehler, *Mechanical Perturbation of Webbed Edges in 3t3 Cells.* Cell Motility and the Cytoskeleton, 1992. **21**(1): p. 15-24.
565. Hughes, M., et al., *Neurite-like structures induced by mevalonate pathway blockade are due to the stability of cell adhesion foci and are enhanced by the presence of APP.* Journal of Neurochemistry, 2010. **114**(3): p. 832-842.
566. Hsie, A.W., C. Jones, and T.T. Puck, *Mammalian Cell Transformations in-Vitro .2. Further Changes in Differentiation State Accompanying Conversion of Chinese Hamster Cells to Fibroblastic Form by Dibutyryl Adenosine Cyclic 3',5'-Monophosphate and Hormones - (Contact Inhibition/Collagen Synthesis/Agglutination).* Proceedings of the National Academy of Sciences of the United States of America, 1971. **68**(7): p. 1648-&.
567. Preston, S.F., et al., *Regulation of Cell-Shape in the Cloudman Melanoma Cell-Line.* Proceedings of the National Academy of Sciences of the United States of America, 1987. **84**(15): p. 5247-5251.
568. Pelletier, S., et al., *Cyclic AMP induces morphological changes of vascular smooth muscle cells by inhibiting a Rac-dependent signaling pathway.* Journal of Cellular Physiology, 2005. **204**(2): p. 412-422.
569. Aslam, M., et al., *cAMP/PKA antagonizes thrombin-induced inactivation of endothelial myosin light chain phosphatase: role of CPI-17.* Cardiovascular Research, 2010. **87**(2): p. 375-384.
570. Zieba, B.J., et al., *The cAMP-responsive Rap1 Guanine Nucleotide Exchange Factor, Epac, Induces Smooth Muscle Relaxation by Down-regulation of RhoA Activity.* Journal of Biological Chemistry, 2011. **286**(19): p. 16681-16692.
571. Zimmerman, N.P., et al., *Cyclic AMP dysregulates intestinal epithelial cell restitution through PKA and RhoA.* Inflamm Bowel Dis, 2011.
572. Jeon, C.Y., et al., *Control of neurite outgrowth by RhoA inactivation.* J Neurochem, 2011.
573. Ramachandran, C., et al., *Effect of Elevated Intracellular cAMP Levels on Actomyosin Contraction in Bovine Trabecular Meshwork Cells.* Investigative Ophthalmology & Visual Science, 2011. **52**(3): p. 1474-1485.
574. Aktories, K., *Bacterial protein toxins that modify host regulatory GTPases.* Nature Reviews Microbiology, 2011. **9**(7): p. 487-498.
575. Moore, R., et al., *C-Difficile Toxin-a Increases Intestinal Permeability and Induces Cl- Secretion.* American Journal of Physiology, 1990. **259**(2): p. G165-G172.

576. Schepis, A., et al., *Vaccinia virus-induced microtubule-dependent cellular rearrangements.* Traffic, 2006. **7**(3): p. 308-323.
577. Burridge, K., L. Molony, and T. Kelly, *Adhesion Plaques - Sites of Transmembrane Interaction between the Extracellular-Matrix and the Actin Cytoskeleton.* Journal of Cell Science, 1987: p. 211-229.
578. Rogers, S.L., et al., *Molecular requirements for actin-based lamella formation in Drosophila S2 cells.* Journal of Cell Biology, 2003. **162**(6): p. 1079-1088.
579. Badley, R.A., A. Woods, and D.A. Rees, *Cooperativity of Concanavalin-a Patching and Its Influence on Cytoskeleton Changes in Fibroblast Rounding and Detachment.* Journal of Cell Science, 1981. **47**(Feb): p. 349-363.
580. Bogatcheva, N.V. and A.D. Verin, *The role of cytoskeleton in the regulation of vascular endothelial barrier function.* Microvascular Research, 2008. **76**(3): p. 202-207.
581. Zlokovic, B.V., *The blood-brain barrier in health and chronic neurodegenerative disorders.* Neuron, 2008. **57**(2): p. 178-201.
582. Shen, L., L.P. Su, and J.R. Turner, *Mechanisms and Functional Implications of Intestinal Barrier Defects.* Digestive Diseases, 2009. **27**(4): p. 443-449.
583. Lucas, R., et al., *Regulators of endothelial and epithelial barrier integrity and function in acute lung injury.* Biochemical Pharmacology, 2009. **77**(12): p. 1763-1772.
584. Pavenstadt, H., W. Kriz, and M. Kretzler, *Cell biology of the glomerular podocyte.* Physiological Reviews, 2003. **83**(1): p. 253-307.
585. Shen, L., et al., *Tight, Junction Pore and Leak Pathways: A Dynamic Duo.* Annual Review of Physiology, Vol 73, 2011: p. 283-309.
586. Daneman, R. and M. Rescigno, *The Gut Immune Barrier and the Blood-Brain Barrier: Are They So Different?* Immunity, 2009. **31**(5): p. 722-735.
587. Morel, N.M.L., et al., *INFLAMMATORY AGONISTS THAT INCREASE MICROVASCULAR PERMEABILITY INVIVO STIMULATE CULTURED PULMONARY MICROVESSEL ENDOTHELIAL-CELL CONTRACTION.* Inflammation, 1990. **14**(5): p. 571-583.
588. Garcia, J.G.N., *Concepts in microvascular endothelial barrier regulation in health and disease.* Microvascular Research, 2009. **77**(1): p. 1-3.
589. Vandenbroucke, E., et al., *Regulation of endothelial junctional permeability.* Ann N Y Acad Sci, 2008. **1123**: p. 134-45.
590. Birukova, A.A., et al., *Endothelial permeability is controlled by spatially defined cytoskeletal mechanics: Atomic force microscopy force mapping of pulmonary endothelial monolayer.* Nanomedicine-Nanotechnology Biology and Medicine, 2009. **5**(1): p. 30-41.
591. Verin, A.D., et al., *Regulation of Endothelial-Cell Gap Formation and Barrier Function by Myosin-Associated Phosphatase-Activities.* American Journal of Physiology-Lung Cellular and Molecular Physiology, 1995. **269**(1): p. L99-L108.
592. Morris, A.J., et al., *Regulation of blood and vascular cell function by bioactive lysophospholipids.* Journal of Thrombosis and Haemostasis, 2009. **7**: p. 38-43.
593. Ivanov, A.I., et al., *Protein kinase C activation disrupts epithelial apical junctions via ROCK-II dependent stimulation of actomyosin contractility.* Bmc Cell Biology, 2009. **10**.
594. Shivanna, M., G. Rajashekhar, and S.P. Srinivas, *Barrier Dysfunction of the Corneal Endothelium in Response to TNF-alpha: Role of p38 MAP Kinase.* Investigative Ophthalmology & Visual Science, 2010. **51**(3): p. 1575-1582.
595. Cioffi, D.L., et al., *TRPing on the Lung Endothelium: Calcium Channels That Regulate Barrier Function.* Antioxidants & Redox Signaling, 2009. **11**(4): p. 765-776.
596. Ereso, A.Q., et al., *Angiotensin II type 2 receptor provides an endogenous brake during inflammation-induced microvascular fluid leak.* Journal of the American College of Surgeons, 2007. **205**(4): p. 527-533.
597. Bodor, C., et al., *Angiotensin II increases the permeability and PV-1 expression of endothelial cells.* American Journal of Physiology-Cell Physiology, 2012. **302**(1): p. C267-C276.
598. Wojciak-Stothard, B., et al., *Regulation of TNF-alpha-induced reorganization of the actin cytoskeleton and cell-cell junctions by Rho, Rac, and Cdc42 in human endothelial cells.* Journal of Cellular Physiology, 1998. **176**(1): p. 150-165.
599. Bayless, K.J. and G.E. Davis, *Microtubule depolymerization rapidly collapses capillary tube networks in vitro and angiogenic vessels in vivo through the small GTPase Rho.* Journal of Biological Chemistry, 2004. **279**(12): p. 11686-11695.
600. Wojciak-Stothard, B. and A.J. Ridley, *Rho GTPases and the regulation of endothelial permeability.* Vascular Pharmacology, 2002. **39**(4-5): p. 187-199.
601. Schlegel, N., et al., *Differential Role of Rho GTPases in Intestinal Epithelial Barrier Regulation In Vitro.* Journal of Cellular Physiology, 2011. **226**(5): p. 1196-1203.
602. Profirovic, J., et al., *Vasodilator-stimulated Phosphoprotein Deficiency Potentiates PAR-1-induced Increase in Endothelial Permeability in Mouse Lungs.* Journal of Cellular Physiology, 2011. **226**(5): p. 1255-1264.
603. Je, H.D., et al., *Protective Effect of Resveratrol on Agonist-Dependent Regulation of Vascular Contractility via Inhibition of Rho-Kinase Activity.* Pharmacology, 2010. **86**(1): p. 37-43.
604. Issuree, P.D.A., et al., *Resveratrol attenuates C5a-induced inflammatory responses in vitro and in vivo by inhibiting phospholipase D and sphingosine kinase activities.* Faseb Journal, 2009. **23**(8): p. 2412-2424.
605. Cain, R.J., B. Vanhaesebroeck, and A.J. Ridley, *The PI3K p110 alpha isoform regulates endothelial adherens junctions via Pyk2 and Rac1.* Journal of Cell Biology, 2010. **188**(6): p. 863-876.
606. Komarova, Y.A., D. Mehta, and A.B. Malik, *Dual regulation of endothelial junctional permeability.* Sci STKE, 2007. **2007**(412): p. re8.
607. Adyshev, D.M., et al., *Differential involvement of ezrin/radixin/moesin proteins in sphingosine 1-phosphate-induced human pulmonary endothelial cell barrier enhancement.* Cellular Signalling, 2011. **23**(12): p. 2086-2096.
608. Turner, J.R., *Intestinal mucosal barrier function in health and disease.* Nature Reviews Immunology, 2009. **9**(11): p. 799-809.

609. Kim, K.S., *Mechanisms of microbial traversal of the blood-brain barrier.* Nature Reviews Microbiology, 2008. **6**(8): p. 625-34.
610. Lemichez, E., et al., *Breaking the wall: targeting of the endothelium by pathogenic bacteria.* Nature Reviews Microbiology, 2010. **8**(2): p. 93-104.
611. Shin, S. and K.S. Kim, *RhoA and Rac1 contribute to type III group B streptococcal invasion of human brain microvascular endothelial cells.* Biochemical and Biophysical Research Communications, 2006. **345**(1): p. 538-542.
612. Vasiliev, J.M., et al., *Rho overexpression leads to mitosis-associated detachment of cells from epithelial sheets: A link to the mechanism of cancer dissemination.* Proceedings of the National Academy of Sciences of the United States of America, 2004. **101**(34): p. 12526-12530.
613. Marchiando, A.M., et al., *The Epithelial Barrier Is Maintained by In Vivo Tight Junction Expansion During Pathologic Intestinal Epithelial Shedding.* Gastroenterology, 2011. **140**(4): p. 1208-+.
614. Cho, K., et al., *Xenopus Kazrin interacts with ARVCF-catenin, spectrin and p190B RhoGAP, and modulates RhoA activity and epithelial integrity.* Journal of Cell Science, 2010. **123**(23): p. 4128-4144.
615. Geny, B., et al., *Clostridium sordellii lethal toxin kills mice by inducing a major increase in lung vascular permeability.* American Journal of Pathology, 2007. **170**(3): p. 1003-1017.
616. Boyer, L., et al., *Induction of transient macroapertures in endothelial cells through RhoA inhibition by Staphylococcus aureus factors.* Journal of Cell Biology, 2006. **173**(5): p. 809-819.
617. Matthews, B.D., et al., *Cellular adaptation to mechanical stress: role of integrins, Rho, cytoskeletal tension and mechanosensitive ion channels.* Journal of Cell Science, 2006. **119**(3): p. 508-518.
618. Trepat, X., et al., *Universal physical responses to stretch in the living cell.* Nature, 2007. **447**(7144): p. 592-+.
619. Mukhina, S., Y.L. Wang, and M. Murata-Hori, *alpha-actinin is required for tightly regulated remodeling of the actin cortical network during cytokinesis.* Developmental Cell, 2007. **13**(4): p. 554-565.
620. Guha, M., M. Zhou, and Y.L. Wang, *Cortical actin turnover during cytokinesis requires myosin II.* Current Biology, 2005. **15**(8): p. 732-736.
621. Carlsson, A.E., *Actin Dynamics: From Nanoscale to Microscale.* Annual Review of Biophysics, Vol 39, 2010. **39**: p. 91-110.
622. Danuser, G. and C.M. Waterman-Storer, *Quantitative fluorescent speckle Microscopy of cytoskeleton dynamics.* Annual Review of Biophysics and Biomolecular Structure, 2006. **35**: p. 361-387.
623. Kittler, R., et al., *Genome-wide resources of endoribonuclease-prepared short interfering RNAs for specific loss-of-function studies.* Nature Methods, 2007. **4**(4): p. 337-344.
624. Hutchins, J.R.A., et al., *Systematic Analysis of Human Protein Complexes Identifies Chromosome Segregation Proteins.* Science, 2010. **328**(5978): p. 593-599.
625. Tatsumoto, T., et al., *Human ECT2 is an exchange factor for Rho GTPases, phosphorylated in G2/M phases, and involved in cytokinesis.* Journal of Cell Biology, 1999. **147**(5): p. 921-927.
626. Hutter, J.L. and J. Bechhoefer, *Calibration of Atomic-Force Microscope Tips.* Review of Scientific Instruments, 1993. **64**(7): p. 1868-1873.
627. Burnham, N.A., et al., *Comparison of calibration methods for atomic-force microscopy cantilevers.* Nanotechnology, 2003. **14**(1): p. 1-6.
628. Muller, D.J., et al., *Force probing surfaces of living cells to molecular resolution.* Nat Chem Biol, 2009. **5**(6): p. 383-90.
629. Thoumine, O. and A. Ott, *Time scale dependent viscoelastic and contractile regimes in fibroblasts probed by microplate manipulation.* J Cell Sci, 1997. **110 (Pt 17)**: p. 2109-16.
630. Mitrossilis, D., et al., *Single-cell response to stiffness exhibits muscle-like behavior.* Proc Natl Acad Sci U S A, 2009. **106**(43): p. 18243-8.
631. Fabry, B., et al., *Selected contribution: time course and heterogeneity of contractile responses in cultured human airway smooth muscle cells.* J Appl Physiol, 2001. **91**(2): p. 986-94.
632. Wang, N., J.P. Butler, and D.E. Ingber, *Mechanotransduction across the Cell-Surface and through the Cytoskeleton.* Science, 1993. **260**(5111): p. 1124-1127.
633. Kasza, K.E., et al., *Magnetic twisting cytometry.* Cold Spring Harb Protoc, 2011. **2011**: p. pdb prot5599.
634. Zhang, H. and K.K. Liu, *Optical tweezers for single cells.* Journal of the Royal Society Interface, 2008. **5**(24): p. 671-690.
635. Ou-Yang, H.D. and M.T. Wei, *Complex fluids: probing mechanical properties of biological systems with optical tweezers.* Annu Rev Phys Chem, 2010. **61**: p. 421-40.
636. Mizuno, D., et al., *High-resolution probing of cellular force transmission.* Phys Rev Lett, 2009. **102**(16): p. 168102.
637. Lincoln, B., et al., *High-throughput rheological measurements with an optical stretcher.* Meth Cell Biol, 2007. **83**: p. 397-423.
638. Knezevic, V., et al., *Isotonic biaxial loading of fibroblast-populated collagen gels: a versatile, low-cost system for the study of mechanobiology.* Biomech Model Mechanobiol, 2002. **1**(1): p. 59-67.
639. Sotoudeh, M., et al., *A strain device imposing dynamic and uniform equi-biaxial strain to cultured cells.* Ann Biomed Eng, 1998. **26**(2): p. 181-9.
640. Young, E.W.K., A.R. Wheeler, and C.A. Simmons, *Matrix-dependent adhesion of vascular and valvular endothelial cells in microfluidic channels.* Lab on a Chip, 2007. **7**(12): p. 1759-1766.
641. Malek, A.M. and S. Izumo, *Mechanism of endothelial cell shape change and cytoskeletal remodeling in response to fluid shear stress.* J Cell Sci, 1996. **109**: p. 713-26.
642. Gabriele, S., et al., *Microfluidic Investigation Reveals Distinct Roles for Actin Cytoskeleton and Myosin II Activity in Capillary Leukocyte Trafficking.* Biophysical Journal, 2009. **96**(10): p. 4308-4318.
643. Rosenbluth, M.J., W.A. Lam, and D.A. Fletcher, *Analyzing cell mechanics in hematologic diseases with microfluidic biophysical flow cytometry.* Lab on a Chip, 2008. **8**(7): p. 1062-1070.
644. Siechen, S., et al., *Mechanical tension contributes to clustering of neurotransmitter vesicles at*

presynaptic terminals. Proc Natl Acad Sci U S A, 2009. **106**(31): p. 12611-12616.
645. Loh, O., A. Vaziri, and H.D.S.M. Espinosa, *The Potential of MEMS for Advancing Experiments and Modeling in Cell Mechanics.* Experimental Mechanics, 2009. **49**(1): p. 105-124.
646. Radmacher, M., *Studying the mechanics of cellular processes by atomic force microscopy.* Meth Cell Biol, 2007. **83**: p. 347-372.
647. Mahaffy, R.E., et al., *Scanning probe-based frequency-dependent microrheology of polymer gels and biological cells.* Physical Review Letters, 2000. **85**(4): p. 880-883.
648. Lam, W.A., et al., *Mechanics and contraction dynamics of single platelets and implications for clot stiffening.* Nat Mater, 2011. **10**(1): p. 61-6.
649. Smith, B.A., et al., *Probing the viscoelastic behavior of cultured airway smooth muscle cells with atomic force microscopy: stiffening induced by contractile agonist.* Biophysical Journal, 2005. **88**(4): p. 2994-3007.
650. Alcaraz, J., et al., *Correction of microrheological measurements of soft samples with atomic force microscopy for the hydrodynamic drag on the cantilever.* Langmuir, 2002. **18**(3): p. 716-721.
651. Gavara, N. and R.S. Chadwick, *Noncontact microrheology at acoustic frequencies using frequency-modulated atomic force microscopy.* Nature Methods, 2010. **7**(8): p. 650-U70.
652. Brangwynne, C.P., F.C. MacKintosh, and D.A. Weitz, *Force fluctuations and polymerization dynamics of intracellular microtubules.* Proc Natl Acad Sci U S A, 2007. **104**(41): p. 16128-33.
653. Park, Y., et al., *Measurement of red blood cell mechanics during morphological changes.* Proceedings of the National Academy of Sciences of the United States of America, 2010. **107**(15): p. 6731-6736.
654. Wildt, B., D. Wirtz, and P.C. Searson, *Programmed subcellular release for studying the dynamics of cell detachment.* Nat Methods, 2009. **6**(3): p. 211-3.
655. Wildt, B., D. Wirtz, and P.C. Searson, *Triggering cell detachment from patterned electrode arrays by programmed subcellular release.* Nature Protocols, 2010. **5**(7): p. 1273-1280.
656. Thomas, A., et al., *Real-time elastography--an advanced method of ultrasound: First results in 108 patients with breast lesions.* Ultrasound Obstet Gynecol, 2006. **28**(3): p. 335-40.
657. Kundu, T., J. Bereiter-Hahn, and K. Hillmann, *Measuring elastic properties of cells by evaluation of scanning acoustic microscopy V(Z) values using simplex algorithm.* Biophysical Journal, 1991. **59**(6): p. 1194-207.
658. Mayer, M., et al., *Anisotropies in cortical tension reveal the physical basis of polarizing cortical flows.* Nature, 2010. **467**(7315): p. 617-21.
659. Ji, L., et al., *Probing intracellular force distributions by high-resolution live cell imaging and inverse dynamics.* Meth Cell Biol, 2007. **83**: p. 199.
660. Lee, J., *The use of gelatin substrates for traction force microscopy in rapidly moving cells.* Meth Cell Biol, 2007. **83**: p. 297-312.
661. Dembo, M. and Y.L. Wang, *Stresses at the cell-to-substrate interface during locomotion of fibroblasts.* Biophysical Journal, 1999. **76**(4): p. 2307-16.
662. Tan, J.L., et al., *Cells lying on a bed of microneedles: an approach to isolate mechanical force.* Proc Natl Acad Sci U S A, 2003. **100**(4): p. 1484-9.
663. Yang, M.T., et al., *Assaying stem cell mechanobiology on microfabricated elastomeric substrates with geometrically modulated rigidity.* Nature Protocols, 2011. **6**(2): p. 187-213.
664. Maskarinec, S.A., et al., *Quantifying cellular traction forces in three dimensions.* Proc Natl Acad Sci U S A, 2009. **106**(52): p. 22108-13.
665. Legant, W.R., et al., *Measurement of mechanical tractions exerted by cells in three-dimensional matrices.* Nature Methods, 2010. **7**(12): p. 969-U113.
666. Dimitriadis, E.K., et al., *Determination of elastic moduli of thin layers of soft material using the atomic force microscope.* Biophysical Journal, 2002. **82**(5): p. 2798-2810.
667. Rosenbluth, M.J., W.A. Lam, and D.A. Fletcher, *Force microscopy of nonadherent cells: A comparison of leukemia cell deformability.* Biophys J, 2006. **90**(8): p. 2994-3003.
668. Webster, K.D., A. Crow, and D.A. Fletcher, *An AFM-Based Stiffness Clamp for Dynamic Control of Rigidity.* PLoS One, 2011. **6**(3): p. -.
669. Chaudhuri, O., S.H. Parekh, and D.A. Fletcher, *Reversible stress softening of actin networks.* Nature, 2007. **445**(7125): p. 295-298.
670. Prass, M., et al., *Direct measurement of the lamellipodial protrusive force in a migrating cell.* Journal of Cell Biology, 2006. **174**(6): p. 767-772.
671. Muller, D.J. and Y.F. Dufrene, *Atomic force microscopy as a multifunctional molecular toolbox in nanobiotechnology.* Nature Nanotechnology, 2008. **3**(5): p. 261-269.
672. Stewart, M.P., et al., *Force probing cell shape changes to molecular resolution.* Trends Biochem Sci, 2011.
673. Evans, E.A. and P.L. Lacelle, *Intrinsic Material Properties of Erythrocyte-Membrane Indicated by Mechanical Analysis of Deformation.* Blood, 1975. **45**(1): p. 29-43.
674. Mitrossilis, D., et al., *Real-time single-cell response to stiffness.* Proc Natl Acad Sci U S A, 2010. **107**(38): p. 16518-23.
675. Radmacher, M., M. Fritz, and P.K. Hansma, *Imaging Soft Samples with the Atomic-Force Microscope - Gelatin in Water and Propanol.* Biophys J, 1995. **69**(1): p. 264-270.
676. Hertz, H., *Uber den Kontakt elastischer Korper.* J Reine Angew Mathematik, 1881. **92**: p. 156.
677. Sneddon, I., *The relation between load and penetration in the axisymmetric boussinesq problem for a punch of arbitrary profile.* Int J Eng Sc, 1965. **3**(1): p. 47-57.
678. Radmacher, M., et al., *Measuring the viscoelastic properties of human platelets with the atomic force microscope.* Biophys J, 1996. **70**(1): p. 556-67.
679. Quist, A.P., et al., *Physiological role of gap-junctional hemichannels. Extracellular calcium-dependent isosmotic volume regulation.* Journal of Cell Biology, 2000. **148**(5): p. 1063-74.
680. Schneider, S.W., et al., *Shape and volume of living aldosterone-sensitive cells imaged with the atomic force microscope.* Meth Mol Biol, 2004. **242**: p. 255-79.

681. Harris, A.R. and G.T. Charras, *Experimental validation of atomic force microscopy-based cell elasticity measurements.* Nanotechnology, 2011. **22**(34): p. 345102.
682. Callies, C., et al., *Membrane potential depolarization decreases the stiffness of vascular endothelial cells.* J Cell Sci, 2011. **124**(Pt 11): p. 1936-42.
683. Vanapalli, S.A., M.H. Duits, and F. Mugele, *Microfluidics as a functional tool for cell mechanics.* Biomicrofluidics, 2009. **3**(1): p. 12006.
684. Kim, D.H., et al., *Microengineered Platforms for Cell Mechanobiology.* Annual Review of Biomedical Engineering, 2009. **11**: p. 203-233.
685. Legant, W.R., et al., *Microfabricated tissue gauges to measure and manipulate forces from 3D microtissues.* Proceedings of the National Academy of Sciences of the United States of America, 2009. **106**(25): p. 10097-10102.
686. Rajagopalan, J. and M.T.A. Saif, *MEMS sensors and microsystems for cell mechanobiology.* Journal of Micromechanics and Microengineering, 2011. **21**(5).
687. Addae-Mensah, K.A. and J.P. Wikswo, *Measurement techniques for cellular biomechanics in vitro.* Experimental Biology and Medicine, 2008. **233**(7): p. 792-809.
688. Remmerbach, T.W., et al., *Oral Cancer Diagnosis by Mechanical Phenotyping.* Cancer Research, 2009. **69**(5): p. 1728-1732.
689. Brangwynne, C.P., *Soft active aggregates: mechanics, dynamics and self-assembly of liquid-like intracellular protein bodies.* Soft Matter, 2011. **7**(7): p. 3052-3059.

Declaration of Originality

I herewith declare that I have produced this thesis without the prohibited assistance of third parties and without making use of aids other than those specified. Notions taken directly or indirectly from other sources have been identified as such. This research has not previously been presented in identical or similar form to any other German or foreign examination board.

The thesis work was conducted from 1st April 2007 to 30th April 2012 under the supervision of Prof. Dr. Daniel J. Müller (Biotechnology Center, Dresden, Technische Universität Dresden and Department of Biosystems Science and Engineering, Basel, ETH Zürich) and Prof. Dr. Anthony A. Hyman (Max Planck Institute for Molecular Cell Biology and Genetics, Dresden).

30th April 2012, Martin P. Stewart

_____